Neuroimaging methods for analysing connectivity in the presence of white matter lesions

Hanna Nowicka

Keble College
University of Oxford

A thesis submitted for the degree of Doctor of Philosophy

Michaelmas Term 2019

Abstract

White Matter Hyperintensities (WMHs) are often observed in the MRI scans of the ageing brain. Previous studies show that the WMH load correlates with cognitive decline, as well as with an increased risk of stroke and dementia. Most of the studies use a global WMH load across the whole brain as the only metric. This thesis proposes new insight into such data by introducing a methodology to analyse the WMH impact on the structural and functional brain connectivity in a localised manner, using white matter tracts. The thesis also supports other studies by exploring the potential impact of WMHs presence on tractography modelling, as well as adapts the method to Multiple Sclerosis (MS) lesion data.

In the first part of the thesis, we presented and evaluated two possible measures of the WMHs impact on the WM tracts from the structural perspective. We showed that despite the different distributions of the two measures, both show a similar relationship with the functional connectivity measure. We explored several possible options for quantifying the resting state functional connectivity between the endpoints of the WM tract in the presence of WMHs. We showed that the choice of connectivity measure (full or partial correlation), as well as gray matter parcellation, made a substantial difference in the results. We also observed variability in the results among the tracts and compared our findings to the results from the literature.

The majority of this work depends on the correct definition of the white matter tracts. Therefore, the second part of the thesis focuses on evaluating the impact of the presence of WMHs on tractography modelling. Despite changes in the microstructural parameters within the WMHs and their proximity, we found no meaningful alterations in the shape of the WM tracts in the presence of WMHs on the tract. Finally, we explored the possibility to apply some of this methodology to data from patients with Multiple Sclerosis, which is the most common cause of neurological disability in young adults. MS lesions have different aetiology to the WMHs but may have a similar appearance. We showed that directly applying the method between those two conditions may not be possible, and we proposed an alternative approach, suited to the MS data.

Neuroimaging methods for analysing connectivity in the presence of white matter lesions



Hanna Nowicka

Keble College

University of Oxford

A thesis submitted for the degree of

Doctor of Philosophy

Michaelmas Term 2019

Acknowledgements

First and foremost, I would like to thank my primary supervisor, Professor Mark Jenkinson. I could not have imagined a better advisor and mentor to lead me through these four years. Completing this thesis would not have been possible without his advice, patience, and support.

I am also very grateful to my other supervisors: Professor Jacqueline Palace and Dr Matteo Bastiani. They shared their expertise, provided invaluable inspiring discussions, and comments about this thesis.

I would like to thank the members of the FMRIB Analysis Group for their advice and support. I am grateful to the Clarendon Fund and the Sloane Robinson Scholarship for funding my studies.

Finally, I would like to thank my friends and family, who have supported me throughout this DPhil, as well as my previous mentors, whose work and guidance have inspired me to pursue this path.

Abstract

White Matter Hyperintensities (WMHs) are often observed in the MRI scans of the ageing brain. Previous studies show that the WMH load correlates with cognitive decline, as well as with an increased risk of stroke and dementia. Most of the studies use a global WMH load across the whole brain as the only metric. This thesis proposes new insight into such data by introducing a methodology to analyse the WMH impact on the structural and functional brain connectivity in a localised manner, using white matter tracts. The thesis also supports other studies by exploring the potential impact of WMHs presence on tractography modelling, as well as adapts the method to Multiple Sclerosis (MS) lesion data.

In the first part of the thesis, we presented and evaluated two possible measures of the WMHs impact on the WM tracts from the structural perspective. We showed that despite the different distributions of the two measures, both show a similar relationship with the functional connectivity measure. We explored several possible options for quantifying the resting state functional connectivity between the endpoints of the WM tract in the presence of WMHs. We showed that the choice of connectivity measure (full or partial correlation), as well as gray matter parcellation, made a substantial difference in the results. We also observed variability in the results among the tracts and compared our findings to the results from the literature.

The majority of this work depends on the correct definition of the white matter tracts. Therefore, the second part of the thesis focuses on evaluating the impact of the presence of WMHs on tractography modelling. Despite changes in the microstructural parameters within the WMHs and their proximity, we found no meaningful alterations in the shape of the WM tracts in the presence of WMHs on the tract. Finally, we explored the possibility to apply some of this methodology to data from patients with Multiple Sclerosis, which is the most common cause of neurological disability in young adults. MS lesions have different aetiology to the WMHs but may have a similar appearance. We showed that directly applying the method between those two conditions may not be possible, and we proposed an alternative approach, suited to the MS data.

Contents

List of Abbreviations **xi**

1 Introduction **1**
1.1 Motivation . . . 1
1.2 Thesis outline and contributions . . . 2

2 Background **5**
2.1 Brain MRI . . . 5
2.2 Brain Ageing . . . 6
2.2.1 White Matter . . . 6
2.2.2 White Matter Hyperintensities . . . 6
2.2.3 Studying brain ageing using Big Data . . . 8
2.3 Structural connectivity . . . 8
2.3.1 Diffusion imaging . . . 9
2.3.2 Models . . . 10
2.3.3 Tractography . . . 13
2.3.4 White matter tracts . . . 14
2.4 Functional connectivity . . . 15
2.5 Multiple Sclerosis . . . 16

3 Measuring structural impact of WMHs on WM tracts **19**
3.1 Introduction . . . 19
3.2 Literature review . . . 20
3.3 Data . . . 22
3.4 Methods . . . 25
3.4.1 Proposed method for quantifying the tract-specific WMH impact . . . 26
3.5 Results . . . 27
3.5.1 Whole brain measures . . . 27
3.5.2 Tract-specific spatial distribution of WMHs . . . 28
3.5.3 Method for quantifying tract-specific impact of WMHs . . . 29
3.6 Discussion . . . 30
3.7 Summary . . . 32

4 Measuring WMHs impact on functional connectivity 35
4.1 Introduction . . . 35
4.2 Literature background . . . 36
4.2.1 Data . . . 37
4.2.2 Timeseries extraction . . . 38
4.2.3 Functional connectivity definition . . . 45
4.2.4 Analysis . . . 50
4.3 Results . . . 51
4.3.1 Parcellations . . . 51
4.3.2 Functional connectivity . . . 54
4.3.3 Relationships between the structural and functional measures 57
4.3.4 Summary of the results across methods and tracts . . . 58
4.3.5 Accounting for confounds in the regression . . . 62
4.4 Discussion . . . 62
4.5 Summary . . . 71

5 Tractography in the presence of White Matter Hyperintensities 73
5.1 Motivation . . . 74
5.2 Introduction . . . 74
5.3 Methods and data . . . 76
5.3.1 General overview of the methods approach . . . 76
5.3.2 Data . . . 77
5.4 Tract shape variability analysis . . . 77
5.4.1 Methods . . . 77
5.4.2 Discussion of the results . . . 79
5.4.3 Conclusion . . . 81
5.5 Voxelwise tractography results comparison . . . 81
5.5.1 Methods . . . 82
5.5.2 Results . . . 85
5.5.3 Discussion . . . 96
5.6 Microstructural parameters analysis . . . 101
5.6.1 Methods . . . 102
5.6.2 Results . . . 103
5.6.3 Discussion . . . 113
5.6.4 Conclusion . . . 115
5.7 Summary . . . 115

6 Tractography in the presence of Multiple Sclerosis lesions 117
6.1 Introduction . . . 117
6.2 Background . . . 118
6.3 Data . . . 119
6.4 Methods . . . 122
6.4.1 Preprocessing . . . 122
6.4.2 Applying previously developed methods to MS data . . . 123
6.4.3 A modified method for MS data – creating two binary classes 124
6.4.4 A modified method for MS data – using the lesion load . . . 127
6.4.5 Additional analysis with healthy controls . . . 127
6.5 Results . . . 128
6.5.1 The two classes approach . . . 129
6.5.2 The scaled lesion load approach . . . 130
6.5.3 Additional analysis with healthy controls . . . 132
6.6 Discussion . . . 133
6.7 Summary . . . 136

7 Conclusions and future work 137
7.1 Conclusions . . . 137
7.2 Future work . . . 139

Appendices

A Spatial distributions of WMHs on each tract over 5000 subjects 145

B Comparison between structural measures for each tract 153

C Functional vs structural connectivity measures for different tracts 167

D Analysis of structural and functional connectivity correlation for subsets of data 173

E Voxelwise tractography analysis results for all the tracts 181
E.1 All the data . . . 181
E.1.1 Two columns in design matrix . . . 181
E.1.2 Relative difference when accounting for confounds – 4 columns in the design matrix . . . 190
E.1.3 Results when contrasts are modified . . . 191
E.2 Subset with narrow age range . . . 198
E.3 Single sex subset within the narrow age range . . . 198

F Summary of microstructural parameters 211

G Multiple Sclerosis application results for all the tracts **215**
G.1 A modified method for MS data – creating two binary classes . . . 215
G.2 A modified method for MS data – using the lesion load 220
G.3 Additional analysis with healthy controls 220

References **231**

List of Abbreviations

BOLD . . . . . Blood-Oxygen-Level-Dependent (signal).

CSF . . . . . Cerebrospinal Fluid.

DMN . . . . . Default Mode Network.

dMRI . . . . . Diffusion Magnetic Resonance Imaging.

DTI . . . . . Diffusion Tensor Imaging.

FA . . . . . Fractional Anisotropy.

FDR . . . . . False Discovery Rate.

FLAIR . . . . Fluid-Attenuated Inversion Recovery.

FSL . . . . . FMRIB Software Library.

GLM . . . . . General Linear Model.

H-O . . . . . Harvard-Oxford (atlas).

L . . . . . Left.

ICVF . . . . . Intra-cellular Volume Fraction.

IQR . . . . . Interquartile range.

ISOVF . . . . Isotropic Volume Fraction.

MRI . . . . . Magnetic Resonance Imaging.

MS . . . . . Multiple Sclerosis.

NODDI . . . . Neurite Orientation Dispersion and Density Imaging.

OD . . . . . Orientation Dispersion.

R . . . . . Right.

ROI . . . . . Region of Interest.

rs-fMRI . . . . Resting-state Functional Magnetic Resonance Imaging.

WM . . . . . White Matter.

WMHs . . . . White Matter Hyperintensities.

1 Introduction

Contents

1.1 Motivation 1
1.2 Thesis outline and contributions 2

1.1 Motivation

White Matter Hyperintensities (WMHs) are the high intensity areas in the white matter visible on T2-weighted MRI scans. Those focal changes, along with atrophy, are the frequently observed changes in ageing brains, as they affect the majority of people over the age of 45 [1]. The WMH load (i.e., total volume of WMHs) in the brain is known to correlate with cognitive decline, physical function like gait [2], and increased risk of stroke and dementia [3].

The majority of the literature uses a single number to describe the scale of white matter damage – either the total brain volume or count of WMHs – and relate that to decline in brain function. This thesis proposes to investigate the impact of WMHs on the brain in a more localised manner, which would provide additional measures of the WMHs impact on specific structure and function. In chapters 3 and 4, we propose methodology that uses multimodal data to quantify

both structural and resting state functional connectivity changes due to the presence of WMHs in relation to particular white matter tracts in the brain.

In the areas of WMHs, the microstructure of the tissue is altered [4]. Because some microstructure parameters are used in the tractography, for in vivo identification of the white matter tracts, there was concern about whether tractography results are reliable in the presence of WMHs. In chapter 5, we approached that problem on three different levels to assess whether tractography results are compromised or not. The White Matter Hyperintensities are only an example of white matter lesions observed in neurological conditions. Focal changes in the white matter of similar appearance but different origin can also be observed in the neuroinflammatory diseases. We also investigated Multiple Sclerosis (MS), which is the most common neurological condition causing disability among adults under 30 years old. In the last technical chapter of the thesis, we explored the possibility to translate some of the methods presented earlier in this thesis from the ageing population to MS patients.

1.2 Thesis outline and contributions

The two main results arising from this thesis are:

1. Adding to existing methodological approaches for analysing the impact WMHs on the brain connectivity (structural and functional) in a more localised manner – in relation to the white matter tracts, which can enrich further findings in the literature using multimodal datasets with lesions.

2. Finding the differences in microstructural parameters inside WMHs overlapping tracts and outside them, as well as some patterns of differences in tractography strength in the presence of WMHs overlapping the tracts. These patterns seem to be modulated by age and sex. However, the lack of strong differences in the centre of the tract, even for our large dataset with a broad age range, suggests that in smaller studies there might not be much impact of WMHs on statistical tests that use tractography values. The results show

that the relationships between WMHs and tractography are complex and lay out the basis for further investigation.

Work presented in this thesis uses structural, functional, and diffusion imaging MR scans data from the ageing population (UK Biobank dataset), as well as Multiple Sclerosis subjects. Chapter 2 introduces neuroimaging concepts on which this work is building.

The first half of the thesis proposes the quantitative measures of WMH impact on structural and functional connectivity in the brain and the relationship between both. It emphasises exploring how the choice of methodology impacts the results of the analysis. That work starts in chapter 3 and is continued in chapter 4. In chapter 3, we showed the spatial distribution of the WMHs on the tracts in the UK Biobank dataset [5]. Then, we compared two measures of structural impact of WMHs on the tract, providing more detailed insight into the data. The first measure is based on the volumetric overlap of the WMH mask with the tract mask and has been used in the literature before. The second measure is based on the fraction of the tract streamlines count passing through the WMH mask, which partially takes into account the location of the lesion within the tract. We compare those measures in chapter 3 and observe a wider distribution of values for the streamlines-based measure, which may mean it provides more information as it describes more variability between the subjects.

In chapter 4, we propose methodology to quantify the resting state functional connectivity measure between the endpoints of tracts with WMHs. We explore various methods and their impact on the final results. That included a choice of the gray matter parcellation for the fMRI timeseries extraction and matching the cortical regions with white matter tracts, timeseries preprocessing, or using full versus partial correlations as a measure of functional connectivity. Then we use the extracted measures to explore the relationship between the structural and functional impact of the presence of WMHs on the white matter tracts using the UK Biobank dataset and compare our results with a similar study from the literature. Finally, we compared the results when exploring the relationship between the functional measures proposed

in this chapter and the use of the two structural measures proposed in chapter 3 and we see little difference between results for both structural measures.

The second half of the thesis supports the above analysis, as well as many neuroimaging studies using tractography in the presence of WMHs. In chapter 5, we investigated concerns regarding the impact that the microstructural changes within the WMHs could have on the tractography results when they are in the proximity of white matter tracts. We examined the variability of the white matter tract shape for subjects with WMHs on the tract compared to the rest of the subjects for 22 white matter tracts in the brain. First, we ran the analysis on a high level, looking at the final tract shape. Then, we proposed a method for comparing the voxel-wise tractography results between the subjects with and without the WMHs on the tracts. We found differences in the subsets of data, where we ensured no correlation between age and WMH load, as well as restricting it to a single sex. However, there were no strong effects seen in the results for the dataset with a large age range when including age and sex as covariates. In the final experiment of chapter 5 we look into the microstructural parameters within and in the proximity of WMHs on the tracts, as well as the rest of the white matter tracts with and without WMHs. That supporting analysis showed that there were changes in the microstructural parameters due to the presence of WMHs, but the way they might affect the final tractography results is not straightforward, and it might be modulated by age and sex, which therefore requires further research. The work presented in chapter 5 used 5000 subjects from the UK Biobank dataset.

In chapter 6, we explored the potential of applying the voxel-wise method proposed in chapter 5 to the Multiple Sclerosis data. We showed that it is difficult to apply the method directly, therefore we also proposed two adaptations of that method, which can be generalised to MS lesions. Additionally, we explore how the method works in a dataset containing MS subjects and matched healthy controls.

2 Background

Contents

2.1 Brain MRI 5
2.2 Brain Ageing 6
2.2.1 White Matter 6
2.2.2 White Matter Hyperintensities 6
2.2.3 Studying brain ageing using Big Data 8
2.3 Structural connectivity 8
2.3.1 Diffusion imaging 9
2.3.2 Models 10
2.3.3 Tractography 13
2.3.4 White matter tracts 14
2.4 Functional connectivity 15
2.5 Multiple Sclerosis 16

2.1 Brain MRI

One of the most important tools used in neuroimaging is Magnetic Resonance Imaging (MRI). MRI is a medical imaging technique that uses combinations of magnetic fields and radiofrequency pulses to allow for in vivo and non-invasive investigation of the structure and physiology of the body.

Using different sequences of pulses – precisely defined times of turning on and

off radiofrequency fields and gradient coils – it is possible to obtain images with different contrasts using MRI. Common ones are structural images (including T1-, T2-weighted, FLAIR), which allow for distinguishing between the tissues, using their different properties. Other types of frequently used MR imaging techniques include: functional (fMRI), diffusion (dMRI), arterial spin labelling and spectroscopy.

MRI is non-invasive, safe, and flexible, what makes it a particularly attractive medical imaging technique to study the human brain, which has an extremely complex structure and function that is still not fully understood.

2.2 Brain Ageing

The brain is constantly changing during an individual's life. Healthy older individuals typically show decreases in both brain size and cognitive function [6] [7]. Neuroimaging allows in vivo and non-invasive investigation of changes in the brain over time and in big populations.

2.2.1 White Matter

In this thesis, we focus on white matter. White matter, which constitutes more than half of the human brain, contains neuronal fibres – the axons. The structure of white matter and its changes are strongly related to cognitive function, learning, information-processing, and also psychiatric and neurological disorders [8]. In humans, axons may be surrounded by a myelin sheath. Myelin is a cell membrane, consisting of multiple lipid layers [8]. Myelin provides electrical insulation and its presence increases the speed of electrical signal conduction along the axon. It is not clear whether changes – in white matter structure or in genes responsible for myelination – are likely causes of psychiatric and neurological disorders or their consequence [8].

2.2.2 White Matter Hyperintensities

A very common finding when looking at MRI datasets from an ageing populations is White Matter Hyperintensities (WMHs). Otherwise known as leukoaraiosis, WMHs

are visible as patches brighter than the rest of white matter on the T2-weighted MRI scans. WMHs have been shown to be associated with impairment in cognition, physical function [2], as well as depression [9], [10], a higher risk of stroke (three times) [3] and a higher risk of dementia (two times) [3]. Here, we mostly discuss the WMHs of presumed vascular origin. However, white matter changes of inflammatory nature in Multiple Sclerosis (lesions) will also be discussed later in this thesis.

WMHs become more common with age [1]. Statistically, nearly 95% of people over the age of 45, and 98% of people over the age of 75 will develop at least one WMH [1]. With increased age there is a higher median volume of WMHs, but their spatial pattern becomes broader [1]. The prevalence of WMHs is related to multiple risk factors, especially vascular ones like hypertension or any changes in blood pressure. Among other risk factors that may cause WMHs, there is also diabetes, smoking and lack of physical exercise. The impact of particular risk factors varies with age [11].

Different changes in the white matter might be related to different underlying pathological changes on the tissue level [12]. The age related changes in white matter are widespread. There is a pattern of changes being most visible in the frontal and parietal brain regions, however for some local areas this trend is reversed [13]. In terms of focal changes in white matter, we broadly distinguish lesions with regard to their location in the periventricular regions, which lie in proximity of the ventricles, and deep white matter regions [14]. Periventricular WMHs are characterised by higher fluid concentration [12]. In deep white matter, WMHs can be a sign of pathological changes of ischemic origin [12]. These can include demyelination and axonal loss [12], which are examples of permanent changes. However, in general, the WMHs can change, and the biology underlying WMHs is complex [15]. Apart from ischemia, there is also an alternative hypothesis explaining the origin of WMHs by linking it to altered CSF circulation [16]. Changes in the blood-brain barrier permeability are also often associated with the appearance of WMHs [16]. The knowledge about the underlying processes comes mostly from

pathology studies, but it is not always possible to relate their results with the findings from an MRI scan [15], [12].

2.2.3 Studying brain ageing using Big Data

There is widespread interest in studying WMH and try to link them with functional and behavioural outcomes. A review from 2019 [17] summarises over 130 studies using the data from 37 datasets. The median size of these datasets was around 1000 subjects.

One of these datasets is the UK Biobank [5], [18], [19]. It is a large study in the United Kingdom with 500,000 participants, aged 40-69 years old at the time of recruitment. It has already been used for a study of the white matter health in ageing [20]. The study found age-related white matter deterioration in association fibres and thalamic radiations.

A tendency to use large datasets in brain ageing research reflects a general trend in neuroimaging research (such as the Human Connectome Project). It is worth noting that these datasets, like the UK Biobank, often contain large quantities of not only imaging data but also genetics, physical measures, and electronic health records [19]. That trend, however, should lead to a reflection about the methodologies used. Using 'big data' in neuroimaging has its advantages but also brings particular challenges [21].

2.3 Structural connectivity

One of the most interesting aspects of the brain is its connectivity. It can be understood as a pattern of relations between the elements building a brain [22]. There are three types of brain connectivity: structural, functional and effective connectivity [23]. Structural connectivity looks at how the white matter fibres pathways connect different brain regions. Functional connectivity looks for functionally related brain regions based on pattern similarity in their blood oxygen levels over time, usually by detecting correlations. Effective connectivity describes

a network of directed interactions between neural systems in a brain. In this thesis, only structural and functional connectivity will be investigated.

2.3.1 Diffusion imaging

To estimate the brain's structural connectivity profile non-invasively and in vivo, we can use diffusion imaging. Diffusion MRI is sensitive to the motion of water molecules at the micrometer scale, usually in the time scale of tens of milliseconds [13]. Measurement of those water molecule displacements can be used to estimate the composition and microstructure of the tissue. The main assumption used in diffusion modelling is that in the white matter diffusion is anisotropic, which means that the diffusion is dependent on the spatial direction [24]. That is caused by the structure of axons, which contain mostly elongated elements, like microtubules and neurofilaments inside of the axon as well as axonal membrane and myelin sheath around the axon.

Diffusion imaging is the only method available to assess brain microstructure in vivo and non-invasively. It requires modelling approaches, due to the fact that dMRI provides only an indirect measure of the anatomical substrate and due to the difference in scales in imaging: even in the most advanced MRI scanners, the voxel size is in the order of a millimetre, while the axons have radii between $0.1-10\mu m$ [13].

Diffusion MRI acquisition Typical diffusion MRI experiments use a spin-echo pulse sequence with two additional magnetic field gradients that make the sequence sensitive to diffusion motion (during the time between when the two gradients are applied). The contrast of the diffusion image depends on the diffusion weighting parameter (called 'b-value') and the direction of the gradient. With the higher b-value, the diffusion contrast (sensitivity to the diffusion) is higher but there is less signal remaining (lower signal to noise ratio). Normally, there are multiple volumes acquired with different gradient directions.

Distortions in diffusion imaging Due to the nature of their acquisition, diffusion-weighted images normally have lower resolution and signal-to-noise ratio than structural images from the same subject. Moreover, they also show substantial image distortions. Some distortions come from the fact that image acquisition in diffusion imaging typically relies on echo planar imaging (EPI), which is very sensitive to the off-resonance field (difference between the field expected and the real field). Changes in the magnetic field result in spin precession frequency changes, which add an off-resonance phase in the EPI data. This results in shift (or warping) of the actual image in the phase-encoding direction. The above effect is often seen around structural boundaries (for example in the proximity of the sinuses, which contain air – in contrary to the tissue around them). Another source of artifacts is the generation of spurious eddy currents, which are induced when the diffusion-weighting gradients are switched on and off rapidly. Apart from distortions due to the field perturbation, there are also significant artifacts arising from motion (whole head movement or cardiac driven pulsations).

There are methods for correcting these artifacts, both at image acquisition (like using parallel imaging) and data postprocessing. To estimate the susceptibility field it is possible to acquire an image in opposite directions along the phase encoding axis and integrate the data from both. Estimating and correcting for eddy currents and subject motion is more complicated but it is also possible using bespoke tools.

2.3.2 Models

The images obtained from diffusion MRI experiments do not provide the underlying tissue microstructure directly. However, that data can be used to fit a model, from which it is possible to infer tissue microstructure.

Diffusion Tensor Imaging Diffusion Tensor Imaging (DTI) [24] is the most widely used model allowing the in vivo study of white matter properties such as axonal organisation [4]. DTI is widely used because it allows researchers and clinicians to estimate microstructural proxy features and the principal diffusion

direction, which can be assumed to correspond to the principal direction of the axons at a given spatial location. [13].

After having acquired at least 6 diffusion weighted volumes using 6 linearly independent diffusion encoding gradient orientations and a b0 (i.e., diffusion unweighted) volume, it is possible to describe the anisotropy of the diffusion by a 3 x 3 tensorial matrix. The three diagonal elements of the tensor matrix are the values of diffusivity along x, y, and z axis. The highest eigenvalue of the tensor is assumed to represent the axial diffusivity – i.e. degree of diffusivity along the main direction of the fibre, and the smaller eigenvalues represent the degree of diffusivity in two directions perpendicular to the main direction. These two smaller eigenvalues are averaged to obtain voxel-wise radial diffusivity values. All three of those eigenvalues averaged together represent the average rate of diffusion in a voxel, which is known as the mean diffusivity parameter (MD). Fractional anisotropy (FA) quantifies the degree of anisotropy, i.e., of directional preference, in a voxel. FA can take values from 0 for fully isotropic diffusion to, theoretically, 1 in the fully anisotropic case. In practice, FA normally takes values between 0.2 to 0.4 in gray matter and between 0.45 to 0.8 in white matter [13]. In white matter, FA is higher in those voxels that contain neuronal fibres aligned mostly in one direction (such as in the body of the corpus callosum) and lower where fibres are pointing in different directions (i.e. crossing or kissing). Diffusion anisotropy can also be reduced as a result of neurological disorders, generally due to tissue degeneration. The main limitation of the DTI model described above is that it can only resolve one principal diffusion orientation per voxel. That means that in the voxels with more complicated fibre configurations, like crossing fibres, the DTI model fails.

Ball and stick model The ball and stick model [25] is a multi-compartment model, which separates the signal contribution from water molecules in two different pools: a free compartment, where molecules freely move in any direction – that is represented as 'a ball', and a restricted compartment, where water molecules are assumed to be moving only along one direction, indicated by 'a stick'. It is

possible to add more than one stick to the ball, if the data suggests that there is more than one direction of fibre populations in the voxel, which is the advantage of this model compared to DTI.

Parameter estimation Parametric models such as the DTI and ball and stick model can be fitted using different approaches. In the case of the ball and stick model, it is not easy to analytically solve the relevant equations. Therefore, a Bayesian probabilistic inference framework is used to estimate the model parameters. Such a framework will estimate both the average parameter values such as, e.g., fibre orientiations, but also their uncertainty. One example of a tool that estimates the parameters of the ball and stick model is FSL's BEDPOSTX – Bayesian Estimation of Diffusion Parameters Obtained using Sampling Techniques [26], [27]. It uses Markov chain Monte Carlo (MCMC) sampling to find the combination of values of the model parameters that would give predictions for the resulting signal, such that it is close to the actual measurements. The downside of the method is that it is computationally expensive.

NODDI Neurite orientation dispersion and density imaging (NODDI) [28] is a model that tries to provide a quantitative description of neurite (i.e. dendrites and axons) features. Two parameters of this model are the intra axonal volume fraction (i.e., considered a proxy for axonal density) and orientation dispersion of the neurites. The model assumes three different water compartments: the intra-cellular one (inside the neurites), the extracellular (space around the neurites), and one describing the space occupied by free water (CSF). From those compartments, it is possible to estimate parameters describing the microstructure, such as intra-cellular volume fraction (ICVF) representing the neurite density, isotropic volume fraction (ISOVF) for extra-cellular free water diffusion and orientation dispersion (OD), which is related to the directional complexity of the fibre (e.g. fanning).

2.3.3 Tractography

The next stage of the analysis, after the estimation of fiber orientation distributions (FODs), is tractography. Tractography uses the output, from the previously described voxel-wise methods that estimate FODs, to estimate structural connections in the white matter.

Deterministic tractography Deterministic tractography reconstructs virtual streamlines by seeding at specific brain location and following the most probable orientation every time it steps in a new voxel. It can only provide a deterministic binary answer (i.e., connected or not connected) and does not provide a measure of 'connectivity weight'.

Probabilistic tractography Probabilistic tractography uses not only the fiber orientation but also its uncertainty estimates to build a spatial distribution of probable paths from any given point. The idea of running such a model is to pick a location, which will be a tractography seed, from which a number of streamlines will be propagated. In every step of propagation the algorithm randomly picks one orientation from the underlying distribution and propagates the streamline along that direction until it hits the voxel border. The process is continued for next streamlines from the seed. As a result, the spatial distribution of the streamlines is built. Then, it is possible to define the path probability in each voxel by calculating a ratio between the number of streamlines passing through the voxel by the total number of samples (streamlines) that left the seed [26]. The result reflects a probability of a tract starting at that seed and going through that voxel. For the whole brain, the result is a path probability map. Its values are often referred to as a 'connectivity strength' but in fact they reflect rather a combination of anatomical connectivity and the robustness against noise.

Connectome The term connectome refers to the whole structural or functional profile of connectivity in the brain [29]. A connectome can be modelled as a graph, which is made up of a set of nodes and edges between them. In mathematical analysis this can be described using an adjacency (connectivity) matrix, where rows and columns represent nodes and entries are the weights of the connection between those nodes. When estimating an individual's connectome, the definition of its nodes is crucial, as it influences the results. In the case like the one presented in this thesis, the connectome consists of the cortico-cortical and cortico-thalamic connections in the adult human brain. Therefore, a node will be a spatial region of interest in gray matter – cortex or thalamus, defined according to some rules. This process is called parcellation and can be done in several different ways. It can be based on anatomical information or functional data patterns. For instance, resting state fMRI data can be used to define functionally related regions with correlated spontaneous activity. This can be done at a subject specific level, at the group level (using methods like dual regression) or by using a predefined functional atlas for a certain population.

2.3.4 White matter tracts

Tractography allows for the virtual dissection of the neuronal fibre bundles in white matter. These white matter tracts connect cortical and sub-cortical gray matter regions. Between the fibres that have both of their ends on the cortex we can distinguish three classes: association fibres, commisural fibres, projection fibres, and limbic fibres.

Association fibres connect cortical regions belonging to the same hemisphere of the brain and can vary in length. Association fibers include: superior longitudinal fasciculus (SLF) with arcuate fasciculus, inferior longitudinal fasciculus (ILF) and uncinate fasciculus (UNC). SLF connects frontal, parietal, occipital and temporal lobes and runs around the insula [30]. ILF consist of long fibres connecting visual areas to the amygdala and hippocampus, as well as short fibres connecting the occipital and temporal lobes [31]. UNC connects the frontal and temporal lobe of the cortex [30]. The inferior occipitofrontal fasciculus (IFO) connects the frontal and

occipital lobes [32]. In both UNC and IFO, three fragments can be distinguished: frontal, insular and parietal [30]. A slightly different example of an association fibre is the cingulum. It connects the cingulate gyrus, which is a part of the cortex in a very medial location, with the entorhinal cortex. The cingulum is part of the limbic system, which is related with behaviour, as well as memory and emotions. In this thesis, the cingulum has been split in two segments: cingulate gyrus and parahippocampal part of the cingulum.

Commisural fibres connect both hemispheres of the brain. The largest bundle is the corpus callosum. In the anterior part of corpus callosum lies the forceps minor (FMI) and in the posterior part there is the forceps major (FMA).

Projection fibres connect the subcortical structures (like thalamus, brainstem, striatum or spinal cord) with cortex. In this thesis, out of those, we will only analyse the thalamic radiations, i.e. tracts that connect the thalamus with cortical regions. The acoustic radiation (AR) starts in the medial geniculate nucleus part of the thalamus and ends in the primary auditory cortex. The anterior thalamic radiation (ATR) connects the dorsomedial nucleus of the thalamus to the prefrontal cortex. Its abnormal characteristics in the right hemisphere are linked with compulsive behaviour problems [33]. The superior thalamic radiation (STR) originates in the ventral nuclear group thalamic nuclei and leads to the postcentral gyrus [34]. The posterior thalamic radiation (PTR) includes part of the optic radiation, which connects the thalamus with the primary visual cortex.

2.4 Functional connectivity

Functional connectivity describes the relationship between the patterns of activity of different brain regions, by looking at the statistical dependencies between them [13]. It is derived from functional MRI data (fMRI). Functional MRI is an indirect measure of neuronal activity in the brain by measuring a blood-oxygen-level dependent signal (BOLD). The idea behind the measurement is that when a certain neuronal population becomes more active, it requires more oxygen. This causes an increase in the amount of oxygenated blood delivered to the active brain region, which can be

detected as a positive BOLD signal response. The BOLD signal can be modelled as a convolution of a hemodynamic response function with the neuronal activity, which means that it has some delay and a lower frequency than the electrical activity of the neurons. These signals are measured as a response to stimuli or when no task is performed by a participant. The latter case is called a resting state study.

In resting state fMRI (rs-fMRI) there are particular types of noise observed. The two main sources of noise are related to motion and scanner hardware [35]. Motion artefacts arise from the movement of the subject in the scanner but also from physiological processes such as breathing and blood vessel pulsation. Hardware noise can include distortions (warps) and drop out – loss of signal in certain regions due to inhomogeneities in the static magnetic field [35]. These problems are also present in diffusion MRI, as mentioned above. Another artifact is signal drift, i.e. a very low frequency trend in the BOLD signal.

Despite the presence of noise and artefacts in fMRI data, with current processing techniques, it is possible to greatly reduce its impact on the analysis. Distortions, which can change the shape of the brain in the image, are corrected using a fieldmap image obtained during data acquisition, which describes the magnetic field inhomogeneity in the scanner. Artifacts related to motion are corrected by registering each 3D volume (data at each timepoint) to the reference image (which could be for instance the middle timepoint volume). This can be followed by slice timing correction, if the volume slices are not acquired exactly in the same time. Finally, data can be filtered. This includes spatial smoothing, which improves the signal-to-noise ratio by adjusting the value at each voxel based on information from neighbouring voxels. It is also possible to perform temporal filtering using a high-pass filter in order to remove the scanner drift artifact.

2.5 Multiple Sclerosis

Multiple Sclerosis is a chronic inflammatory demyelinating disease which affects the central nervous system. It is one of the most common neurological causes of progressive disability among young adults in the western world [36]. Its peak onset

occurs around 20–30 years old [36]. MS changes the structure of the brain, causing axonal losses and inflammation, as well as brain atrophy.

There are four distinct types of MS development: clinically isolated syndrome, relapsing remitting MS, secondary progressive and primary progressive MS [37]. The most common type is relapsing remitting MS, which is characterised by the appearance of relapses (attacks) of neurologic symptoms and remissions (recoveries). The diagnostic criteria for Multiple Sclerosis are based on clinical assessment with support of magnetic resonance imaging [38].

Axonal loss, which is considered to be a marker of disease progression, is partially correlated with the number of lesions observed on T2-weighted MRI [39]. These lesions, as well as cortical atrophy, are the main signs of MS on conventional MRI [40]. In Multiple Sclerosis the white matter lesions can be pathologically classified into different types [41]. Generally, an MS lesion is defined (according to the McDonald criteria [42], [38]) as a hyperintense area, of at least 3 mm of length, visible on a T2-weighted (or proton density weighted) MRI scan.

3

Measuring structural impact of WMHs on WM tracts

Contents

3.1 Introduction 19
3.2 Literature review 20
3.3 Data 22
3.4 Methods 25
3.4.1 Proposed method for quantifying the tract-specific WMH impact 26
3.5 Results 27
3.5.1 Whole brain measures 27
3.5.2 Tract-specific spatial distribution of WMHs 28
3.5.3 Method for quantifying tract-specific impact of WMHs . 29
3.6 Discussion 30
3.7 Summary 32

3.1 Introduction

Over the last few years White Matter Hyperintensities (WMHs) have been extensively investigated and linked with increased risk of stroke, dementia and cognitive decline [3]. Most of these reported studies were looking only at the total volume or count of WMHs in the brain as a global measure that might correlate with other clinically relevant features. The objective of this part of the work was to find out

whether it would be possible to break down those effects to specific parts of white matter. Therefore, the starting point of this work is to define the local measures of WMHs presence in the brain. We realised that specifying the regions of the brain solely based on its structure, would not be adequate for that purpose, as ultimately the interest focuses on the impact on the function of the brain. Therefore, we propose to using the white matter fibres architecture as a starting point of a more local-effect focused approach.

In this first, shorter research chapter we present the data used as well as the general approach to work with structural and diffusion MRI (dMRI) data, which will be used also in the following chapters. Then, two approaches that quantify the structural 'impact' of WMHs on white matter tracts are introduced and discussed– one that is seen often in the literature, and a novel approach that is proposed here. This chapter is very closely connected with the one that follows (4), where the focus is on investigating the local impact of WMHs on the functional connectivity of the brain. They are presented as two separate chapters for clarity, but their results are linked and will be interpreted together.

3.2 Literature review

Local approaches to study WMHs in brain, although frequent in pathology studies, are rarely used in studies in vivo. The majority of MRI studies look only at the total WMH volume [17].

Recently, some studies investigated relationships between the presence of WMHs and functional decline in a more localised manner. One of the studies used 14 predefined brain regions for parcellation [43]. The authors only acquired structural images (T1-, T2-weighted and FLAIR) and looked at functional assessments over the next seven years, as well as at clinical events (like stroke). Their segmentation into brain regions included: brainstem, cerebellum (both not included in this work), bilateral frontal, occipital, temporal, and parietal lobes; and bilateral anterior and posterior periventricular white matter. Out of all those regions they found that only the volume of periventricular white matter hyperintensities was particularly

associated with faster functional decline. Typically, this is the region with the highest prevalence of WMHs [14] [44]. The authors of the work [43] conclude that the volume of periventricular WMHs could be used to predict accelerated functional decline.

Another example of a study that has also taken the approach to look locally at the WMHs impact on the WM tracts was published by Langen et. al. [45]. In this study, the authors used the data of 1584 participants of the Rotterdam Study to investigate the tract-specific effects of WMHs on functional connectivity. They used the overlap of the WMH mask transformed to the diffusion space with the tract masks divided by the tract volume as the local WMH structural impact measure. Their results showed that the tract-specific WMH load varied greatly for different tracts and, to much smaller extent, between the hemispheres as well. Moreover, the relationship between the WMH load and the functional connectivity was found to be highly dependent on the tract and brain hemisphere. As this study has a very similar aim, although different methodology, especially in the last stages, we will discuss results from this and the next chapter in comparison with the ones presented in that publication.

Another study [44] also looked at the relationship between WMHs and cognition, investigating both the impact of total WMH volume in the brain and effects specific to the location of the hyperintensities. Their approach to incorporating the spatial information was based on creating WMH occurence maps for each of the cognitive factors considered. The results showed that the WMHs in frontal white matter corresponded to a decrease in executive function, WMHs in the parieto-temporal area corresponded to negative memory function and WMHs in the upper deep white matter (which includes corticospinal tract) were related to reduced motor speed performance.

A study published in 2018 [46] focused on investigating microstructural parameters of white matter on the tracts as a function of distance from the WMHs using structural and diffusion scans. That study is limited to only the corticospinal tract, which we did not investigate in this thesis, and from other studies (like [45] described above) we know that there is high variability in the WMH impact between

the tracts, therefore the study might not be easily generalisable. For corticospinal tract they found that the tracts with WMHs have lower density (expressed as a ratio of number of fibres divided by number of voxels belonging to the tract) than the tracts with no WMHs. They also show that the diffusion parameters are altered not only in the WMHs are but also their proximity, and they relate it to the Wallerian type degeneration pattern.

Here, we propose the use of white matter tracts to define local white matter ROIs in which we will investigate the impact of WMHs. The next step is to define the best way to quantify the phenomena of interest. The simplest measure that can be used is volumetric overlap between the WMH mask and the tract mask. This measure is consistent with the usual definition of total WMH load in the brain and was used with regard to WM tracts in the [45] study. We were also interested in whether there could be another way to quantify that impact, in order to take into account also other information, such as WMH locations on the tract. We believe that there could be a difference in the consequences of WMHs depending on how much of the crossectional area through the tract is left intact. Work from 2013 addressed a similar problem in tractograms. The tool the authors proposed was called NeMo [47], which stands for Network Modification tool workflow. It requires providing a mask of where there are pathological changes in WM and then the standard set of tractograms is used as a reference to find streamlines that would travel through those areas. Building on the assumption that with changes in white matter there will come the alteration in the related gray matter regions they use the map of those changes to predict changes in functional connectivity graph.

3.3 Data

UK Biobank dataset This chapter, as well as chapters 4 and 5, use data from the UK Biobank dataset [5]. Out of the subjects with complete sets of structural, resting state functional and diffusion data, a subset of 5000 subjects was randomly selected. UK Biobank brain imaging data is also available in the form of partially

or fully postprocessed images, with results of most common types of modelling provided [18]. For the majority of the work in this thesis the preprocessing of the data is done as in that pipeline, unless otherwise stated.

Acquisition parameters of UK Biobank data used in the thesis All the data were collected with the same scanning protocol, at three sites on identical 3T Siemens scanners [18]. T1-weighted structural images (one volume per subject) were acquired with 1mm isotropic resolution and using 3D MPRAGE. T2-weighted FLAIR images (one volume per subject) were collected with a 3D SPACE acquisition that used fat saturation. Voxel size for the T2-weighted FLAIR scans was 1.05 mm x 1mm x 1mm. Diffusion-weighted images were acquired using two shells: with $b = 1000s/mm^2$ and with $b = 2000s/mm^2$. There were 50 diffusion directions acquired for each shell, selected in the way that neither of those combined 100 directions were the same. The phase-encoding direction for the diffusion-weighted scans was anterior-posterior. The acquisition also included images with $b = 0$: 5 volumes for the anterior-posterior phase decoding direction and 3 volumes for the posterior-anterior direction. Scans with a posterior-anterior phase-encoding direction were collected to allow fieldmaps for distortion correction to be computed. The resolution of the diffusion MRI scans was 2mm x 2mm x 2mm, which resulted in a 104 x 104 x 72 voxel image size. Resting state functional scans were acquired with a resolution of 2.4 mm x 2.4 mm x 2.4 mm, with TE/TR = 39/735 ms, and a multiband factor of 8. There were 490 timepoints collected for each subject.

Selected aspects of the UK Biobank data preprocessing pipeline UK Biobank data was extensively preprocessed as a part of the preparation of data for sharing with researchers. The details can be found in the publication that describes the data processing as well as the quality control of the data [18]. The data used in this thesis benefited from that processing before further analysis was done.

Generally, the steps applied to the images started by converting from DICOM to NIFTI format, performing gradient distortions corrections, then cutting down the field of view. Then, the linear and non-linear transformations to the standard atlas

space were calculated. Subsequently, brain extraction, defacing, and segmentation of brain structures were performed.

For T1 images, which are used as the reference for registrations, linear and non-linear registrations to the MNI152 space were performed. The exact process was relatively complex (due to the defacing and very bright carotid arteries) and the details can be found in the main pipeline publication [18]. T1-weighted images were also used for tissue-type segmentation and subcortical structure segmentation. The T1-weighted image was also used to estimate the bias field.

The T2 FLAIR image is (after gradient distortion correction) linearly transformed (with six degrees of freedom) to the T1-weighted image space and all the further processing is done there. Therefore, in the further processing steps described in this thesis, one can assume that the T2 FLAIR image is in the same space as the corresponding T1-weighted image. Therefore, for instance, the MNI152 version of the T2 FLAIR image also uses the registration warp calculated between the T1-weighted image and MNI152 space. The bias field correction for the T2-weighted image was done based on the field estimate from the T1-weighted image as well.

The fieldmaps were generated from the $b = 0$ dMRI images for geometric distortion correction of the dMRI and fMRI data. Diffusion data is also corrected for other distortions including those induced by eddy currents and head motion. Resting state fMRI data is also appropriately corrected. In addition, any structured artefacts were removed from the fMRI data using tools based on independent component analysis.

White matter tracts Analysis presented in this thesis focuses on 22 white matter tracts. These are automatically generated for each subject using the AutoPtx tool [48]. Out of those, we discarded the tracts that went through the regions, where our semi-automated WMH detection algorithm, BIANCA [49], is not trained to detect hyperintensities. We excluded also the corticospinal tract, middle cerebellar peduncle, and medial lemniscus as they go through the brainstem

or the cerebellum – we kept only the tracts that either connect cortical areas on both ends or connect thalamus with cortex.

Tracts were analysed in each hemisphere separately, there were also two callosal tracts that connect both hemispheres. The tracts that were used included (for both hemispheres): association fibres: superior longitudinal fasciculus (slf), inferior longitudinal fasciculus (ilf), inferior fronto-occipital fasciculus (ifo), uncinate fasciculus (unc); thalamic projection fibres: acoustic radiation (ar), anterior thalamic radiation (atr), posterior thalamic radiation (ptr), superior thalamic radiation (str); limbic system fibres divided into cingulate gyrus part of cingulum (cgc) and parahippocampal part of cingulum (cgh) separately; as well as forceps major (fma) and forceps minor (fmi) from the callosal fibres.

3.4 Methods

Whole brain measures To characterise the subset of 5000 UK Biobank subjects, the data about their age as well as the total WMH volume was extracted. The WMH volume was assessed as in the main UK Biobank pipeline [18] using the BIANCA algorithm [49] from the FSL package. The result from BIANCA is a probability map of WMHs in the brain, which was thresholded at 0.8 and binarised.

The distribution of age and total WMH load was plotted against each other to give a qualitative overview of the relationship between both, as well as ensure that sample used is representative of the UK Biobank.

Tract-specific WMH load As the focus of this work is on investigating the impact of WMHs with respect to the white matter tracts they are on, the next step was to visualise the distribution of WMHs on the individual tracts.

For each voxel on each of the tracts we calculated how many subjects would have this voxel classified as WMH. The distribution of that count was plotted using the 'hot' scale on top of the blue outline of the average tract shape for each of the analysed tracts. The raw counts of the number of subjects for whom a given voxel

was classified as WMH are given, in order to ensure that the variability between maximum counts of WMHs per voxels for tracts is presented.

3.4.1 Proposed method for quantifying the tract-specific WMH impact

Instead of volumetric overlap, as a way of quantification of WMHs on a tract, an alternative measures, based on the tractography streamlines, is proposed here. This could add to the characterisation of the WMHs impact as it better reflects how much of the tract was left intact. It also allows us to investigate local changes (both within and outside the WMHs) on the sub-part of each tract that goes through one (or more) WMHs. The idea was that the number of streamlines that belong to the tract (i.e. reach the target) and also, at the same time, go through the area where there are lesions, might represent the degree to which the tract is affected by the lesions.

The calculation of the proposed measure is performed by running tractography twice and summarising the results. Once, the tractography is run according to the UK Biobank pipeline [18]: using ProbtrackX2-GPU [50], [26] with the set of masks from AutoPtx [48]. The only change here was that the random seed was set to a constant to ensure consistency between both runs. The second tractography was performed by adding the WMHs as one waypoint mask. The output of this second tractography run consists only of the tract-specific streamlines that went through at least one hyperintensity region (therefore might be directly affected by the presence of WMHs). The result is the ratio of this output (streamlines that went through at least one hyperintensity) divided by the total number of streamlines from the first tractography run for that subject.

Comparison with the overlap measure We plotted the scatter plot of the 'pure volumetric' overlap measure on the x axis and the one using tractography information, based on the ratio of the streamlines, on the y axis. We want to investigate here is only the variability introduced by using different methods. Therefore, it is important to reduce the intersubject variability due to other confounds, like head size. For that reason, for this comparison the results of

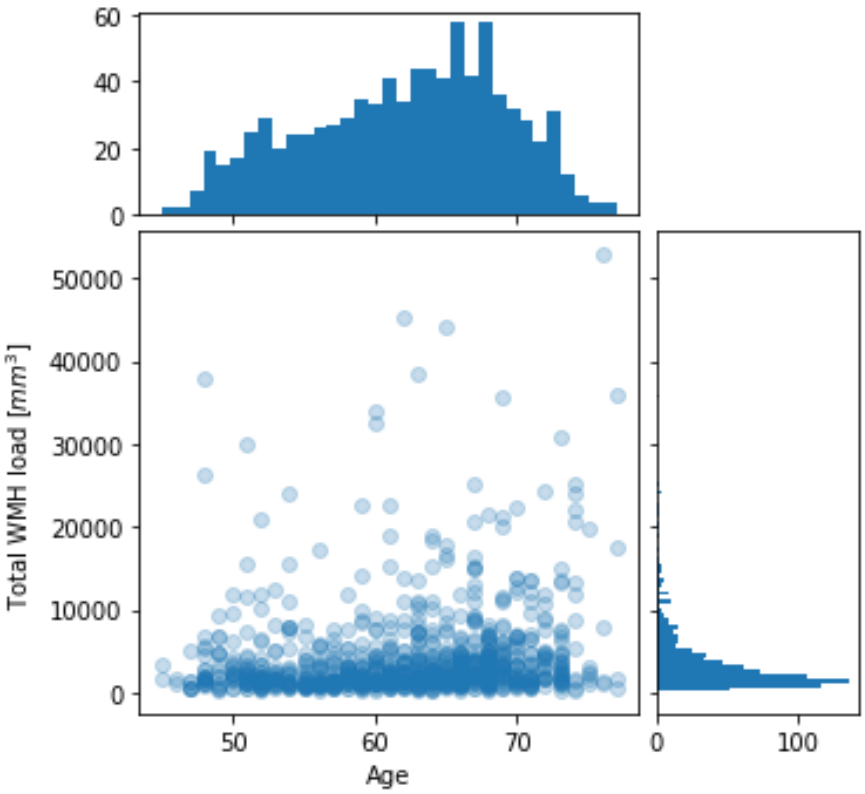

Figure 3.1: Figure presents the distribution of the total WMH load for the whole brain in relation to the subject's age in the subset of 5000 UK Biobank subjects.

the overlap measure were also scaled – divided by the number of voxels belonging to this particular tract for the given subject. That was calculated using the *fslstats* command from the FSL package [51].

3.5 Results

3.5.1 Whole brain measures

Figure 3.1 presents the distributions of age and WMHs for subset of UK Biobank data. The distribution of age is slightly skewed towards older participants but generally seems to cover the whole range of the older population. The distribution of total WMH load is heavily skewed towards smaller numbers, although with non-zero median. This could be expected as it is assumed that UK Biobank participants are healthy older individuals.

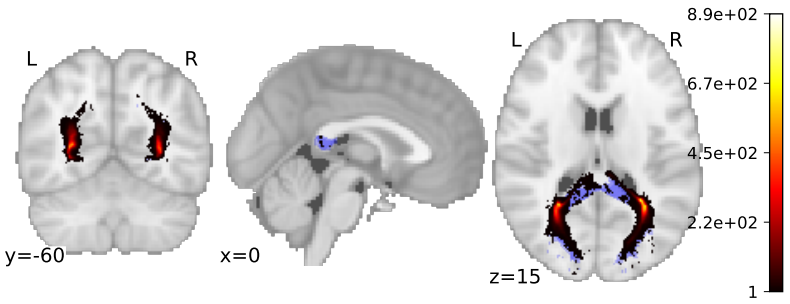

Figure 3.2: The spatial distribution of WMHs (in black–red colour map) visualised on the average FMA tract mask (in blue). The colour from black through red to white reflects the number of subjects for whom a given voxel was counted as a part of a WMH.

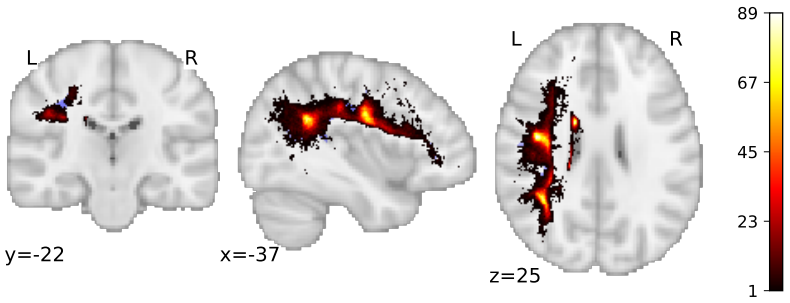

Figure 3.3: The spatial distribution of WMHs (in black–red colour map) visualised on the average SLF left hemisphere tract mask (in blue).

3.5.2 Tract-specific spatial distribution of WMHs

We plotted how many times a given voxel in the tract was classified as part of a WMH in the analysed subset of 5000 subjects. The heatmaps for each tract can be found in appendix A. Here, example heatmaps are presented for the FMA (figure 3.2) and SLF in the left (figure 3.3) hemisphere. By looking at the colourscales of those maps it can be observed that the maximal counts of WMHs at any given voxel over all the subjects varies between the tracts, with tracts that pass close to the ventricles having higher counts of WMHs. Interestingly, if we sorted the tracts according to those maxima it would not necessarily reflect the number of subjects with WMHs on given tracts (this is presented in more detail in chapter 5, in particular see table 5.1). The patterns of WMH distributions were varied between the tracts. In general, it can be said that for the majority of the tracts the WMHs would be mainly detected in certain regions of the tracts rather than spread uniformly over the whole volume of the tract.

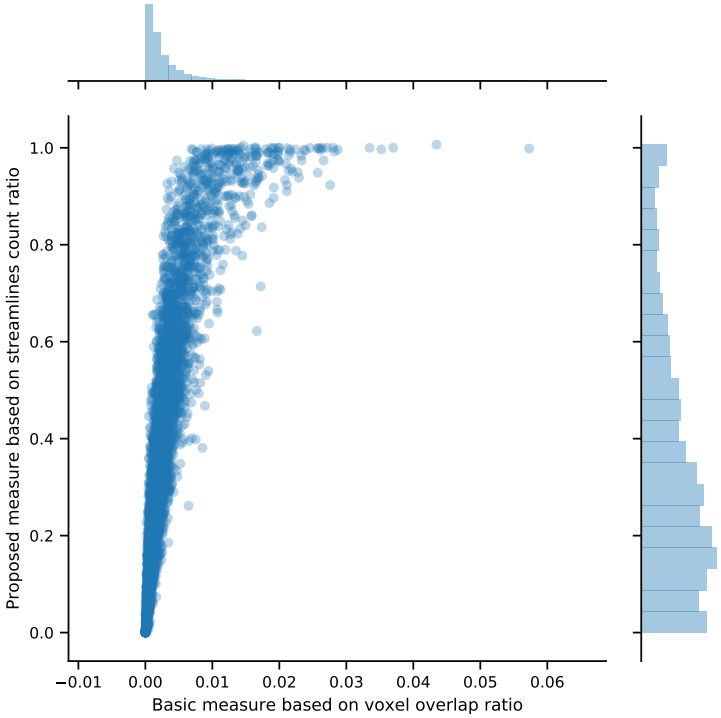

Figure 3.4: Comparison between results obtained with both structural measures for the FMA tract.

3.5.3 Method for quantifying tract-specific impact of WMHs

Finally, we present results of quantifying the WMHs on the tracts. The scatterplots with results for all the datapoints (5000 subjects) for each tract are presented in appendix B. An example plot for the FMA tract is presented below (figure 3.4) showing the joint distributions of two measures, where each point represents one subject.

The x axis shows the normalised total volumetric overlap of the WMH mask with the subject specific tract mask and on the y axis – the proposed measure of ratio of tract streamlines that pass through at least one WMH mask. Both measures are ratios, so effectively the values that they can take are between 0 and 1.

The joint distribution of the two measures for FMA (figure 3.4) shows that for this tract the streamline-based measure returns values over the whole 0–1 range, and only after it saturates does the overlap measure start to take higher values, although still under 0.06 for all the 5000 subjects analysed. Patterns for the other tracts are described in appendix B.

3.6 Discussion

This chapter looked at the characteristics of the structural data used in this thesis. The spatial distribution of the WMHs on the white matter tracts among the subset of 5000 subjects from UK Biobank were presented. Finally, a new way to quantify the WMH load on the tracts was proposed and compared with the local measure seen previously in the literature.

The majority of analysed subjects have non-zero total WMH load but under $10.000mm^3$. The small WMH load is expected, as UK Biobank is a dataset of largely healthy older participants. The fact that the load is rarely zero might come from the fact that a small number of WMHs are often detected in the healthy population as well, but it is also important to take into account that the semi-automatic method for WMH detection that was used might not be perfect and it might result in some false positives. Since BIANCA was proposed [49] and used as a standard in UK Biobank pipeline, there was new work published [52], that acknowledges the limitation of that method and proposes a better way of thresholding the WMH probability map for more accurate segmentation. It might be useful in the future to update this analysis with segmentations from that updated version of the algorithm.

The tract-specific WMH load varies between the tracts. That can be observed both in terms of the frequency of how many times a given tract was affected as well as in the width of the spatial distribution of WMHs within the tract mask. Both of these observations are not surprising as we know from the literature that there are certain locations in the brain that have higher prevalence of WMHs than others [53]. That was also shown in the literature for tracts specifically [54]. With regards to the spatial distribution within the tract mask, the WMHs are relatively concentrated for most of the tracts. That suggests that within a tract the locations in which WMHs are detected are quite similar between subjects. They are also highly consistent between hemispheres, showing symmetrical patterns for all the tracts.

The last part of this chapter compared the proposed method of quantifying the WMHs on the tract using two measures: the ratio of tractography streamlines that go through the WMHs, with the simpler measure based on the volumetric overlap

of WMH mask with the tract mask. Both of those numbers were scaled – divided by the total number of streamlines on the tract and by the total tract volume, respectively. This was done in order to allow comparison between the subjects (and account for intersubject variability like head size) but also between the methods. That was necessary but it could have affected the distributions.

The distributions of results obtained with the two measures vary, despite the fact that they were calculated for the same set of subjects. The streamline-based method generally has a wider distribution than the volumetric overlap one. A wider distribution means that the measure takes more values, therefore it might be more useful in describing the data. Of course, the data can be transformed (by applying a mathematical function e.g. log) so it is not possible to directly conclude that the wider distribution will translate to a more useful measure. However, the example of the FMA tract (figure 3.4) suggests that if we tried to apply the method to analyse more severe types of lesions than WMHs, it might not be that useful – as in the case of more affected tracts it saturates at a value of one and does not allow for analysing the further differences between them.

The two measures discussed in this chapter focus on quantifying two different aspects of how WMHs can affect the structure of WM tracts. They are designed to be complementary: one focuses on the total volume of changes, the other accounts for the maximum cross-sectional area of the tract being affected. The volume of WMHs is likely to be strongly correlated with other measures, such as the number of WMHs that overlap with a tract, or the average count of the number of WMH voxels traversed for each streamline. In contrast, the streamline-based measure used here should be able to represent the maximal extent of disruption to the total tract signal, related to the amount of cross-sectional area being affected, independently of any other WMHs that might be present on the tract with a smaller cross-sectional overlap. It is this independence that we valued as well as the potential interpretation based on how many streamlines might be compromised in terms of signal transmission. It still might be useful, however, to combine the results from both of these measures or to include other measures. This can be

done by some operation combining different values (e.g. multiplication) or by the addition of a new method for quantifying the impact of WMHs on WM tracts. An example of such a measure could be calculating how many voxels of the WMHs were traversed by each streamline or how many isolated WMHs appear on streamlines belonging to the tract. It is not entirely straightforward to interpret most of these measures, especially when combined. For example, a combined measure would be likely to struggle to resolve the case where multiple smaller WMHs affect the same number of streamlines as one large hyperintensity of the same volume. One of the aims of this chapter was to propose a second measure that would add information – in isolation or in combination with – the measure based on the total WMH volume overlapping the tract. The results of this chapter show that the streamline-based measure is often not strongly correlated with the volume-based measure. That suggests that it can be a good candidate to be used either instead of the volumetric measure or in combination with it, depending on a particular study.

The presented results were calculated for the binarised version of the BIANCA-derived WMH probability map with a set threshold. However, it would be good to use the unthresholded probabilities and let them inform the measures. It is not possible to feed a non-binary mask into the tractography algorithm used here (ProbtrackX2) but it is possible to threshold the WMH probability map on different levels and run the tractography algorithm multiple times to construct a more advanced measure combining values obtained at different probability levels.

3.7 Summary

This short chapter introduced the structural data and measures that the further chapters will build on. The characteristics of the data were presented as well as a new method to quantify the structural impact of the WMHs on white matter tracts was presented. The majority of the subjects have a small but non-zero total WMH load. Its spatial distribution varies between the tracts but not that much between subjects. For quantifying the WMH load on the tracts, the method proposed here, based on the streamlines ratio, seems to return a wider distribution

of the results for most of the tracts than using the volumetric overlap between the WMH mask and a tract. The next chapter will use the metrics derived here to look at the relationship between structural and functional impact of WMHs on the tracts. It will also add to the evaluation of those two metrics by investigating their relevance to intersubject variability in functional data.

4

Measuring WMHs impact on functional connectivity

Contents

4.1 Introduction 35
4.2 Literature background 36
4.2.1 Data 37
4.2.2 Timeseries extraction 38
4.2.3 Functional connectivity definition 45
4.2.4 Analysis 50
4.3 Results 51
4.3.1 Parcellations 51
4.3.2 Functional connectivity 54
4.3.3 Relationships between the structural and functional measures 57
4.3.4 Summary of the results across methods and tracts . . . 58
4.3.5 Accounting for confounds in the regression 62
4.4 Discussion 62
4.5 Summary 71

4.1 Introduction

The previous chapter presented the approaches to quantifying how the white matter tracts can be affected by the WMHs from the structural perspective. This chapter explores possible methods to measure also their 'functional impact' with respect

to the structural one. Part of that work is proposing an appropriate definition of the measure of functional connectivity between the ends of the tracts. That can be done in multiple different ways. This chapter introduces and compares various approaches to calculating functional connectivity for tract-specific analysis and indicates the effect of those decisions on the results. Eventually, the functional measures of the WMHs impact on the tracts are related to the structural measures, discussed in the previous chapter.

4.2 Literature background

The presence of the WMHs in elderly subjects - both in the whole brain and in particular brain locations - has previously been linked to the functional changes in the brain. Medical studies focused on the behavioural observations, for example, the publication by Murray et al. [55], which highlights executive function as the main cognitive measure that is affected by the WMHs, especially those in the parietal lobe. Another publication [56] used Rotterdam study data to explore the relationships between the WMH-related changes in connectivity and cognitive measures. The latter was represented by the composite cognitive score based on the results from 5 cognitive tests. They defined 'disconnectome' and analysed disconnectivity due to the WMHs (accounting for the WMH load on a global and local level). Their findings suggest that there can be a relationship between the executive function score and appearance of the WMHs in all the connections between the brain lobes.

However, as mentioned in chapter 3, there are also examples of the studies that relate the WMHs to the measures derived from functional connectivity. We mentioned there a study [45] that showed that the correlation between the WMH load (measured by volumetric overlap) on a tract and functional connectivity between the ends of that tract varies between the tracts. They found the relationship between the WMH load on the tracts and the functional connectivity to be different between the tracts and also not necessarily consistent between brain hemispheres [45].

Another relevant study was done by Taylor et al. [57], where they did a similar analysis, focused on the Default Mode Network (DMN). Using data from 78 subjects

with Alzheimer's Disease at different stages they investigated the relationship between the volume of overlap of the WMHs on the tracts and functional connectivity between the ends of the tracts that belonged to the DMN. They extracted the DMN using ICA and used that for the parcellation. Using that definition did not allow them to analyse the FMA and FMI tracts. From the tracts linking the DMN areas that were analysed in that work, they found a significant negative correlation between the WMHs measure and functional connectivity for the IFO tract. As they combined the MRI data with PET scans in this study, they came to the conclusion that the WMH load causes an additional effect to the increased amyloid levels in reducing the functional connectivity. Additionally, in this work the authors analysed the distribution of the WMHs on the tracts, showing that among the tracts belonging to the DMN they analysed the highest WMHs load was on the IFO and the SLF, as the WMHs mostly appear in posterior and anterior periventricular areas [57].

In late life depression patients, where the WMHs also appear due to the vascular changes, Wu and colleagues [58] have found significant negative correlation between the WMH load (log-transformed, normalised) and measure of the DMN connectivity (particularly in the medial frontal region). Similarly, work [59] has described a significant negative correlation between the WMH load and resting state connectivity measures in the default mode network in subjects with mild cognitive impairment. It is important, however, to remember that the presence of the WMHs often coincidence with other changes, like atrophy, degeneration or appearance of the amyloid deposition [59] and that might cause ambiguity in the interpretation of the results.

4.2.1 Data

Data used in this chapter is the same subset of the 5000 UK Biobank subjects as in the previous chapter. Here, apart from the structural and diffusion data, also resting state functional MRI (rsfMRI) data was used. Six subjects were excluded from this analysis due to the problems with their data (either diffusion or functional scans), therefore, in this chapter, the results are presented for 4994 subjects.

The rsfMRI data consists of 490 timepoints with $TR = 0.735s$ [5]. The spatial resolution is $2.4mm$ [5]. The preprocessing and cleaning of the rsfMRI data were done in the UK Biobank pipeline [18]. To avoid resampling of the functional data, both structural and diffusion data were registered to the functional space at the beginning of this analysis, where needed.

4.2.2 Timeseries extraction

ROI definition To measure the functional connectivity between the gray matter regions linked by the tract of interest, it is crucial to define the spatial extent of those regions. They will constitute the nodes of the investigated connections, therefore their definition can largely affect the results of the analysis and their interpretation.

In this work, we consider the 22 white matter tracts (see 3.3) out of which some connect cortical regions, while others run from the thalamus to cortex. For each of those tracts calculating correlations requires a correct definition of the cortical region that will be regarded as the tract ending.

There are multiple approaches available to perform the cortex parcellation. Two most popular methods include using an atlas-based parcellation and a data-driven node definition. Here, we only explore the use of the former. That is because the interpretation and application of the atlas-based solutions to new datasets would be more straightforward, than the data-driven parcellations.

There are two different atlas-based approaches that we explored: using the Harvard-Oxford (H-O) structural atlas [60] and the Yeo functional atlas [61]. First, the Harvard-Oxford atlas needed to be slightly adapted to allow for differentiation of the corresponding regions into two separate hemispheres. For each tract ending, we manually selected the H-O regions that tract endings were reaching and classified them as biologically plausible or ones that are probably overlapping only with some spurious connections.

The second solution we propose is based on using the Yeo atlas [61], which is a functional atlas. We decided to use the 17 parcel version of the atlas. That was to ensure that in case of partial correlations there are some regions left to regress



Figure 4.1: Visualisation of the Yeo atlas used for parcellation: 17 cortical parcels from the original Yeo atlas, with added thalamus mask. That atlas was later masked by a subject-specific gray matter mask. Each voxel belongs to only one parcel. Parcels are non-contiguous, which means that two or more spatially separated regions may be marked with the same colour (as they constitute the same parcel).

out after eliminating those that could touch the tract ending. We added the binary thalamus mask (containing both hemispheres of the thalamus) as the 18th parcel.

The atlas that was eventually used is shown in figure 4.1. The thalamus mask, which is added to the original cortical parcellation, might seem large, but it will be reduced by masking with the subject-specific thalamus segmentation when extracting the timeseries. Similarly, the regions are big but they will be masked by subject-specific gray matter segmentations extracted from the T1-weighted image and registered to the functional space.

In the case of the Harvard-Oxford atlas, after careful consideration of the images and literature, we made a list of regions for each tract ending that can plausibly, from the biological perspective, constitute an ROI for timeseries extraction (i.e. they do not contain spurious connections). This list of regions was then provided to the timeseries extraction procedure and the associated binary masks were used to extract the average timeseries from the four-dimensional image (i.e. timeseries of 3D images).

In the case of the Yeo atlas, the situation was slightly more complicated because it is a functional atlas. Since its parcels are derived from resting-state networks they are non-contiguous. A parcel being contiguous means that it is a single 'blob' of voxels that are spatially adjacent to one another. A non-contiguous parcel means that it contains multiple 'blobs' that are not spatially connected to one another.

In this project we work with white matter tracts and are interested in functional connectivity between the regions at the two endings of a given tract. It is highly probable that two such tract endings might connect regions belonging to the same resting-state network. In this situation the two endings of the same tract would overlap with regions having the same label. Therefore, in this case, if we simply extracted the timeseries for each label from the Yeo atlas by combining it with the tract image, we would end up with two identical timeseries (as the timeseries for each end would be extracted using voxels sharing the same label from the Yeo atlas - that is, disconnected regions but all part of the same 'parcel'). In order to allow for the automated timeseries extraction for each separate tract ending in this situation, additional processing was required.

The first step of that processing included slight adaptation of the Yeo atlas (presented in figure 4.1) based on the Harvard-Oxford atlas, in such way that the Yeo atlas defines the spatial extent of the ROIs (to ensure the parcellation is being driven by the functional atlas) but the labels also include coding information from the H-O atlas. As the H-O atlas is split into two hemispheres, and also thanks to the fact that it has contiguous parcels, it provides the necessary information for automatic distinguishing one end of each tract from all the others, while also taking into account biological plausibility of the tract streamlines, since these had been verified manually. Therefore, the final ROIs for the functional (Yeo) parcellation were defined for each tract in such a way that only the voxels delineated by both atlases were included.

An example of how such an ROI looks is presented in figure 4.2. It depicts the regions corresponding to two endings of the SLF tract in the left hemisphere in two distinct colours. The regions marked with a partially opaque colour represent the voxels that were not in the final version of the atlas, and hence did not contribute to the signals associated with the tract endings or any of the signals used for regression in the partial correlations. Those voxels belonged to the ROIs in the Harvard-Oxford atlas but were not present in the Yeo atlas, and it is the latter that drives the segmentation in the second (functional) approach to ROI definition.

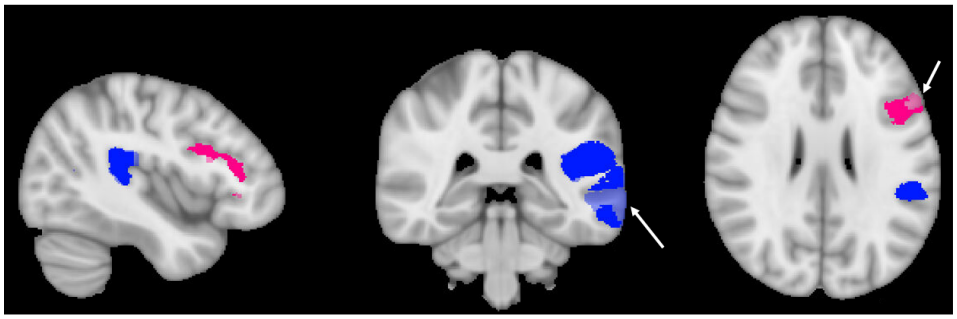

Figure 4.2: This example image presents regions from two endings of the SLF tract in the left hemisphere plotted on top of the standard brain. Pink represents voxels at one end of the tract, blue represents voxels at the other end. Arrows highlight the places with lighter colouring, which correspond to voxels that belong to the parcel according to the H-O atlas but according to the Yeo atlas they are not included in the ROIs, and hence they are not included in any of the timeseries calculations that we make when using the functional (Yeo) atlas approach.

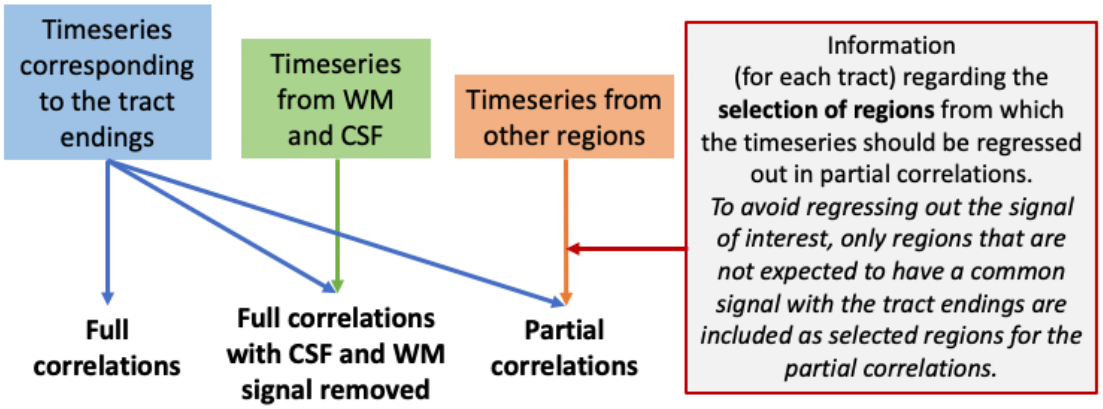

Figure 4.3: Overview of timeseries types needed for functional connectivity correlations.

Timeseries extraction For this work we extract the timeseries in three separate processes. This is because different types of timeseries are required for different parts of the analysis. Figure 4.3 presents this in a simple overview.

Extraction of 'timeseries from other regions' (the orange box in figure 4.3) is the most straightforward. To extract those timeseries, the atlas was masked by the subject-specific gray matter mask, both registered to the functional space. It resulted in 18 average timeseries – one per atlas label. Each of them was a simple mean of the timeseries from each voxel in that region. These timeseries are only used in the partial correlations as regressors (described later in more detail).

'Timeseries corresponding to the tract endings', presented in figure 4.3 in the

blue box, are the main signals of interest. Their extraction was performed in a weighted manner. The weights were proportional to the tractography results, so that timeseries from voxels with a higher probability in the tractography outputs for the tract of interest had higher weights. The process overview is presented in figure 4.4. The left hand side presents the processing related to the ROI definition, while the right hand side presents the algorithm responsible for the voxel weighting. The latter part starts from the image of the WM tractography probabilities, registered to the fMRI space and thresholded at a low threshold. Liberal thresholding allows for more voxels to contribute to the timeseries average, which can help with improving the signal to noise ratio. For the same reason, a one voxel dilation was performed as the next step. Because the definition of the parcel happens independently (in the pipeline on the left hand side), the dilation of the tract did not create any risk of including voxels from outside of the atlas parcel of interest or from outside the gray matter mask. The image of the WM tract obtained in this way was used for weighting the fMRI data, from which the timeseries are extracted. Timeseries are extracted, for each region, using the atlas defined as it was described above, masked by the GM and thalamus masks (as indicated in the left hand side of figure 4.4) and using the weighted fMRI data (as indicated in the right hand side of figure 4.4).

Figure 4.5 presents the process of extracting the timeseries used for regressing the WM and CSF signals (shown in the green box in figure 4.3). The subject-specific WM and CSF masks are registered to the fMRI space and processed (as described in figure 4.5) before being used to extract the average timeseries: one for the WM area and one for the CSF area.

As will be explained in subsection 4.2.3 in more detail, we consider three types of correlations to describe the functional connectivity in this thesis. Those include: partial correlations, full correlations, and full correlations with the removal of the CSF and WM signals as potential contamination. Each of those correlations is calculated using a slightly different set of functional timeseries. Figure 4.3 presents which type of extracted timeseries is used in which correlation. The timeseries marked by the blue box will be required in each type of correlation. This is because

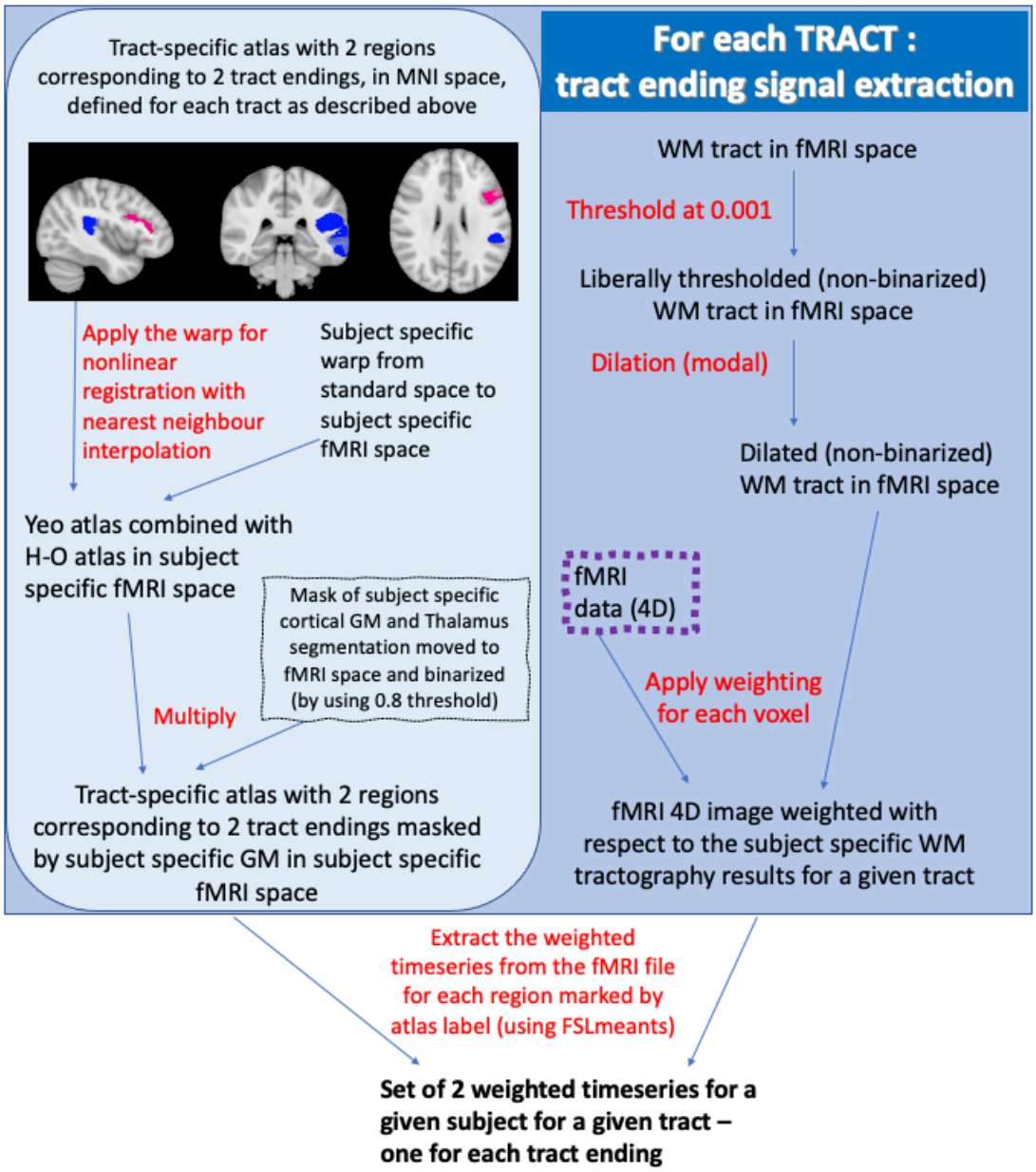

Figure 4.4: The illustration above presents the steps involved in extracting timeseries for each tract ending (in a weighted manner) for each subject. On the left side, a lighter coloured box contains the definition of the ROIs based on an atlas described in the previous subsection. On the right side, the preparation of the fMRI data with weights for a given tract is explained. Weighting of the fMRI data was performed by using the thresholded and dilated *tractNorm* image in subject specific fMRI space.

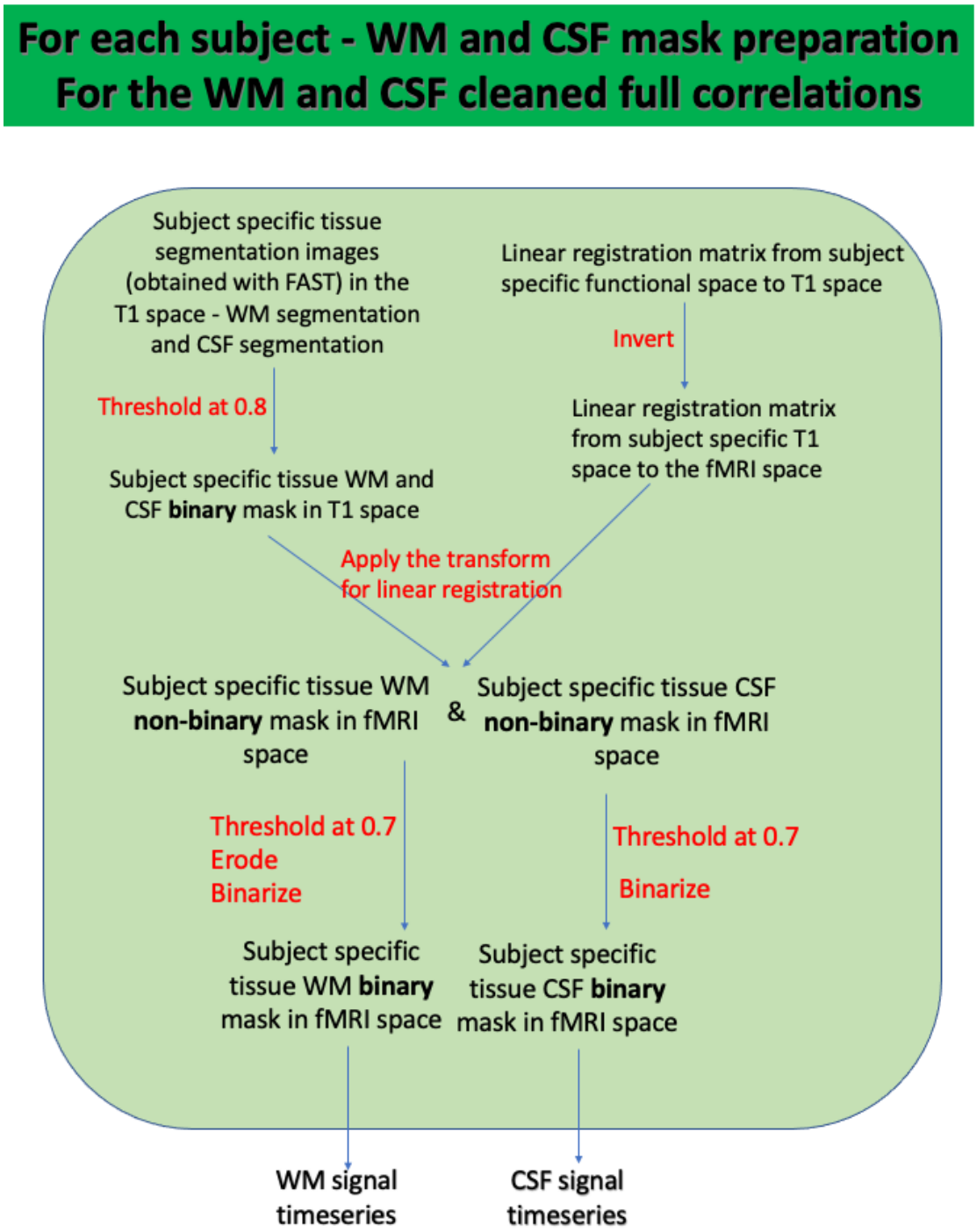

Figure 4.5: This figure presents the steps leading to the extraction of the timeseries from CSF and WM regions. The WM mask was additionally eroded by one voxel in fMRI space to additionally ensure no overlap with any GM.

these are the signals from the tract endings. Therefore, these two timeseries are the ones that drive the correlation of interest. Since we will also calculate a correlation with the WM and CSF signals removed, we also need WM and CSF timeseries (green box in figure 4.5). Partial correlations require the information that was needed for the previous corrrelations as well as timeseries from other regions in the gray matter (orange box) which will be regressed out (process described in more detail later, in subsection 4.2.3). As these regions are, by definition, not overlapping with the white matter tract that is currently being analysed, the 18 timeseries (represented by the orange box) are not weighted. The use of these will allow us to regress out their potential infuence on correlations. However, we want to avoid losing the signal of interest. Therefore, in figure 4.3 we can also see the box with the red edge, which represents a set of additional information that is used when determining what signals are used in the partial correlations. It is a text file with a list of timeseries corresponding to the regions that do not belong to the same functional network as the endings of the tract, and therefore these can be safely regressed out in partial correlations for a given tract. The script then uses that list to inform the FSLNets algorithm, for each tract, which timeseries to include in partial correlation calculations for each tract.

4.2.3 Functional connectivity definition

Functional connectivity can be defined in more than one way. The most popular functional connectivity measure is the correlation between the timeseries. It can be either full (Pearson) correlation or partial correlation, each expressing different aspects of connectivity.

Full correlations

Full correlation is the most straightforward way to estimate the edges in functional connectivity. It is based on calculating the Pearson correlation coefficient between the (average) timeseries from two regions of interest. In this work, those will be the two regions coming from the two tract endings, masked by a subject specific

gray matter mask. The timeseries will be averaged in a weighted manner, i.e. the timeseries from voxels that have higher probability of being connected to the WM tract will have higher weights.

In the case of full correlations it is important to take into consideration the global signal and its potential impact on the results. One option to address that problem could be performing global signal regression (removing the average timeseries calculated using all voxels in the brain or GM), however we decided against it. The reason for that was that it will contain, to some degree, the gray matter signals of interest and therefore could cause a change in the structure of the brain connectivity [35] or a shift in the correlation values (e.g. from positive to negative) making the interpretation of the results of this work highly problematic.

As an alternative to straightforward full correlation, we explored the effect of removing any potential contamination caused by the white matter and cerebrospinal fluid (CSF) and included this as a second option in the presented results. We believed it was essential to evaluate the importance of that option as after moving the analysis to the functional space, due to the lower spatial resolution of the images, the partial volume problem becomes more substantial. Any potential signal from non-GM regions should not be related to the neuronal activity and can add noise, possibly structured noise [35]. It is worth mentioning, however, that regressing out these components may not always be the best option because, on the other hand, WM signals coming from veins and venous pulsations might be correlated with the BOLD signal [35]. To regress the WM and CSF signal, for each subject, conservative masks of those regions were constructed from their T1-weighted structural images and registered to the functional space with relatively conservative thresholding before binarisation (at 0.7 as shown in figure 4.5). The WM mask was eroded by one voxel (in fMRI space) to additionally ensure no potential overlap with GM. The CSF mask was not eroded due to the relatively small amount of CSF. Therefore, there is a chance that there was a small amount of GM signal included in the CSF timeseries. If that was the case, regressing out the CSF timeseries could act to a small degree like a global signal regression (which might not be optimal, as discussed

earlier). The resulting WM mask contained only deep white matter and the CSF mask contained ventricles and several voxels within wider sulci in the cortical folds.

Correlations were calculated using the FSLNets implementation [62], which includes r to z transformation of the results. This operation, known also as a Fisher transformation, is commonly applied to the connectivity estimates in order to stabilise the variance of correlation values [63]. It is particularly useful when analysing correlations that fluctuate over time but also in other situations when an unbounded, more normal, distribution of the correlation values could be advantageous. The Fisher transformation takes the correlation coefficients r, which are between -1 and 1, and transforms them to z (with limits in $-\infty$ and ∞) using the formula 4.1:

$$z = \frac{1}{2} \ln \left(\frac{1+r}{1-r} \right) \tag{4.1}$$

Since this is commonly used notation, that transform is also known as an r to z transform, and it is also sometimes noted as $z = arctanh(r)$. The distribution of the values of z can be approximated by the Gaussian distribution [63]. All the functional connectivity values plotted in this chapter are these z-transformed values.

Partial correlations

An alternative to using full correlations is using partial correlations, which remove the indirect connectivity effects. The idea behind partial correlation is to add an additional step before calculating the correlation between two regions of interest: to regress out the signal (timeseries) from regions that are not in the pair of interest. Partial correlation measures the pairwise relationship between the variables (timeseries in this case) while removing the linear effect of other variables [64]. In this case, the other variables would be the timeseries from other regions of the brain. Partial correlation calculation can be performed slightly differently depending on the data and research question, and a choice of its parameters can influence the results.

We can describe that problem mathematically (in matrix form to account for multiple timeseries that are regressed at the same time) as:

$$y = X\beta + e \tag{4.2}$$

If we describe the number of timepoints as m and the number of regressors as n, then in equation 4.2: y is a vector of size (1 x m), X is a matrix of regressors, β is a vector of scaling parameters (of size (1 x n)), and e is a vector of size (1 x m) representing some noise.

Regressing out the all the other nodes' timecourses is equivalent to finding the inverse covariance matrix. It can be done through ordinary least squares (OLS):

$$\beta = (X^T X)^{-1} X^T y \tag{4.3}$$

The term $(X^T X)^{-1}$ in equation 4.3 is often poorly conditioned and does not allow for robust computation of the inverse. That is especially true if there is high multicollinearity (correlation between variables), as this causes variances to be so large that they are difficult to estimate and perform accurate calculations on. In such cases, it is possible to make it better conditioned by using regularisation. One of the methods used for regularisation is ridge regression. The idea is to add a small value to the diagonal elements of the correlation matrix. That increases the bias and reduces the variance, or instability of the inverse. The formula for ridge regression regularisation can be written as:

$$\beta = \left(X^T X + \rho I\right)^{-1} X^T y \tag{4.4}$$

In equation 4.4 I stands for an identity matrix, and ρ is a parameter, which controls how much the regularisation impacts the results. The method for deciding on the value of the ρ parameter will be described in the next subsection.

The solution can then be described as an optimisation problem of finding the β value that minimizes the right hand side of the equation:

$$\beta = argmin \left(\|X\beta - y\|^2 + \rho\|\beta\|^2\right) \tag{4.5}$$

To calculate partial correlations in this work we used the FSLNets toolbox[1].

[1] https://fsl.fmrib.ox.ac.uk/fsl/fslwiki/FSLNets

Finding the optimal ρ value To find the optimal ρ parameter for the ridge regularisation in our partial correlations, we performed some empirical quantitative optimisation. The optimisation was based on finding the ρ value that corresponds to the maximum correlation between the subject and the group-average network matrices (netmats) [65]. First, the group average netmat was calculated using partial correlation with $\rho = 0.01$. Second, for each subject there were subject-specific netmats calculated for each ρ, across a range from 0.001 to 0.7 (with irregular sampling, see figure 4.9). Then each of those was correlated with the group average netmat, to give one correlation value per subject per ρ. Finally, those values were averaged across subjects for each ρ value and plotted on a graph that on the x axes has ρ and on the y axis has z-transformed r (average correlation coefficient). Then the maximum value from that graph was identified and the corresponding ρ was used in the analysis. The results from this analysis, leading to the decision of using $\rho = 0.035$, are presented in 4.3.2. For reference, the ρ parameter used in L2 regularisation in the UK Biobank pipeline was much higher: 0.5 [18], however, the timeseries correlated there were derived from data-derived ICA components, not an atlas-based parcellation like here.

Quality assurance of the timeseries for non-tract endings In partial correlations, the main signals of interest are the signals from the two endings of the tract, as in full correlations, however we also use the signals from all the other parcels, not touched by the tract, and regress them out. To ensure the quality of those signals as well, we explore the timeseries obtained by visualising their spectra in the frequency domain. In the Results section 4.3.1 we will show the spectra. Since we observe there that the timeseries from one region of the Yeo atlas (the region labelled as 10) was particularly noisy (a tail of raised higher frequencies, with timeseries also missing for some subjects, which is not shown in the figure), this region was excluded and not used in the partial correlation analysis.

4.2.4 Analysis

In the analysis presented in this chapter, we want to explore the relationship between the structural and functional measures of WMH impact. For example, we present scatter plots of the structural measure on the x axis and the functional measure on the y axis. We consider here two structural measures, which were compared in chapter 3. The first one was the streamline based measure, expressed as the ratio between the number of streamlines going through at least one WMH mask to the total number of streamlines in the tract. The second one was the overlap measure (ratio of the number of voxels of tract overlapping with the WMH mask to the total number of voxels in the tract). In that latter case, due to values being very small, we used the log of that value on the x axis instead. Because that measure was often zero, its value was increased by the very small constant number before applying the log transformation, to avoid infinite values. As the dependent variable, we consider three different cases of the functional connectivity definition, as mentioned above. One of them is from partial correlation with regularisation, and the other two use full correlation. There is a difference between the two full correlation measures. In case of the first one, we use the signals simply as described before, assuming that the gray matter mask was correct. For the other one, we assume that there might be a problem with the partial voluming and we 'aggressively' regress out the white matter and CSF signals from the timeseries, before calculating the full correlation. In the Results section, we present 6 scatterplots, showing each combination of those measures, for two selected tracts. Then, we present results for each of the 22 tracts for one selected combination of those measures. Each scatterplot shows 4994 points, which are the measures for each analysed subject. For each possible scatterplot (from those combinations of 6 cases and 22 tracts, not all shown) we calculate the correlation between the two measures, using Spearman correlation. That returns a rank-order correlation coefficient (and p-value) without assuming a normal distribution of the data. All those correlation coefficients are then summarised in barplots 4.3.4.

Accounting for the confounds In any analysis like this one, it is important to take into account other factors that can influence the results [21]. As there were a lot of other options in the analysis, showing the influence of the confounds on each of them would be difficult to follow. Therefore, for one of the final versions of the methodology, we show the analysis done with the basic confounds normally accounted for in the studies. Here we fit the model when accounting for the age, sex and head size. We decided to take those factors in particular, so as to be able to compare our results to the ones from [45], where those confounds were included. The values of confounds for each subject were taken from the UK Biobank data. Age and headsize data was normalised (removed mean and standarised variance) before using it in the model.

4.3 Results

This section presents the exploration of possible approaches to investigating the functional impact of the WMHs on the tracts with regard to their structural effect. The previous chapter discussed the two possible approaches to quantifying the structural impact. This section of this chapter first shows some of the exploration done to decide how to quantify the functional connectivity impact. Then, for some of the discussed options, it relates the structural measure with the functional measure, aiming at both presenting the impact of the chosen method on the final results, as well as trying to answer the question about what is the relationship between the structural and functional impact of the WMHs on WM tracts.

4.3.1 Parcellations

This subsection analyses the quality of the timeseries from the regions of interest for the two atlases used. Timeseries used here come from the cortical regions masked only by the subject-specific gray matter mask. Therefore, those are not the same timeseries that will be primarily used in the endpoint analysis in this chapter (as those will be also weighted according to the tractography results). The reason for that is to compare the quality of the timeseries from two atlases, without the

influence of other factors. These timeseries are used in the partial correlations analysis (where they represent the other nodes in the network that are regressed out).

Harvard-Oxford atlas parcellation Figures 4.6 and 4.7 present the frequency spectra of the timeseries from H-O regions. The standard H-O cortical atlas was divided to have separate regions for the two brain hemispheres. Therefore, the corresponding regions from two hemispheres here are separated by 48 (i.e. both 49 and 1 according to the notation here would be a region labelled 1 in the original H-O atlas). Thalamus was not included in this analysis.

Figure 4.6 shows the spectra of each ROI separately (in blue), with a dotted black plot in the background of each, which represents the average spectra. It can be seen that the low frequency signal dominates, as expected. However, for some of the regions the tails are raised, which suggests a substantial influence of signals of higher frequency than BOLD. That contamination is clearly visible in figure 4.7, which shows all these spectra in one image. It can be noted that while the spectra for the majority of timecourses (as well as the average one) look correct, there are many timeseries with high frequency components. There is a peak that can be observed in one of the high frequencies but it originates in the data, therefore the parcellation used has little impact on it.

Yeo parcellation Figure 4.8 shows the frequency spectra of timeseries from regions of the Yeo atlas, based on data from all the subjects. Generally, the shape of spectra are correct – only for three regions are raised tails observed. Those regions are the thalamus (timeseries number 18 in figure 4.8), and those from the regions labelled there as 9 and 10. Number 9 is a region that consists of two spatially separate clusters: temporal pole and inferior temporal gyrus. Number 10 is a single region of orbital frontal cortex. That region is particularly problematic in the functional imaging [66], as was also mentioned in the original atlas description [61]. For some subjects the timeseries of that region were corrupted, therefore region number 10 was excluded from being used in the partial correlations. Similarly, as in the case



Figure 4.6: The timeseries spectra for each of the 96 GM regions based on the H-O atlas parcellation calculated over 2000 UK Biobank subjects. Black dotted lines indicate the average timeseries spectrum for reference. Corresponding left and right regions of the brain are shown opposite each other in the same row.

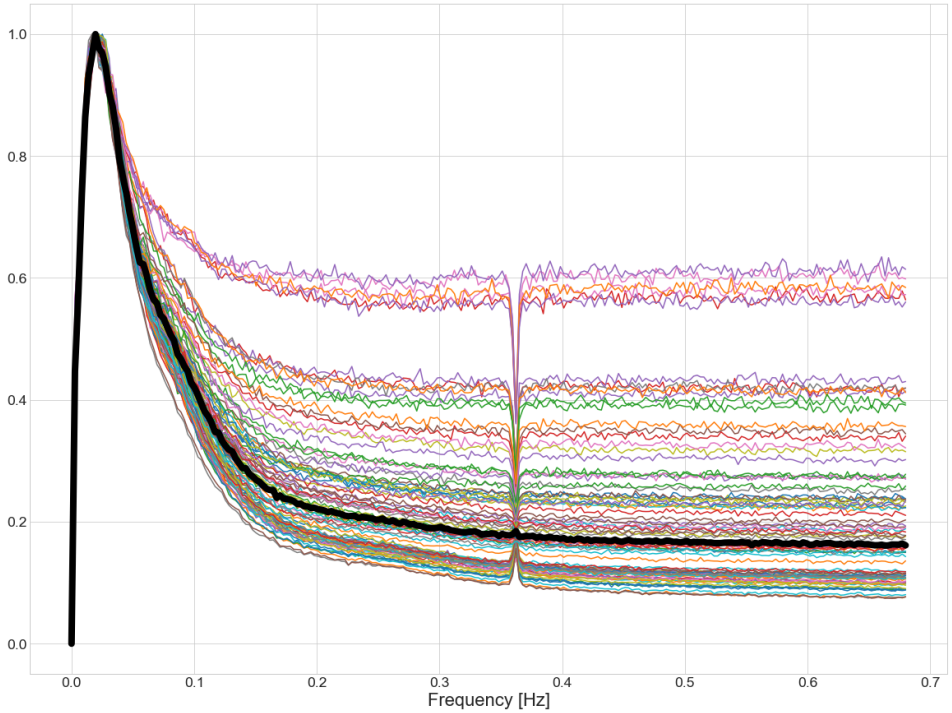

Figure 4.7: Figure shows the spectra of timeseries for each of the 96 GM cortical regions based on the Harvard Oxford atlas parcellation plotted in the same picture. Each coloured line shows spectra from a H-O region (the same as single subplots in figure 4.6). The thick black line indicates the spectrum of the average timeseries. All spectra were calculated using the data from over 2000 UK Biobank subjects.

of the H-O parcellation, there is a peak observed at a single high frequency, which is related to the data and its standard preprocessing in the UK Biobank pipeline.

4.3.2 Functional connectivity

Optimal ridge regression parameter for partial correlation When using the partial correlations with regularisation as a measure of functional connectivity, it is necessary to decide on the weight that regularisation will have in the model. This paragraph describes the exploration of the various weights to find the optimal parameter for the ridge regression.

Figure 4.9 presents the values of the average correlation coefficient (z-transformed) for various values of the ρ parameter in regularisation. The optimal ρ value would correspond to the maximum on that plot. We can see that the results slightly vary between the tracts but the general shape of the dependency between ρ and the

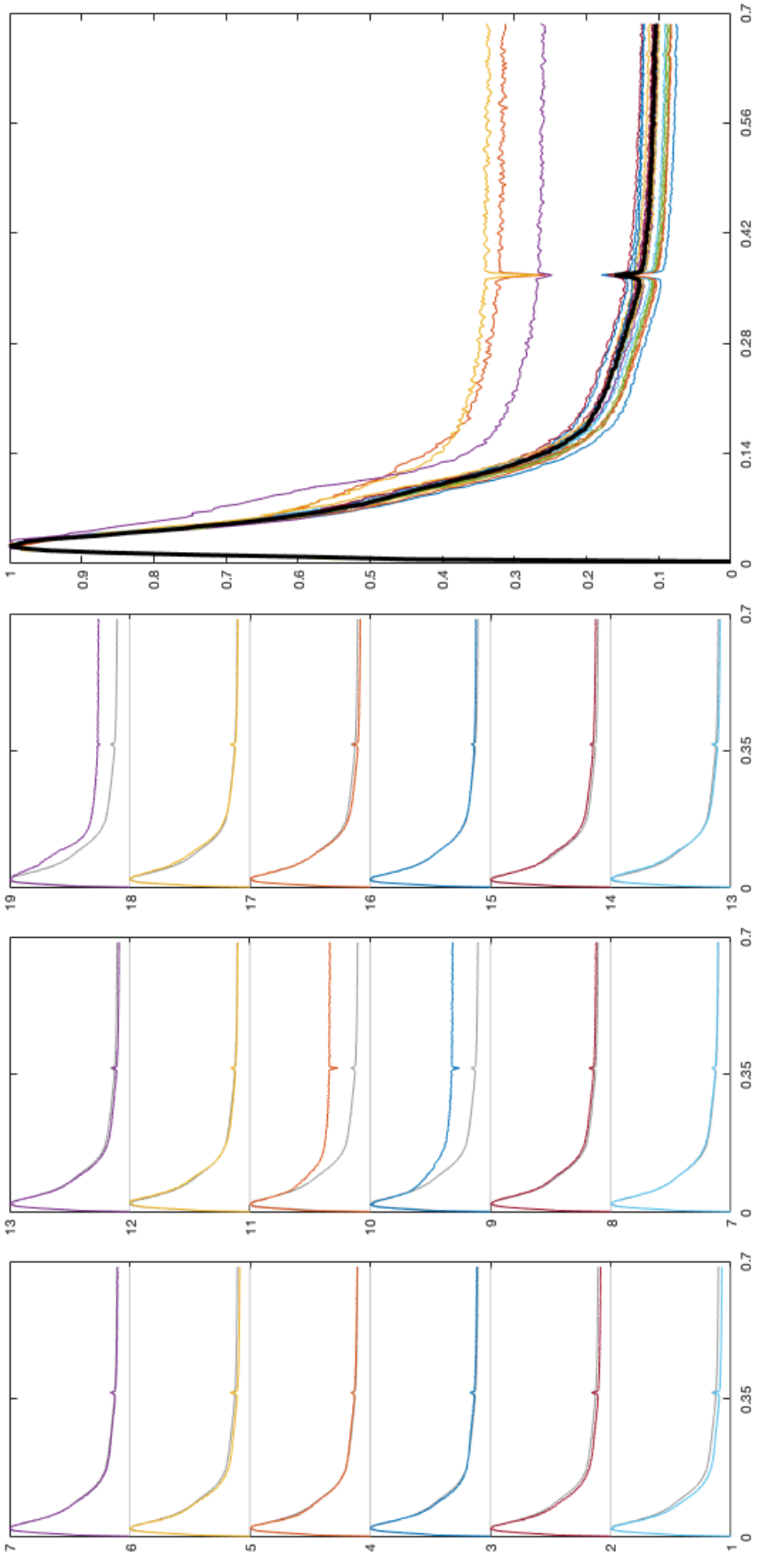

Figure 4.8: Frequency spectra of timeseries from 17 regions of the Yeo atlas (1-17) and the thalamus (18). On the left side, each timeseries spectrum plotted in colour with the gray reference of the average spectra, on the right side all of 18 spectra plotted simultaneously.

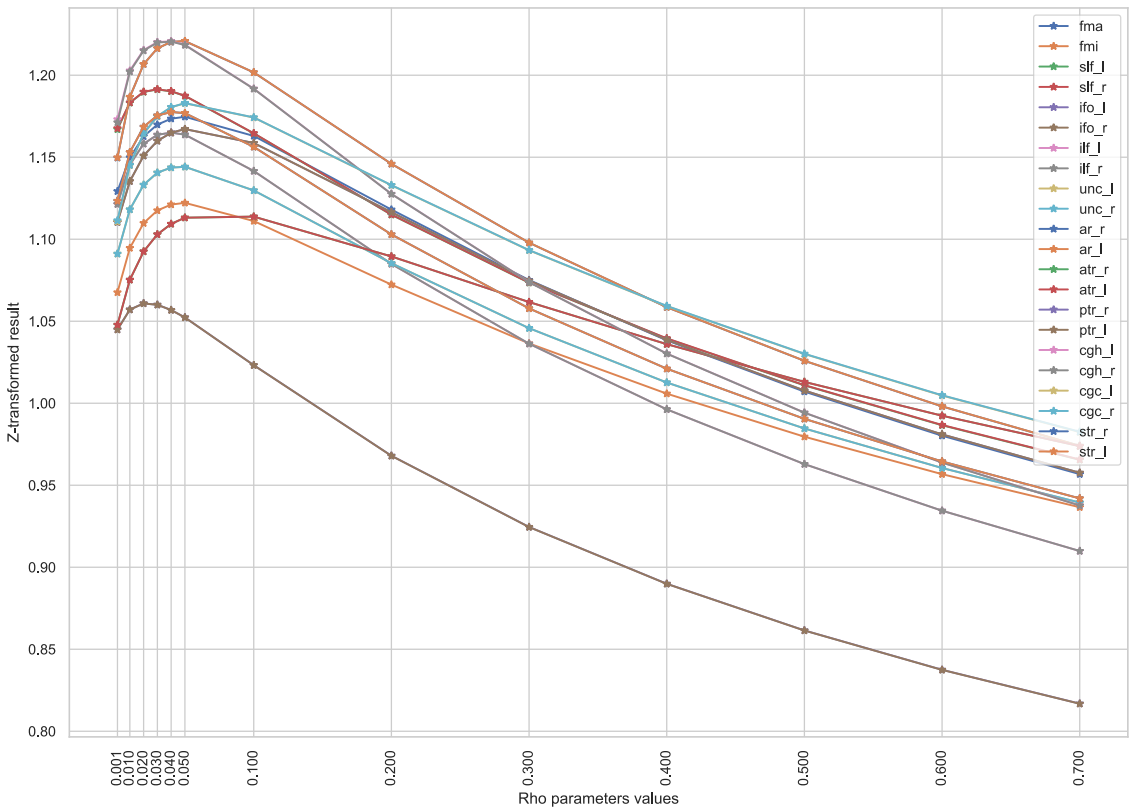

Figure 4.9: Results of calculations in order to find the optimal ridge regression parameter for each tract. Each tract is coloured differently. On the x axis there are different values of the ρ parameter, on the y axis there is a z-transformed average correlation coefficient between the subject-specific partial correlation with given ρ with the group full correlation result.

result are consistent between the tracts. There is also some variability between the maxima of different tracts. They all seem to fall around small values (no higher than 0.1) but higher than zero. Despite that it looks like there are fewer lines on the plot than the 22 tracts mentioned in the legend - this is just the result of plotting when the results for the symmetric tracts in both hemispheres were so strongly similar (after the closer look it is possible to see small differences). For the majority of the tracts, we can observe that they have a maximum peak between 0.03 and 0.05. Based on those results we decided to set $\rho = 0.035$ as the optimal parameter for the partial correlations here.

4.3.3 Relationships between the structural and functional measures

Comparison of results obtained with different methods

In this subsection, there are results obtained with different combinations of the methodological approaches described above. The results are shown for two of the tracts: FMA (figure 4.10) and left hemisphere PTR (figure 4.11). Those two tracts were selected because the results for the PTR were relatively similar to the results for other tracts, and results for FMA are distinctively different. The latter is most likely due to the fact that the FMA has much higher WMH load than other tracts because of its anatomical position. Therefore we believe it is important to analyse it separately.

Two structural impact measures discussed in the previous chapter are used in the plots here in two columns. The plots on the left hand side use the measure based on the streamline ratio, of tract streamlines that go through the WMHs to the total number of the streamlines. The plots on the right hand side use the log of the measure based on the volumetric overlap of the WMH mask to the whole tract volume. Because there were multiple instances when that measure would be zero, to calculate its log, the measure was increased by $\varepsilon = 0.00001$. In the three different rows there are three chosen options of quantifying the functional connectivity. The first two are based on the full correlation, the last one uses partial correlation. The difference between the first one and the second one is that the first one used functional data as it was, when in the second one there was an additional preprocessing step done of removing any potential contamination from the WM and CSF, in case if there was any noise due to the partial voluming.

Figure 4.10 shows results for the FMA tract in 6 different versions of the analysis. In all six cases, regardless of the methods used, for this tract we observe a statistically significant correlation between the structural and functional measures. It means that with an increased structural impact of the WMHs on FMA, there is an associated decrease in the functional connectivity. This agrees with the intuition from visual inspection of the first four plots (that use the full correlation

for functional connectivity), but it is very hard to see on the two plots in the bottom row, where partial correlations are used. All the functional connectivity measure values there are very close to zero (under 0.001). Figure 4.11 shows the same comparison for the PTR from the left hemisphere. In this tract there are more data points where the structural measure is zero or close to it. Here, there is a negative trend but the correlation is not significant for any of the cases. Similarly as before, the functional connectivity measure based on the partial correlations is very small. The difficulty of finding the best methodology is also caused by the variability between the results for different tracts. Here, we presented 6 cases for two selected tracts. A similar analysis was also done for the rest of the tracts. Subsection 4.3.4 presents the summary of those results, and the scatterplots for all the tracts can be found in appendix C along with their description.

4.3.4 Summary of the results across methods and tracts

Here, we present a summary of the results for all the cases and all the tracts combined. For each case we have calculated the Spearman correlation coefficient between the structural and functional measure and plotted the results for all the tracts for a particular condition on the barplots from 4.12 to 4.16. The correlations that were statistically significant (after the multiple comparisons correction) are marked with an asterisk.

Plots 4.12 and 4.13 present the correlation coefficients for the same functional connectivity data (using full correlation) but different structural measures. Regardless of the structural measure used, there were significant negative correlations observed for FMA, FMI, SLF and UNC (both hemispheres), ILF R, ATR (both hemispheres) and PTR R. That is half of the analysed tracts. The differences include that in the case of the streamlines structural measure the CGC L showed significant negative correlation and in case of the overlap measure the AR L showed a significant positive correlation.

The plots 4.14 and 4.15 are also very similar between each other. The functional connectivity measure used for both of those plots was calculated using the full

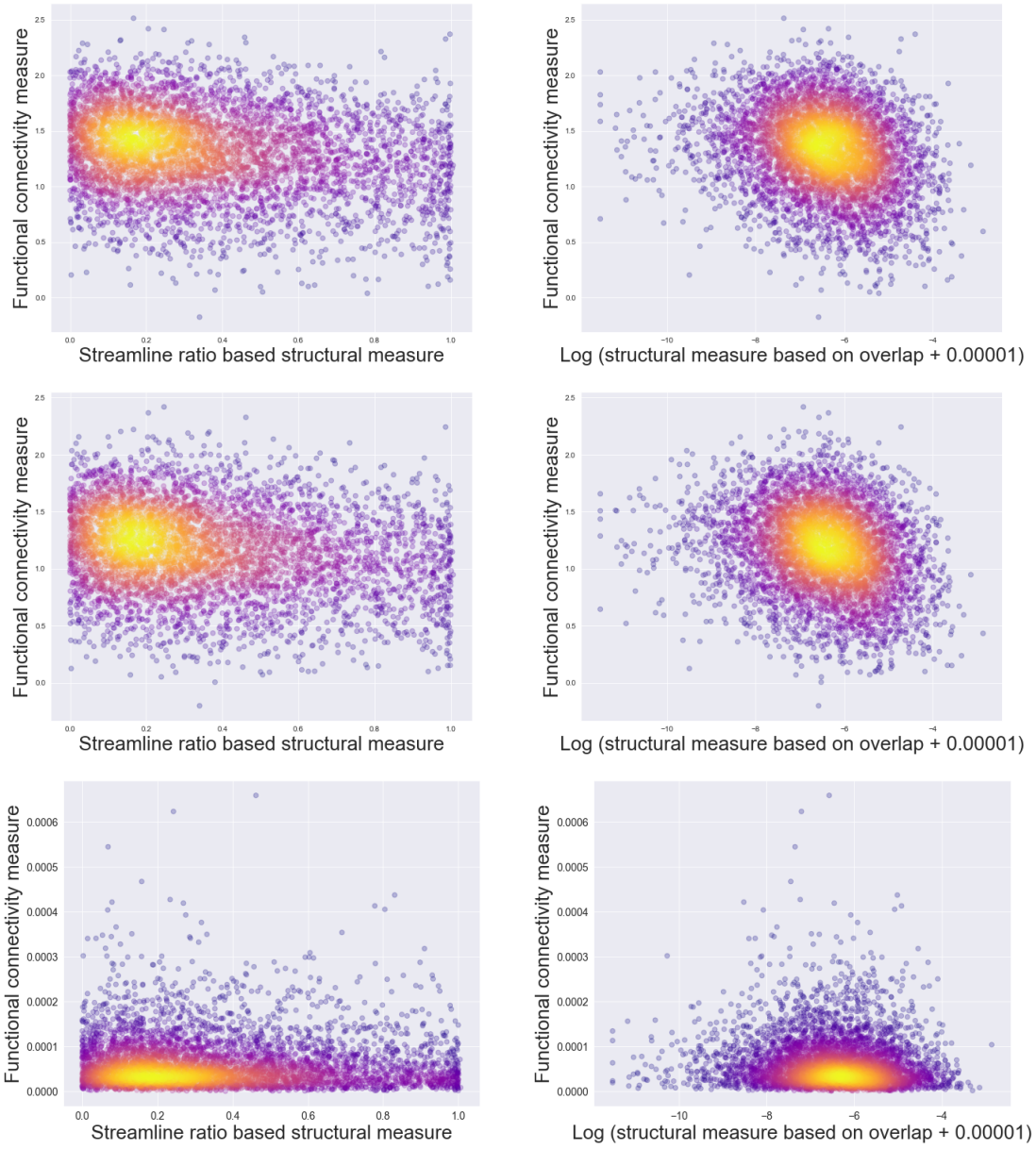

Figure 4.10: Comparison of the results for the FMA tract using different methods. All the panels show scatter plots of the relationship between the structural measure of the WMHs on the tract and functional connectivity measure. All functional connectivity measures (shown on y-axes) were r to z transformed. Plots on the left hand side use the structural measure based on the streamlines ratio and plots on the right hand side use the log of the measure based on the overlap (increased by a small number).
In the top row, plots use the full correlation for the functional connectivity measure.
In the middle row, plots for the functional connectivity measure use also the full correlation but in this case, it was calculated after aggressive removal of possible WM and CSF signal contamination. In the bottom row, the functional measure is calculated using the partial correlation (with rho=0.035).

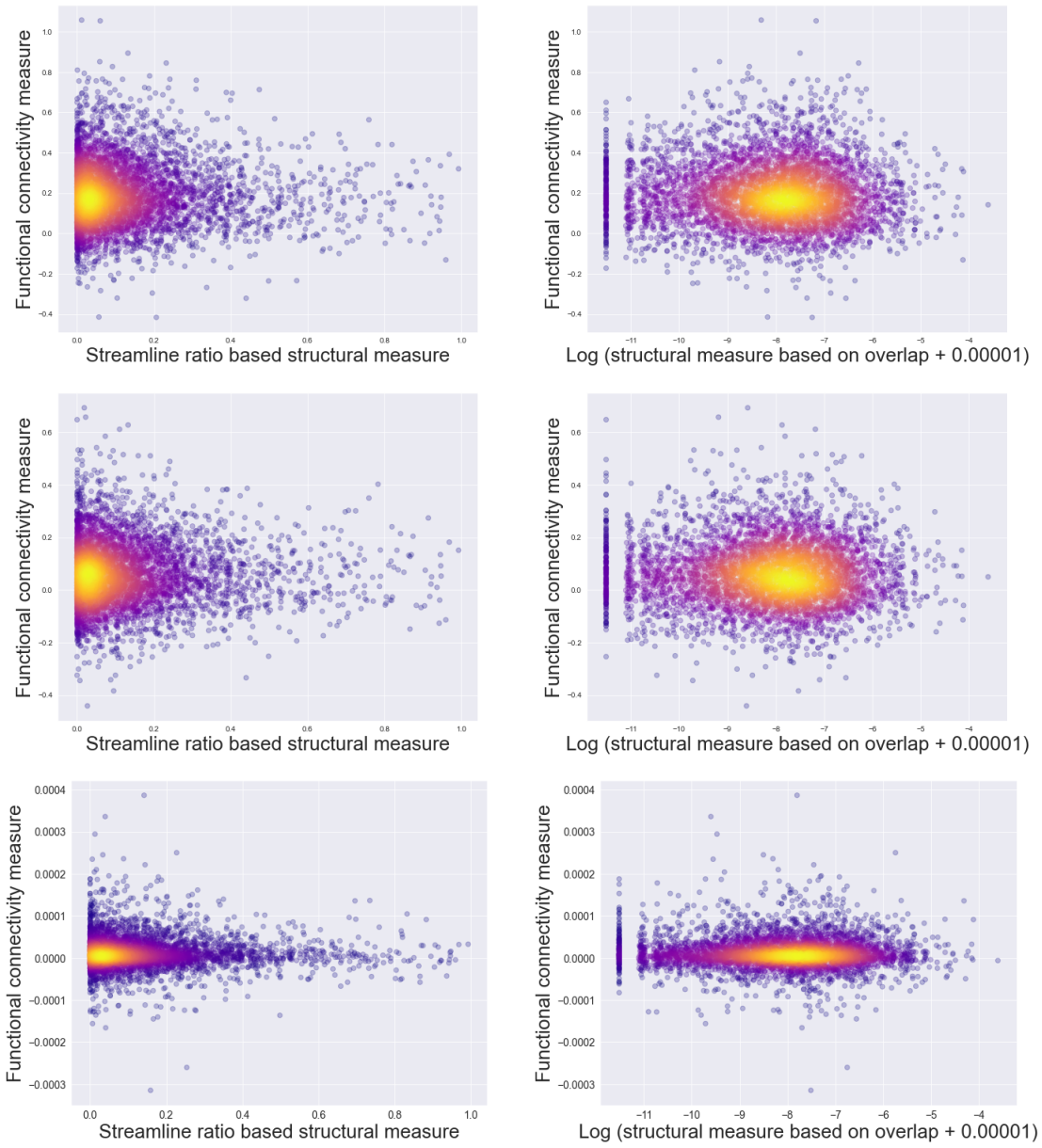

Figure 4.11: Comparison of the results for the PTR tract in the left hemisphere using different methods.
All the panels show scatter plots of the relationship between the structural measure of the WMHs on the tract and functional connectivity measure. All functional connectivity measures (shown on y-axes) were r to z transformed. Plots on the left hand side use the structural measure based on the streamlines ratio and plots on the right hand side use the log of the measure based on the overlap (increased by a small number).
In the top row, plots use the full correlation for the functional connectivity measure.
In the middle row, plots for the functional connectivity measure use also the full correlation but in this case, it was calculated after aggressive removal of possible WM and CSF signal contamination. In the bottom row, the functional measure is calculated using the partial correlation (with rho=0.035).

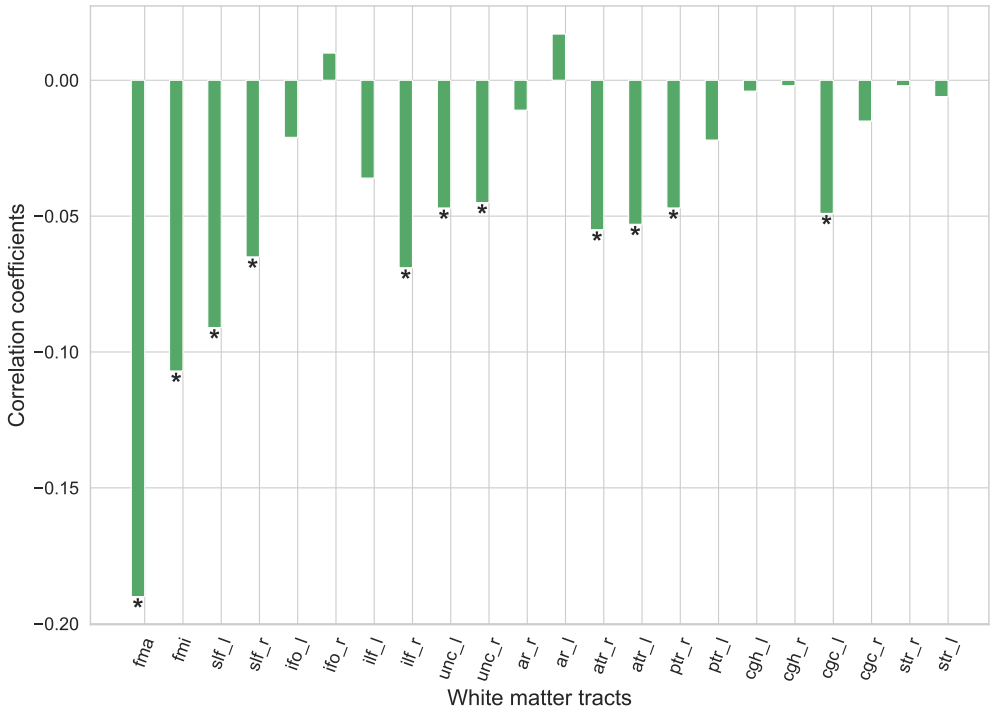

Figure 4.12: Presentation of the correlation coefficients for the relationship between the structural measure based on the ratio of streamlines and the functional connectivity measure based on full correlation. No confound regression was done to the functional signal. The correlations significant after Bonferroni correction are marked with an asterisks.

correlations after aggressive removal of potential WM and CSF signal contamination from the timeseries. As in the previous figure, the first plot 4.14 uses the structural measure based on the overlap and the second one 4.15 uses the measure derived from the volumetric overlap of WMHs with the tract. In both cases, there were significant negative correlations found between the structural and functional measure for the FMA, FMI, SLF L and a positive correlation for the IFO R. In case of the overlap measure there is also a significant negative correlation observed for the UNC in the right hemisphere.

From figure 4.16 we can see that with partial correlations for the functional measure the correlations are much smaller - the scale of the results is around 3 times smaller than it was in case of full correlations. Only FMA shows a significant negative correlation and STR R shows significant positive correlation. However, the correlations are very small.

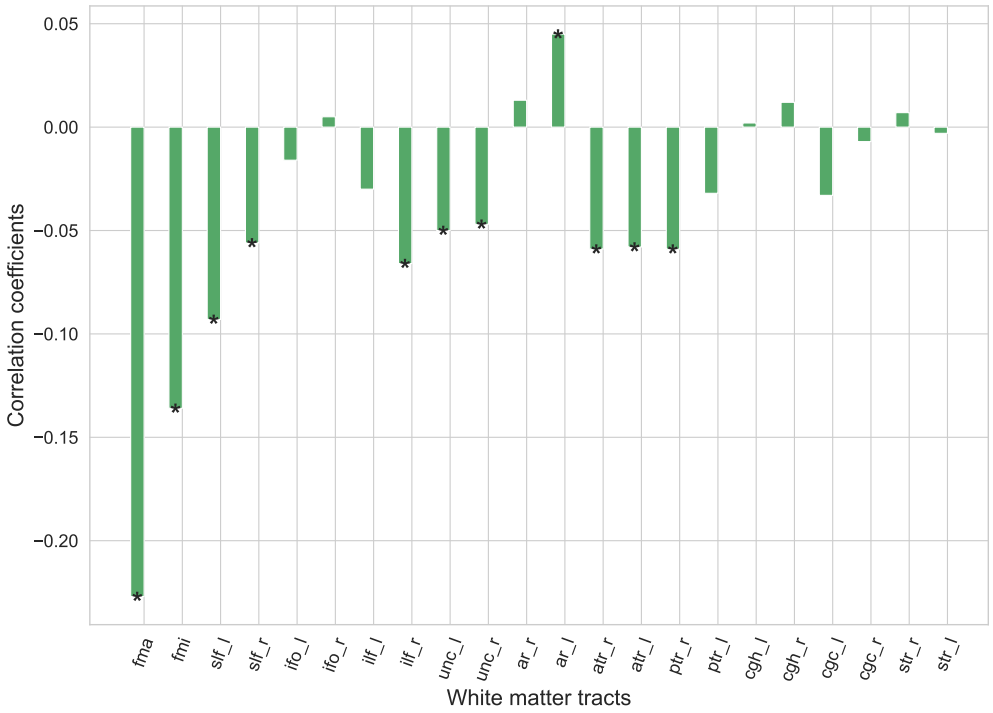

Figure 4.13: Presentation of the correlation coefficients for the relationships between the structural measure based on the overlap and the functional connectivity measure based on full correlation. No confound regression was done to the functional signal. The correlations significant after Bonferroni correction are marked with an asterisks.

4.3.5 Accounting for confounds in the regression

Being aware that the results might be impacted by confounds, we also calculated the results when taking into account the potential effect of the confounds like age, sex and head size. This was done for one case only, with respect to the measures used. That is, the data used for this analysis was the streamlines based structural measure and full correlations with no global regression (in figure 4.10 the corresponding plot would be in the top left corner). The results presented in figure 4.17 are regression coefficients, not correlation coefficients, to allow for comparison of the results with a publication that also addressed this issue [45].

4.4 Discussion

This chapter presents a set of experiments aiming at evaluating the sensitivity and specificity of different methods to quantify tract-specific functional connectivity

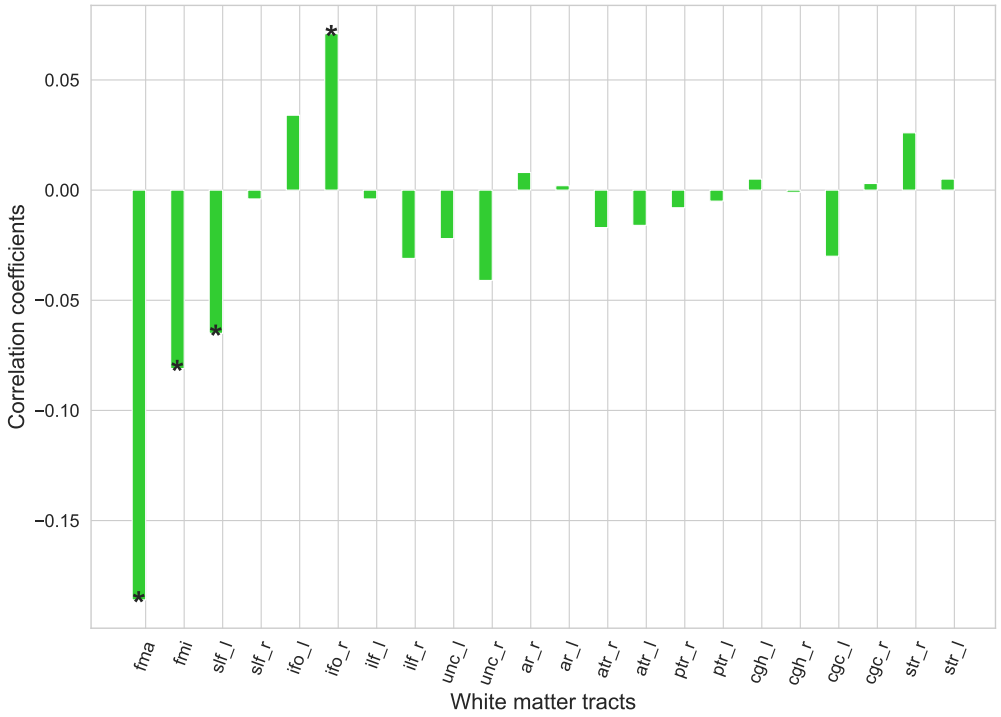

Figure 4.14: Presentation of the correlation coefficients for the relationships between the structural measure based on the ratio of streamlines and functional connectivity measure (based on full correlation) after regressing the WM and CSF signal from the timeseries. The correlations significant after Bonferroni correction are marked with an asterisks.

in the presence of WMHs in a cross-sectional dataset. First, we have presented possible choices of approaching the problem. Then, we show the results obtained using some of the combinations of those choices.

Gray matter parcellation The fMRI data is collected for each voxel independently, however, when looking at functional connectivity, usually information from voxels with similar timeseries is combined to form the nodes of the network. The definition of the nodes has a great impact on the further analysis and results. Our initial choice, i.e. the structural atlas (Harvard-Oxford atlas), allowed for easy identification of regions that belong to each tract. However, after careful analysis, we found out that the cortical parcellation based on the structural information can be inconsistent with the borders of some functionally meaningful regions. That showed in the spectra of the timeseries from the regions from the H-O parcellation. This also would affect the results if we used the partial correlations to define the

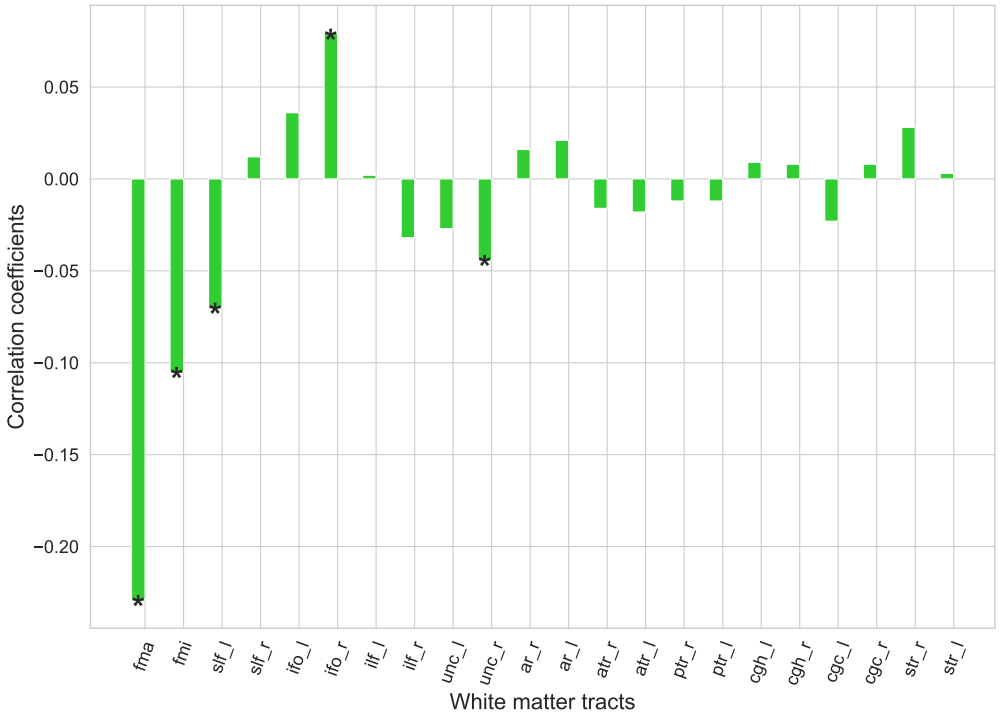

Figure 4.15: Presentation of the correlation coefficients for the relationships between the structural measure based on the overlap based measure and the functional connectivity measure (based on full correlation) after regressing the WM and CSF signal from the timeseries. The correlations significant after Bonferroni correction are marked with an asterisks.

functional connectivity. For this reason, we suggest that it is much better to use an atlas based on the functional data.

Another functional data driven option that could be considered would be a data driven parcellation (for example, the ICA based approach [67], [68]). In this case, as we were more interested in optimising the methodological approach (rather than in the correlations between the structural and functional measures themselves), we tried to avoid any strictly data-driven approach, to improve the replicability of this method on other datasets as it also ensures easier interpretation of the used regions. That comes firstly from the fact that such study-specific data-driven parcellations, even if obtained with the same methods, are often noisy and could differ markedly for different data and the boundaries of the parcels might be difficult to precisely describe using the literature and atlases. The second reason is that running such parcellation heavily depends on the choice of parameters, such as dimensionality

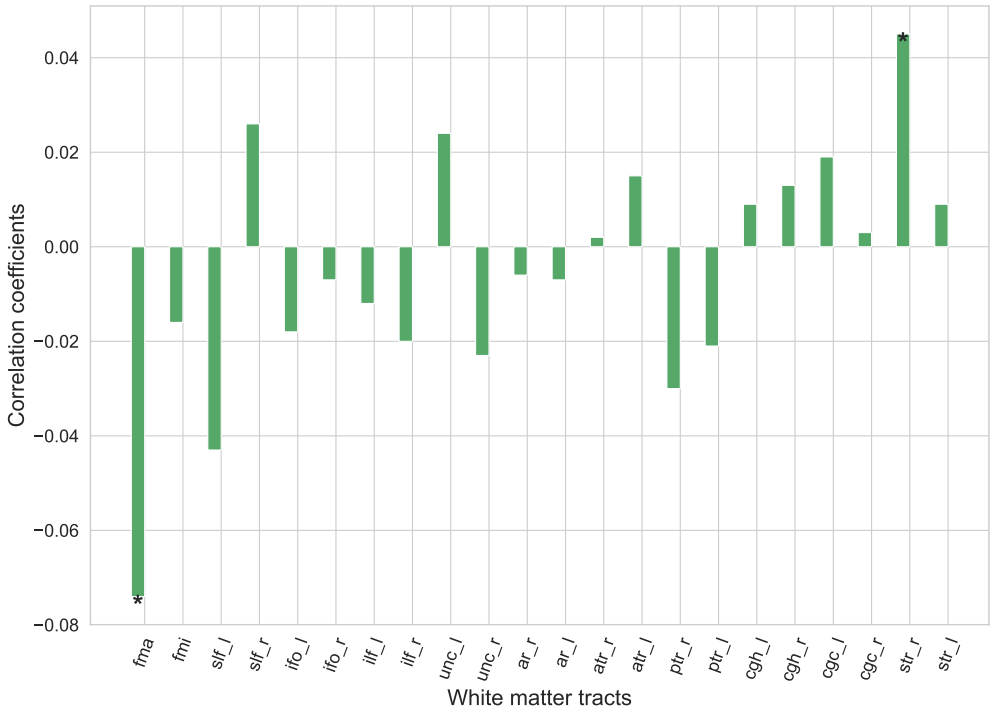

Figure 4.16: The correlation coefficients for the relationships between the structural measure using the streamlines based measure and functional connectivity measure based on the partial correlations with regularisation (rho=0.035). The correlations significant after Bonferroni correction are marked with an asterisks.

(number of ICA components). That brings additionally uncertainty and problems when comparing the final results between studies. In our final parcellation, we combined the H-O regions defining the tract endings prepared previously to be able to extract timeseries separately for two endings of the tract, even if they belong to the non-contiguous regions of the same network in the Yeo atlas, to be able to compute the timeseries from the two ends of the tract separately. Ideally, if doing this work again, we would take some more general approach to define the two tract endings on the Yeo parcels. That could, for example, be based on separating the different areas belonging to the same network into separate ones but with keeping the information about the previous labels for partial correlations purposes. That kind of solution would also minimise the impact of the removal of one noisy region (10) from the Yeo atlas – we would be able to remove only the part of it that is in the problematic part of the brain and, if good enough quality, still use the rest of that parcel to have that signal to regress.

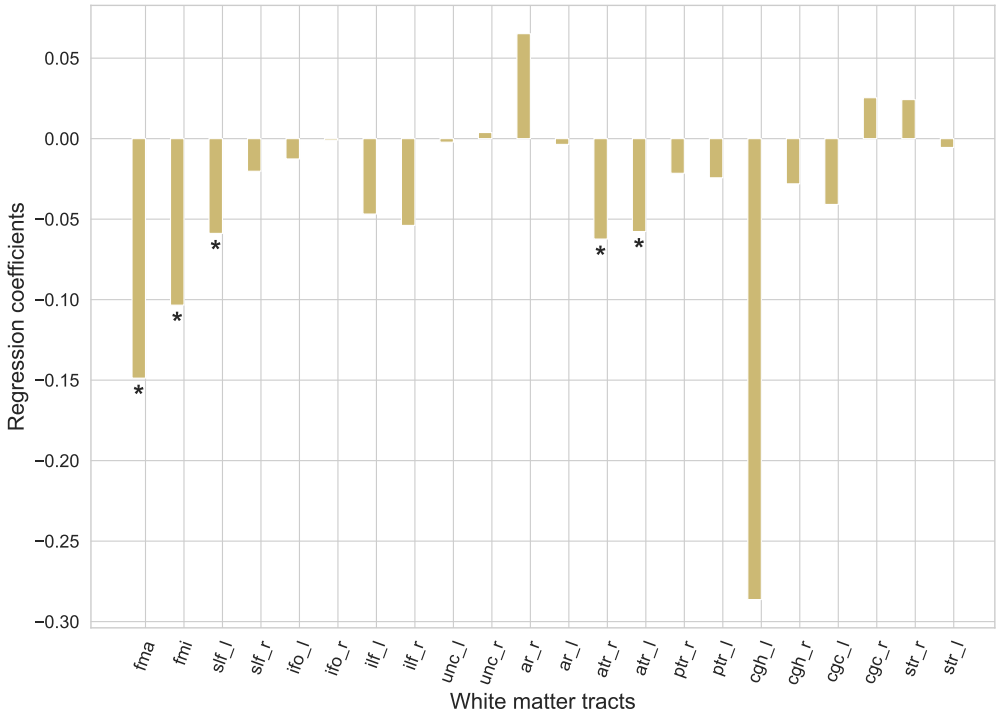

Figure 4.17: Presentation of the **regression** coefficients when accounting for confounds (age, sex, head size). Note that this time the values plotted are regression coefficients, not correlation coefficients. Asterisks mark the statistical significance of the coefficients after the Bonferroni correction.

Timeseries extraction One of the problems encountered with the timeseries extraction was that after registering the data to the functional space (which has lower spatial resolution), the number of voxels belonging both to the tract and gray matter was very low (sometimes under 10 voxels). That raised our concern about the quality of the signal that would be taken as an average from so few voxels. For that reason, we dilated the subject-specific tract endings masks by one voxel. As we were using the voxel-wise weighting of the timeseries when averaging the timeseries from the region, the idea was that those voxels would still have relatively low weights but as we were combining the signals from more voxels, that would improve the signal to noise ratio. Nevertheless, it would be interesting to consider other options for ensuring reliable signal extraction.

Regularisation in partial correlations One of the considered options for defining functional connectivity was based on using regularised partial correlations.

The optimal weight parameter for the regularisation was found to be $\rho = 0.035$. The results slightly varied for different tracts but they were nearly identical for, separately considered, symmetrical tracts in both hemispheres. The results for all the tracts also fall in a similar range and their function with regard to ρ was consistent. That suggests that the method of finding that parameter, that normally is applied to all the considered connections, without specifying the tracts separately, can be used here as well. The value of $\rho = 0.035$ is different from the value used in the UK Biobank pipeline ($\rho = 0.5$) [18]. However, in that work, the timeseries were not extracted using atlas-based parcellations, like here, but from ICA components, which could lead to different results.

Relationships between the structural and functional measures Generally, most of the correlations between the structural and functional measures of the WMH impact on the tract were negative. Therefore, if the WMH effect on the structure of the tract is larger, the functional connectivity is smaller between the ends of the tract. Such relationships were statistically significant for some tracts more often (with various methods) than for others. Among tracts that have shown such relationships were FMA, FMI (callosal tracts) and SLF in the left hemisphere. These are the tracts on which WMHs were detected for the majority of the subjects. In the callosal tracts we observed WMHs for most of the subjects (more than 98%, see the table 5.1 in the next chapter), while SLF had around 80% subjects with WMHs. For many of the subjects, the quantity of WMHs was non-zero but small. Such a non-uniform distribution of the amount of the 'structural impact' between the subjects raises the question of whether that can impact the results of the rank-based correlation values discussed in this chapter. Therefore, we address that concern with an additional analysis in Appendix D. We find that either including or excluding the subjects with a small, non-zero amount of WMHs does not result in any notable changes to the correlation values. The observation of primarily negative correlations agrees with intuition. However, there were also cases of significant positive correlations. That would mean that for those tracts

with the increase of WMH impact on tract structure, the functional connectivity increases. There can be multiple explanations of those observations. For example, when it is observed for the IFO (in the right hemisphere), it is a long tract that runs in the proximity of the ventricles, so it might be an effect of indirect connectivity. It is also possible that there is some compensatory effect. From the analysis point of view, it is possible that some of those correlations are not linear, as we assumed. Finally, removing components from the signal, as it was done with removing the potential contamination of the CSF and the WM signals from the timeseries, often can cause shift (or even change of sign) in the correlations [35].

Comparison with the results from the literature The results of the regression, while accounting for basic confounds, were not very similar to the ones from the most comparable publication [45]. We analysed the same set of the white matter tracts, and also did that for tracts in both brain hemispheres separately (apart from callosal fibres). However, there were many differences in the methodology, which might be (but do not have to be) the cause of the difference in the results. First, they used a surface-based approach for parcellation. We have not considered surface-based methods as at the time we did not have suitable computational resources for required computations. Their parcellation led to 241 parcels and was followed by an automatic removal of the parcels that had no overlap with the raw, unthresholded tract. In the work presented in this thesis, we carefully selected the parcels (from the modified H-O atlas) based on the thresholded tract model that was a result of averaging all the tracts from the subjects with no WMHs on a given tract. That should have led to the more conservative choice of the regions included as a part of the tract, eliminating spurious connections and ensuring consistency between the subjects (in case subject's tractography estimates would be different due to the presence of WMHs, see the next chapter 5). Other basic differences include that here we used the weighted average for generating the timeseries, and the authors of the publication [45] only considered full correlations as the measures of the functional connectivity.

Variability between the methods Some choices of methodology make more difference to the results than others. The effect might vary from simply changing the values of observed results, to making the analysis more difficult or interpreting the results ambiguous. One of the main difficulties, while preparing this work, was the unpredictable scale of the impact of one of the methodology choices, which often required re-running the analysis from the beginning.

Some of those observations were different than expected. For instance, from subsection 4.3.4 it can be inferred that the choice of the structural measure has much less impact on the observed relationships than the choice of the functional measure. In chapter 3 there were substantial differences between the distributions of both proposed structural measures. However, regardless of the measure used, we observe a similar pattern of correlations between the structural and functional measures.

Another example is related to the choice of atlas. For instance, in the beginning, it seemed natural to use the structural atlas based parcellation for this work, while the functional one was in the end much more appropriate.

Potential future directions The topic of describing the effects of the WMHs based on their location is now starting to be explored systematically, but there is much more that can be done in this area.

The first clear direction of research that could support this work would be to investigate how those connectivity changes derived from fMRI data correlate with measures that normally are related to them, like the ones related to cognition. A big part of neuroscience research was based on case studies of patients with lesions in particular regions of the nervous system showing certain symptoms [69]. With the development of neuroimaging, it became possible to investigate the lesions not only from wounds (e.g. gunshot wounds) but also stroke or Multiple Sclerosis lesions. As mentioned in section 4.2, there are now studies that relate executive function to the localisation of the WMHs. Having access to such a broad resource as the UK Biobank, it seems like the natural next step to combine the results of those cognitive tests to the connectivity measures discussed here. Another interesting

project would be to use machine learning to attempt to predict the changes in the functional connectivity (or maybe, even further, the fMRI signal itself) based on the structural impact of white matter changes on the tracts.

Limitations One limitation of this work is that we considered here only selected tracts (selection of the tracts was explained in chapter 3). Related to that is the issue that in case of the long tracts with multiple endings we only took into consideration the furthest ends, ignoring the other regions, still connected to the tract, hence sharing the signal. We made sure that those issues are not affecting the partial correlations (regressing out signal from those areas could potentially remove all the signal of interest), however it would be good to discover a way to address that issue in more detail.

Another limitation is that we did not have a chance to explore the effect of the outliers in calculating the correlations. We tried to reduce the potential bias by using the rank-based correlation coefficient but there can be more work potentially done to compare the results obtained here with the ones with some more robust method of fitting the regression or consider removing the outliers. The latter is a difficult point because it is both unclear where to put the threshold on the structural measure and because potentially those 'more affected' subjects are providing very important insights into the relationship we are investigating (we currently assume all subjects in the dataset are healthy).

There are also certain limitations related to the interpretation of the results due to the large number of subjects used in this study. In case of a large dataset, like the UK Biobank, it is important to be careful when interpreting the classic measures of statistical significance, as it is not necessarily a guarantee of a biologically meaningful effect [21]. Another issue is that this kind of work would be ideally done in a longitudinal manner, while here we worked with a cross-sectional dataset. That might have led to other factors and inter subject variability affecting the results.

The final point to mention is the possible concern that the tracts we use as a point of reference in space might not be correctly modelled due to presence of the WMHs. Since the whole work in this and previous chapter rely on the assumption of correctly performed tractography modelling, this is what the next chapter of this thesis addresses. There is no ground truth available that would allow us to fully validate the methods and the results presented in this chapter, as it often is a case in the medical imaging, but at least the work presented in the next chapter supports the assumption of the correct tract definitions being used here.

4.5 Summary

This chapter proposes the methodology for investigating the impact of WMHs on functional connectivity in the brain. Building on the previous chapter, it uses the white matter tracts for description of the local environment, therefore it aims at defining the functional connectivity between the endpoints of the tracts in the gray matter. This chapter explores many of the choices that have to be made to propose such methodology as well as indicates their impact on the results. That includes issues like choice of the gray matter parcellation and the method of ensuring that only voxels belonging to the tract are considered, functional connectivity definition and the pre-processing of the data, or impact of the confounds and outliers on the results. We observed high variability of the results between the tracts. The results suggest that the choice of the structural measure of the WMH effect on the tract had a smaller impact on the results than the choice of the functional connectivity measure. While defining the functional connectivity between the tract endpoints, we found it was very important to correctly extract the timeseries. That included the tract ending region definition and checking the quality of the average signal from them. We believe that provides useful recommendations for similar future analysis using big datasets like UK Biobank or similar.

5

Tractography in the presence of White Matter Hyperintensities

Contents

5.1 Motivation 74
5.2 Introduction 74
5.3 Methods and data 76
5.3.1 General overview of the methods approach 76
5.3.2 Data 77
5.4 Tract shape variability analysis 77
5.4.1 Methods 77
5.4.2 Discussion of the results 79
5.4.3 Conclusion 81
5.5 Voxelwise tractography results comparison 81
5.5.1 Methods 82
5.5.2 Results 85
5.5.3 Discussion 96
5.6 Microstructural parameters analysis 101
5.6.1 Methods 102
5.6.2 Results 103
5.6.3 Discussion 113
5.6.4 Conclusion 115
5.7 Summary 115

5.1 Motivation

In ageing white matter, in the areas containing WMHs, parameters like Fractional Anisotropy (FA) are altered compared to the 'healthy' tissue [4]. These microstructural tissue changes might affect tractography – virtual (in vivo) dissection of white matter tracts. Using the UK Biobank study data, this chapter aims to add to the literature by investigating whether the presence of WMHs can indeed affect white matter tract modelling.

5.2 Introduction

Tractography modelling is the main tool available for investigating the white matter tracts noninvasively in living humans. However, most of the algorithms for running the tractography are developed primarily to work on a healthy population. Even in those, relatively the easiest cases, tractography faces many still unsolved challenges. Those include problems like finding the exact tract terminations [70] or gyral bias (a tendency for algorithms to stop fiber tracking on gyral crowns, compared to the banks of sulci) [71]. In cases of ageing brains, there is potential for even more disruptions in tractography modelling due to altered tissue characteristics. As mentioned in the previous chapters, it is known that white matter parameters are changed in the presence of WMHs. Variations in the DTI measures like FA and MD that can be observed between the subjects are strongly correlated with the total WMHs volume and a measure of WMH intensity on the FLAIR image [72]. Additionally, it was shown (using TBSS) that FA decreases strongly within the area of WMH, but also in its proximity [4].

Validation of tractography, although important, is challenging. The first reason for that is that there is no ground truth available. There are multiple studies, reviews, and competitions aiming in the validation of the tractography in a general sense, as well as relating it to the histological imaging. Here, we are assuming that the tractography in the subjects with no WMHs is performed correctly and only looking at whether it is altered when WMHs are present on the white matter

tracts. One work on that topic was described in an ISMRM conference abstract from 2017 [73]. The authors focus on the fact that WMHs can have an impact on tractography indirectly – by affecting the fibre tracking mask if it is not corrected to include WMHs in WM segmentation results. They also conclude, however, that the principal orientation distribution function direction is not altered in the WMH areas. Their conclusion was a suggestion to correct the tracking masks in the presence of WMHs. The question asked by the authors of that work was undoubtedly the right one, however, the methodology used there could be improved. First of all, the authors checked only the impact of the WM mask when WMHs are not counted as WM. Also, the dataset used for that study was very small (5 subjects). Few studies addressed similar problems, but they focused on the whole tractograms. One example was the NeMo tool [47] mentioned in chapter 3. It requires a mask of WM pathological locations and the standard set of tractograms, which is used as a reference to find streamlines that would travel through those areas.

Accurate tractography modelling is undoubtedly important in research studies. However, there are also many clinical applications of tractography, which rely on its results not only for disease diagnosis and progress monitoring but also for procedures planning, where errors in modelling can more directly have severe consequences. Tractography is used, often in addition to the diffusion modelling, in managing and treatment of many neurological diseases. In stroke cases, it allows for identification of the exact white matter pathways that were affected, which can help to interpret the symptoms [74]. It is also used to investigate the adaptive changes and rewiring after the stroke. Tractography is also useful for neurosurgical planning. In epilepsy, apart from direct tract visualisation, tractography helps reducing the risks and predicting outcomes of surgery [75], [76]. In functional neurosurgery, like deep brain stimulation, the tractography can assist in more precise electrode placement planning in depression [77]. There is also increasing use of tractography in Multiple Sclerosis patients, primarily in assessing and explaining pathological changes and their relation with disability scores but also other changes

that can be linked to functional adaptation [76]. Chapter 6 describes the use of tractography in MS in more detail.

5.3 Methods and data

5.3.1 General overview of the methods approach

The aim of the work presented in this chapter is to investigate whether the presence of WMHs of vascular origin on the WM tracts affects the tractography results for those bundles. In order to perform the full analysis of this problem we decided to analyse the data on three different levels.

- *Global tract shape changes:* Starting from the top level, of the most general standard outcome of the whole tract modelling process – tract shape – comparing its variability for the subjects with WMHs on that tract to those with none. Section 5.4 presents that analysis, which uses the Dice coefficient values for the thresholded and binarised tract images, and the distributions of that score for both subsets of subjects, separately for each tract.

- *Local tract probabilities changes:* That is followed by the more quantitative analysis of the actual values obtained with the tractography modelling for each voxel, which correspond to the probability of the particular voxel being a part of the tract. For that purpose, we adapted a voxelwise General Linear Model to investigate the differences between the distributions of those values for subjects with and without WMHs on each tract, for three subsets of the data. That analysis is described in section 5.5.

- *Microstructural tissue changes:* Finally, section 5.6 looks at the microstructure level, to explore whether the tissue properties modelled using the diffusion data do actually differ in and around the WMH areas from the normal appearing white matter parts of the tracts. It is necessary to look at that variability on a very low level of diffusion data modelling in order to explain the changes observed at the higher levels.

The more detailed explanation of the methods in each of those three parts is described in the sections below.

5.3.2 Data

For the analysis presented in this chapter the same subset of the UK Biobank cohort was used as in the previous chapter. That is 5000 subjects randomly selected from all the available subjects (around 12,000 subjects, who had complete data, at the time of analysis). For some parts of the analysis two subjects were discarded due to errors in the Diffusion Tensor Model results. Analysis was done for 22 WM tracts, as in the previous chapters. When taking a closer look at the data, it can be observed that there is quite high variability in the number of subjects that have WMHs overlapping with the tract, which differs between the 22 tracts.. If we define the *nonaffected tract* in a particular subject as one that has no voxels marked as WMHs overlapping with the thresholded and binarised tract, the number of subjects with nonaffected tract varies greatly between the tracts, such that some had very few examples of nonaffected tracts. The exact numbers are presented in table 5.1.

5.4 Tract shape variability analysis

The first analysis of this chapter looks at the whole tracts, in order to assess whether the tract shape, as a final outcome of tractography after postprocessing, is different in the presence of WMHs or not. Of course, there is no ground truth in that case, the actual real shape of the tract is unknown, so it is necessary to define tractography reliability in some other way. Generally, the approach here is to define an 'expected' shape based on the data from the nonaffected tracts and compare the variability in divergence from it for affected and nonaffected tracts.

5.4.1 Methods

Since there is no ground truth in tractography modelling, it is important to define some point of reference to which the shape of the subject specific tract will be compared. For that purpose, I define the *average nonaffected tract*, which is

Table 5.1: This table presents the number of subjects with nonaffected tracts out of 5000 analysed for each WM tract analysed in this chapter. In red, there are marked tracts for which over 99% of the tracts had some WMHs on them. In orange – highlighted cingulum – the only tract for which less than half of the subjects had WMHs.

WM tract	Left (L) or right (R) hemisphere	Number of subjects with no WMH detected	Percentage of subjects with nonaffected tract
IFO	L	74	1.48%
IFO	R	24	0.48%
SLF	L	1031	20.62%
SLF	R	883	17.66%
ILF	L	148	2.96%
ILF	R	44	0.88%
UNC	L	1100	22.00%
UNC	R	1309	26.18%
FMA		6	0.12%
FMI		65	1.30%
AR	L	1196	23.92%
AR	R	1046	20.92%
ATR	L	12	0.24%
ATR	R	53	1.06%
CGC	L	2811	56.22%
CGC	R	3399	67.98%
CGH	L	3256	65.12%
CGH	R	3213	64.26%
PTR	L	179	3.58%
PTR	R	72	1.44%
STR	L	811	16.22%
STR	R	987	19.74%

constructed from a subset of the data. For each tract, the subset of subjects for whom that tract is nonaffected (have no overlap with WMHs mask) was defined (see 5.1) and a sum of those images (thresholded at 0.001 and binarised) was computed. Then, that sum was normalised (value at each voxel was divided by the highest value in the sum image) so the maximum value was 1 for each sum. Subsequently, that normalised sum image was thresholded at 0.1 (10 percent of the maximal value), in order to exclude the voxels that belong to the tract only for few subjects, to ensure that this reference average nonaffected tract is as general as possible.

In the next step, for each of the 5000 subjects, and for each tract, their subject specific tract was thresholded at 0.001, binarised and compared to that average

nonaffected tract. The comparison was done using the Dice coefficient, defined as in the equation below, where X is the subject specific binary tract mask and Y is the average nonaffected tract binary mask. The more similar masks are, the higher Dice index. Dice index values have values from 0 to 1, but that range is not linear.

$$Dice = \frac{2|X \cap Y|}{|X| + |Y|} \tag{5.1}$$

For each tract the subjects can be assigned to one of the two groups depending whether that tract was nonaffected for that subject as described in table 5.1. Then the Dice coefficient results were plotted separately for each of those two groups to see how their distribution differs. Differences between the groups were tested for significance using a t-test with Bonferroni correction. The hypothesis would be that the presence of WMHs causes the tract shape to deviate more from the average nonaffected tract than for the nonaffected tracts. Therefore, we would suspect that for the affected subjects the Dice coefficient value would be significantly lower on average than in the nonaffected cases, if the WMHs were having an effect on the tractography.

5.4.2 Discussion of the results

The distributions of Dice coefficient values for all the subjects for both groups were plotted in figure 5.1.

A significant difference ($p < 0.001$ after Bonferroni correction) between the Dice coefficient for both groups was detected for some of the tracts: AR for both left and right hemispheres, left and right SLF, right IFO, right ILF, right PTR, as well as for the FMA. Visual inspection of figure 5.1 suggests that the differences are not very big – apart from one tract, FMA. That can be explained by the fact that the FMA, which runs close to the ventricles, where WMHs are detected for most of the subjects (see WMH spatial distribution maps on the tract 3.5.2). In the analysed subset of data, that was particularly notable for FMA – as shown in table 5.1, only 6 out of 5000 analysed subjects were nonaffected for that tract. That means that 4994 subjects were compared to the average of 6. That clearly could

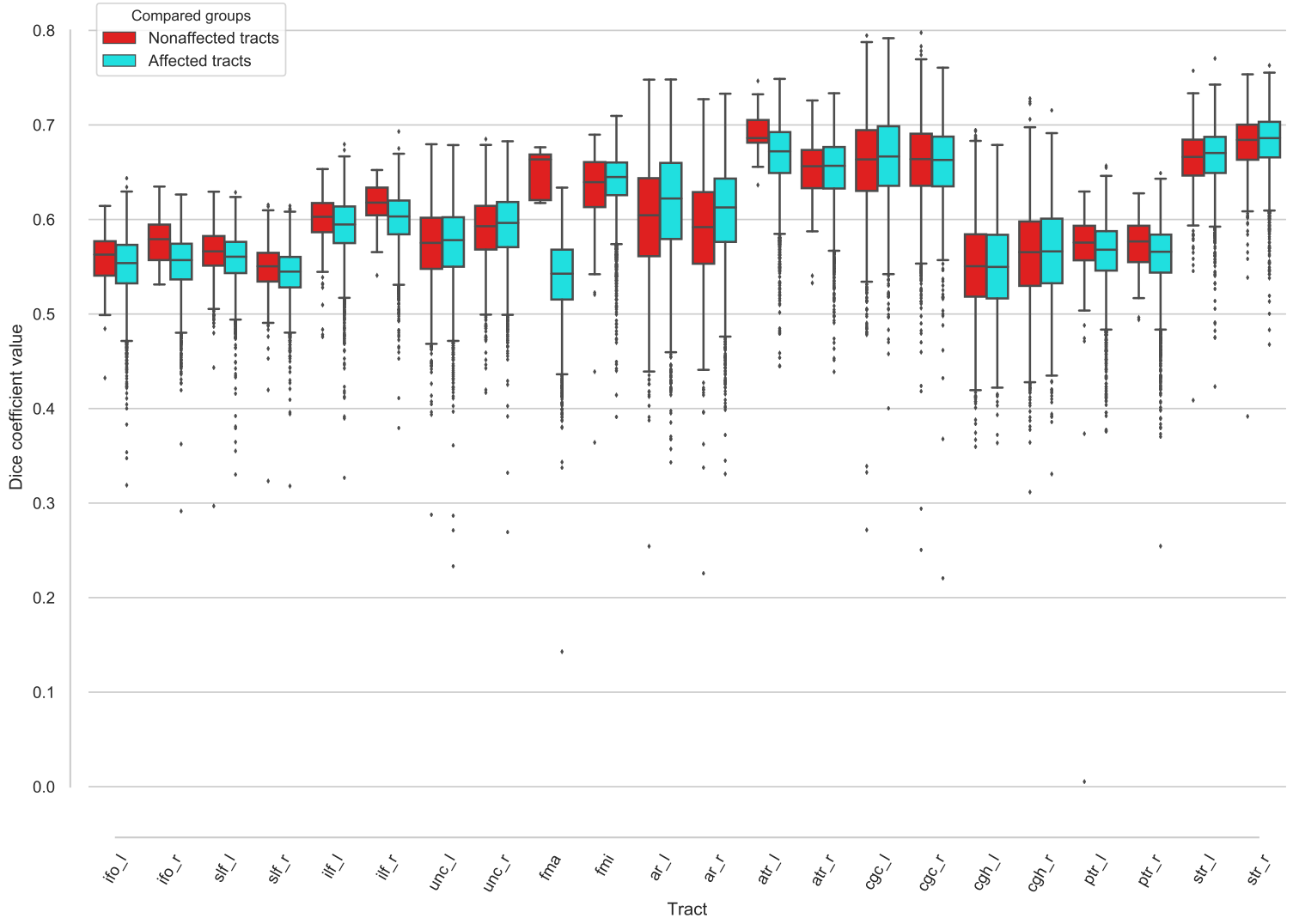

Figure 5.1: Distribution of Dice coefficient values in groups with nonaffected tracts (red) and affected tracts (light blue) subjects for each tract. Significant differences were found for AR (both hemispheres), SLF (both hemispheres), IFO right hemisphere, ILF right, PTR right and FMA tracts.

have affected the results for that tract and therefore I would not trust the difference seen on the plot to be meaningful. That leads to another point of discussion that needs to be mentioned: the method proposed here is imperfect because we are comparing tracts belonging to two different classes to the average of data from one of those classes. That could affect the results, making the differences between classes bigger and potentially the distribution of the Dice coefficient for the affected tracts wider than the one for the nonaffected tracts (based on how the reference average nonaffected tract was constructed).

Additionally, in cases like this, when the differences are significant but look very small there comes a question about whether the statistically significant results are meaningful. When using such a large amount of data, like here, it is much easier to obtain statistically significant results even when there might not be any biologically meaningful effect (in terms of percentage of variance explained in the data) [21].

5.4.3 Conclusion

When comparing the shape of the tracts, the differences between the variability of the tracts with WMHs and without WMHs overlap from the 'expected' average shape were small, and although statistically significant for some tracts, the results do not suggest that the presence of WMHs on the tract would substantially change the shape of the tract obtained with the tractography modelling.

5.5 Voxelwise tractography results comparison

The previous section investigated the final shape of the tract as a binary mask. As a next step, this section looks at the tractography results in more detail, comparing the probability values obtained from tractography for every voxel of the image. For each tract, subjects were assigned to one of two classes (nonaffected or affected, as before) and the General Linear Model (GLM) on a voxelwise level was used to estimate whether the are differences in streamline proportion – the scaled probability value in each voxel which is the result of running tractography.

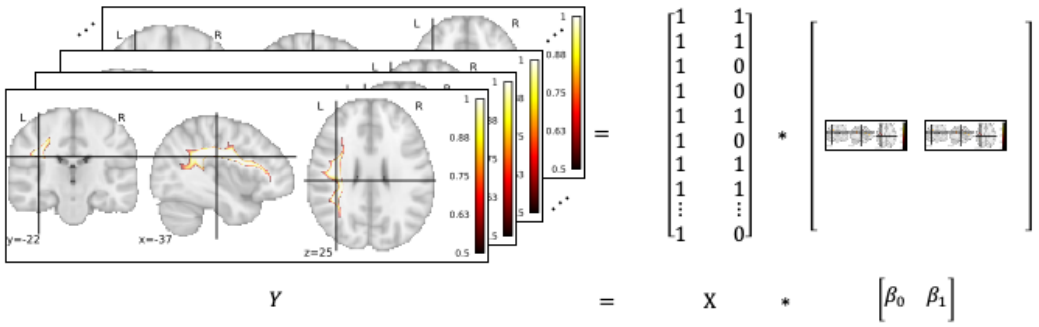

Figure 5.2: Ilustration of the general idea of the voxelwise GLM model used in this part of the work. Y is data (here: tractography results), X - design matrix, β are coefficients.

5.5.1 Methods

Explanation of the method proposed

The values analysed in this part of the work are path probabilities images. These are numbers of streamlines in each voxel divided by the total number of streamlines that belong to the tract. The results were obtained with ProbtrackX2-GPU [50] [26] through AutoPtx [48] tools from the FSL package [51]. Tractography parameters, as well as preprocessing steps, were set as in the UK Biobank pipeline [18] with one small change – the seed for initialisation was set to a constant, instead of being random.

Those results were fed to a GLM model (as presented in 5.2): normalised tractography results (3D files) as an input (data, Y), design matrix (X) with a column containing values of zeros or ones, depending whether the tract has a hyperintensity in it or not (as well as a column of ones for a mean, and columns with subjects' age and sex to account for them as confounds). We designed the analysis, prepared the data, design matrix, and did the postprocessing but the voxelwise GLM implementation used here was written by Tom Maullin[1] [2].

[1]https://github.com/TomMaullin/BLM-py/releases/tag/v1.0.1
[2]https://github.com/TomMaullin/BLM/releases/tag/v1.0.3

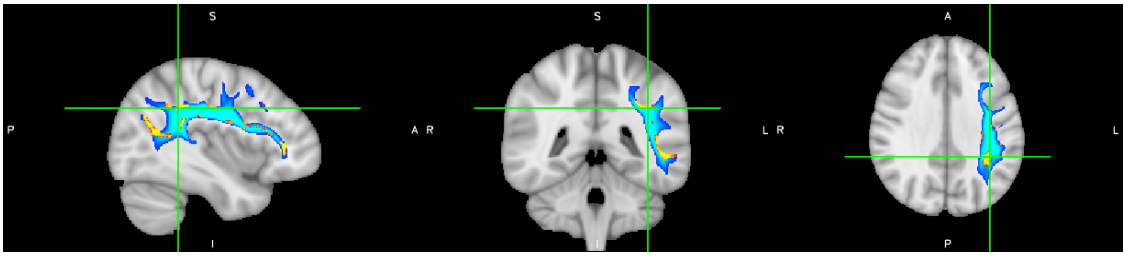

Figure 5.3: Example of uncorrected p-values (yellow) on the SLF L tract (blue).

GLM results postprocessing The results of the voxelwise GLM implementation we used are not corrected in any way that would take into account the neighbourhood voxels information (clusters). Instead of looking at the p-values of clusters distribution (example image of uncorrected p-values is shown in figure 5.3) we decided to look at the scaled effect size. The p-values show results regarding the ratio of the mean difference to the standard error without taking into account the size of the difference. In large datasets it can often be the case that very small effects can create significant results as the standard errors can become very small, but such small effect sizes are not of particular interest in studies with more typical sample sizes. Consequently, we will instead show the effect sizes, scaled with respect to the mean tractography values, to more intuitively put into perspective the magnitude of the change. In addition, it can be seen that the locations of statistically significant clusters did not overlap well with the high probability of WMHs appearance (which were presented earlier in subsection 3.5.2). Therefore, we moved to displaying the effect size, which should let us draw more informed conclusions.

Effect size is related to the β coefficient (see 5.2). β can be interpreted as a difference: it represents value for WHM case minus value for a non-WMH case. It can take both positive and negative values, as in this case the effect of the WMH on the tractography can be either way.

Results presented below are using the transformed β values to reflect the relative differences, rather than absolute values. For each voxel the value of β was divided by the mean of tractography strength (results from tractography in *tractNorm* image) for all the subjects. That allowed us to present the difference as a percentage with

reference to the tractography values. In the results below the analysed area of the tract is only the overlap with the average nonaffected tract, as defined above.

Evaluation of the method on the UK Biobank data

We used the proposed method to investigate the voxelwise differences in the tractography results between subjects with and without WMHs on their tracts, for different subsets of UK Biobank data. The null hypothesis here would state that there is no difference between the classes.

All the data To begin with, we run the analysis for the whole dataset used in the previous parts of the thesis, consisting of 4998 subjects from the UK Biobank (the same selection of 5000 subjects as before with 2 excluded due to some problems with their tractography results). We perform the analysis twice, with different sets of covariates. Firstly, with the simplest possible analysis – using a design matrix X consisting of only two columns: one with the classes encoded as 0/1 and another with all ones to account for the mean. Secondly, a very similar analysis was run but this time the design matrix also includes age and sex as covariates. The second version reflects the approach we wanted to take to find the results, while the first one is more aimed at testing if this method is sensitive enough to detect any changes, regardless of whether they are driven by WMHs, age or sex.

Subset with a narrow age range Global WMH load is often reported to be correlated with age [78]. To ensure that it does not affect the results we select a subset of the subjects within a narrow age range –between 65 and 71 years old – using a selection process that also ensures that there is no linear correlation between the age and WMHs in that group. The subset contained 1010 subjects, which constitutes more than 20% of the original subset of the data used in the thesis, and hence should have a statistical power that is only slightly reduced.

We ran the analysis with a similar design matrix to that used before. The design matrix had 4 columns: mean (constant: 1), WMH presence on the tract (binary variable: 0 or 1), age, and sex. In all the previous analyses we only included one

contrast, which selected WMH presence (i.e. using the order of columns mentioned above, the contrast would be [0, 1, 0, 0]). Here, we performed that analysis but also additionally we added 2 separate contrasts, as if we were looking into each other factor (i.e. [0, 0, 1, 0] where 1 is age and [0, 0, 0, 1] where 1 is sex), hoping that it will provide further insights into the performance of the method. The analysis included all the tracts apart from FMA, because in the selected subset there are no subjects without WMHs on this tract.

Single sex subset within a narrow age range Then we split this narrow-age subset further into two groups based on their sex, to remove any possible effect that sex could have on the results. The subsets have 523 female subjects, and 487 male subjects. We ran the analysis again for all the tracts apart from the FMA. In this analysis, the design matrix had 3 columns: mean, WMH presence on the tract (binary variable), and age. The contrast was applied with regard to the WMH presence (i.e. [0, 1, 0]) and only those results are presented.

5.5.2 Results

In this part of the work, the results presented are the relative β values – scaled by dividing by the mean of tractography strength for voxels. They were then masked by the average nonaffected tract mask and plotted on the standard brain template used here as a spatial reference. The purpose of masking was to visualise only the data for voxels that would actually be expected to be part of the tract. The average nonaffected tract masks used are quite liberal (they exclude only voxels that would belong to the tract for fewer than 10 percent of the nonaffected subjects), therefore it should not limit our ability to see the differences. Moreover, if there were any dramatic deviations in the tract shape from the standard one, having a constant number of particles used in tractography means that then we would see also much lower tract probabilities in the region where the tract was expected to run. That justifies using the mask for allowing for clearer visualisation without concerns over misinterpreting the results. In the plots of the results presented

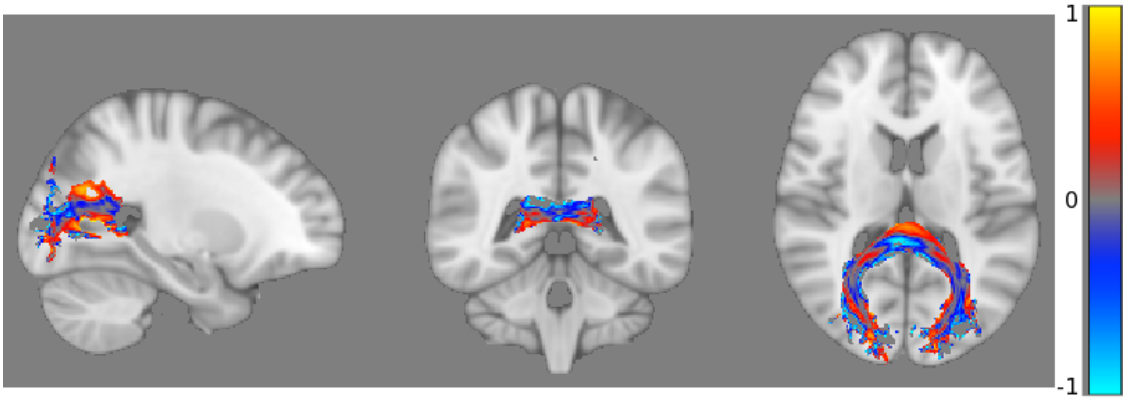

Figure 5.4: Scaled β values from the voxelwise GLM comparison between cases of presence and absence of WMHs for the FMA tract.

on the tracts, negative values are shown in shades of blue, and positive values in shades of red, with colour being brighter closer to the extremes and reaching gray for the values around zero.

Results for different tracts, conditions, and their description can be found in appendix E. Below there are results for selected tracts for different types of analyses to allow for comparing them.

All the data First, we look at the results when using the design matrix X with only two classes (i.e. WMH presence on the tract, as a binary variable, and the mean). Figure 5.4 shows the results for the FMA tract. The results look symmetrical between the hemispheres, with both positive and negative results present. The positive values (shown in red) are mostly observed on the medial side of the tract (on the side of the ventricles).

Then, we look at the results that use the same data but the design matrix X in the model consists of 4 columns: mean, WMH presence, age, and sex. Results for the FMA tract are shown in figure 5.5. After regressing out the difference introduced by age and sex there is very little effect left. There are very few voxels marked in red or blue there, though they still form a smooth pattern, but only around the tract endings and edges.

In order to look into that change in more detail, we also show example visualisations for the second case, when different regressors are used. That is, we

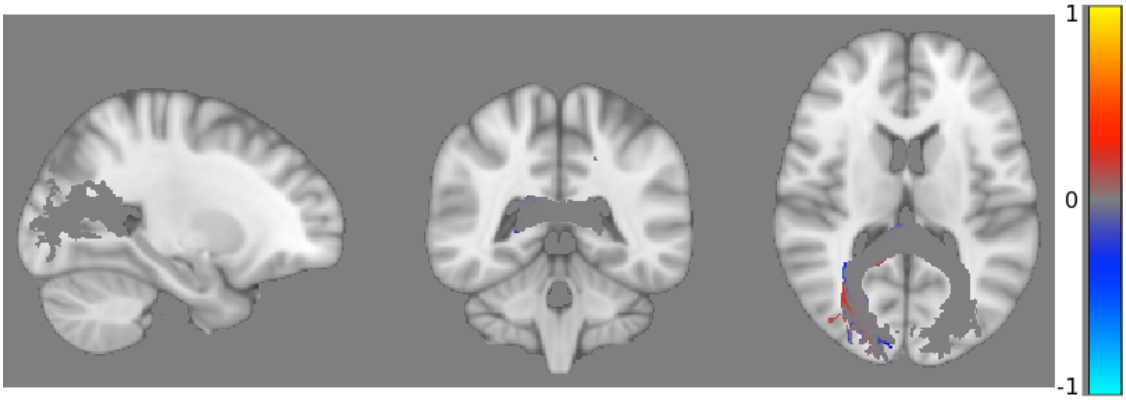

Figure 5.5: Scaled β values from the voxelwise GLM comparison between cases of presence and absence of WMHs for the FMA tract with correction for age and sex.

form separate contrasts for each of the WMH, age and sex regressors such that 1 is assigned to the regressor under consideration and 0 to the other regressors, i.e. [0,1,0,0], [0,0,1,0], [0,0,0,1]. This is still the analysis run on the whole dataset (of 4998 UK Biobank subjects).

As examples, we show these results for the ILF (figure 5.6) and the STR (figure 5.7) in the right hemisphere. We chose to show the results on those two tracts instead of the FMA to allow for comparisons with results for other subsets of data, and we have no results for the FMA for the cases presented next due to there being no subjects without WMHs on the FMA tract in the smaller subsets. Results for the other tracts can be found in appendix E. For both the ILF and the STR in the right hemisphere, we observe some clusters of positive and negative betas for the WMH regressor and for sex, although they are not very strong.

Subset with a narrow age range In this part we present the additional analysis for the subset of the UK Biobank data with a narrow age range. The subset was selected in such a way that WMHs and age are uncorrelated, in order to see whether the results still hold for that group. We sampled a subset of 1010 subjects (over 20% of the data used in the thesis) that fall within a narrow age range, to ensure that there is no correlation between age and the total WMH volume for those subjects. Selected subjects were between 65 and 71 years old (inclusive). The results of the correlations between WMH presence and age, calculated using this subset were as

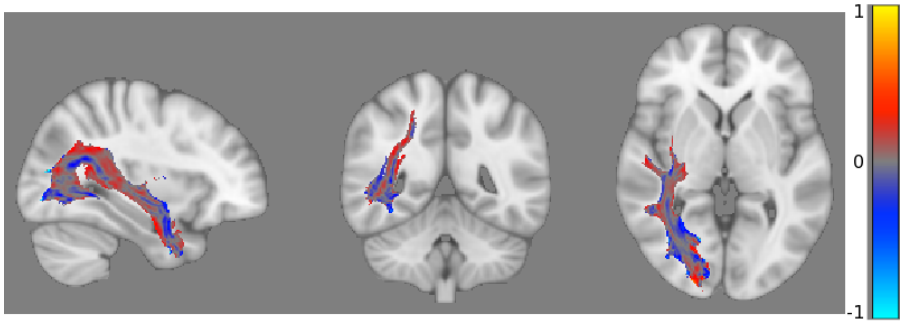

(a) Results for the case of the contrast focusing on WMH presence (default) for the ILF R tract on 4998 subjects.



(b) Results for the case of the contrast focusing on age for the ILF R tract on 4998 subjects.

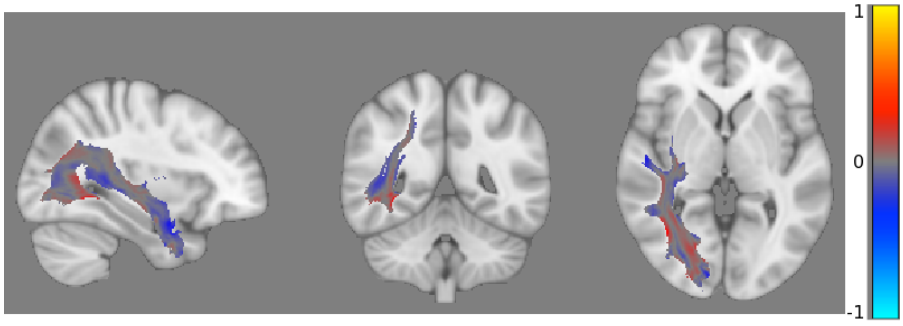

(c) Results for the case of the contrast focusing on sex for the ILF R tract on 4998 subjects.

Figure 5.6: Results showing the analyses for all 4 contrasts for the ILF R tract on the whole UK Biobank data subset used in the thesis (around 5000 subjects).

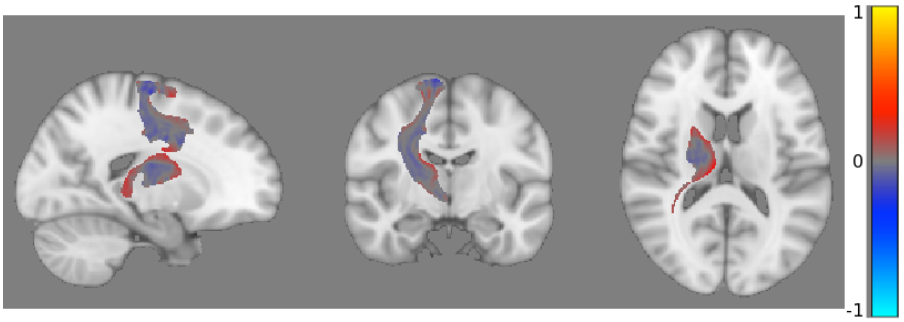

(a) Results for the case of the contrast focusing on WMH presence (default) for the STR R tract on 4998 subjects.

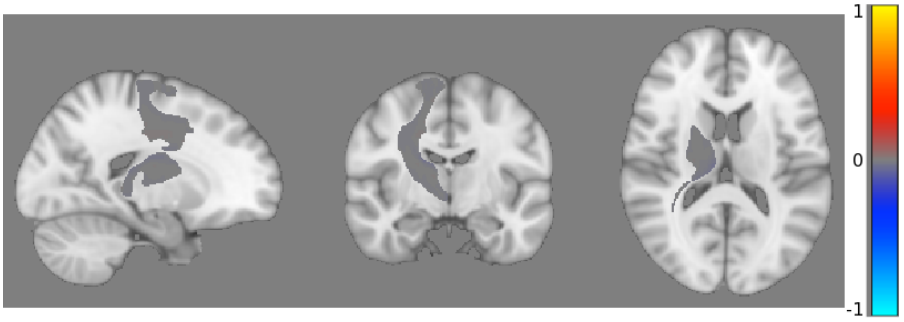

(b) Results for the case of the contrast focusing on age for the STR R tract on 4998 subjects.

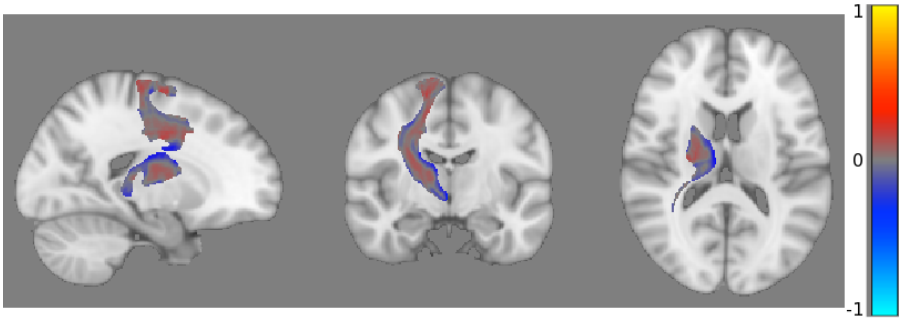

(c) Results for the case of the contrast focusing on sex for the STR R tract on 4998 subjects.

Figure 5.7: Results showing the analyses for all 4 contrasts for the STR R tract on the whole UK Biobank data subset used in the thesis (around 5000 subjects).

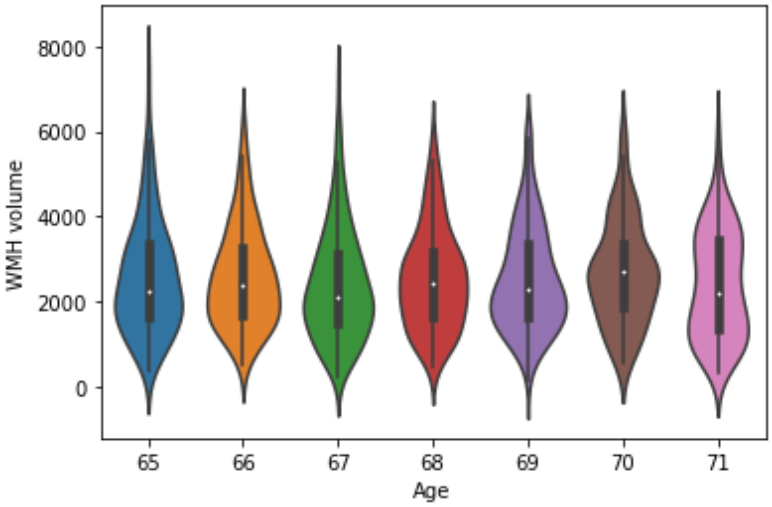

Figure 5.8: Distributions of WMH volumes (in mm^3) for each yearly age range used in the subset of data (1010 subjects).

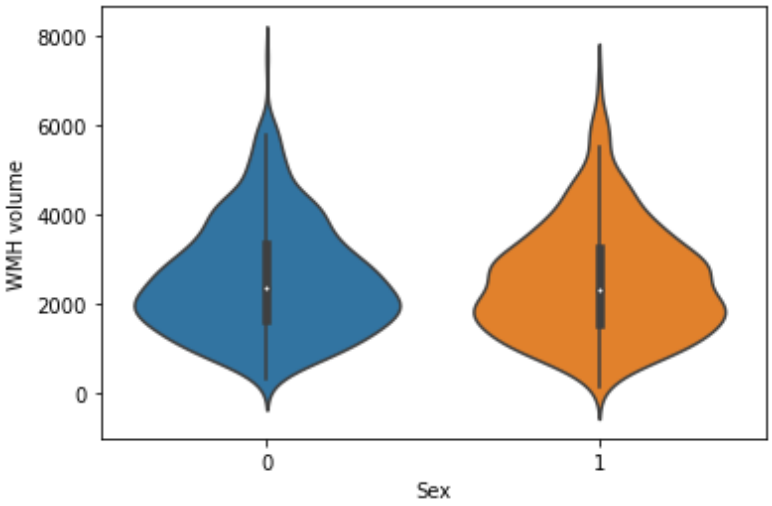

Figure 5.9: Comparison of the WMH volume distributions for each sex used in the subset of data (1010 subjects). WMH volume is in mm^3 and sex is coded with 0 being female and 1 being male.

follows: the Spearman correlation value for that subset was 0.005 with a p-value of 0.886, and the Pearson correlation value was: -0.006 with a p-value of 0.858.

Figure 5.8 presents the distributions of total WMH volume for the selected subjects for each age. Figure 5.9 presents the distributions of total WMH volume for the selected subjects for each sex. We performed a T-test to investigate whether there is a difference in WMH volume between the sexes, as an equivalent of calculating the correlation value for binary data. Results of the T-test were as follows: T-

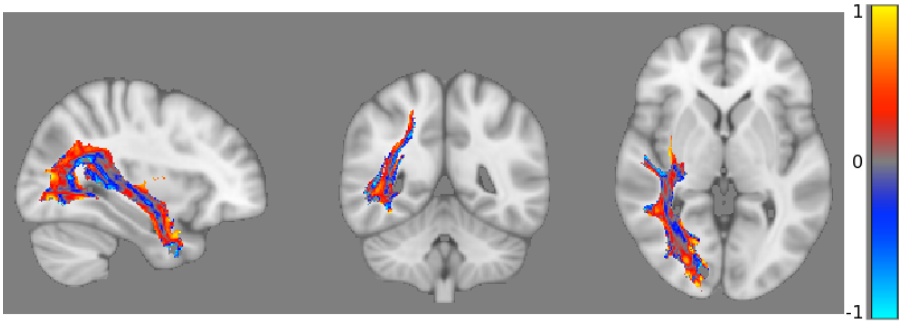

(a) Results for the case of the contrast focusing on WMH presence (the default contrast of interest) for the ILF R tract on the subset of 1010 subjects within a relatively narrow age range.

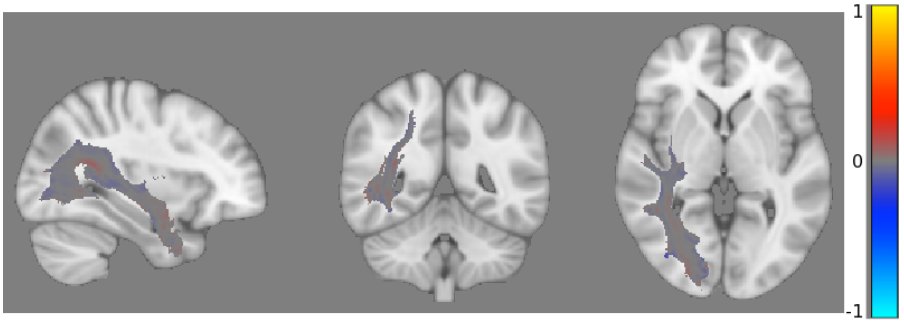

(b) Results for the case of the contrast focusing on age for the ILF R tract on the subset of 1010 subjects within a relatively narrow age range.

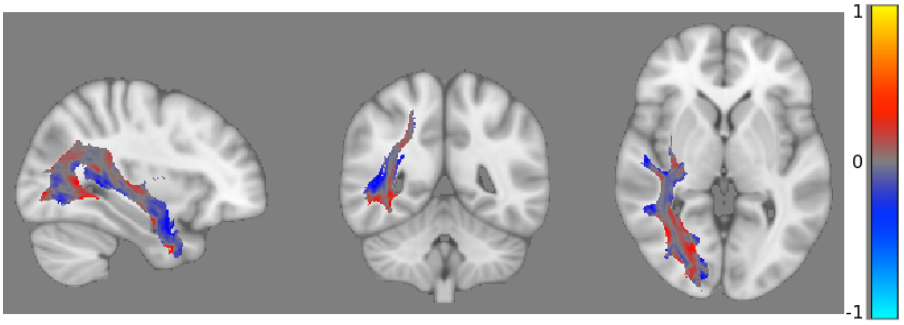

(c) Results for the case of the contrast focusing on sex for the ILF R tract on the subset of 1010 subjects within a relatively narrow age range.

Figure 5.10: ILF in the right hemisphere on the narrow age range subset.

statistic=−0.590, p-value=0.555. Therefore, there is no evidence to imply that the distributions of WMH volume differ between the sexes in this subset of data.

In figures 5.10 and 5.11 the results are presented in the following order from the top down in each tract's figure: first, the contrast with respect to WMH presence; second, the contrast with respect to age; third, the contrast with respect to sex. We included age for completeness, even though we would not expect strong results

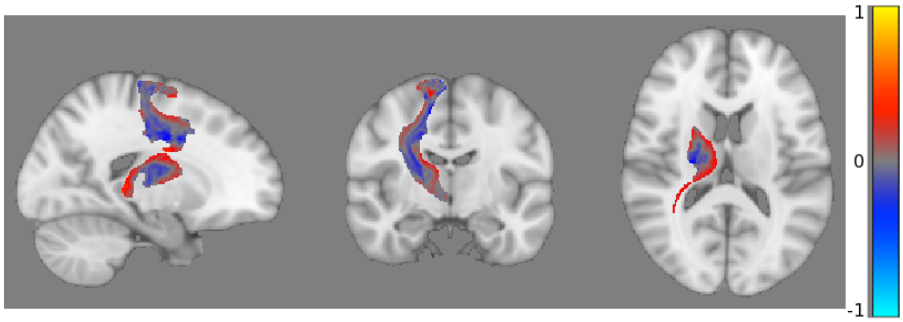

(a) Results for the case of the contrast focusing on WMH presence (the default contrast of interest) for the STR R tract on the subset of 1010 subjects within a relatively narrow age range.

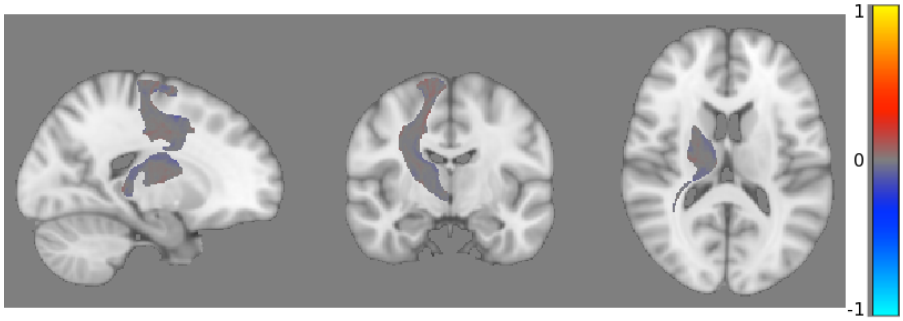

(b) Results for the case of the contrast focusing on age for the STR R tract on the subset of 1010 subjects within a relatively narrow age range.

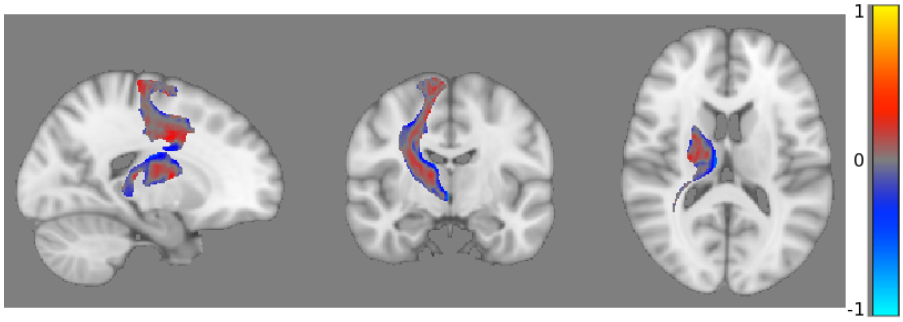

(c) Results for the case of the contrast focusing on sex for the STR R tract on the subset of 1010 subjects within a relatively narrow age range.

Figure 5.11: STR in the right hemisphere on the narrow age range subset.

for age here as we purposefully chose the subset from a relatively limited age range.

Figure 5.10 shows the results for the ILF tract in the right hemisphere using the subset of 1010 subjects of similar age, with no correlation between the age and WMH load. Again we visualise 3 different contrasts to investigate the method in depth, although of course we are eventually interested in the one focused on WMH presence on the tract. We can observe much stronger relative betas here compared to using the whole dataset of 5000 subjects. The contrast for sex is also stronger, and there is nearly no effect of age. For the STR in the right hemisphere (figure 5.11) we see a similar pattern: there are stronger effects in the WMH focused contrast when only a subset is used compared to the whole (4998 subjects) dataset (figure 5.7), nearly no effect for age, and moderate effect for sex. Additionally, we can see that the shape of the patterns of high (positive and negative) betas for WMHs and sex are very similar. The colours are opposite, however that should not be of interest, as sex was coded as a binary variable arbitrarily. That means that if we coded sexes with opposite numbers, we would get opposite signs of the effect for the sex contrast.

Single sex subset within a narrow age range Finally, we present the results for a dataset that is split even further, where a narrow age range subset is divided into two subsets with a single sex each. Here, we are only showing the results for the WMH contrast, as this is what we are interested in, but also because here we have removed the effect of age by using a narrow age subset with no correlation between age and WMH load (and corroborated by the previous age contrast results in the narrow age range set), as well as all the effect of sex by considering only single sex groups.

From figures for the ILF 5.12 and STR 5.13 tracts, we observe that the scaled effect is showing different patterns for different tracts. The patterns vary slightly between the two hemispheres but less than between different tracts. We can also compare these results with the previous results for the bigger datasets presented above. We observe that generally the effects are stronger now in the limited age and sex subsets.

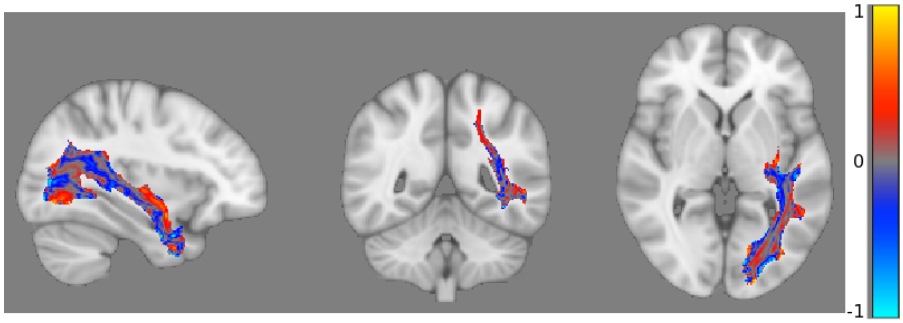

(a) Results for the case of the contrast focusing on WMH presence (default) for the ILF L tract on 523 female subjects.

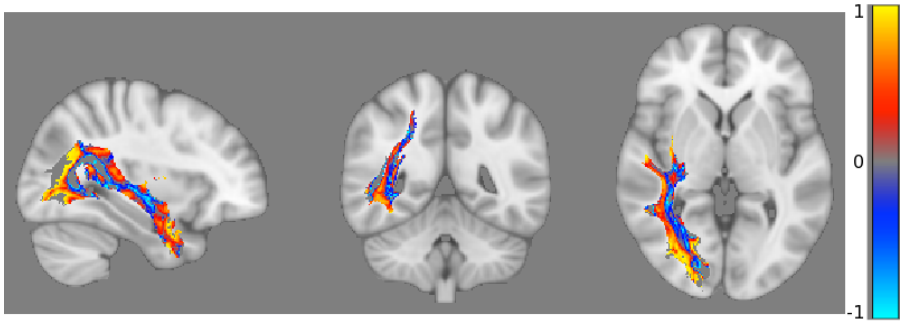

(b) Results for the case of the contrast focusing on WMH presence (default) for the ILF R tract on 523 female subjects.

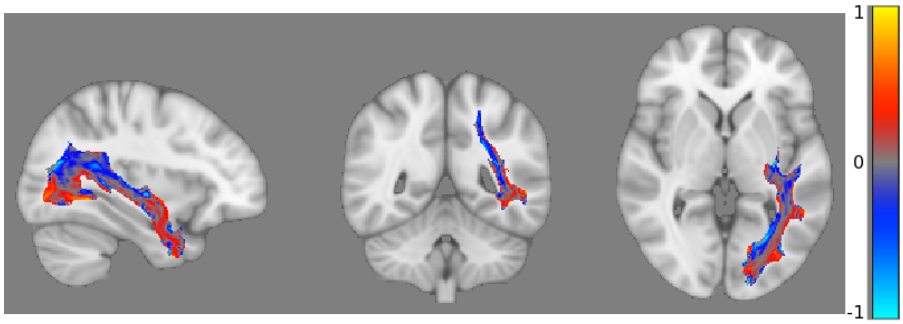

(c) Results for the case of the contrast focusing on WMH presence (default) for the ILF L tract on 487 male subjects.

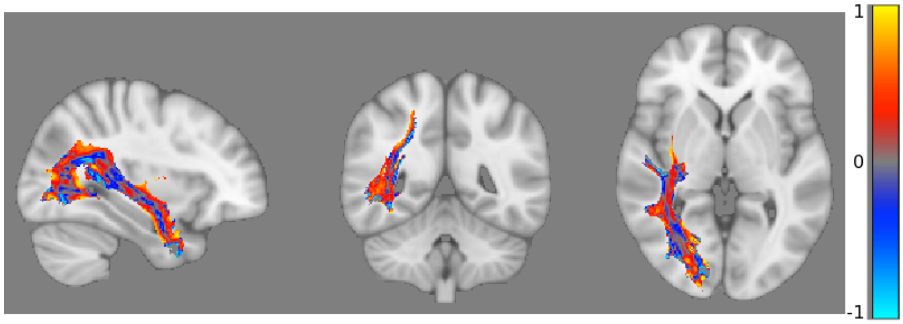

(d) Results for the case of the contrast focusing on WMH presence (default) for the ILF R tract on 487 male subjects.

Figure 5.12: Results for the case of the contrast focusing on WMH presence (default) for the ILF tract on a subset of subjects within a narrow age range and within single sex groups.

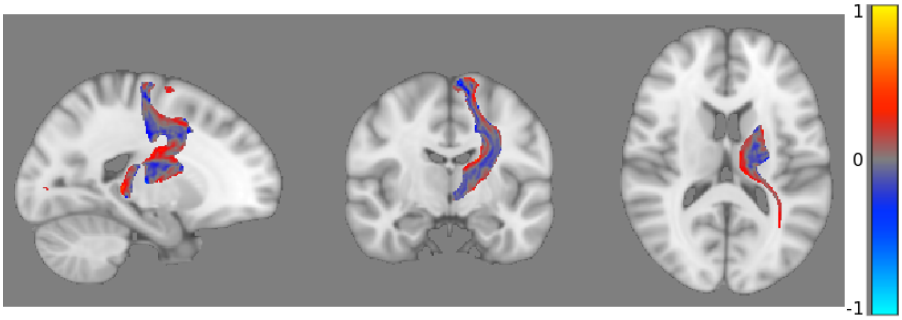

(a) Results for the case of the contrast focusing on WMH presence (default) for the STR L tract on 523 female subjects.

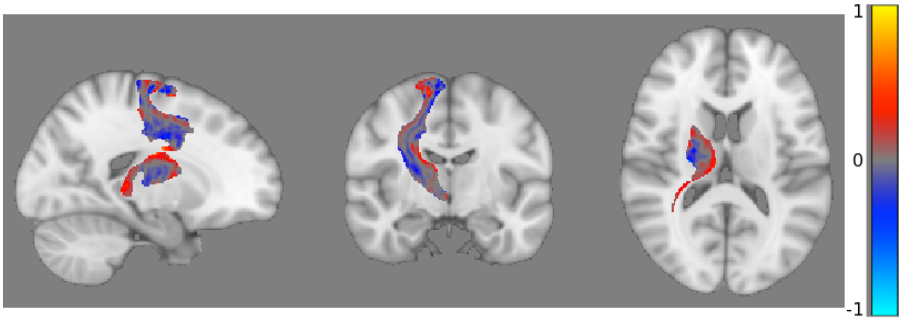

(b) Results for the case of the contrast focusing on WMH presence (default) for the STR R tract on 523 female subjects.

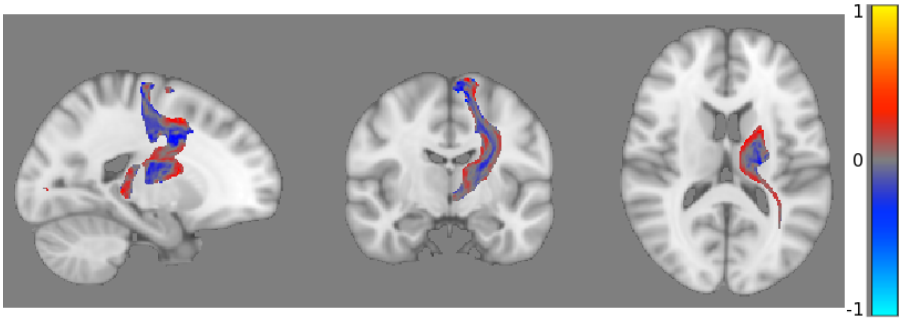

(c) Results for the case of the contrast focusing on WMH presence (default) for the STR L tract on 487 male subjects.

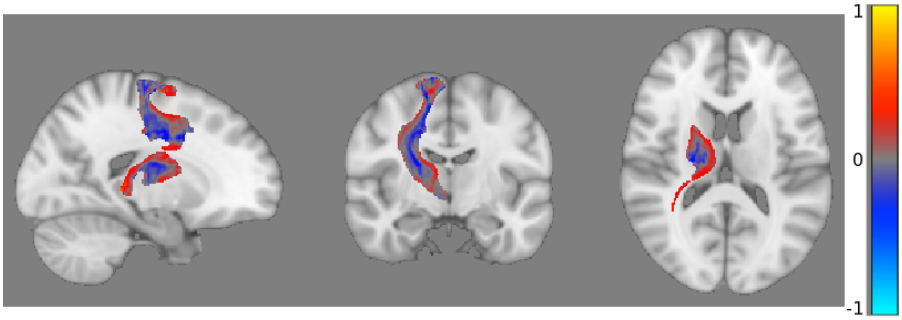

(d) Results for the case of the contrast focusing on WMH presence (default) for the STR R tract on 487 male subjects.

Figure 5.13: Results for the case of the contrast focusing on WMH presence (default) for the STR tract on a subset of subjects within a narrow age range and within single sex groups.

5.5.3 Discussion

The proposed method showed both positive (marked in red) and negative (in blue) values of the relative β. Results differ between the tracts, depending on the particular design matrix that is used. The important point with regard to all of the tracts is that we can observe spatial patterns of certain types: neighbouring voxels have similar values, and the change of the patterns is also quite smooth along the tract. This is very reassuring as in the method itself there was no enforcement of spatial smoothness or any postprocessing using the neighbourhood information. That means that it was possible for the neighbouring voxels to have very different values if the method was not reliable. Results however show otherwise, which suggests that the information obtained with the method is meaningful. The patterns observed are also typically similar between both hemispheres for the same tract and analysis settings, which is also reassuring.

Values used here were scaled in each voxel by the dividing by the mean tractography strength, which is averaged over subjects for each voxel. Scaling was done consistently, using the same values for all the analyses presented, which means dividing by the mean from the whole dataset, regardless of the size of the subset of data used for a particular analysis.

The results of the investigation of the voxelwise impact of WMH presence on the tractography results differed depending on what data was used for the analysis. Each of the three experiments was based on the same overall dataset, just using a more narrow or wide subset of the same 5000 subjects from the UK Biobank. We observed that the relative β values tend to be higher (on a positive or negative side) for the more narrow, smaller subsets of similar age and the same sex rather than in the bigger dataset.

In the first analysis, using a full dataset of 5000 subjects, when the design matrix X contained only binary information about WMH presence as well as the mean, we observed moderately strong effect sizes. That suggested that there is a voxelwise change in the tractography results, although it is not clear whether

that is due to WMH presence on the tract or some other factor like age or sex, that could be correlated with WMH load.

In the second analysis, also using the full dataset, but when the design matrix X also included age and sex regressors, we observe the effect to be split between WMH presence and sex regressors. The split might be coming from the interaction between the variables or driven by noise, though in the latter case this should be evident by a noisy spatial structure. The effect, even if split, does not dissapear – it can be still observed, thanks to the fact that we are looking at the estimated contrast of the parameter estimates. If we were looking at the statistics that divide the estimates by the expected variance, we might have observed that the results of the individual contrasts would disappear. That could have happened even if the contrast of parameter estimates was large, due to the large variance of the contrast of parameter estimates (related to the fact that the design matrix may contain highly collinear columns and so its inverse can contain very large values). The fact that the effect is split between WMHs and sex might suggest that there is very little or no age-related effect. However, when we performed a similar analysis on the subset of data where there is no correlation between age and WMH load, we observed stronger effects. That might suggest that there is some interaction or nonlinearity with age, and the effect might be stronger or weaker for populations of certain ages.

A valuable extension to this work would be repeating the analysis for narrow age range subsets of data with different age ranges and comparing the results between them. It might be the case that the relationships for different age ranges are opposite and cause the overall linear effect to fade. It is also important to mention, that for the analysis presented we did not use all the 65–71 year old subjects from the dataset but instead we sampled subjects within this age range in such a way that their WMH load and age were uncorrelated. It seems unlikely that this selection process would have a large impact on the results but in future work, it might be useful to double check that.

In the last version of the analysis, where we analysed subsets containing a single sex and within a narrow age range, we observed relatively similar patterns between

the sexes and hemispheres, but sometimes varying in strength between the sexes. That might suggest an interaction, as an observed effect is likely to be due to the WMH presence but its strength may be modulated by sex.

From the results presented in this work, it looks like the patterns of effect size for WMH presence and sex tend to be opposite, but that is just a matter of coding (0 as female, 1 as male), therefore if we swapped the coding of sex we would observe the patterns being similar. The interaction might not be the key to explaining the results but should be taken into account in future work. In general, there have been contradictory studies published in the literature, both reporting the effect of sex on the diffusion measures in ageing (due to a higher diffusion in the direction perpendicular to the tract) [79], as well as a lack of such an effect [80].

One of the limitations of this work is that we only included the most basic covariates of age and sex, but future work should extend to other relevant variables, for instance, related to cardiovascular health like hypertension, and interactions between those variables as well. Furthermore, future work could report other statistics, such as p-value, for the regions with high effect size, and take that into consideration when comparing the models.

It is not clear why in this work we observe the effect to partially disappear in the larger sample. It might require extensive future experiments to be able to answer that question with confidence. However, the observations from this work, such as larger age ranges resulting in weaker results, effects being split, and regressors possibly being correlated, should be highlighted, as they might be important for interpreting other large studies. Future analyses should also include some regressors to account for these possible effects.

Often, an observed pattern in the results from the WMH presence contrast would be that there are more positive (red) values closer to the centre of the brain and negative ones (blue) towards the outside. That could be interpreted as increased probabilities of voxels belonging to parts of the tract closer to the ventricles and lower tractography probabilities closer to the cortex in the case when WMHs are present.

It is not possible to rule out that it might be related to other white matter changes happening in the brain, for example, due to neurodegeneration. That could include atrophy or any real biological changes in neighbouring structures such as the ventricles. There might also be real biological changes related to the tract itself and its size or shape. They could impact the observed differences either directly or by the impact they have on tractography results, or a combination of both.

Another possibility is that such differences are driven by purely methodological factors. White matter varies more across individuals than, for example, gray matter structures. This may lead to residual misalignments across white matter tracts from different subjects, which appear as statistically significant differences, especially at locations close to tissue boundaries. To try and minimise this, we have used a non-linear registration approach [81], which was already part of the standard UK Biobank pipeline [18]. Non-linear registration approaches, thanks to their higher degrees of freedom, do a better job at registering brain structures across individuals, when compared to linear approaches [51]. It is important to mention that if the registration uses the T1-weighted images then some information about the white matter (its anatomy and pathology) will not be available to the registration, which may result in mis-registration. Such mis-registrations may either be random in nature or have a consistent bias, or a combination of both. In the case of a consistent bias that is related to the presence of WMHs at any location along the tract, there would be some pattern that could be observed in the results. These patterns would look like positive changes along one side of a tract and negative ones along the other side, in the case that the mis-registration was a translation of the tract. Alternatively, it could result in consistent signs on both sides of the tract, in the case that the mis-registration was due to a scaling of the tract, or just a change on one side, in the case of a combination of translation and scaling. However, all of these patterns may also be the result of true biological changes. To determine whether the observed changes are due to mis-registration or not it would be necessary to investigate alternative registration methods, especially ones

that could make use of the diffusion images and the information that these contain about the white matter structure. Future work should explore these issues further.

Discussion of potential alternative analysis approaches

In analyses like the ones presented here, there are different approaches that could be taken, resulting in slightly different variations of the results. As in many biomedical imaging problems, there is no ground truth here so it is not possible to delineate with certainty the actual white matter tracts for a particular individual. When asking the question whether the tractography is disrupted by the pathology, it might not be possible to disentangle the effects of pathology-related disruption to tractography modelling and diffusion data, pathology-related white matter tract displacement, or other effects, from normal inter-subject variability in tract shape. Depending on the research question, different analysis approaches might be more appropriate. In the case of this work there is a spectrum of methodological possibilities that could be considered, and subject-specific diffusion data might have larger or smaller influence on the results, depending on the choices made. On one end of the spectrum, it could be possible to use predefined standard white matter tracts from an atlas, registered to the subject-specific T1-weighted image, instead of relying on tractography modelling results. That approach would have the advantage of not using the potentially pathology-disrupted diffusion data – that is, it would result in standardised tracts, not impacted by potential problems with the diffusion acquisition, noise, and for small pathologies such as WMHs, unlikely to interact with the pathology itself. The disadvantage of such an approach would be that it would suffer from inaccurate anatomical localisation due to the fact that T1-weighted images lack details in the white matter structures. That could be solved by a hybrid approach, for example registering the standard predefined white matter tract to the structural image but also using the subject-specific FA map to drive the registration. That approach uses diffusion data, which could be disrupted due to pathology, like the WMHs. That disruption is of interest in the present work, but on the diffusion level does not necessarily fully represent subject-specific differences in the underlying

anatomical tract. At the other end of the spectrum are approaches that rely fully on the acquired diffusion data, by using it to run the tractography modelling in order to define the tract shape. These methods of segmenting the WM tracts are the most likely to be perturbed by the presence of pathology, such as WMHs. Therefore, it was deemed to be the most appropriate to be used in this work, as it should be the most sensitive test of the hypothesis, that the tractography results are affected by the presence of WMHs. Ifsubstantial perturbations were observed, the other two methods would be worth investigating as potential alternatives.

The results observed from the method used here suggests that it allows for investigation of the voxelwise variability between the tractography strength for two classes (e.g. with and without any WMH voxels on the tract), returning consistent, spatially smooth patterns of scaled effect sizes. However, the results for the analysed dataset of healthy participants from the UK Biobank suggest that the investigated relationships are not straightforward. Including age and sex covariates makes the effect seem very small, even in a large dataset such as this one. Therefore, in smaller samples, with less statistical power, the collinearity between covariates can reduce the reported results (compared to the effect size) and it would be unlikely that the effects discussed here would be a source of false positives for tractography. That suggests that the results from other studies are plausible to be valid on the whole. Nevertheless, this work suggests that effects of WMHs and other WM pathologies should be factored into analyses. In future, more work should be done to improve our understanding behind factors driving the effects here. Analysed relationships, at least for this population, do not seem to be captured well by the linear models that we used. In future work, other, more complex models should be tested as well.

5.6 Microstructural parameters analysis

The last section of this chapter explores the variability in the microstructural parameters in regions of the tracts affected by WMHs.

At the beginning of this chapter the question asked was whether there is impact on the tractography results due to the WMHs changing the microstructure. However,

as results above do not show very much difference it might be due to the actual lack of differences but also it would be possible that either the methodology is insensitive or there is just no change in the brain microstructure due to the presence of WMHs, so that there is no impact on the tractography results. Therefore here the distributions of average values among subjects of the microstructural parameters are presented from two models using the diffusion data. Those include FA from the DTI model [24] and OD, ICVF, ISOVF from the NODDI model [28].

5.6.1 Methods

In this analysis the distributions of average values of microstructural parameters within four mutually exclusive classes were compared. The first class contained the whole tracts with no WMHs, which was compared with the following classes defined by subsets of voxels in tracts containing WMHs: overlap of the WMH with tract, WMH proximity on the tract, and the rest of the tract.

WMH mask used here was defined as in the previous subsections. The tract mask used was thresholded at 0.001 and binarised, which is consistent with the subsection 5.4 of this chapter but different to the subsection 5.5.

To extract the values for comparison, firstly subjects were separated into the affected and nonaffected cases. As previously, that classification was done separately for each tract. For the nonaffected subjects, the values for all the voxels on the given tract were extracted and averaged for each subject. That became the first analysed class, shown on the left hand side in the boxplots below.

For the subjects with WMH overlap with the tract, the tract area is split into three separate classes. First class covers the area marked as a WMH – which in figure 5.14 is represented by the areas where yellow overlaps with blue. The second class includes the tract area in the proximity of WMHs but not within the WMH itself. That is defined by the dilation of the BIANCA mask with a $3mm$ kernel (voxel $\approx 1mm$) and is marked in figure 5.14 with the red colour. Therefore, this class is represented by the areas of overlap of red and blue from figure 5.14. Finally, the rest of the tract voxels (not overlapping with the two classes just described) constitute

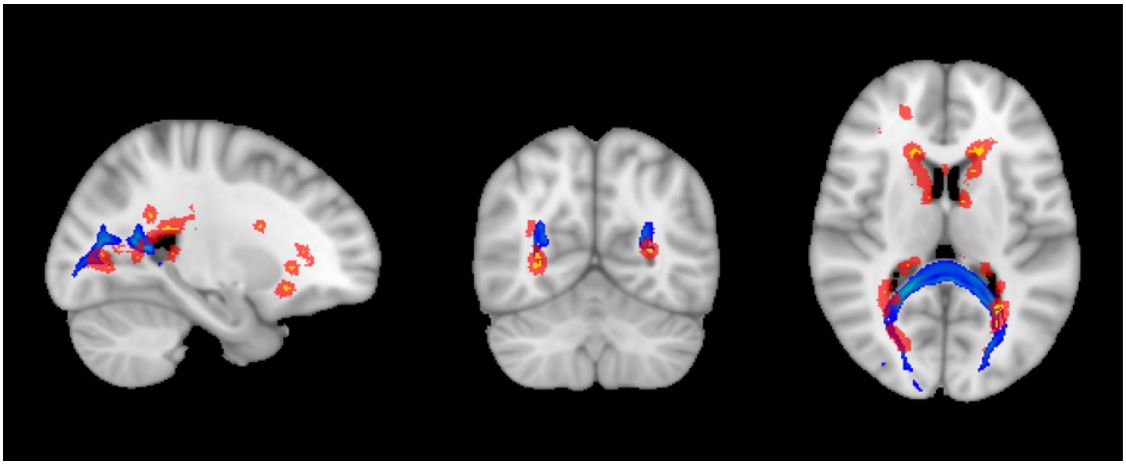

Figure 5.14: Visualisation of the three classes of voxels used for the affected tracts. The WMHs are marked in yellow and the areas in 3mm proximity around them are marked in red. The rest of the example tract is presented in blue.

the last class, that is shown in figure 5.14 in blue. As result, there were four mutually exclusive classes of voxels created. In plots presented below, each box represents the distribution of average values of a given parameter within a class for a given subject.

Two variations of this analysis were performed: (i) including all voxels; and (ii) including only voxels with a single fibre direction, as determined by ProbtrackX. This is important because NODDI, which parameters we also investigate here as well, is a single fibre model, as opposed to ProbtrackX. Therefore, this allows us to see whether crossing fibres or other 'problematic' cases could have affected our results and conclusions.

5.6.2 Results

Results for all voxels on the tract

FA Figure 5.15 shows the distributions of the average FA value for different parts of the tract. FA varies from just below 0.2 to just above 0.4 for most of the cases. From figure 5.15 it can be observed that the average FA drops (to different extents) in the WMH areas compared to the 'healthy' tissue for most of the tracts (apart from ILF R, PTR R and STR in both hemispheres). The most pronounced difference is visible in the FMI.

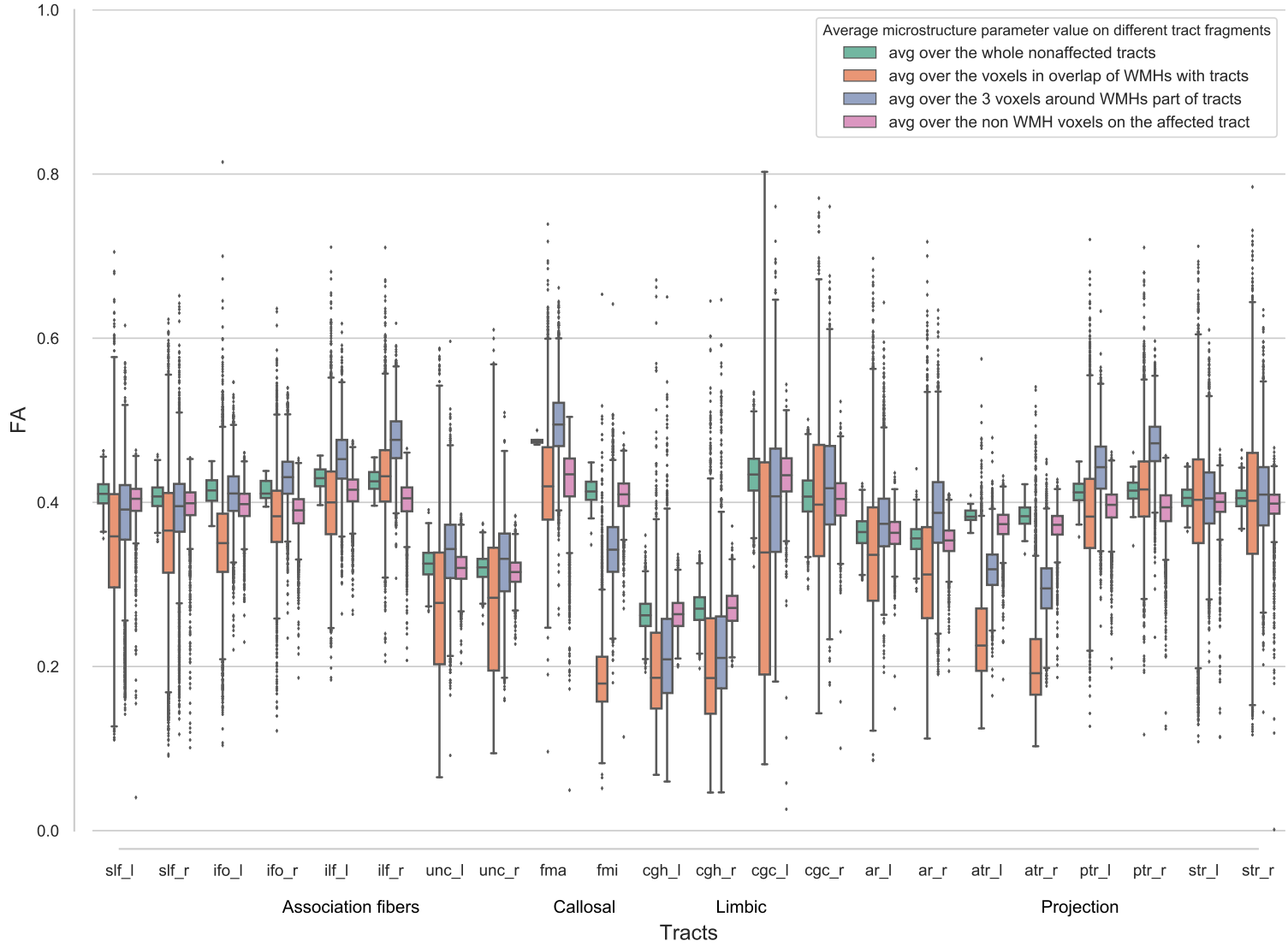

Figure 5.15: Comparison of average FA between the classes.

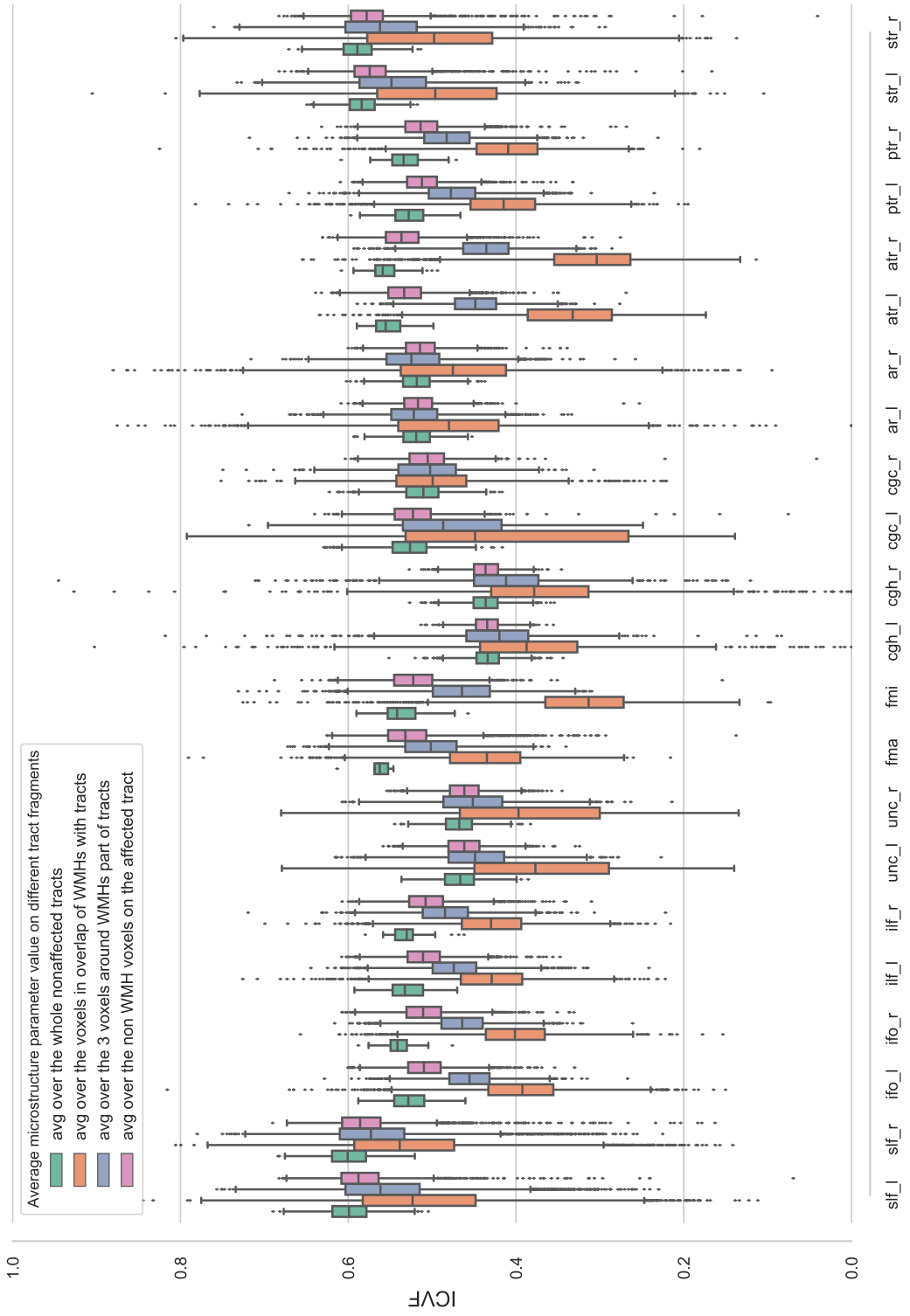

Figure 5.16: Comparison of average ICVF between the classes.

ICVF Similarly, FMI together with ATR, which is also in the frontal part of the brain, show the biggest drop in ICVF for the WMH voxels compared to non WMH voxels (figure 5.16). A substantial decrease is also visible in PTR and IFO. For the region around the WMH compared to in WMH itself, ICVF then increases for all tracts but one. The values vary from around 0.3 to around 0.6, with most of them being around 0.5.

ISOVF From figure 5.17 we can observe the increase of ISOVF in WMH areas compared to the non-affected tract measures for all the tracts but STR, CGC R, and UNC. The most pronounced changes are visible in FMI, CGH, and AR. For the tracts that show that increased values in WMH voxels, the values for the voxels in proximity of WMHs are between the values for WMH and non-WMH voxels. That suggests that there the presence of hyperintensities might be affecting the free water diffusion in and around the WMH areas.

OD Looking at figure 5.18 we can see that in general, the OD values tend to be in the range from 0.1 to 0.5, mostly around 0.25. This agrees with the values that are presented in the literature. For the non-WMH voxels the values stay at this level for PTR and STR as well as all the association fibres apart from UNC.

Summary To make it easier to see the trends and compare them between the parameters, the same results are presented in appendix F, where they are averaged over both hemispheres.

It can be seen that there are decreases in FA in the WMHs areas, which coincidence with the decrease in the ICVF and increase in the ISOVF, which might be a sign of axonal loss. In the WMH area OD decreases as well in all the association fibres and most of the projection ones (apart from ATR). If there is axonal loss, then it might mean that the remaining fibres show less dispersion.

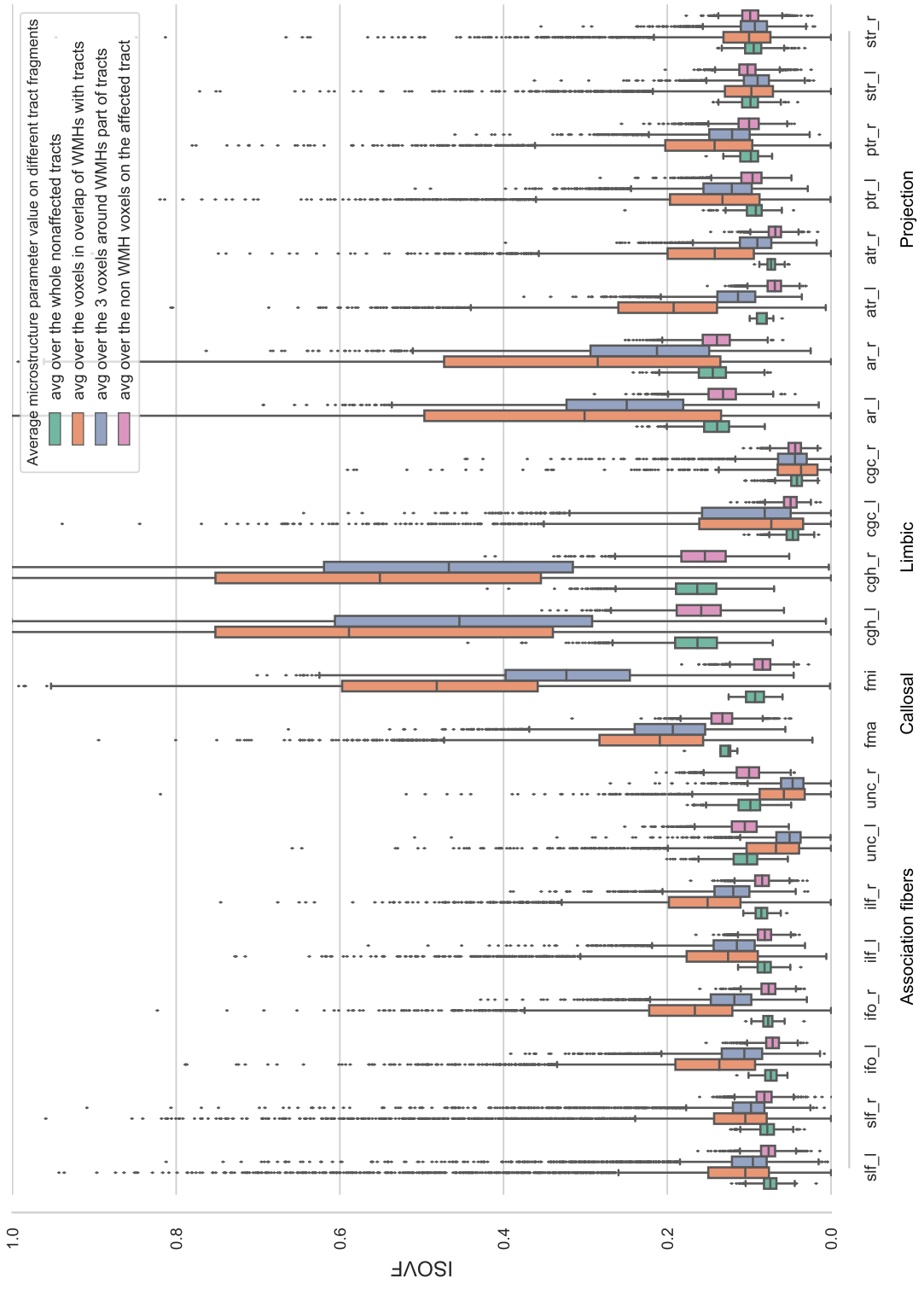

Figure 5.17: Comparison of average ISOVF between the classes.

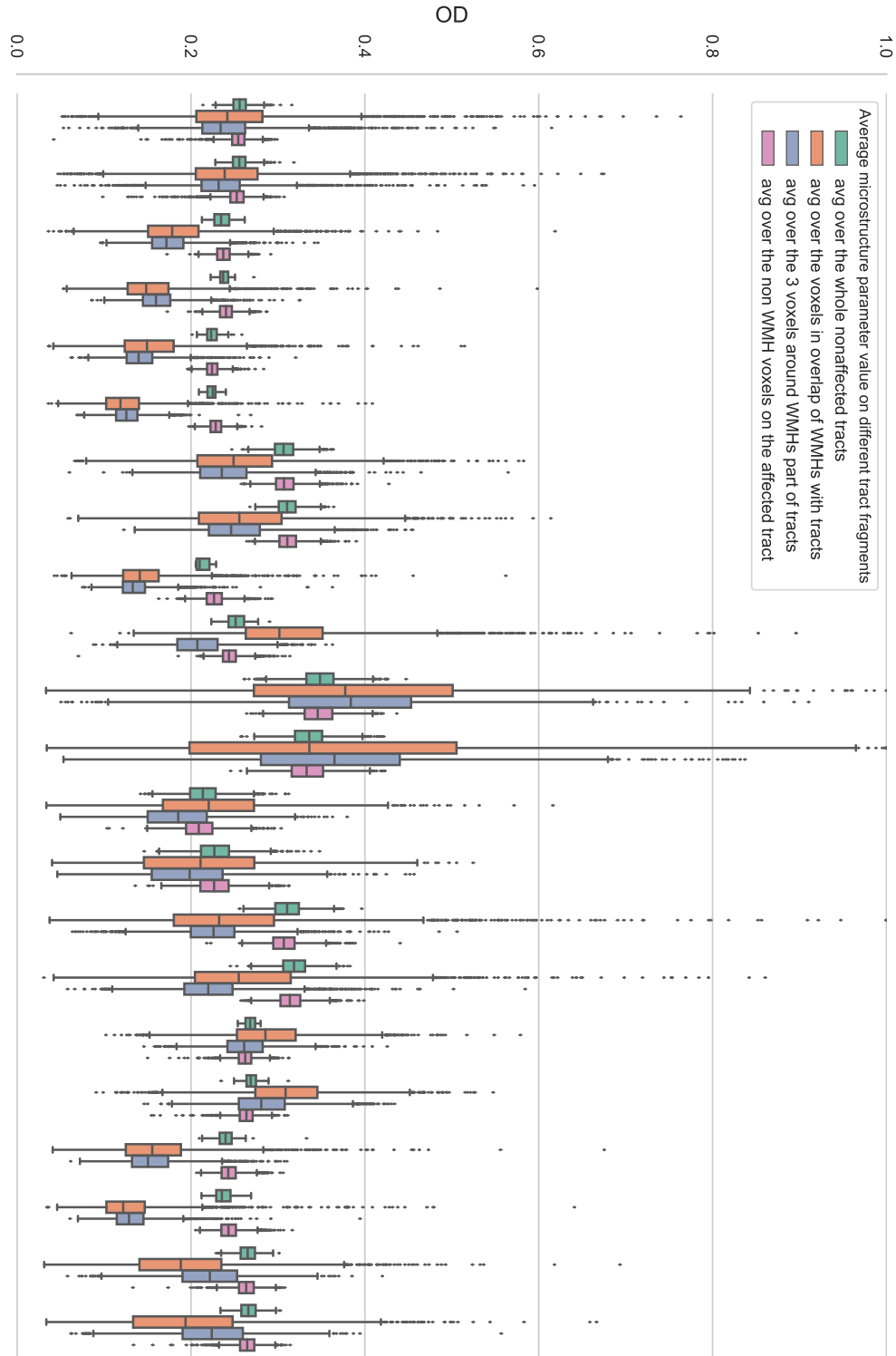

Figure 5.18: Comparison of average Orientation Dispersion (OD) between the classes.

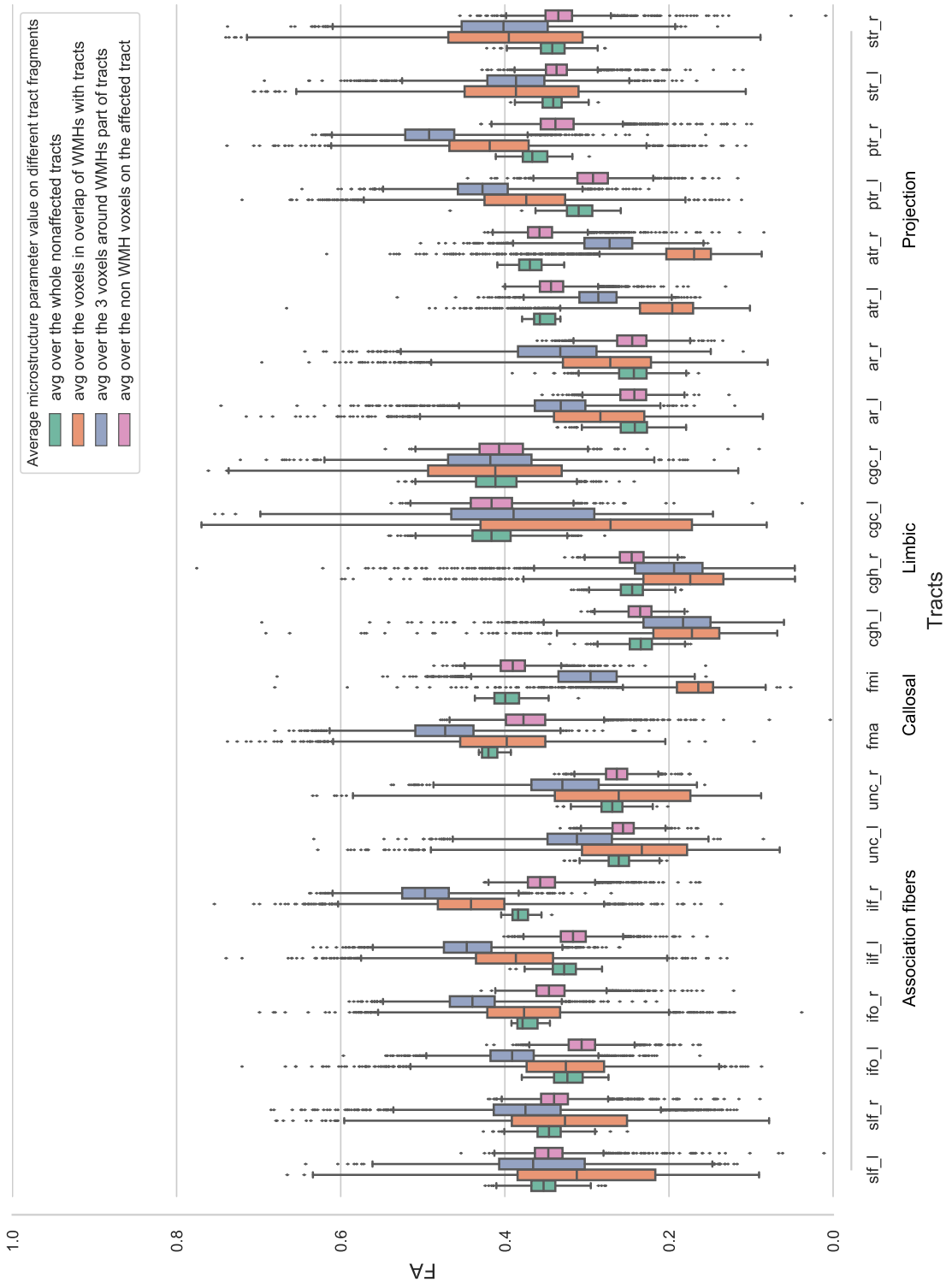

Figure 5.19: FA parameter values using only voxels that support a single fibre direction.

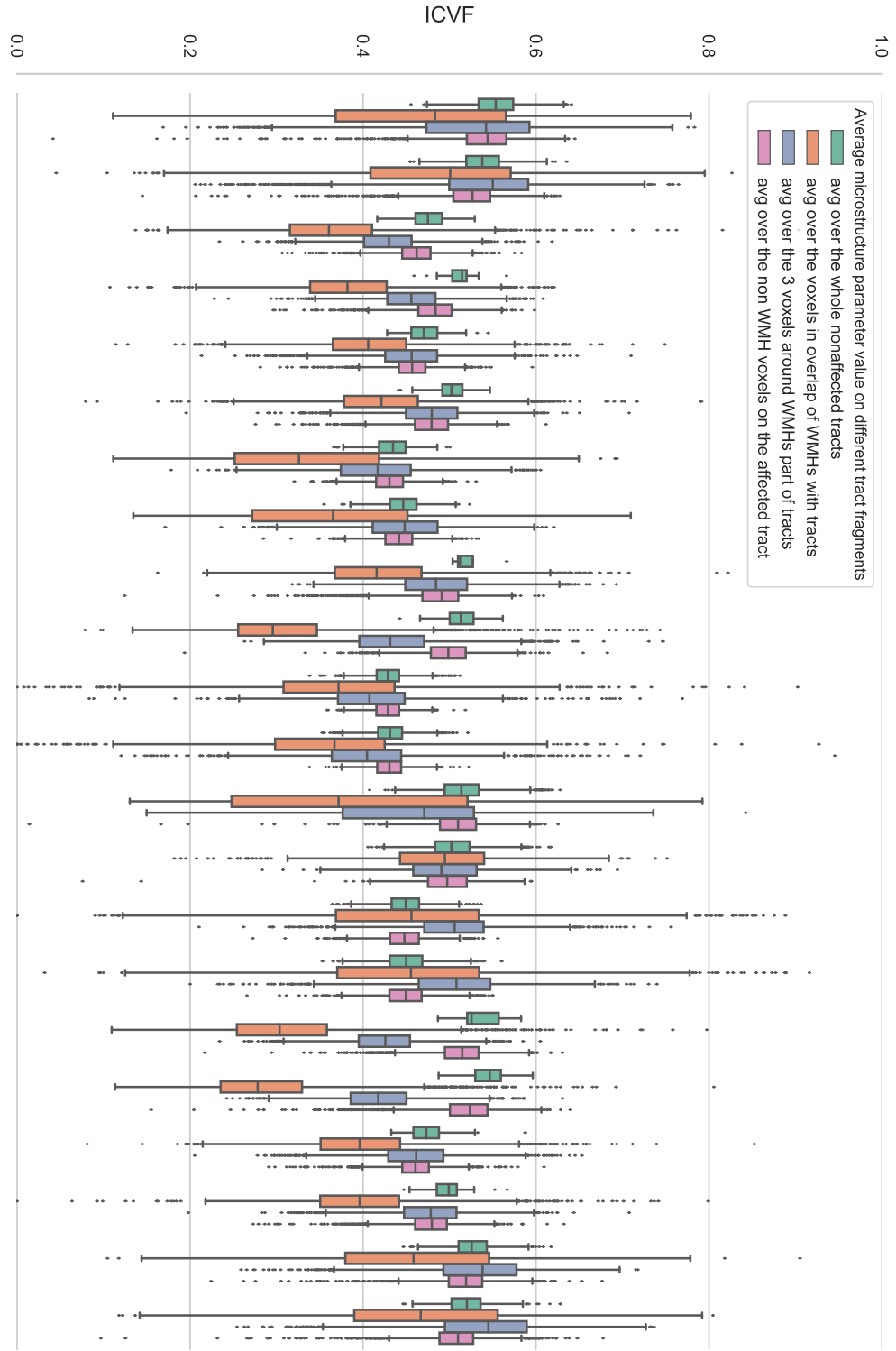

Figure 5.20: ICVF parameter values using only voxels that support a single fibre direction.

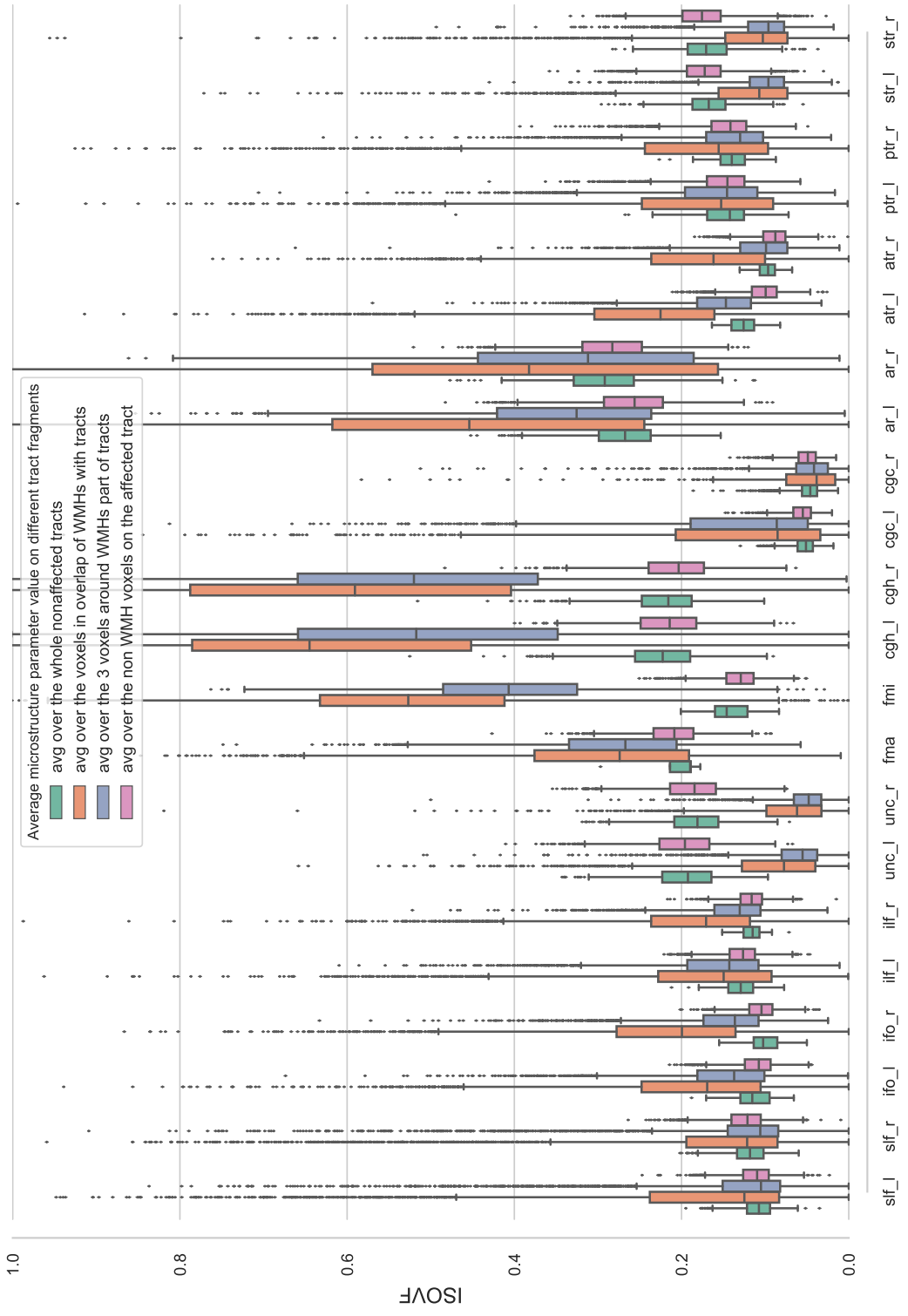

Figure 5.21: ISOVF parameter values using only voxels that support a single fibre direction.

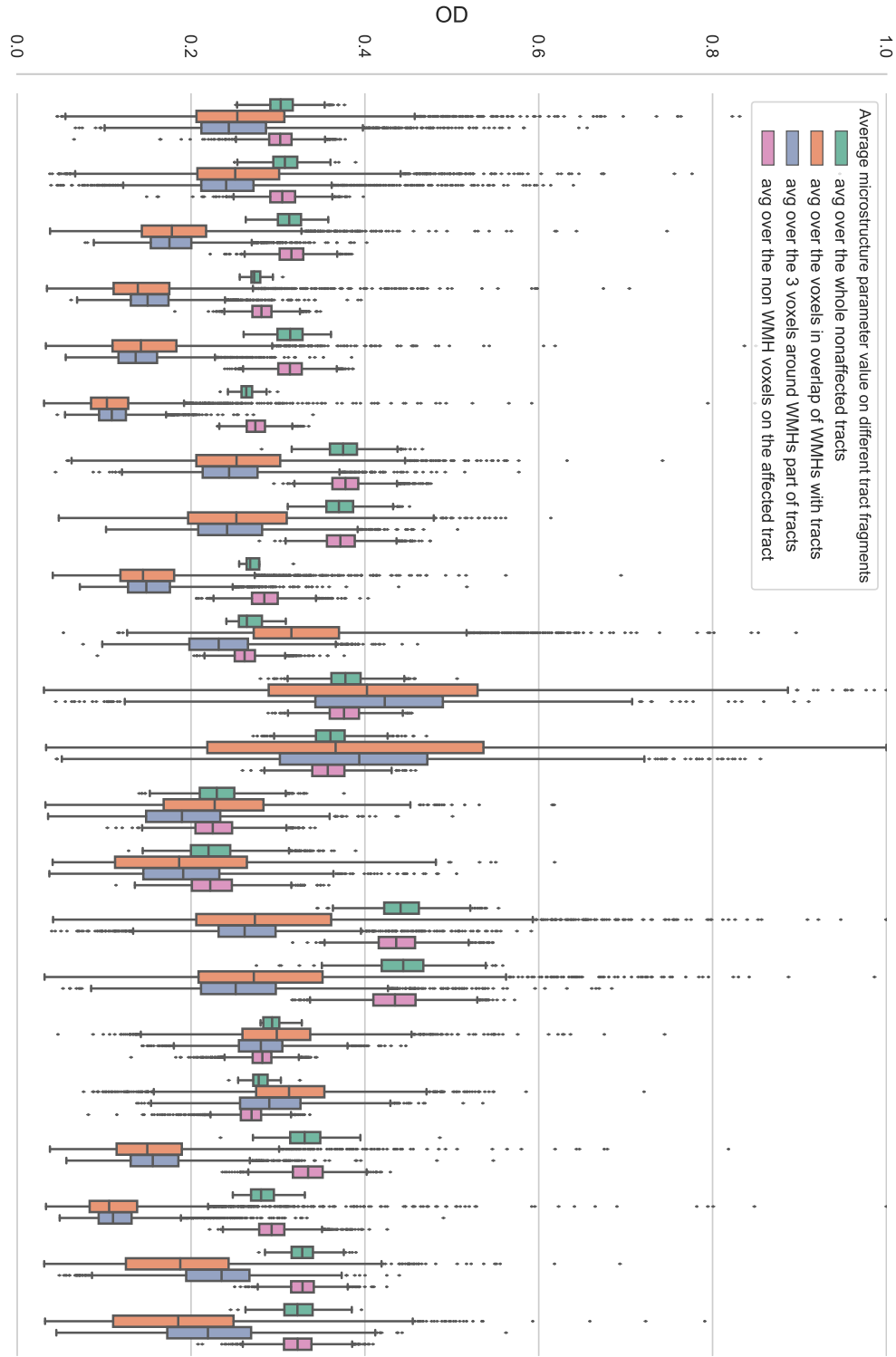

Figure 5.22: OD parameter values using only voxels that support a single fibre direction.

Results for voxels with only single fibre fitted

FA values seem to be generally lower, when taking only single fibre voxels into account – see figure 5.19. Also for ICVF (figure 5.20) the observations are similar to the ones for all the voxels. Also, in general for most of the cases the ICVF values are smaller than when are all the voxels included in the analysis. In general, figure 5.21 looks quite similar to the one including all the voxels, although the values tend to be slightly higher in this case. Figure 5.22 again looks very similar to the previous OD plot (for all the voxels). One thing that differentiates these plots is that in most of the tracts the IQR is slightly higher when using only single fibre voxels.

In general, there are differences in IQR (size of boxes and whiskers) for the values between the classes (colours). Those can be explained by the fact that there was a different number of voxels used to calculate each subject-wise average for each given class (i.e. there are fewer voxels within the WMHs on the tract than outside, data not presented here). Similarly, differences in IQR for certain classes between the tracts can be explained by the different number of subjects classified as affected for different tracts (see table 5.1) . It might be also worth noting that there were far fewer voxels taken to calculate the points to the second series of figures (5.19 to 5.22). Despite the concern that this difference might cause the results to be less reliable, in the end it can be seen that the results are similar, therefore the single fibre voxels analysis supports the previous part.

5.6.3 Discussion

The results show that the microstructural parameters in the areas of the tract marked as within and in the proximity of the WMHs are different than the rest of the tract. The effects are stronger strictly in the WMH area compared to just outside of it. At the same time, even for tracts that contain WMHs, the part of the tract that is not in the near proximity to the WMHs rarely shows values deviating from the ones for the nonaffected tracts.

The fact that the results for WMH proximity are often between the results for averages within WMHs and the rest of the tract suggests that it might be worth,

in the future, doing a more detailed analysis comparing separately the parameters in the distance of one, two and three millimetres from the WMHs border. As it was suggested in the literature [46], the patterns of diffusion characteristics along the tracts might be related to distance from WMHs.

It could also be possible to expand the analysis to other microstructural parameters. For example, thanks to the Bayesian framework used to estimate fibre orientations using FSL's BEDPOSTX, it would be possible to investigate the uncertainty of the spherical polar coordinates of the samples from the principal fibre direction distribution. That kind of analysis would be more focused on the model fitting aspect than the current use of OD values, as OD is not used in the fibre tracking algorithm. To conduct such an analysis it would be necessary to first address the problem that it is not currently possible to identify (a posteriori) which estimated fibre population is consistently used to track a specific fibre tract in a probabilistic tractography algorithm. Therefore, it would be necessary to design an algorithm to match fibre populations within the same voxel to be able to compare the spherical polar coordinate uncertainties. Currently, the presented work uses the OD estimate from the NODDI model as an approximation of such uncertainties. OD aims to quantitatively capture the degree to which fibres disperse around the main estimated axis, while spherical polar coordinate uncertainties taken from BEDPOSTX estimates would require some filtering or processing to avoid them being a complicated mix of fitting errors from a multi-fibre model, the underlying fibre dispersion and image noise. Although OD is also influenced by image noise, it is easier to interpret and not tied to the more complicated tractography modelling, including the model selection aspect. Therefore, in future work, expanding the analysis to include the BEDPOSTX spherical polar coordinate uncertainties, although more complex, would be a valuable additional analysis, as those parameters would be derived from the same model that had been used for tractography modelling.

The size of the parameter differences between the WMH area and outside of it varies greatly between the tracts. It would be interesting trying to explain why it is

the case. Of course, the number of WMHs, their volume and volume of the tract differ between the tracts as well. That is consistent with the literature, where it was reported that the most affected tract is FMA, then PTR, IFO, FMI and ILF [54]. It is not clear, however, how that would introduce such a variability. It might be worth checking whether the WMHs in deep white matter show different effects than the rest.

5.6.4 Conclusion

As expected from the literature, the microstructure in WMH areas is altered, with ISOVF increasing and FA, OD, and ICVF decreasing for most of the tracts. The size of effects varies largely between the tracts.

5.7 Summary

This chapter focused on investigating whether the presence of the WMHs on the WM tracts substantially affects the results of tractography modelling. The analysis shows that despite the altered microstructural parameters in the WMHs areas, and voxels in their proximity, the final tract shapes do not vary much from the tracts with no WMHs based on the Dice index analysis. The method we proposed to investigate the tractography strength in particular voxels for subjects with WMHs shows patterns of differences that are likely to differ with age and sex, and might be driven by biological changes or methodological interactions or both. Although there is evidence of some changes in tractography related to WMHs, the lack of strong changes in the centre of the tracts when analysing a broader age range, with covariates for age and sex, suggest that in smaller studies the statistics are probably not going to be impacted strongly, because of reduced power relating to smaller sample sizes and correlations between regressors. This work suggests that the investigated relationships are not straightforward and are not captured well by a linear model, and thus further investigations into these effects are warranted.

In the next chapter, the same methodology is adapted to be applied to the Multiple Sclerosis subjects data. There, in contrary, MS lesions are signs of more

severe damage to WM than age-related WMHs in healthy brains but the number of available scans for analysis is substantially lower.

6

Tractography in the presence of Multiple Sclerosis lesions

Contents

6.1 Introduction 117
6.2 Background 118
6.3 Data 119
6.4 Methods 122
6.4.1 Preprocessing 122
6.4.2 Applying previously developed methods to MS data . . 123
6.4.3 A modified method for MS data – creating two binary classes 124
6.4.4 A modified method for MS data – using the lesion load 127
6.4.5 Additional analysis with healthy controls 127
6.5 Results 128
6.5.1 The two classes approach 129
6.5.2 The scaled lesion load approach 130
6.5.3 Additional analysis with healthy controls 132
6.6 Discussion 133
6.7 Summary 136

6.1 Introduction

Although the White Matter Hyperintensities typically observed in ageing and vascular disease have a different pathogenesis from Multiple Sclerosis lesions, both

of those changes may have a similar appearance [82]. Multiple Sclerosis lesions are usually more prominent than the WMHs of vascular origin. Therefore, their impact on tractography has been already studied much more extensively in the literature.

Using our proposed methodology to assess the potential impact of hyperintensities in white matter on tractography results, which was presented in previous chapter 5, as well as capitalising on the availability of a small dataset of scans of MS subjects collected with the same protocol as the UK Biobank data used in the previous chapters, this chapter aims to explore the potential of translation of selected methods proposed in this thesis to MS subjects.

6.2 Background

In Multiple Sclerosis some of the changes, e.g. non-lesional damage and cortical damage, are not visible on conventional MRI. It also can not distinguish between oedema, demyelination and axonal loss in observed lesions, which vary in their clinical significance. One of the techniques increasingly used to study Multiple Sclerosis [76] is tractography.

Tractography is performed in patients with Multiple Sclerosis with the hope that it can add useful information to conventional imaging. It has the potential to provide novel quantitative measures of pathologies leading to disability, improving the prediction of the clinical disability, compared to approaches based only on standard clinical diagnostic tools. This can be particularly useful in the case of analysis focused on white matter tracts and their contribution to functional changes, as connectivity measures based on tractography were shown to correlate with disability better than FA [76].

The presence of MS lesions can be a potential obstacle in correct tract path estimation [76]. In general, in the white matter of multiple sclerosis patients, the diffusivity is higher and fractional anisotropy is lower than in the white matter of the healthy individuals [83]. Reduction in the FA value is most prominent in the MS lesions but, thanks to studies based on diffusion MR imaging, it was shown that these values are also abnormal in so-called 'normal appearing white matter' [83].

The fact that FA is lower than normal can result in termination of the tractography-led path too early or cause errors around the lesion areas [76]. This is because low values of FA are one of the two most often used rules in tractography algorithms (next to the high curvature of the streamline) to stop streamline propagation [13].

Recently, Lipp and colleagues [84] have focused on the effect on tractography in the presence of MS lesions, where they investigate the topic in much more detail. Their approach uses both real data for 135 participants (T1-weighted, T2-weighted FLAIR, and diffusion scans), as well as simulated diffusion data. Their analysis was conducted only on two tracts: the cortico-spinal tract (CST) and the arcuate fasciculus (ARC, which historically was believed to be part of the SLF tract discussed in this thesis, but it is a different, separate tract [85]). One part of their analysis was similar to the analysis presented in the first section of the previous chapter 5.4. For 29 patients and 19 matched controls, they had the tracts defined based on the diffusion data twice: manually dissected (virtually), as well as extracted the specific tracts from the whole-brain tractograms. Then, they calculated the anatomical overlap between them, expressed by a weighted Dice coefficient, and reported 'modest anatomical correspondence'. Following this they report that MS related abnormalities affect fibre orientation distributions estimation. The effect on the reconstruction was dependent on the algorithm used: in case of the tensor-based approach, there was observed early termination of the streamlines, while in case of the constrained spherical harmonic deconvolution the impact was visible as spurious streamlines. Despite that, and the high prevalence of MS lesions in the CST and ARC regions, Lipp and colleagues showed that the tract segmentations results were not affected, and lesions were not found to be omitted by tractography algorithms.

6.3 Data

Multiple sclerosis subjects

Data used in this chapter consisted of scans of 15 subjects with relapsing-remitting Multiple Sclerosis, provided by Dr Silvia Messina. All subjects were Caucasian, aged between 31 and 56 (with average age of 44 years old and standard deviation of

Table 6.1: Total lesion volumes for each MS subject. Presented numbers are based on manual annotations of the lesions by a clinical expert on the T2-FLAIR images.

Subject identifier	Total volume [voxels]	Total volume [mm^3]
006	39001	21602.41
008	52800	29245.61
017	12473	6908.72
039	16440	9106.02
041	6510	3605.85
045	45428	25162.31
049	17108	9476.02
053a	8018	4441.12
054a	107842	59733.08
055a (excluded)	59347	32871.94
056a	17002	9417.31
057a	10800	5982.05
063a	15013	8315.61
065a	8924	4942.95
077a	11430	6331.01

6.5 years), there were 8 female subjects. We used the T2-weighted FLAIR scans for lesion delineation, diffusion-weighted MRI scans for structural connectivity analysis. T2-weighted FLAIR MRI scans had a spatial resolution of $0.43mm$ x $0.43mm$ x $3mm$ and dimensions: 512 x 512 x 48, while the diffusion MRI scans had resolution of $2mm$ x $2mm$ x $2mm$ (field of view $210mm$ x $210mm$, 72 slices). Diffusion data were acquired with 100 diffusion directions (50 $b = 1000s/mm^2$, 50 $b = 2000s/mm^2$, 8 volumes with no diffusion weighting), repetition time of $3600ms$, echo time of $92ms$. The scans were acquired using a 3 Tesla MRI scanner. The diffusion data acquisition protocol was based on the protocol of the UK Biobank [5], which was used in the previous chapters. This should allow the methodology developed in the previous chapters to be used with only minimal modifications. One of the subjects (with an identifier 055a) was excluded from further analysis, due to problems with their diffusion imaging data. Therefore, the analysis was done for 14 subjects. Characteristics of lesion volumes for all the subjects are presented in table 6.1. The spatial distribution of the lesions for the 14 subjects is presented in figure 6.1.

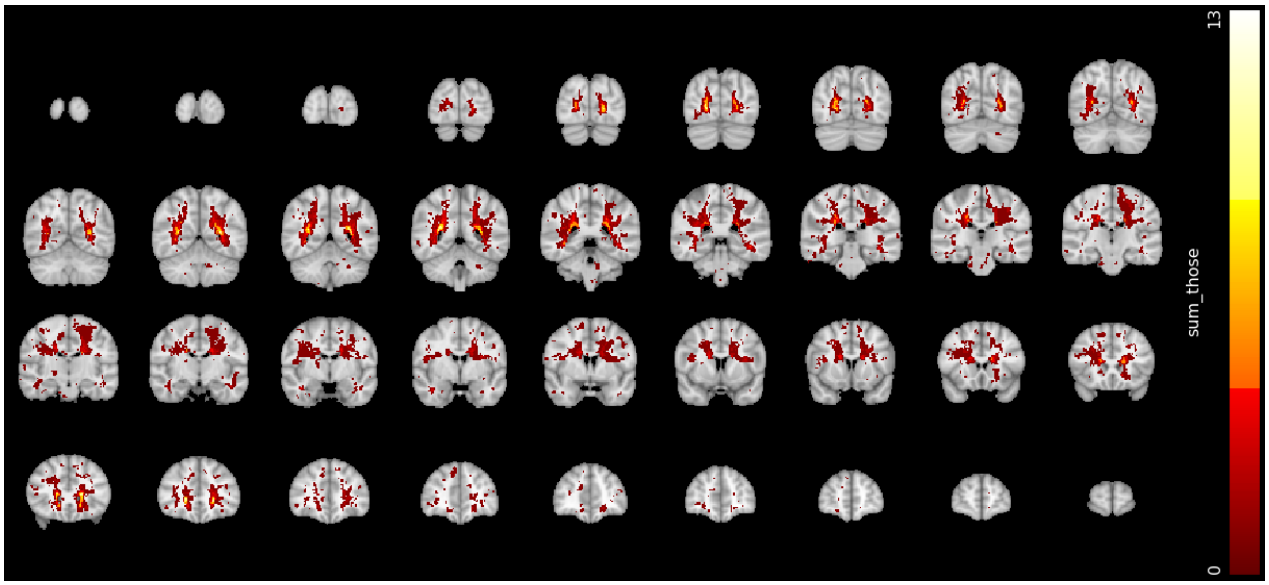

(a) Coronal view.

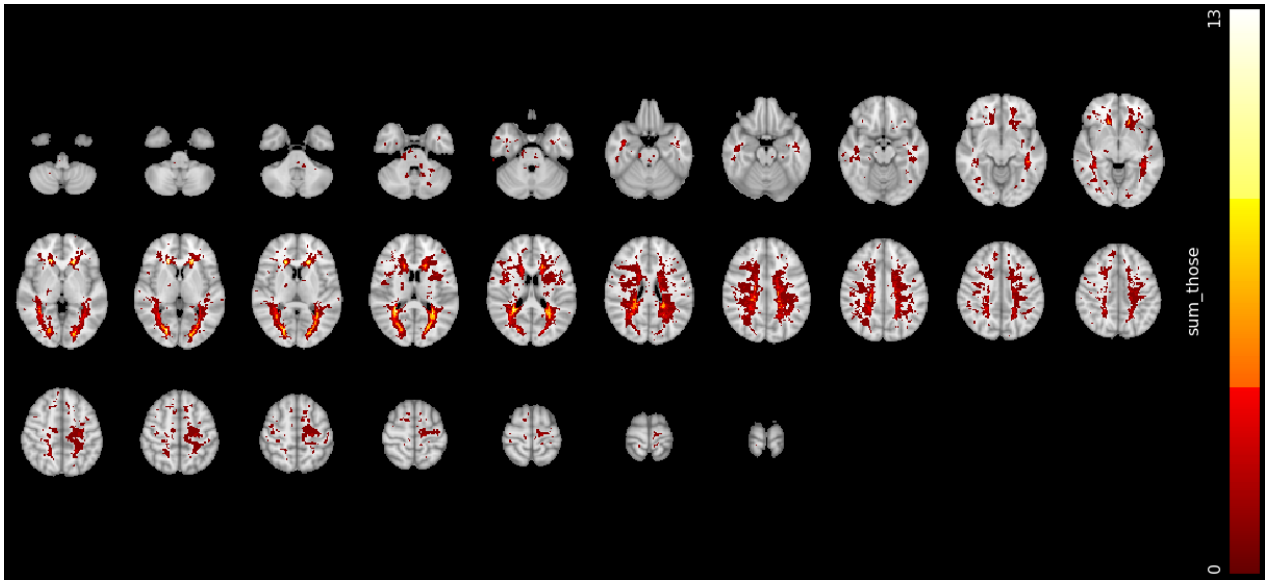

(b) Axial view.

Figure 6.1: Sum of the lesion masks across 14 subjects. Colour scale indicates the number of subjects that had a particular voxel classified as a lesion, with the numbers varying from 1 (in dark red) to 13 (in bright yellow).

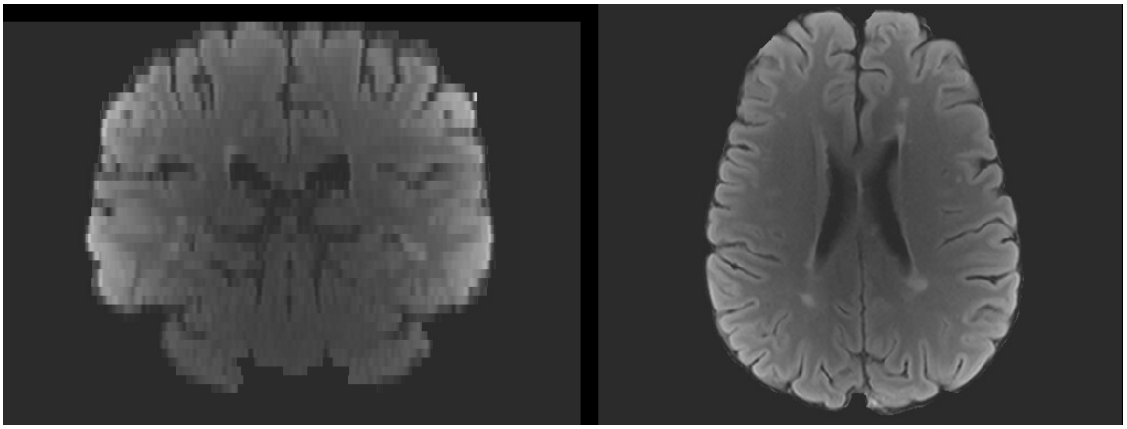

Figure 6.2: Example of a FLAIR image for one subject in coronal and axial views.

Healthy controls

After presenting two variations of the method using MS subjects' data only, we also evaluate one version of the method that uses both the MS subjects and the healthy controls. Healthy controls were partially age and sex matched. They also were scanned in the same scanner and with the same MRI sequence as the MS subjects. The control cohort consisted of 18 healthy participants (8 male, 10 female), with an average age of 39 years old (standard deviation: 13 years). Fifteen of the participants were Caucasian, two were Asian, and one had mixed ethnicity.

6.4 Methods

6.4.1 Preprocessing

Manual annotations of the lesion delineations were done by an expert, originally on the FLAIR volumes. An example of such an image is presented in figure 6.2 and its annotation in figure 6.3.

The diffusion data was first processed in an analogous manner to the UK Biobank pipeline [18]. That included correcting for eddy currents and movement artefacts, estimating voxel-wise fibre orientation distributions using FSL's BEDPOSTX [26] [27], and extracting white matter tracts using probabilistic tractography. For each subject, we virtually dissected the same 22 tracts as in the previous chapters. Examples of the tracts modelled and their overlap with MS lesions are presented in

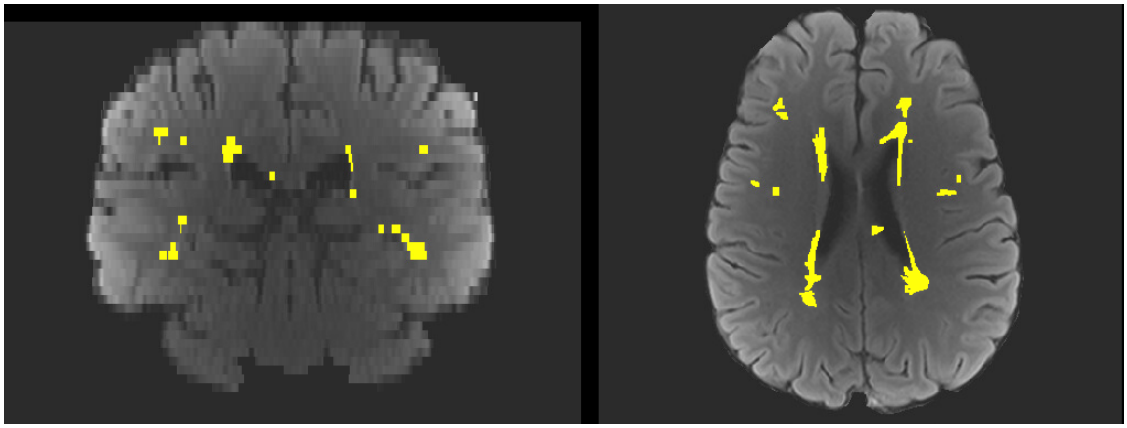

Figure 6.3: Example of the same view (as in Figure 6.2) of the FLAIR image of one subject with binary mask of manual annotations of the lesions.

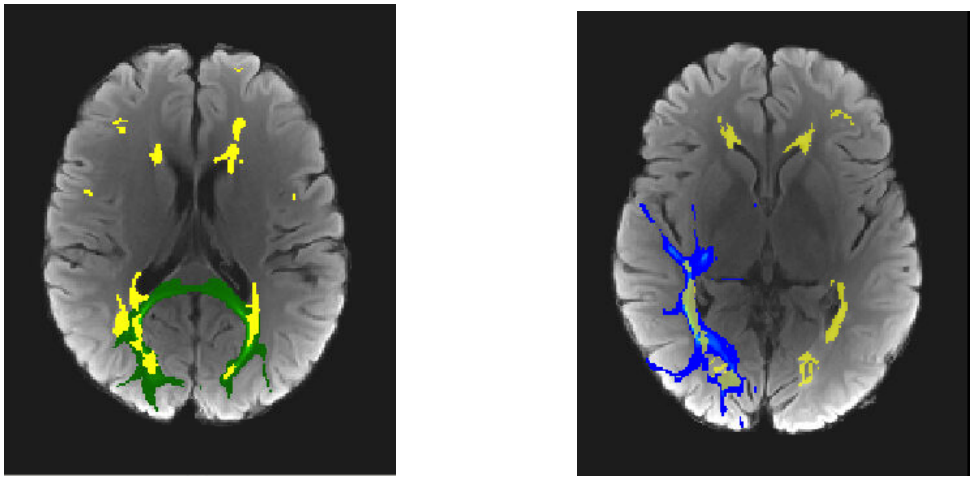

(a) FMA tract (green) with lesions (yellow) **(b)** ILF R tract (blue) with lesions (yellow)

Figure 6.4: Example tracts with manually annotated lesions (in yellow) on the FLAIR images in MNI space.

figure 6.4. Healthy control scans were preprocessed in the same way. The images were checked by clinical experts for incidental findings. As none were found, we consider healthy participant data to have no lesions, and so in the analysis we assign their lesion volume to be equal to 0.

6.4.2 Applying previously developed methods to MS data

In chapter 5, two methods were proposed for assessing the difference in the tractography results due to the presence of WMHs. Those methods assumed the existence of the two separate subsets of data: a subset of subjects with WMHs

on the investigated tract and a subset with no WMHs.

Therefore, the first step in trying to apply the methods to MS data was identifying those subsets in the new dataset. In the previous chapters, tract probability volumes were thresholded either at 0.001 or 0.01, depending on the application, therefore for testing the prevalence of lesions on the tracts here, those two separate thresholds were also used. A lower threshold means that the tract mask is going to be larger (i.e., potentially increasing the number of false positive connections), which was necessary previously, for example, when working in the functional space, where there is a lower spatial image resolution. Results of volumetric overlap (in voxels in MNI space) for both lower and higher thresholds are presented in tables 6.2 and 6.3, respectively. It is clear that in case of the lower threshold, most of the tracts have lesions in all the subjects. In case of the higher threshold, over half the tracts still have lesions in nearly all the subjects. That suggests that the methods used previously for WMHs cannot be applied to MS lesions without modifications.

Supporting the analysis with healthy control data

A potential limitation of the work presented in this chapter is the relatively small number of Multiple Sclerosis subjects available. It is much smaller than the UK Biobank, but it is important to note that often studies on disease populations can be around this size. In an attempt to alleviate this problem, in the last part of this work, we additionally explored how using healthy control data in addition to the MS subject dataset would impact the performance of the proposed method.

6.4.3 A modified method for MS data – creating two binary classes

The most similar approach to the one applied to the WMHs in the UK Biobank would be to arbitrarily divide the subjects into two classes. In case of this data, the classes would effectively correspond to high lesion load vs low lesion load, rather than indicating the presence or absence of the lesions as before. However, the decision about where to put the threshold of the lesion load dividing subjects into these two groups was not straightforward. We considered several options for an appropriate

Table 6.2: Results of the number of voxels of volumetric overlap between the lesion mask and the tract, when the lower threshold was applied to the tractography results.

tract subject	ar_l	ar_r	atr_l	atr_r	cgc_l	cgc_r	cgh_l	cgh_r	fma	fmi	ifo_l	ifo_r	ilf_l	ilf_r	ptr_l	ptr_r	slf_l	slf_r	str_l	str_r	unc_l	unc_r
006	148	193	1150	499	29	13	0	36	3253	1290	2377	3642	1878	3523	1919	2734	202	739	937	371	166	35
008	122	351	1578	1044	0	67	85	103	6145	2435	2302	4035	3764	6017	2119	3267	1903	1949	1688	1510	231	168
017	75	83	110	93	0	0	0	0	1445	173	1031	207	1574	875	1135	311	381	874	189	41	14	32
039	58	7	48	71	0	48	0	0	2797	110	1030	1261	945	1358	1180	1408	61	272	574	383	23	0
041	94	14	340	179	0	3	0	0	1675	324	568	566	588	763	664	535	41	8	35	446	150	28
045	194	18	1286	657	2	27	91	50	2521	1665	3918	1917	4544	2884	2274	1678	265	488	427	95	129	166
049	43	153	638	438	0	0	42	0	2852	1000	911	892	791	830	653	746	277	373	56	86	677	183
053a	83	0	300	384	0	0	0	5	1862	397	969	1420	1115	1629	588	968	80	32	67	5	45	9
054a	1163	1069	3121	1983	0	245	0	2	8491	4360	9132	6432	7362	8582	3897	5362	8173	6448	5787	1843	1510	186
056a	164	86	530	690	25	0	4	0	1129	941	993	1054	892	919	350	419	238	69	705	346	232	202
057a	35	24	810	236	30	0	3	0	715	808	968	374	726	391	189	293	410	273	280	272	276	62
063a	186	46	333	472	61	1	0	0	2347	1765	505	871	846	1361	282	1051	438	465	366	147	52	37
065a	165	137	463	205	0	0	0	24	52	623	271	206	382	219	23	73	322	164	244	178	294	71
077a	24	0	45	82	0	0	23	106	2054	377	325	1085	651	1049	427	375	0	49	8	18	62	37

Table 6.3: Results of the number of voxels of volumetric overlap between the lesion mask and the tract, when the higher threshold was applied to the tractography results.

tract subject	ar_l	ar_r	atr_l	atr_r	cgc_l	cgc_r	cgh_l	cgh_r	fma	fmi	ifo_l	ifo_r	ilf_l	ilf_r	ptr_l	ptr_r	slf_l	slf_r	str_l	str_r	unc_l	unc_r
006	36	50	317	37	10	9	0	0	1377	280	794	1119	654	1450	1057	1380	0	25	17	6	0	0
008	48	80	109	14	0	30	0	26	1883	173	442	982	517	738	541	747	207	16	190	196	11	27
017	11	23	1	5	0	0	0	0	550	31	149	0	193	87	342	80	0	36	34	0	0	17
039	26	0	0	0	0	7	0	0	1117	16	51	223	94	116	422	337	0	3	222	85	6	0
041	16	2	63	12	0	0	0	0	546	48	13	32	116	45	234	159	9	0	0	124	1	0
045	21	0	179	90	0	0	44	21	1281	211	1221	496	1677	808	1212	877	17	19	0	0	3	34
049	2	22	58	47	0	0	20	0	996	85	118	24	111	221	223	317	23	5	0	0	66	9
053a	28	0	41	70	0	0	0	0	696	41	77	392	60	231	127	379	0	0	18	0	1	0
054a	431	319	888	394	0	245	0	0	3040	1342	2055	1280	1443	1268	1377	1538	1369	757	1086	567	354	26
056a	107	42	96	206	0	0	0	0	626	34	163	199	233	149	114	125	56	0	110	72	11	54
057a	2	3	131	22	25	0	0	0	205	96	305	38	23	61	78	124	0	0	6	55	0	17
063a	41	4	66	32	2	0	0	0	1067	362	72	49	89	176	54	388	25	0	43	5	0	0
065a	71	13	87	44	0	0	0	0	10	59	20	40	43	14	0	31	11	0	49	24	4	0
077a	0	0	2	14	0	0	7	26	930	8	25	217	53	50	165	115	0	0	0	0	14	19

criterion for dividing subjects into subgroups. We found it challenging to decide on a single threshold value for all the tracts (whether that was a value in volume of overlap or as a quantile of the volume distribution for a given tract) nor on arbitrarily dividing the dataset in half regardless of the actual lesion distribution (for some tracts more than half of the subjects would have no lesions on a tract). Therefore, to explore that approach, despite this difficulty, we divided the data into two classes but, given the above, those classes did not always have the same number of subjects.

6.4.4 A modified method for MS data – using the lesion load

The arbitrary division of the data into two groups presented above may not be the optimal approach when subjects have different lesion loads. The aim is to visualise the differences caused by that load, and if within group pair-wise differences in load are comparable to between group differences, the approach presented above might not be the best. Therefore, we also propose another approach. Instead of using a binary regressor, we used a regressor with scaled values of lesion load for each subject on a given tract. In other words, instead of using only 0 or 1 for each subject, we used a continuous variable that represented the lesion load.

6.4.5 Additional analysis with healthy controls

To support the analysis of the MS data we additionally present an analysis that is expanded to also use the age-matched healthy participants. The aim was still to use the method proposed in chapter 5 with as little modification as possible. For the analysis, we again used a similar design matrix as in the UK Biobank analyses, which contained 4 columns: a column for the mean, one for the scaled lesion load on a specific WM tract (the same values as in 6.5.2), one to account for age, and one for sex. The contrast for the GLM analysis was [0, 1, 0, 0], which means that we will present the effect with regard to the lesion volume but accounting for age, sex, and the overall mean. In chapter 5, where we applied the method to the UK Biobank data, we used a binary regressor of 0 when there were no WMHs on the

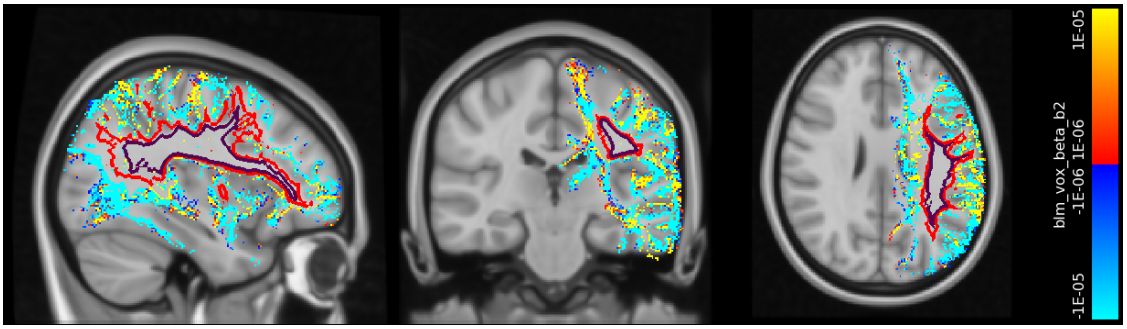

Figure 6.5: Example of non-cleaned results when using the two classes approach for the SLF L. The results are the β values from the GLM model, scaled to represent the relative effect size with regard to the tractography results. The purple (inner) contour depicts the part of the tract that belongs to more than 5 subjects, while the orange (outer) contour shows the part that belongs to more than one subject. We can observe that most of the results lay outside of the larger contour.

tract and 1 if there were any. In the MS application, due to most of the tracts having some lesions on the tract, such an approach would effectively represent whether the subjects are in the MS or healthy participant group. That would answer a slightly different research question than the one focused on the presence of lesions on the tracts. Therefore, we used here a combined approach of repeating all the steps from the chapter 5 analysis but as the regressor we used the scaled lesion load, as in 6.5.2 section. That means that this is a volumetric lesion load scaled linearly in such way that the most affected subject is assigned a value of 1, and others have assigned, proportionally, a value between 0 and 1. In the case of healthy participants, the lesion load was always zero.

6.5 Results

Results presented in this section, as in section 5.5 of the previous chapter, are calculated for each voxel independently. The results in each voxel are the values of the effect size β from the GLM model, divided by the average values from tractography. That way, the effect size results presented in figures are relative to the tractography results.

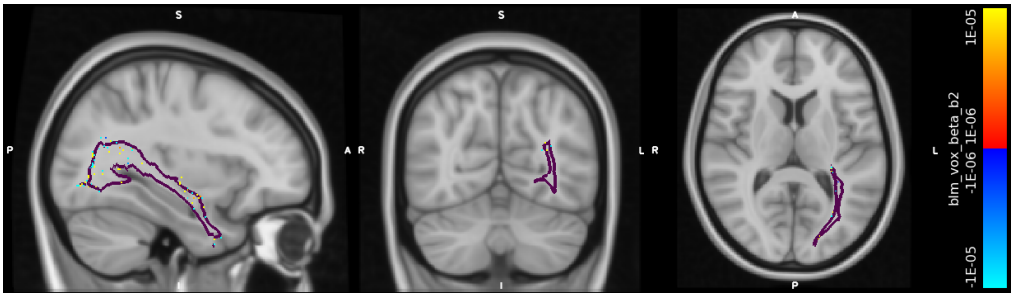

(a) ILF L

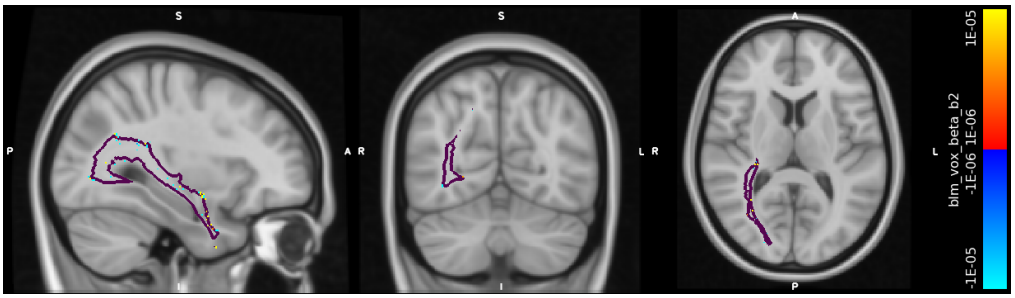

(b) ILF R

Figure 6.6: Results for the case of artificially dividing the dataset into two binary classes for the ILF tract.

6.5.1 The two classes approach

Figure 6.5 presents results as they were obtained using the SLF L as an example. There were points representing results in areas that did not plausibly belong to the tract, due to keeping very low tract probabilities that are due to noise or unwanted crossovers into other tracts. Therefore, in the figures presenting results for this variation of the method (examples for ILF 6.6, STR 6.7, as well as all the other tracts in appendix G.1) these points are removed, or 'cleaned', leaving only results that fell within the tract. We decided to use a liberal definition of that area, as follows: we thresholded all the subjects' tracts at the lower threshold (0.001) and kept here only results for the voxels that belonged to the tract for more than one subject. Since the idea of the analysis is comparison between the cases, if the result belonged to the tract only for one subject, then it is difficult to consider it meaningful.

Figures 6.6 and 6.7 present example results for ILF and STR tracts respectively, for the variation of the method, when subjects were assigned to binary classes. In the majority of the images, there are only a few voxels left after the cleaning,

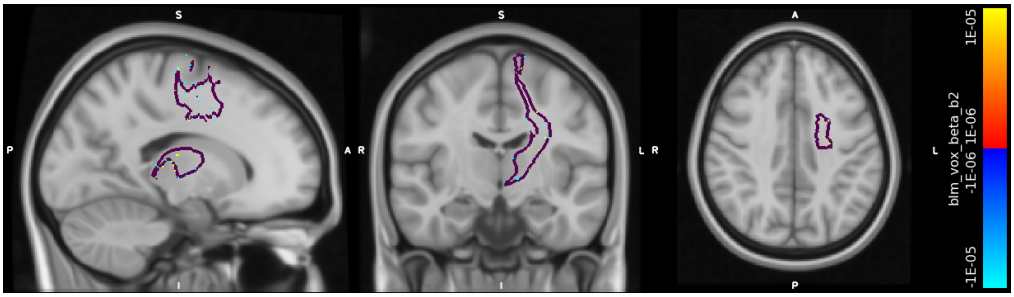

(a) STR L

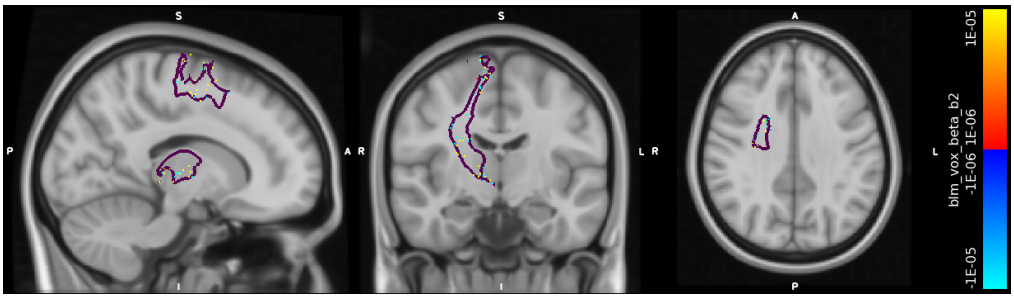

(b) STR R

Figure 6.7: Results for the case of artificially dividing the dataset into two binary classes for the STR tract.

despite using a colourscale that includes also very small values. The voxels that light up in the results do not express any patterns, nor we are not observing any similarity between the neighbouring voxels.

6.5.2 The scaled lesion load approach

In the second variation of the analysis we present the results for when lesion load was used as a regressor. Example figures for ILF 6.8 and STR 6.9, as well as figures for other tracts in appendix G.2 show that in that case, the results are more consistent between the tracts, therefore it was possible to use the same colour scale for all. As in the previous chapter on WMHs, we can observe spatial clusters of similar results for neighbouring voxels. That is the main strength of this approach compared to the one presented above (in subsection 6.5.1). Since the analysis is performed for each voxel independently, similar values in results for neighbouring voxels are reassuring. We can see that the clusters presenting a non-zero effect size are mostly around the edges of the standard tract mask.

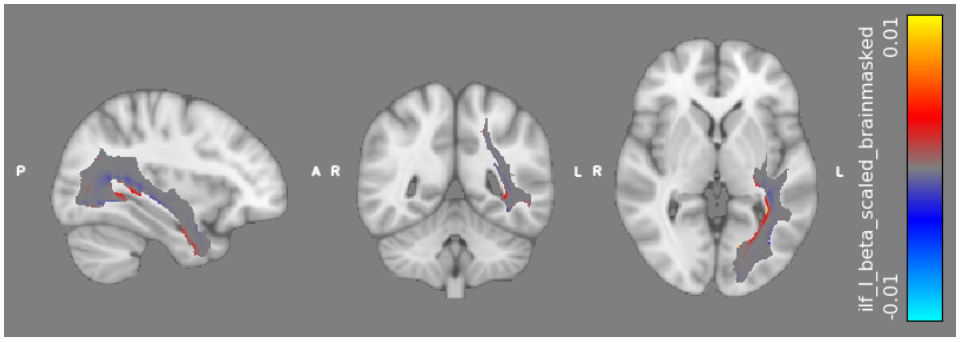

(a) ILF L

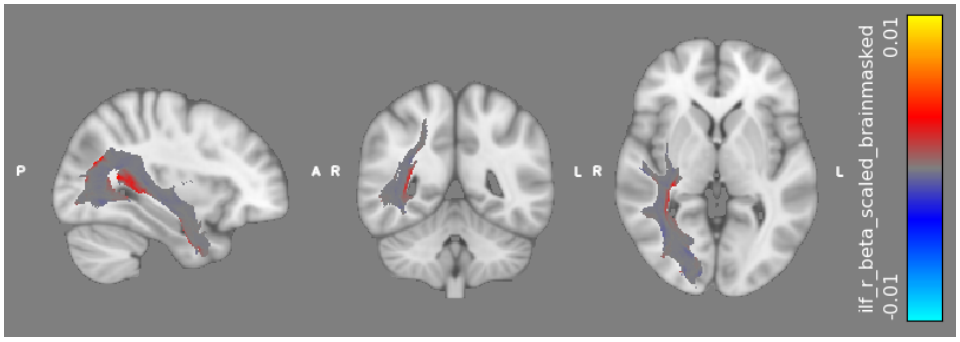

(b) ILF R

Figure 6.8: Results for the case of using the lesion load as a regressor for the ILF tract.

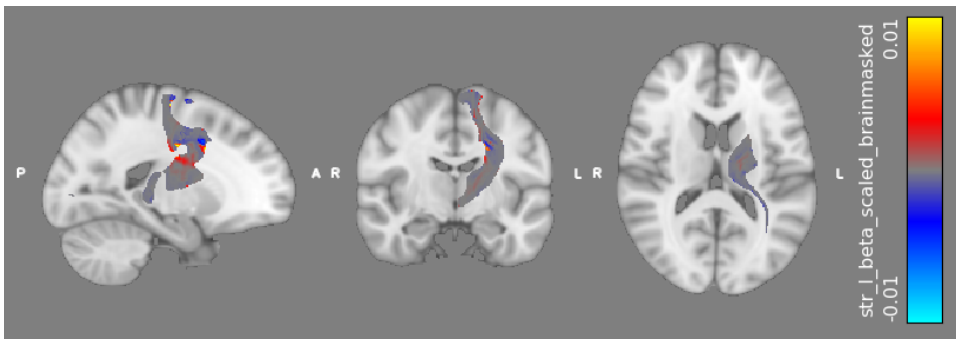

(a) STR L

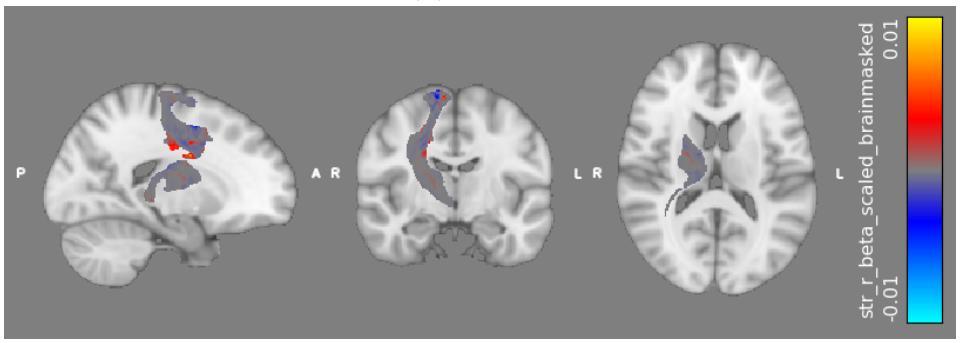

(b) STR R

Figure 6.9: Results for the case of using the lesion load as a regressor for the STR tract.

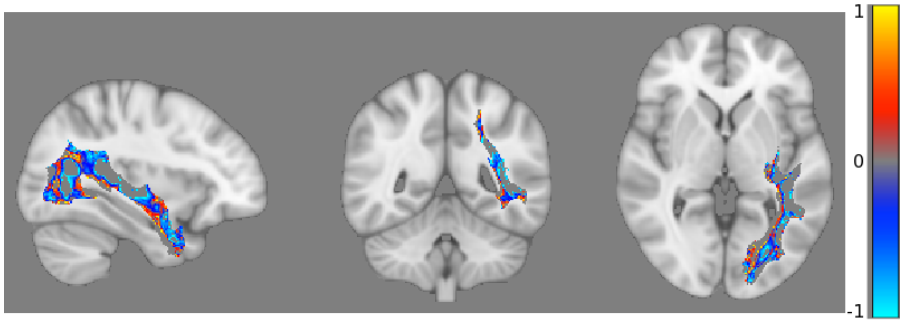

(a) ILF L

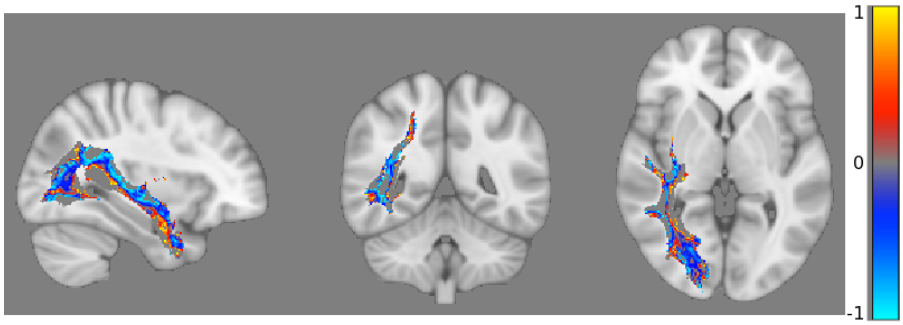

(b) ILF R

Figure 6.10: Results for the case of using the lesion load as a regressor in the analysis of combined MS subjects and healthy controls for the ILF tract.

6.5.3 Additional analysis with healthy controls

Finally, we present the results for the combination of MS subjects and healthy controls. As before, the values presented in the results are scaled β values (scaled effect size). For this analysis, they were scaled with regard to the average tract image that included all subjects used here, both MS subjects and healthy controls.

The results when using both MS subjects and healthy controls are presented in figures 6.10 for the ILF tract, figure 6.11 for the STR tract, and in appendix G.3 for all the other tracts. In this version of the analysis, the figures resemble much more closely the ones obtained when investigating the impact of WMHs in the UK Biobank, with respect to the observed scale of the relative effect size. The value of the relative β is higher than in the analysis using only MS subjects. Non-zero results cover a bigger part of the tract but are slightly more noisy in the sense of forming clusters of positive or negative effects.

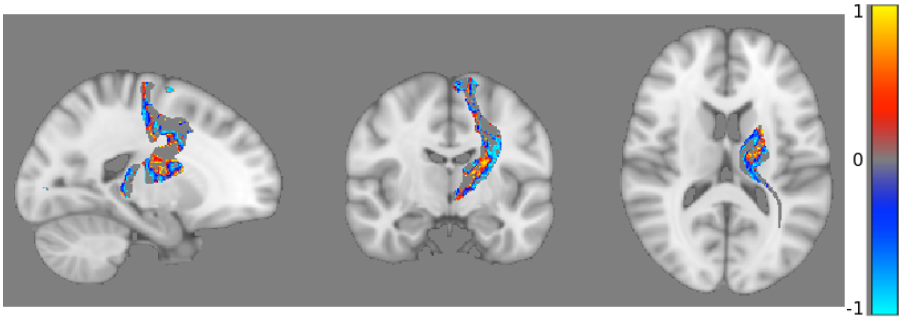

(a) STR L

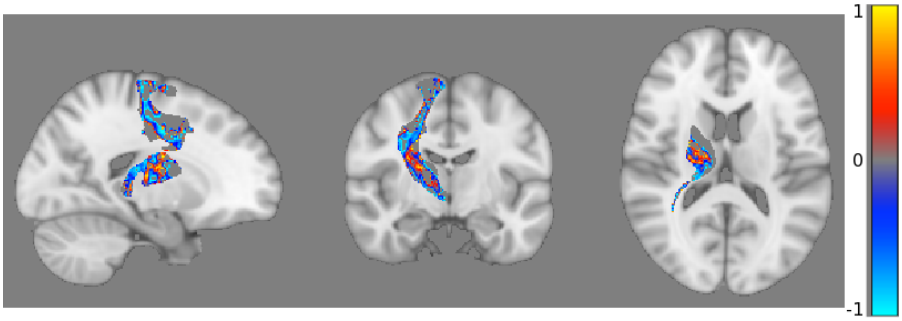

(b) STR R

Figure 6.11: Results for the case of using the lesion load as a regressor in the analysis of combined MS subjects and healthy controls for the STR tract.

6.6 Discussion

In this chapter, we use voxelwise modelling to assess the spatial variability of the tractography results in the presence of MS lesions on white matter tracts. We propose a modified version of the method presented in the previous chapter, where the lesions we focused on were white matter hyperintensities of vascular origin. We found that the analysis proposed there cannot be directly applied to a subset of MRI scans of MS subjects without modifications. The direct reason was that there were too few subjects with no lesions on a given tract. Therefore, we propose to modify the method by using a regressor with values representing the lesion load instead of using binary classes. That allowed us to obtain a similar type of result compared to what we found in the previous chapter.

In the results of the analysis including a matching dataset of healthy controls, we can observe that the relative effect sizes are higher than in the results without the healthy controls. That could come from the fact that now we are comparing

two distinct groups – subjects diagnosed as having MS and healthy controls.

The results are, however, this time not as 'smooth' as in case of analysing data with WMHs of presumed vascular origin – which might come from the smaller dataset size than that used in chapter 5 but it is not clear what causes such an effect here. The lack of a smooth pattern of changes makes the interpretation of the results very difficult.

We can see that now, when also taking into account healthy controls, we can visualise results with the same scale as we did for the UK Biobank experiment in chapter 5. The colorbar is now -1 to 1 (colours are clipped in that range as well).

The difference between results for the two hemispheres was observed for the CGC tract. In the approach that divided the MS subjects into two classes, in subsection 6.5.1, we also observed higher values for the CGC in the left hemisphere, which should not be surprising because it was a subset of the same data with a slightly different approach.

Including healthy controls alongside MS subjects aimed, partly, at addressing the issue of the relatively small size of the dataset used. However, using both MS subjects and healthy controls in the same analysis brings additional issues. The simple one is that in the case of the MS subjects, not all of them had lesions on all the tracts, and it is unclear how that should be coded in the design matrix. If a bigger dataset was available, that could be fixed by selecting a subset of MS subjects to be used per tract. Here, we only coded the volume of lesions on the tract (in mm^3), and therefore MS subjects with no lesions on a specific tract might have been interpreted by the models in the same way as healthy controls. We made a decision to approach it this way because it allows for the analysis with regard to MS lesions. However, it highlights a limitation of the work related to the fact that then we are not able to control for other factors that differentiate the two groups, in addition to the lesions. Those factors might include the 'normal appearing white matter' or atrophy. If we decided to code subjects into binary groups depending on whether they are MS subjects or healthy controls, that could lead to uncertainties about whether the differences we see are due to different

tractography results or other factors. Alternatively, other analyses where more groups were introduced, or more complicated sets of regressors used, would end up with problems related to statistical power again, due to the low number of subjects. The analysis approach that we decided to use here might have contributed to the fact that the results of the analysis are more 'noisy' than the ones for UK Biobank. Future work should include investigating this issue further.

One of the contributions of this chapter is providing an insight about how well different variations of the method designed for the analysis of data with WMHs of presumed vascular origin performed on the MS specific data. There are several possible reasons behind the need to adapt the methods before applying them to the MS population. MS lesions are different from the WMHs of vascular origin, and they are also more spatially inhomogenous. In particular, there can be different underlying effects behind the MS lesions, like gliosis, demyelination, or axonal degeneration. In this chapter, we assumed all MS lesions were of the same type – however, in the potential extension of this work, it would be valuable to differentiate the lesions. This can be done, for example, by analysing the appearance of the lesions on multiple structural images of different types, (e.g., using the T1-weighted images to identify the 'black holes') or by using quantitative measures derived from diffusion weighted imaging.

If we consider translation of this method to the clinical setting, it is important to note that the data used here had acquisition parameters like the UK Biobank. This is a strength of that dataset, as the scans have a good spatial resolution and diffusion acquisition parameters, which is advantageous for the analysis. However, clinical MS scans typically have different parameters, therefore to fully evaluate the potential of clinical translation, an additional analysis on such datasets would be required.

In the future, it would be invaluable to expand that analysis to the tracts of interest in the MS studies, and most importantly, the corticospinal tract. This is because that tract is often investigated in MS research as its characteristics are strongly related to disability. We have not included it because we used the same tracts as in the previous chapters that focused on the UK Biobank data, where

lesions (WMHs) were detected using the BIANCA software, and this algorithm currently does not support that area. However, in the case of the MS dataset, we use manual annotations for the lesions and therefore it would have been possible to include that tract in the analysis.

It is of growing importance to address the effect of MS lesions on tractography results as there is a great interest in using multimodal MR imaging in MS. The importance of the multimodal approach has been underlined almost two decades ago [86]. Cercignani and colleagues in their review article from 2018 [87], remind readers that diffusion tractography is used for defining the pathways that can also be related to the specific functional networks, which, eventually, gives a chance to put the local white matter disruption in a functional context. For that, however, it is important to be careful with using tractography in a clinical setting [76].

6.7 Summary

In this chapter, we present the method for investigating the impact of MS lesions on white matter tracts in a voxelwise manner. It is an adaptation of the method presented in the previous chapter for WMHs of vascular origin in the UK Biobank data. We found that directly applying the same methodology from that dataset to the smaller dataset of the MS patient population was not possible, despite the fact that both sets of scans were collected with the same protocols. We explored using two different modifications of the method and we found that using a continuous regressor representing a lesion load gave better results than arbitrary division of subjects to subsets with low and high lesion loads. That addressed the problem of a different distribution of MS lesions in white matter tracts, which we pointed out as one of potential obstacles for translation of the methods between those populations. Moreover, we explored an analysis on the combined MS subject dataset with the dataset of matched healthy controls.

7

Conclusions and future work

Contents

7.1 Conclusions 137
7.2 Future work 139

7.1 Conclusions

In this thesis, we focused on investigating elements of the methodology for analysing the impact of white matter focal lesions on the brain and its structural and functional connectivity. We focused particularly on the White Matter Hyperintensities of presumed vascular origin and Multiple Sclerosis lesions. We used multimodal MRI data and, in part of the thesis addressing WMHs, we used a large UK Biobank dataset.

In the first two results chapters, we presented and evaluated the methodological approaches to quantifying the impact of WMHs on the structural and functional connectivity of white matter tracts they affect. That allows for the local description of the WMHs effects in the brain, compared to the more traditional approach of using a single measure for the whole brain.

We showed that for the majority of the subjects, the WMH would be visible in similar spatial locations within the tracts. We compared two approaches to quantifying the structural effect of the WMHs on the tracts: using the volumetric overlap ratio between the WMH mask and the tract mask and using the proposed ratio of tractography streamlines that pass through the WMH mask to the total number of streamlines within the tract. The second approach resulted in a wider distribution of the values among the subjects for most of the tracts, which may suggest it is more informative for further analysis.

After this we proposed the methodology for analysing the impact of WMHs on the resting state functional connectivity in the brain in relation to particular white matter tracts. We explored the impact of multiple methodological choices required for that task. They included possible definitions of tract endings in gray matter, where we showed the advantage of using a functional atlas for gray matter parcellation, as well as comparing results for partial correlations with full correlations (with different preprocessing). We compared the results of correlations between the structural and functional impact of WMHs for two structural measures and we found very little difference between both, compared to the differences between the functional measures.

In the two research chapters that followed, we investigated the variability of tractography results in the presence of the lesions. First, we performed an extensive analysis for the data with WMHs of vascular origin, then we adapted part of it to the MS lesions data. In WMHs we first investigated the variability of the white matter tract shape for the subjects with WMHs on the tract compared to the rest of the subjects for 22 white matter tracts in the brain and the differences we found were very small. Then, we proposed a method for comparing the tractography results on a voxel-wise level between the two groups of the subjects: with and without the WMHs on the tracts. The effect sizes we found were not very strong in the centre of the tract for the large dataset when including age and sex as covariates. The results for smaller sets of data with a narrow age range and single sex show stronger effect sizes and suggest that the observed differences in tractography strength might be

modulated by age and sex. The observed relationships do not seem to be captured well by the linear model and require further investigation. We supported these analyses by exploring the tissue microstructure parameters within the WMHs as well as in their proximity with the rest of the white matter tracts, and we found patterns of differences. That suggests that there are differences in the microstructure parameters, but they do not necessarily translate to the differences in tractography results. In the final research chapter, we explored the potential of applying the voxel-wise analysis of tractography results to the Multiple Sclerosis data. We found that some method modifications were necessary, and we proposed two approaches to address that. Since there were very few subjects with no lesions on given tracts, we attempted: 1. the arbitrary division of subjects into two groups (with small or large lesion load), 2. using a continous variable describing the lesion load, instead of binary classes. We found that the latter version of the method performed better, therefore we presented additional results using that version of the method on the dataset with both MS subjects and healthy controls.

7.2 Future work

The thesis covers a wide range of analyses of white matter lesion impact on brain connectivity. Moreover, that opens a scope for the potential future work that could follow on the findings from this thesis. We summarise the selected directions for such work below.

First of all, in this thesis, we focused on investigating changes in ageing. However, we used crossectional datasets, i.e. using single timepoint data for each subject, and we looked at the differences relative to their age or lesion load. Therefore, ideally, we would be interested in repeating these analyses using longitudinal data. That would allow for modelling of the subject-specific trajectories of changes related to age (and disease progression in case of MS). Such an approach would account for intra-subject variability and provide more certainty that the changes we observed are indeed due to ageing.

Another aspect of the dataset we used in this thesis is its size. In future work, it would be valuable to put more emphasis on the 'big data' aspect of the UK Biobank. To start with, the UK Biobank is a very rich dataset, with many non-imaging variables, and it would be very interesting to explore their interactions with our findings. We would like to see in the future those measures to be included in the work. For example, to compare the rs-fMRI connectivity within certain networks to the results from the relevant behavioural or cognitive tests, which are available in the UK Biobank. Other aspects related to the size of the dataset may include exploring the impact of other confounds than the ones we included in the thesis or mitigating the effect of the outliers on the statistics.

Only a part of this thesis was translated to Multiple Sclerosis lesions. In future, it would be good to translate other methods from WMHs to MS lesions. It would be particularly interesting to try applying the measures of structural and functional connectivity to the MS data. When applying more methods from WMH data to MS data, it will be important to take into account more carefully the issues specific to MS lesions, that do not apply to WMHs. That includes, for example, the fact that in MS it is much more common to observe juxtacortical and infratentorial lesions, which also relates to the importance of shifting the focus to a slightly different selection of the white matter tracts to analyse (e.g. to include the corticospinal tract). By increasing the emphasis on the translational aspect, apart from proposing new or adapted methods, which would already be an important contribution, we would gain an opportunity to compare closer the effects of both types of the lesions on the connectivity. Generally, approaching those questions from the more generic perspective, rather than performing disease-specific studies, may provide a wider insight into the impact of white matter changes in the brain. On the other hand, stronger focus on the particular disease is also valuable. For example, differentiating the MS lesions in different stages for the analysis would be also interesting.

It is worth noting that we used here mostly 'classical' statistical approaches. With the development of machine learning methods, there might arise further ideas to expand the analyses presented in this thesis. For example, it would be interesting

to see whether it is possible to predict the functional connectivity between the ends of the white matter tract, given its structure. That could also lead to finding a better measure of the structural impact of WMHs on the tract. Using machine learning would be particularly interesting when it would include multimodal information and different measures to those we discuss in this thesis. However, even a simple analysis combining measures from the thesis would give us better insight into the white matter changes. For example, we could take a look at the voxelwise differences in the tractography results (as in chapters 4 and 6), it would be interesting how they correlate with spatial distributions of the lesions on the tracts (as presented in the chapter 3). We hope this thesis provides a good reference for future work on the local WMH impact on brain connectivity, especially using large datasets, and serves as a starting point for further studies.

Appendices

A

Spatial distributions of WMHs on each tract over 5000 subjects

The figures below show how many times a given voxel on the tract was classified as a part of a WMH in the analysed subset of 5000 subjects. The colourscales of those maps, presented on the right hand side of the images, are independent for each tract, so the fact they have different maxima also presents the variability here.

In callosal tracts we can observe clear focal points where most of the WMHs are detected. In the FMA (figure A.1) that area is bigger than for FMI (figure A.2), where the voxels with highest counts are more concentrated. WMHs tend to appear symetrically in both hemispheres but not in the central part of the tract. For some of the subjects WMHs were also detected closer to the endings of the tracts,

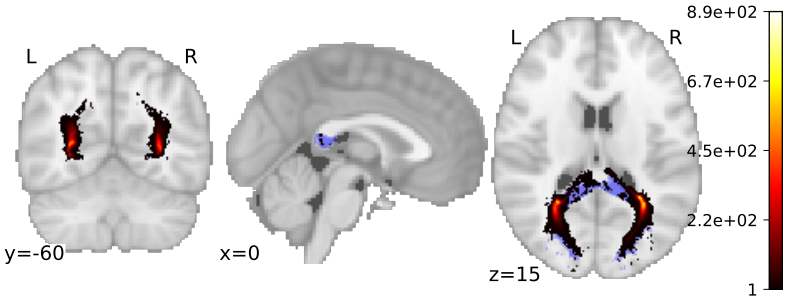

Figure A.1: The spatial distribution of WMHs (in black–red colour map) visualised on the average FMA tract mask (in blue). The colour from black through red to white reflects the number of subjects for whom a given voxel was counted as a part of a WMH.

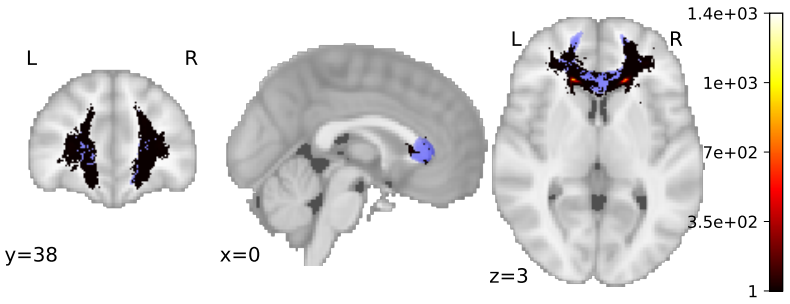

Figure A.2: The spatial distribution of WMHs (in black–red colour map) visualised on the average FMI tract mask (in blue).

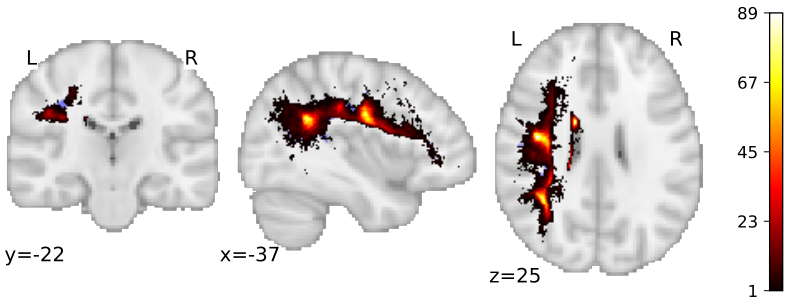

Figure A.3: The spatial distribution of WMHs (in black–red colour map) visualised on the average SLF left hemisphere tract mask (in blue).

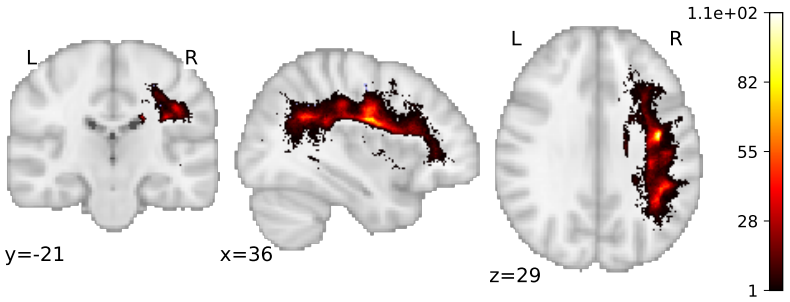

Figure A.4: The spatial distribution of WMHs (in black–red colour map) visualised on the average SLF right hemisphere tract mask (in blue).

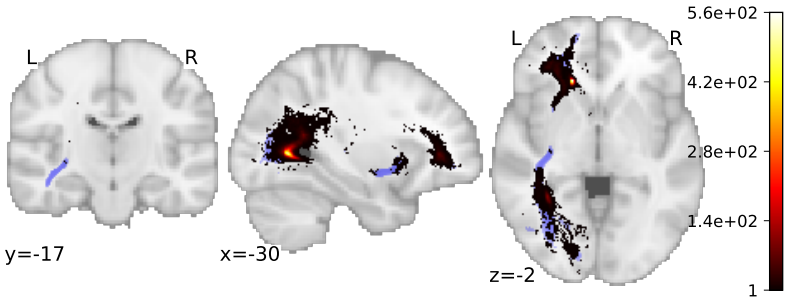

Figure A.5: The spatial distribution of WMHs (in black–red colour map) visualised on the average IFO left hemisphere tract mask (in blue).

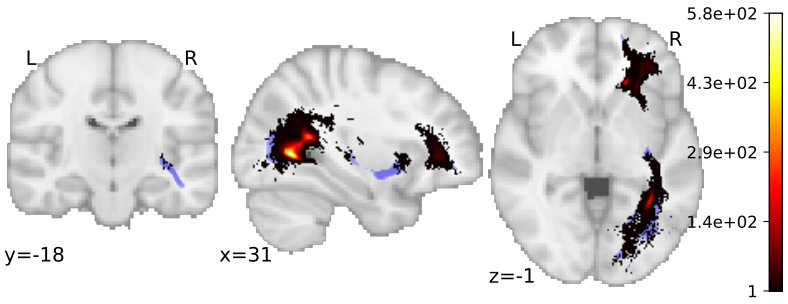

Figure A.6: The spatial distribution of WMHs (in black–red colour map) visualised on the average IFO right hemisphere tract mask (in blue).

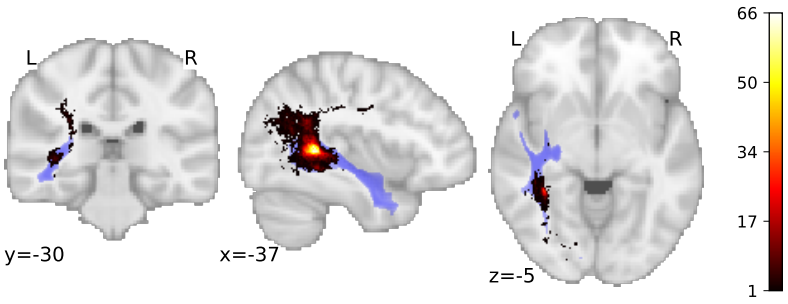

Figure A.7: The spatial distribution of WMHs (in black–red colour map) visualised on the average ILF left hemisphere tract mask (in blue).

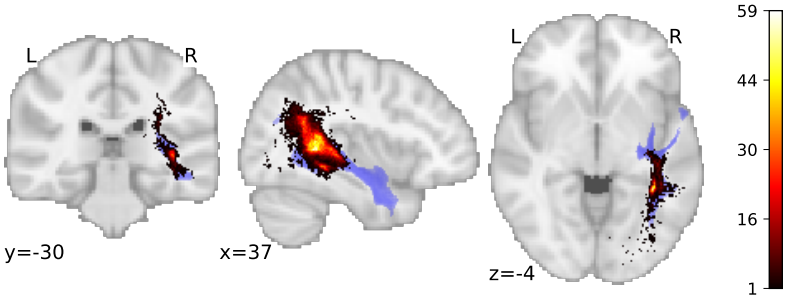

Figure A.8: The spatial distribution of WMHs (in black–red colour map) visualised on the average ILF right hemisphere tract mask (in blue).

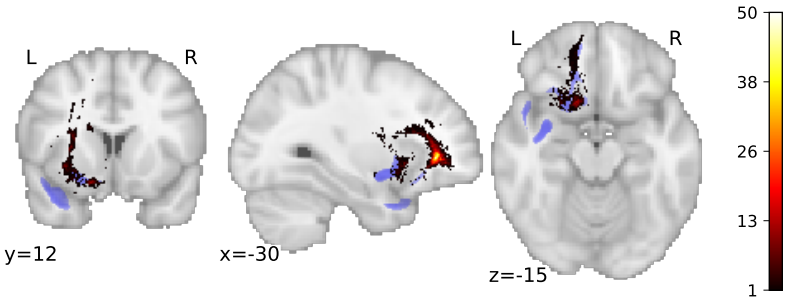

Figure A.9: The spatial distribution of WMHs (in black–red colour map) visualised on the average UNC left hemisphere tract mask (in blue).

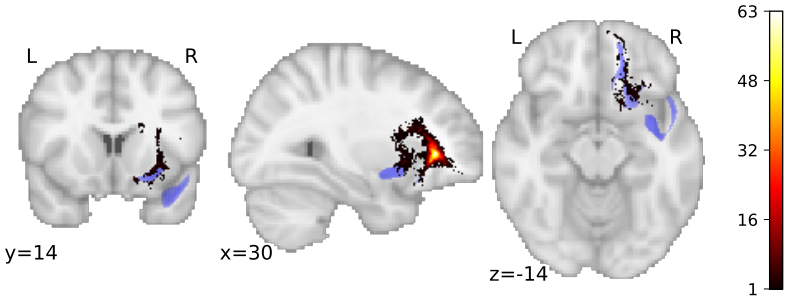

Figure A.10: The spatial distribution of WMHs (in black–red colour map) visualised on the average UNC right hemisphere tract mask (in blue).

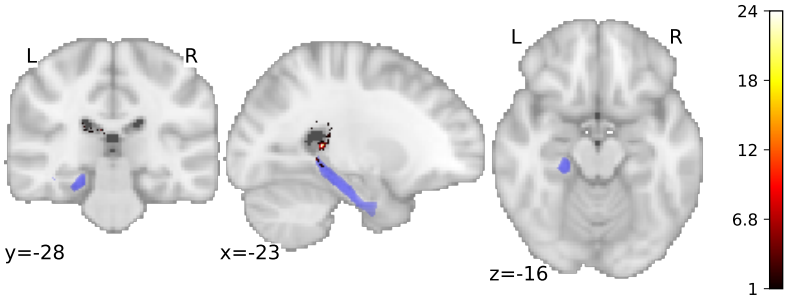

Figure A.11: The spatial distribution of WMHs (in black–red colour map) visualised on the average CGH left hemisphere tract mask (in blue).

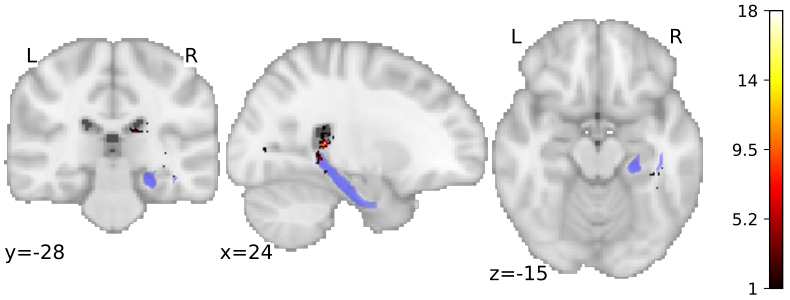

Figure A.12: The spatial distribution of WMHs (in black–red colour map) visualised on the average CGH right hemisphere tract mask (in blue).

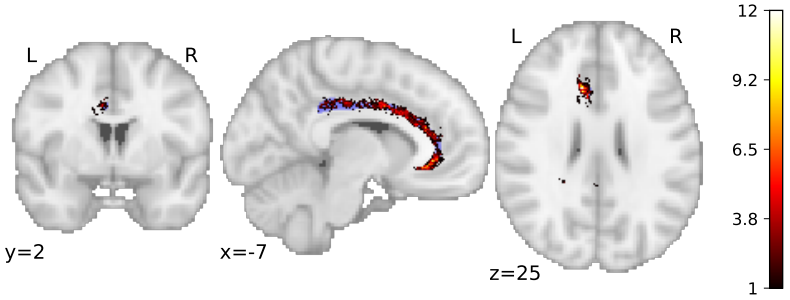

Figure A.13: The spatial distribution of WMHs (in black–red colour map) visualised on the average CGC left hemisphere tract mask (in blue).

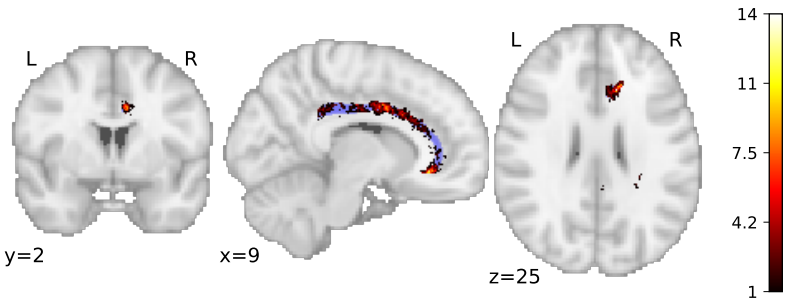

Figure A.14: The spatial distribution of WMHs (in black–red colour map) visualised on the average CGC right hemisphere tract mask (in blue).

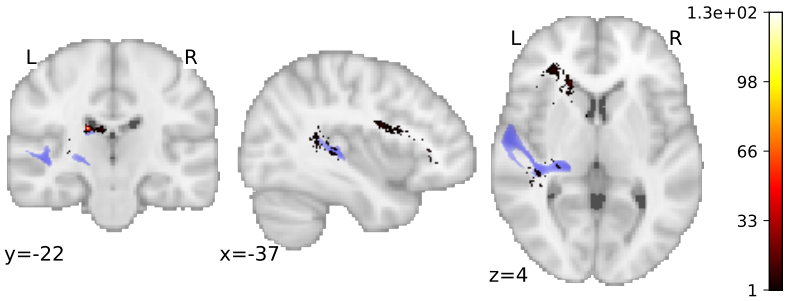

Figure A.15: The spatial distribution of WMHs on the AR left hemisphere tract.

towards the cortex. A different situation can be observed in the SLF in both hemispheres(figures A.3, A.4). Here, it seems like the whole main part of the tract is similarly affected by the WMHs. This pattern is unique, and not repeated for the other tracts. In the IFO (figures A.5, A.6) it is mostly the endings that are affected, while the central part of the tract is left relatively free of WMHs. In the ILF (figures A.7, A.8) there is a strong bias for WMHs to be based in the top part of the tract and in the UNC (figures A.9, A.10) in the frontal part. For limbic system fibres the counts are very low. In the CGH (figures A.11, A.12) they are limited to the top part as it was previously noted in the UNC but in the case of the CGC (figures A.13, A.14) it can be observed that hyperintensities are spread along the whole tract.

In similar visualisations for thalamic projections it can be observed that WMHs are always focused further from thalamus, in the parts of the tract leading to the cortex. It is important to note that the postprocessing mask in the WMH detection algorithm used (BIANCA) excludes the thalamus, which can have some impact on

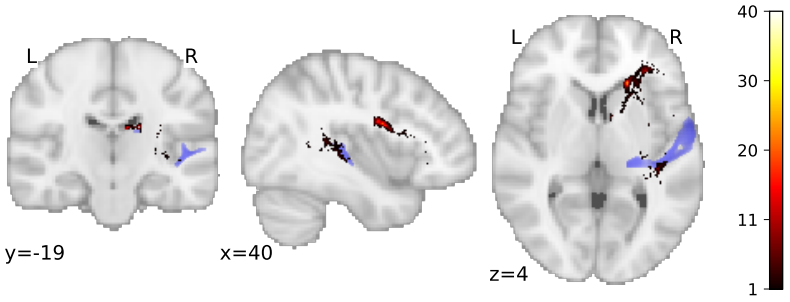

Figure A.16: The spatial distribution of WMHs on the AR right hemisphere tract.

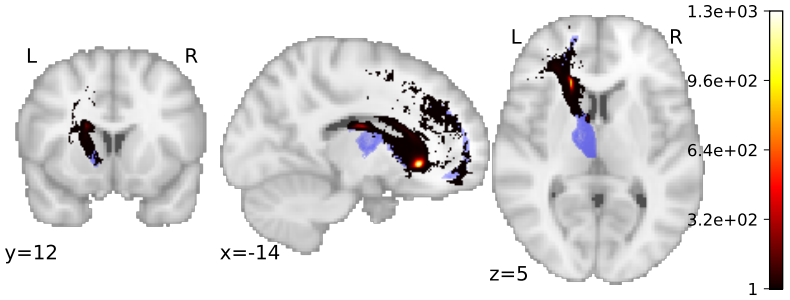

Figure A.17: The spatial distribution of WMHs on the ATR left hemisphere tract.

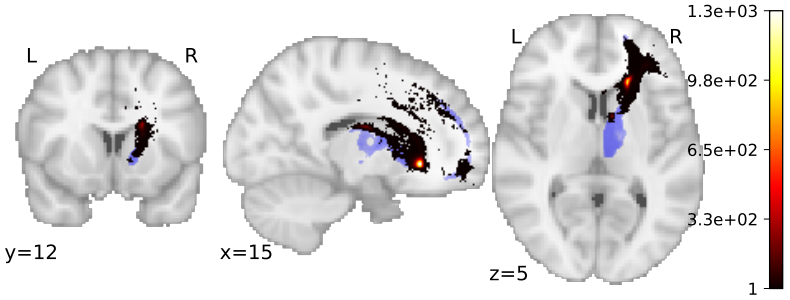

Figure A.18: The spatial distribution of WMHs on the ATR right hemisphere tract.

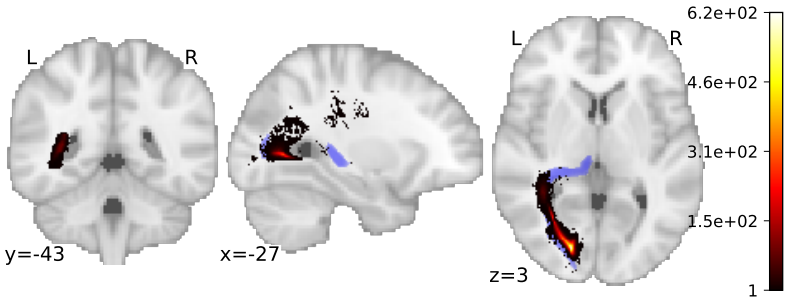

Figure A.19: The spatial distribution of WMHs on the PTR left hemisphere tract.

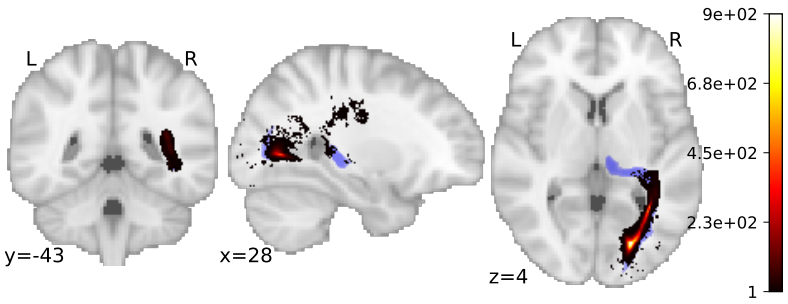

Figure A.20: The spatial distribution of WMHs on the PTR right hemisphere tract.

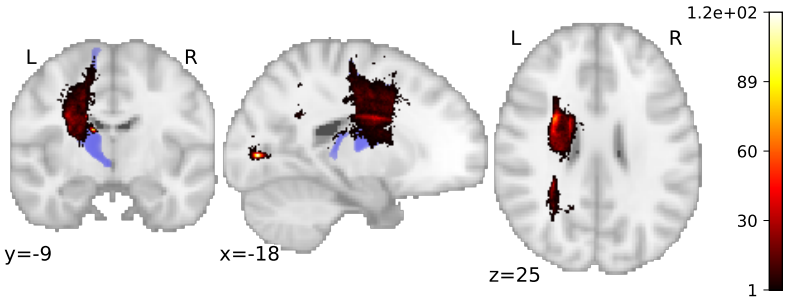

Figure A.21: The spatial distribution of WMHs on the STR left hemisphere tract.

that result. The pattern is not that clear in the case of the AR (figures A.15, A.16), which has relatively low maximal counts, but that pattern is striking in the cases of both ATR and PTR for both hemispheres (figures A.17, A.18, A.19, A.20). In the STR (figures A.21, A.22) the maximal counts are more broadly distributed but, similarly, there are no WMHs closer to the thalamic end of the tract.

In summary, the patterns and number of counts for WMH distributions vary between the tracts. Despite that, it can be observed that for the vast majority of the considered tracts the WMHs are detected in particular regions rather than spread along the whole length of the tract. That is true in particular for the

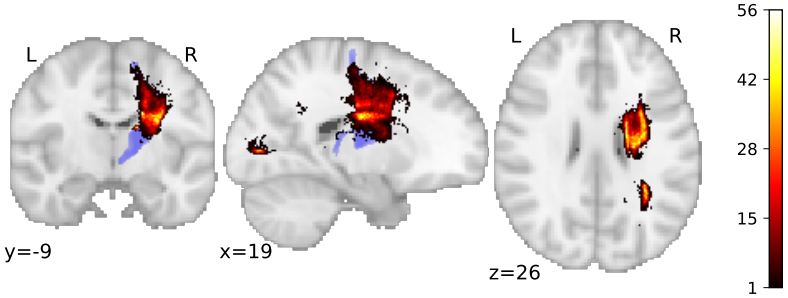

Figure A.22: The spatial distribution of WMHs on the STR right hemisphere tract.

association fibres. The exception for that pattern is the SLF for both hemispheres, where most of the voxels have some overlap with the WMH mask for some subjects. Also in the limbic tracts similar maximal counts were reported for most of the tracts but the counts there were lower.

B

Comparison between structural measures for each tract

The scatter plots (in figures B.1 to B.22) present the joint distributions of two measures, where each point represents one subject. On the x axis there is the normalised total volumetric overlap of the WMH mask with the subject specific tract mask. On the y axis there is the proposed measure of ratio of tract streamlines that pass through at least one WMH mask. In theory, the range of values for both measures is between 0 and 1.

The joint distribution of the two measures for FMA (figure B.1) is very distinctive between the tracts. The streamline-based method gives values in the whole available range. There is a bias towards lower values, however the distribution of the values is much more uniform than for other tracts. For similar values of the volumetric overlap, the streamline ratio values vary, and similarly, all the streamlines are marked as affected for different volumes of WMHs on the tract, but understandably that starts only from a certain level of overlap. The results look very different for FMI (figure B.2). Here, both distributions are one-sided with zero being the peak for the streamline ratio values. Apart from one outlier subject, all the overlap measures are very close to each other, while the streamline ratio values spread over half of the scale for most of the subjects. In the SLF (figures B.3, B.4) for the less

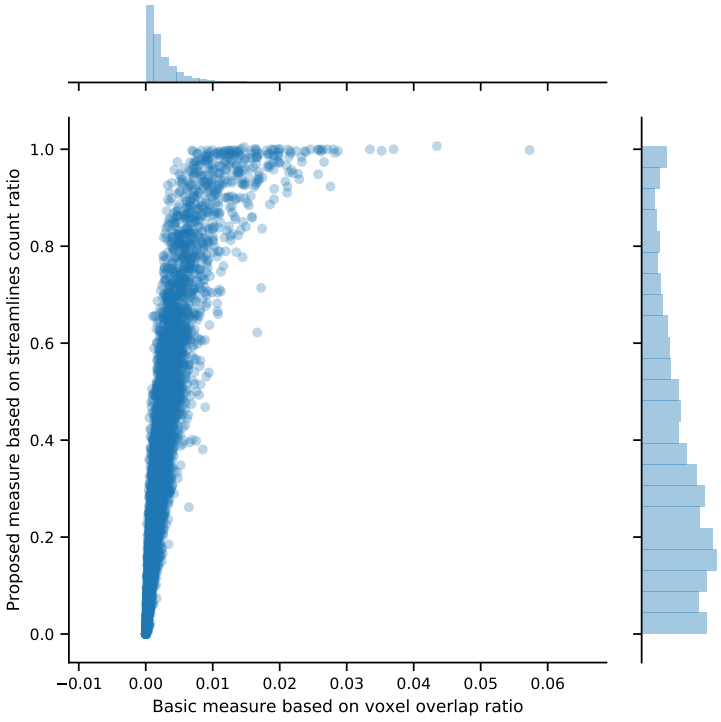

Figure B.1: Comparison between results obtained with both structural measures for the FMA tract.

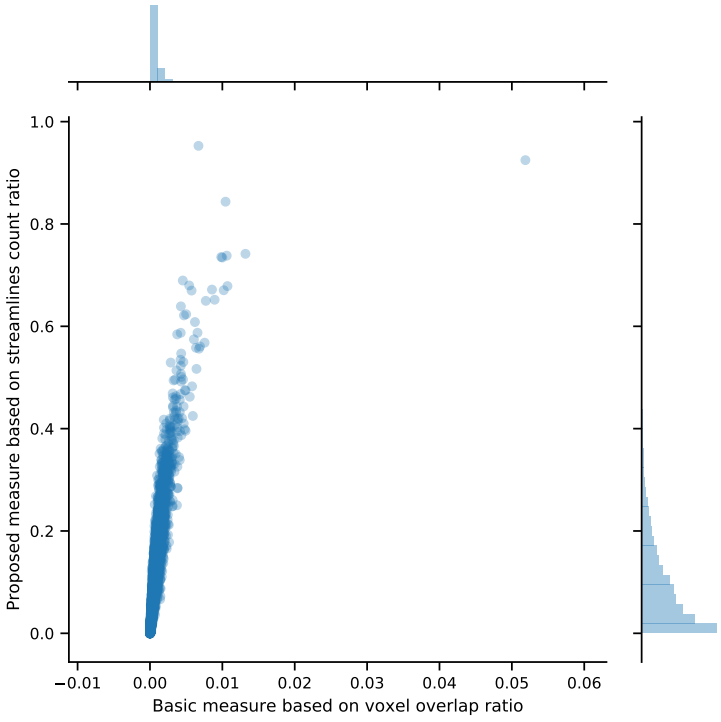

Figure B.2: Comparison between results obtained with both structural measures for the FMI tract.

affected subjects, which constitute a majority, they have similar volumetric overlap but varied streamline-based measures (as for the FMI). However, for subjects with higher WMH loads, the pattern resembles more the one shown for the FMA and qualitatively it looks like an increase of the overlap measure relates strongly to an increase in the ratio measure. Both types of distributions nevertheless are very narrow and are peaked at zero. Distributions are visibly wider in the case of the IFO (figures B.5, B.6). Here, the overlap results seem to have a slightly wider distribution than in the previous tracts, however, it is important to see that the scale on the x axis is different than before. The streamlines measure has a much wider distribution, especially in the right hemisphere. Again, most of the subjects have small WMH loads but this time the overlap seems to have a wider distribution. A very similar pattern can be observed in the ILF (figures B.7, B.8). Here, as well, the right hemisphere seems to have slightly more varied measures. In the UNC (figures B.9, B.10) both types of measures give results close to zero. The relative values are higher for the streamlines based measure, which also results in a slightly wider range of obtained values but both distributions are around zero. A similar situation, even to a higher extent, can be noted for the limbic system fibres (figures B.11, B.12, B.13, B.14), where both measures are strongly clustered around zero. The values obtained are so small (for example, not exceeding 0.005 for the overlap measure for CGH L) that it is difficult to discuss them as meaningful. For the CGC the scale of the results is bigger, but apart from some outliers, the majority of points are still grouped around zero.

There is some slight variation in the patterns observed for the thalamic tracts. In the AR (figures B.15, B.16), it is different from the previous cases as the streamline-based ratio is more narrow and does not reach 1, while the measure based on the overlap is relatively wide (up to above 0.1). That might have, however, affected the visualisation of the relationship between the measures for the smaller values, so it is difficult to draw conclusions for that case. The rest of the thalamic tracts show patterns more similar to the ones from the association fibres. In the ATR (figures B.17, B.18) and PTR (figures B.19, B.20) the distributions of

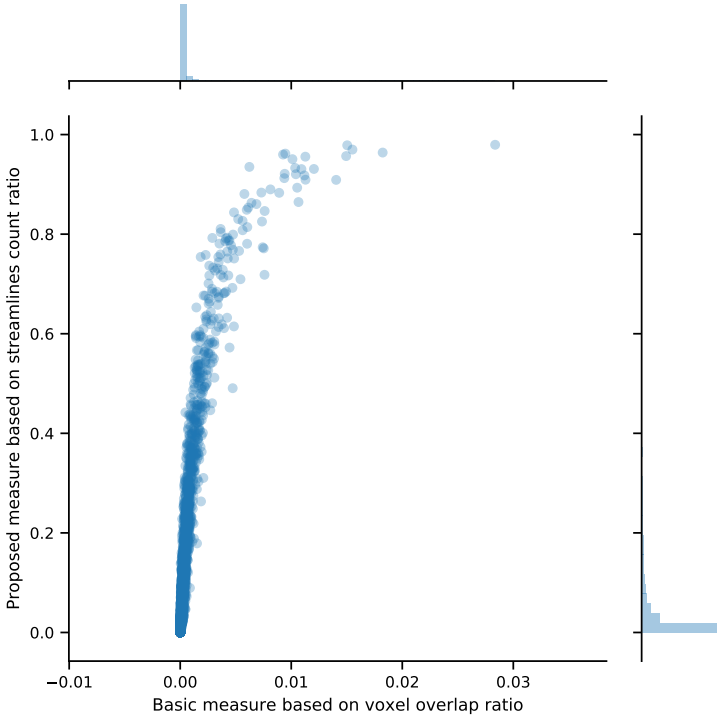

Figure B.3: Comparison between results obtained with both structural measures for the SLF L tract.

the streamline-based measure reach nearly halfway up the scale for most of the subjects, i.e. the majority of them obtained values between 0 and 0.5. For the STR (figures B.21, B.22) even though the scatter plot looks quite similar, the histograms suggest that the streamline-based measure does not have a distribution as wide as in the case of the ATR and PTR.

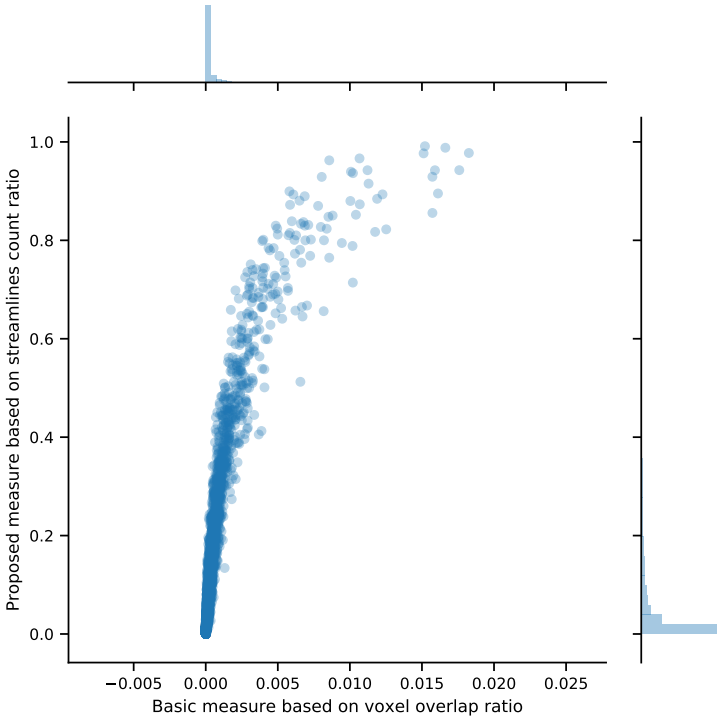

Figure B.4: Comparison between results obtained with both structural measures for the SLF R tract.

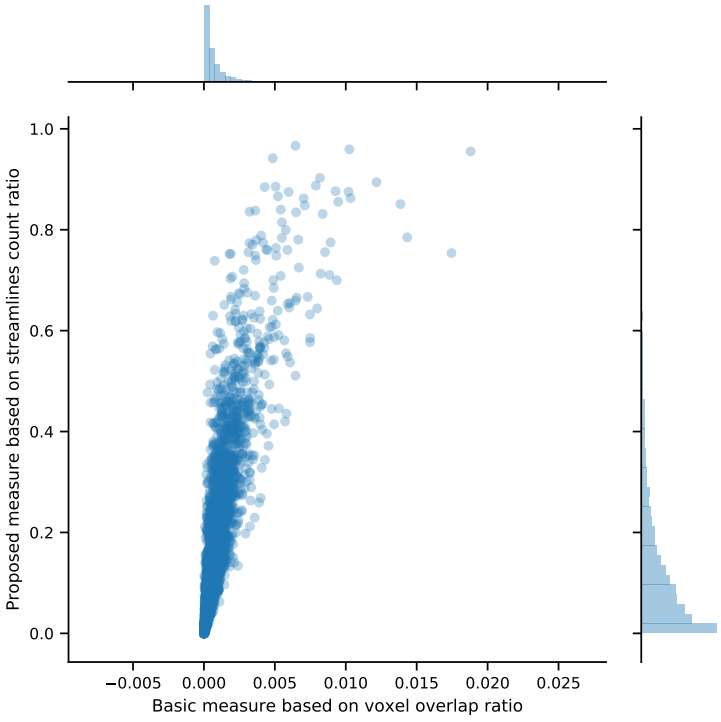

Figure B.5: Comparison between results obtained with both structural measures for the IFO L tract.

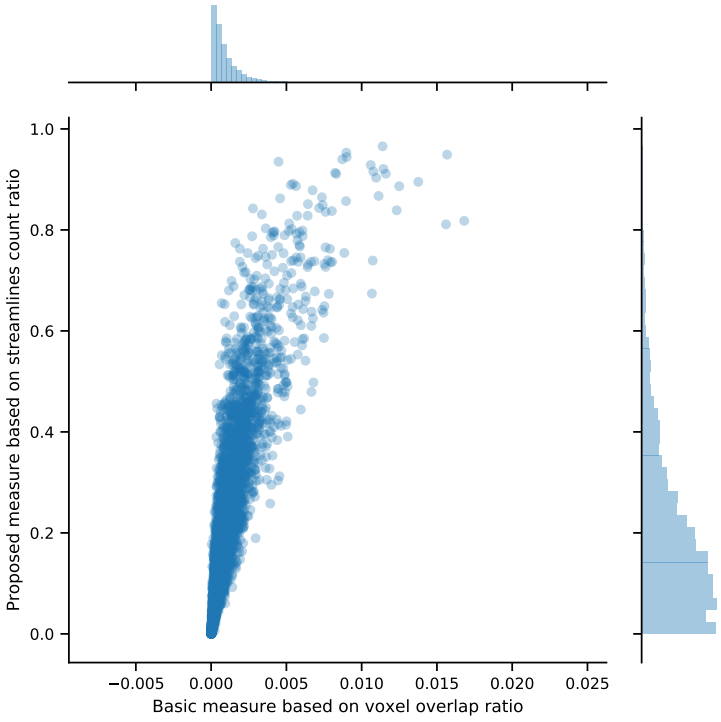

Figure B.6: Comparison between results obtained with both structural measures for the IFO R tract.

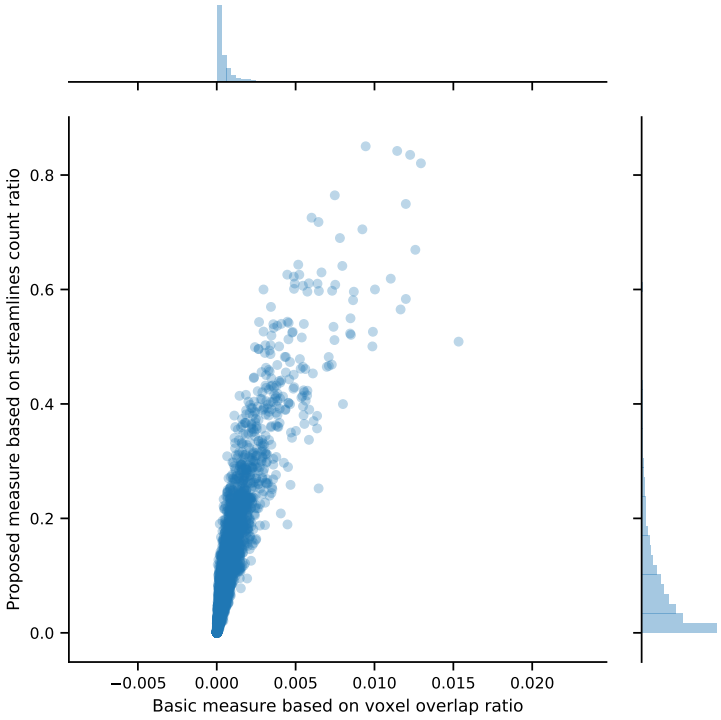

Figure B.7: Comparison between results obtained with both structural measures for the ILF L tract.

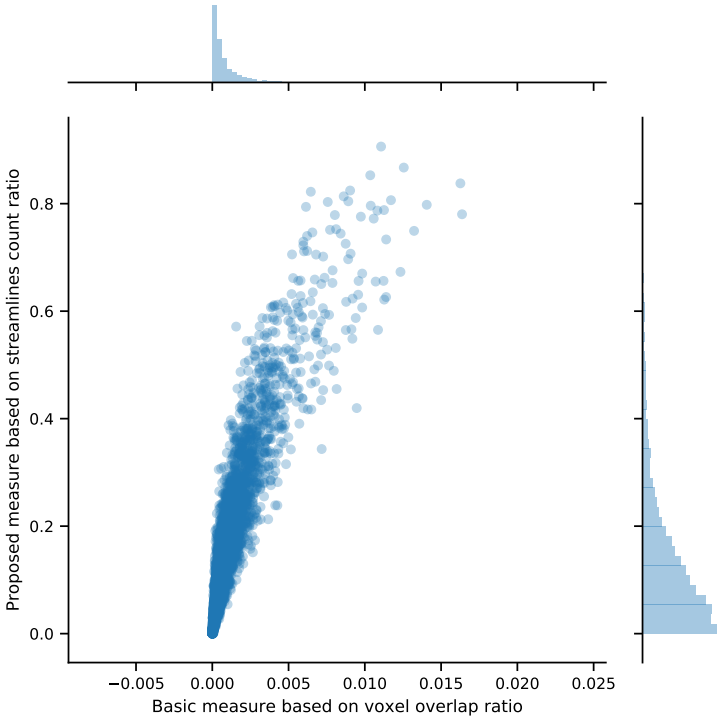

Figure B.8: Comparison between results obtained with both structural measures for the ILF R tract.

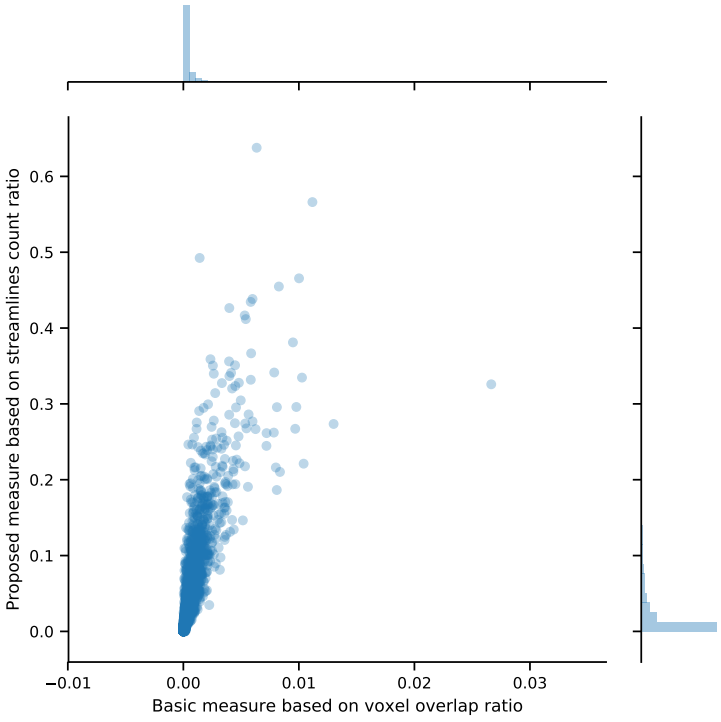

Figure B.9: Comparison between results obtained with both structural measures for the UNC L tract.

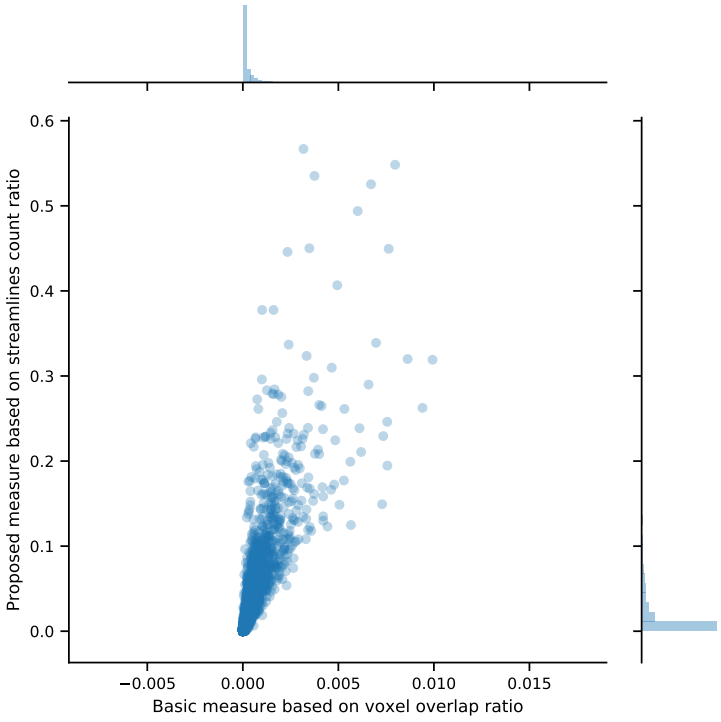

Figure B.10: Comparison between results obtained with both structural measures for the UNC R tract.

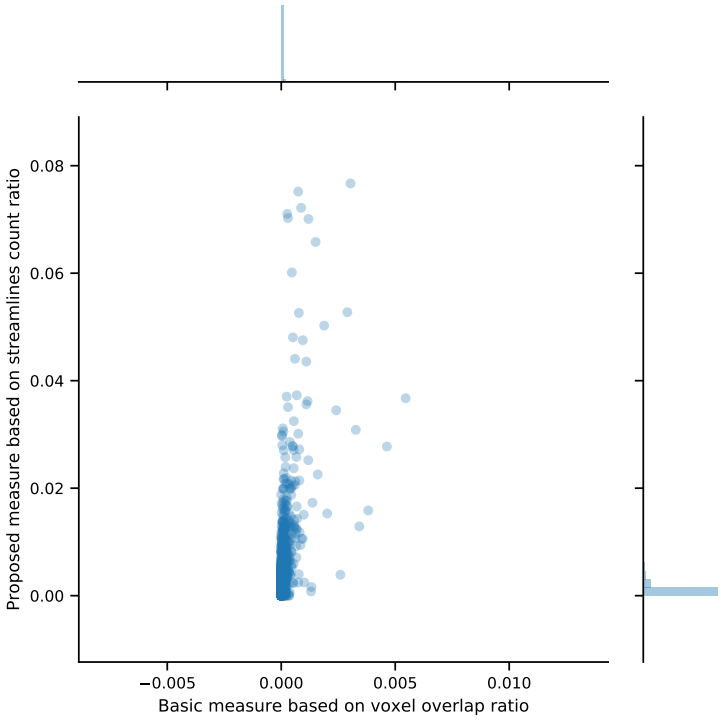

Figure B.11: Comparison between results obtained with both structural measures for the CGH L tract.

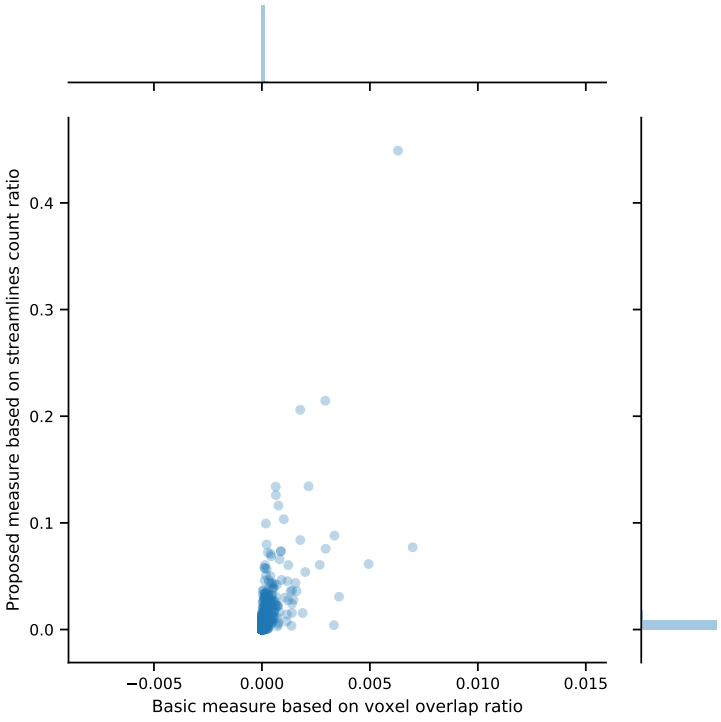

Figure B.12: Comparison between results obtained with both structural measures for the CGH R tract.

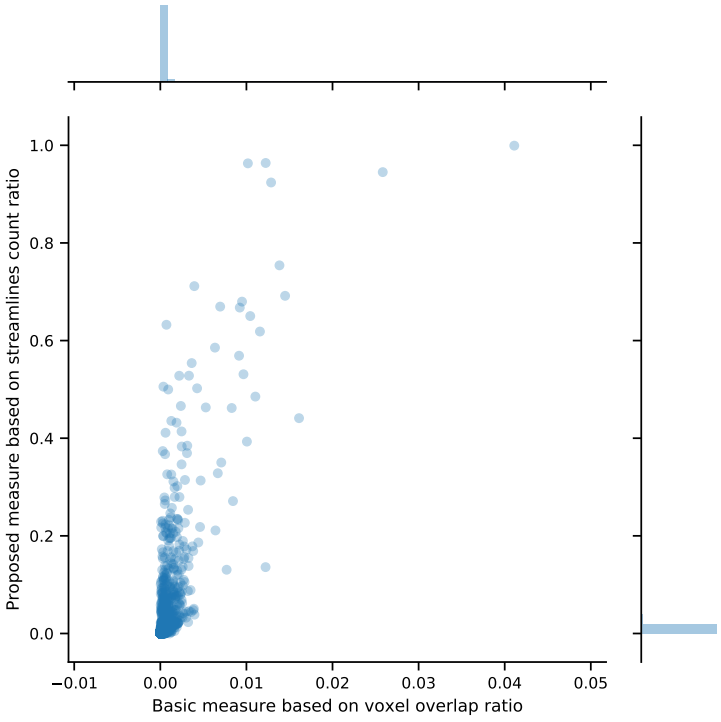

Figure B.13: Comparison between results obtained with both structural measures for the CGC L tract.

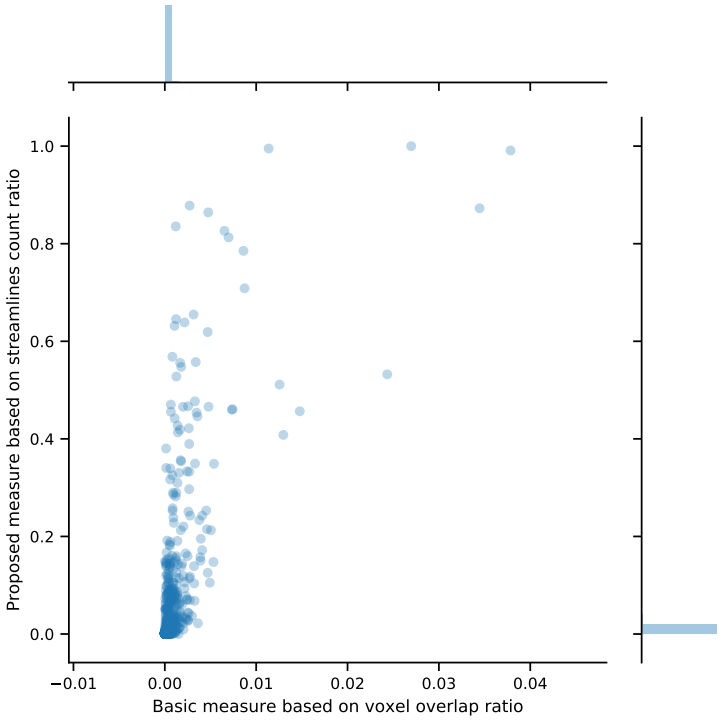

Figure B.14: Comparison between results obtained with both structural measures for the CGC R tract.

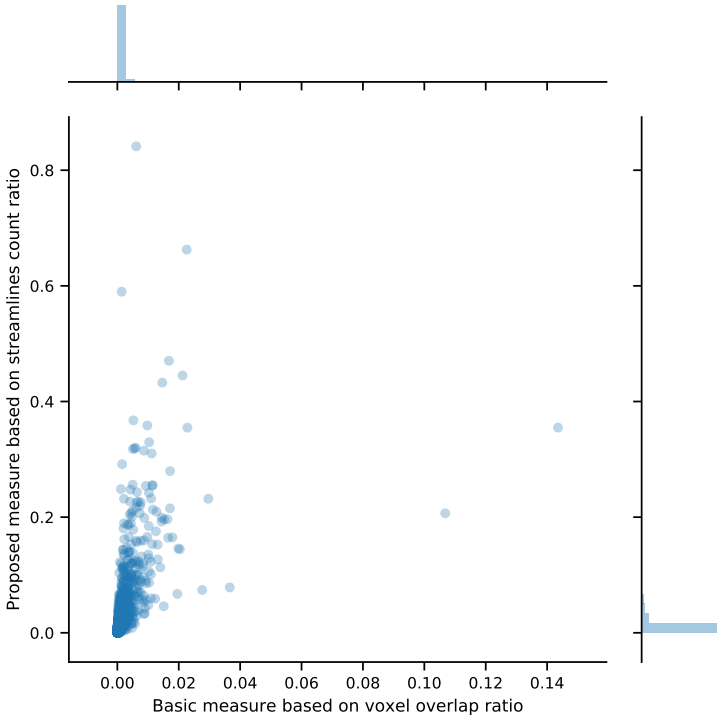

Figure B.15: Comparison between results obtained with both structural measures for the AR L tract.

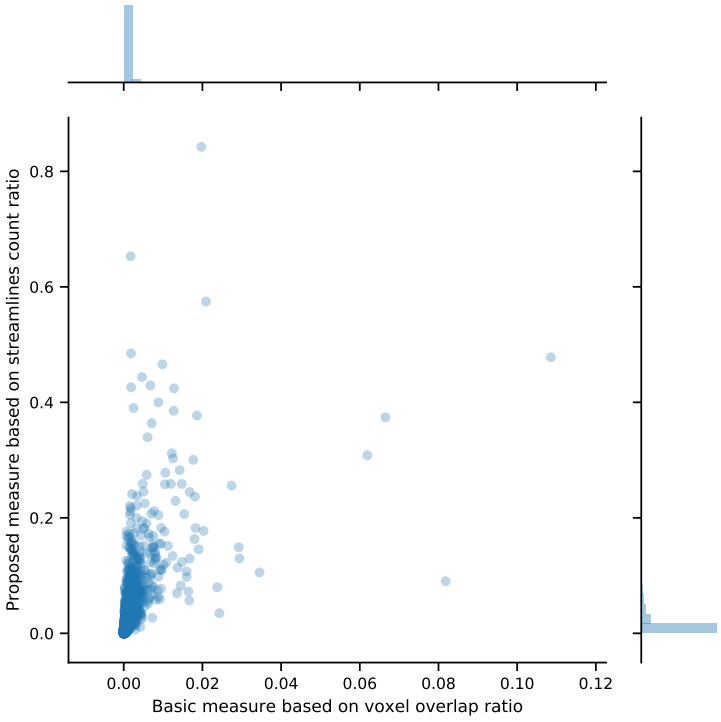

Figure B.16: Comparison between results obtained with both structural measures for the AR R tract.

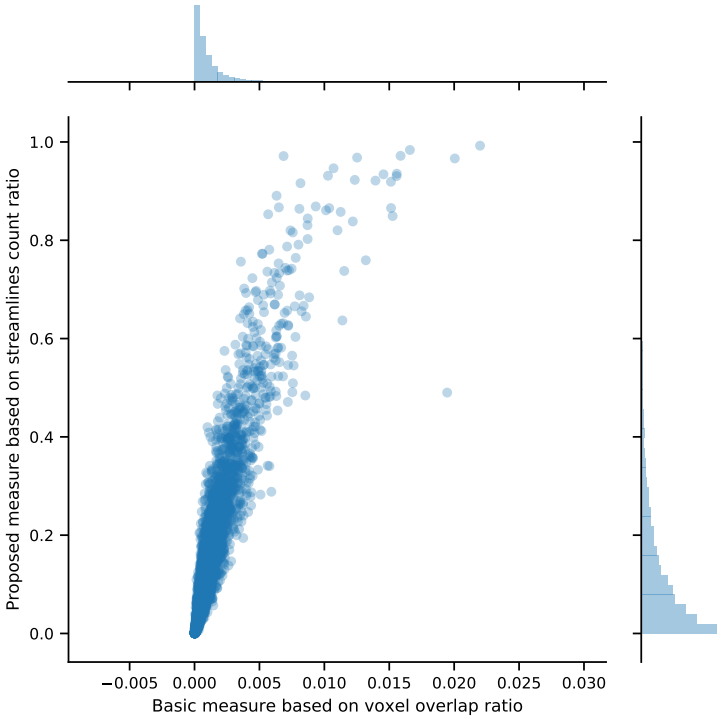

Figure B.17: Comparison between results obtained with both structural measures for the ATR L tract.

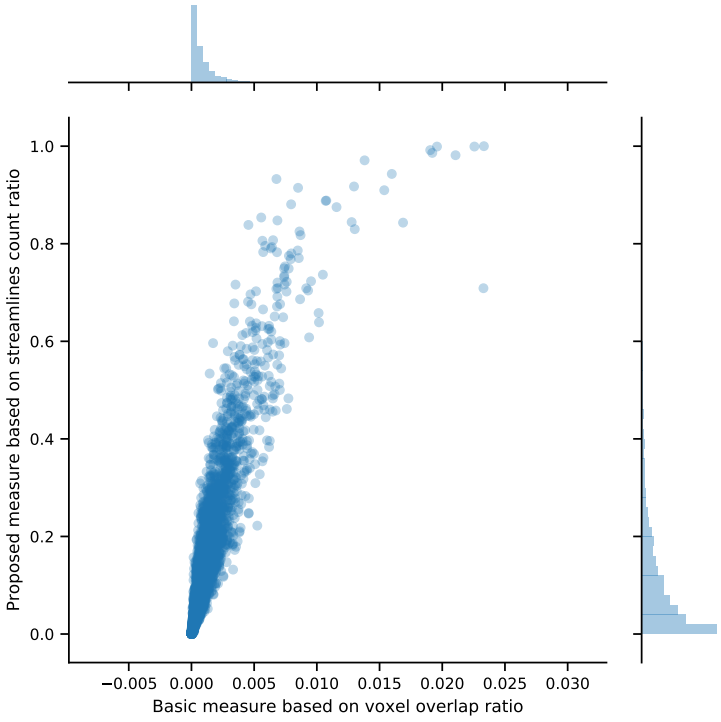

Figure B.18: Comparison between results obtained with both structural measures for the ATR R tract.

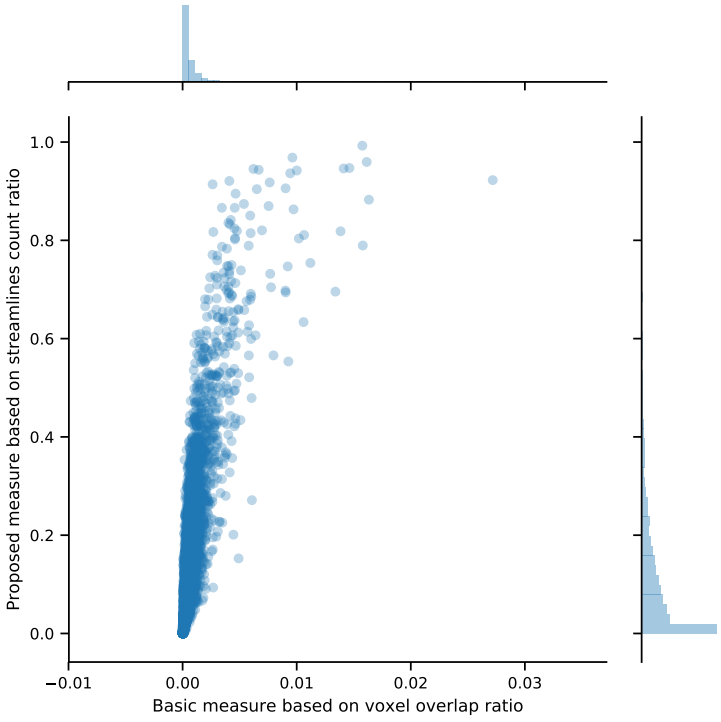

Figure B.19: Comparison between results obtained with both structural measures for the PTR L tract.

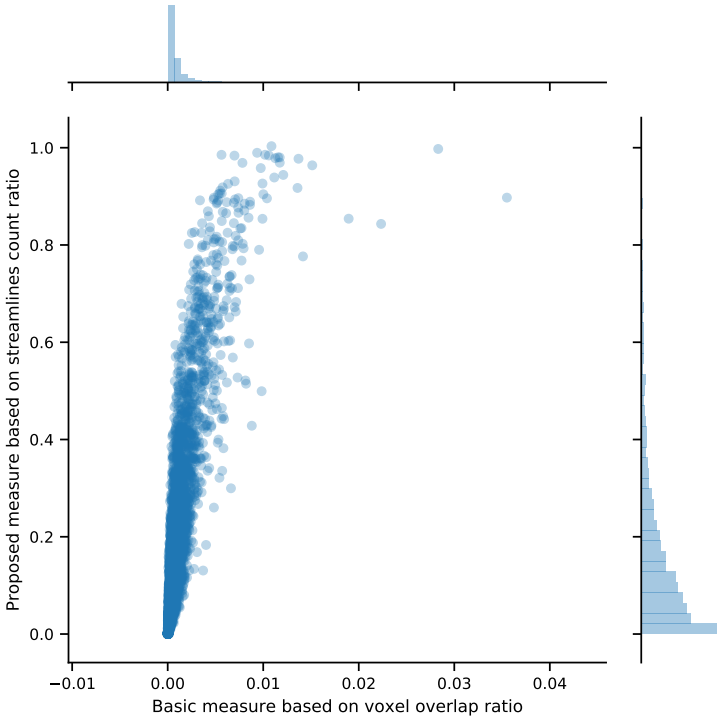

Figure B.20: Comparison between results obtained with both structural measures for the PTR R tract.

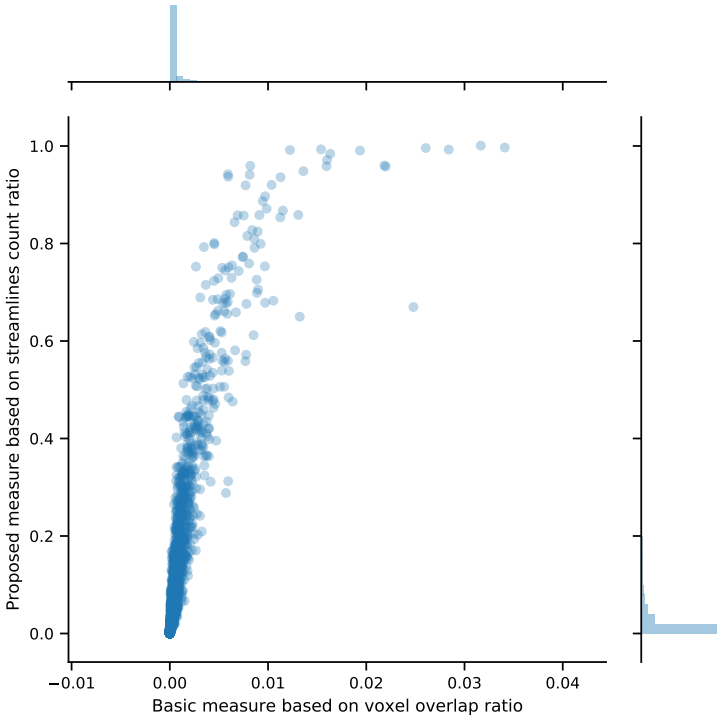

Figure B.21: Comparison between results obtained with both structural measures for the STR L tract.

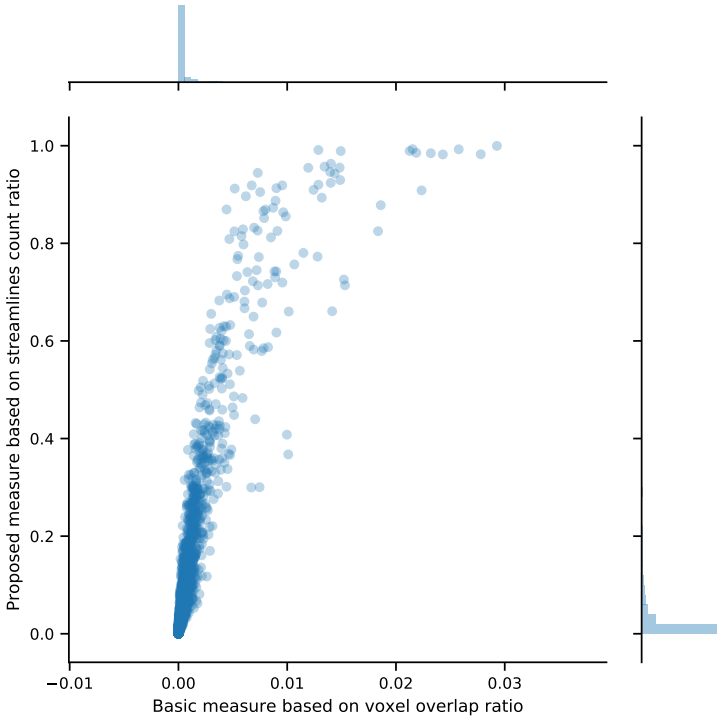

Figure B.22: Comparison between results obtained with both structural measures for the STR R tract.

C

Functional vs structural connectivity measures for different tracts

Figures C.1 to C.11 present the data for all the tracts. They were calculated using the full correlation (without regressing out CSF and WM) as a functional measure plotted against the streamline based structural measure. This corresponds to the top left hand case subplots in figures 4.10 and 4.11.

The distributions of the measures varied between the tracts (note that the range of values on both axes are not constant). For all but two tracts (IFO R and AR L), the trend is negative, i.e. with increased structural WMH impact there is an observed decrease in the functional connectivity, however not all of those relationships are statistically significant. In these plots, we show the regression coefficients (right bottom corner of each scatter plot), while correlation coefficients (and their significance) are going to be presented in figure 4.12. From there we can read which of those relationships were significant after Bonferroni correction for the majority of the tracts. That includes FMA and FMI, SLF and UNC for both hemispheres, ILF R, as well as CGC L and, from the thalamic tracts, ATR (both hemispheres) and PTR R.

For the callosal tracts (figure C.1) we observe the significant negative correlations for both tracts. For FMA, the points are quite disperse but the negative trend is

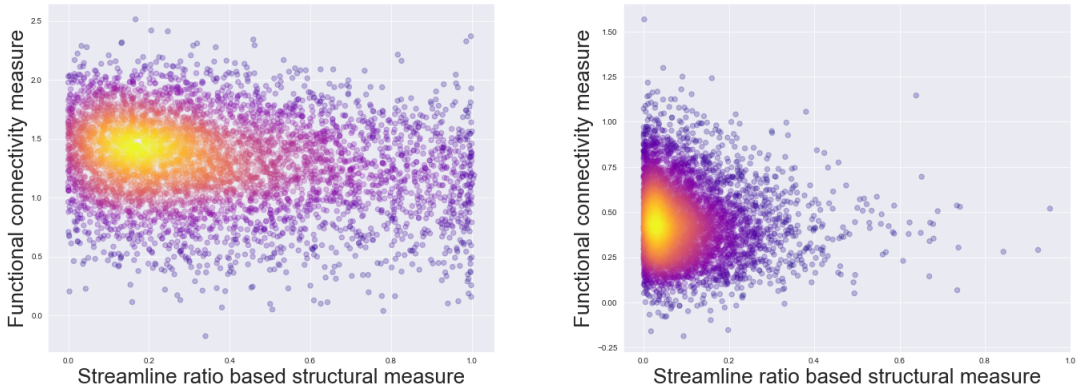

(a) FMA **(b)** FMI

Figure C.1: Scatter plot of the relationship between the structural measure of the WMHs based on the streamlines ratio and the functional measure (full correlation, r to z transformed) for the callosal tracts: FMA (left hand side), FMI (right hand side).

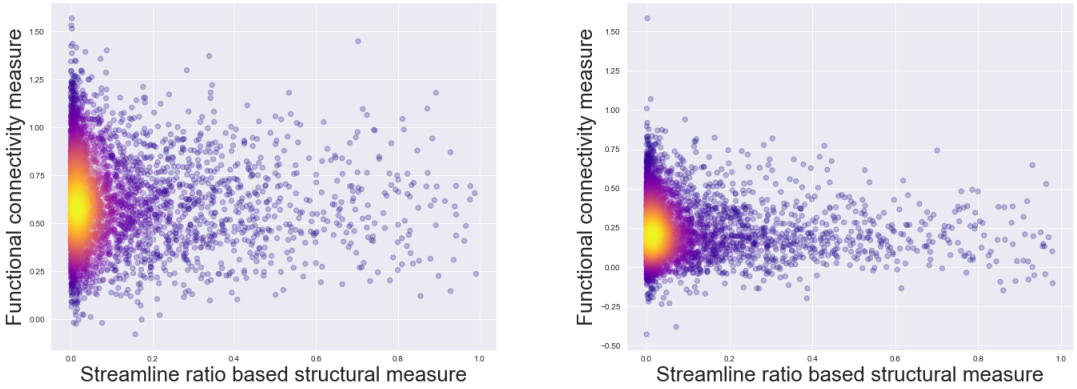

Figure C.2: Scatter plot of the relationship between the structural measure of the WMHs based on the streamlines ratio and the functional measure (full correlation, r to z transformed) for the SLF tract: for right hemisphere (left hand side), for left hemisphere (right hand side).

clearly noticeable. For FMI, as most of the structural measures are smaller than half, there might be a bit stronger influence from the outliers causing that negative correlation, however it is the case that many of the outliers with higher structural measures have a relatively low functional measure. That is even more strongly visible in other tracts, first in the association tracts and then, very strikingly, in the CG tracts (figures C.6 and C.7). That is understandable as most of the subjects had very low WMH loads on the CG tracts, however that opens a discussion point about the importance of addressing the problem of the outliers in future work.

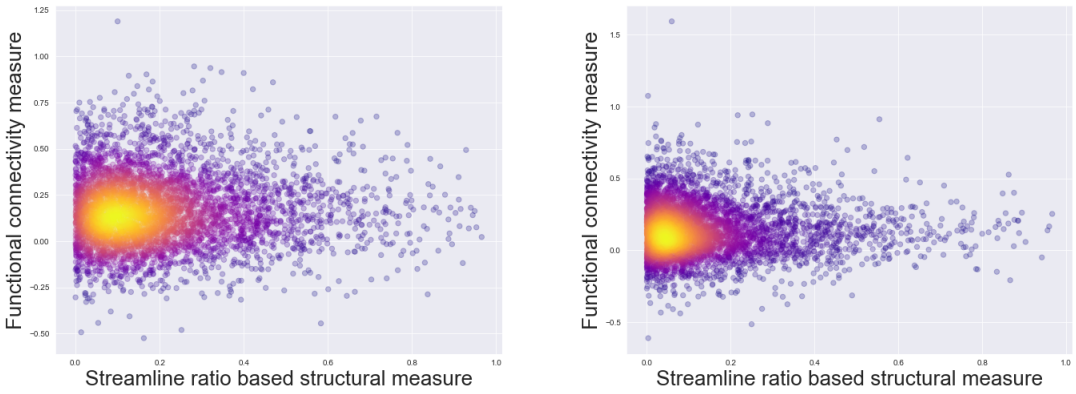

Figure C.3: Scatter plot of the relationship between the structural measure of the WMHs based on the streamlines ratio and the functional measure (full correlation, r to z transformed) for the IFO tract: for right hemisphere (left hand side), for left hemisphere (right hand side).

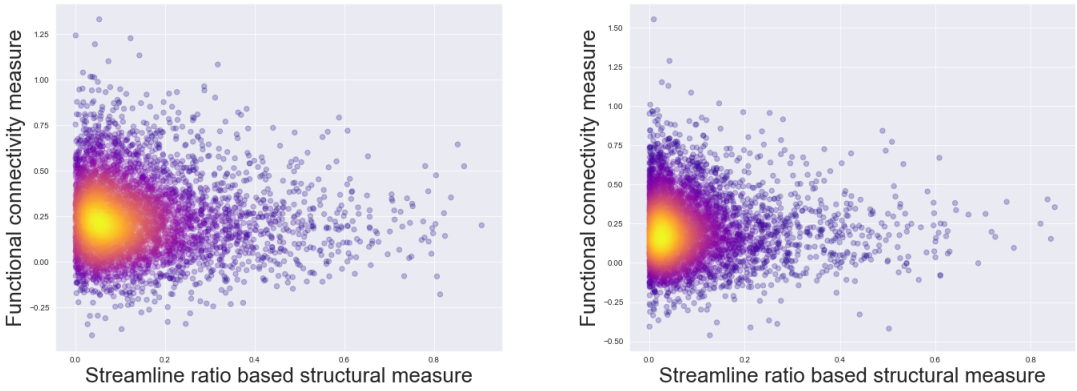

Figure C.4: Scatter plot of the relationship between the structural measure of the WMHs based on the streamlines ratio and the functional measure (full correlation, r to z transformed) for the ILF tract: for right hemisphere (left hand side), for left hemisphere (right hand side).

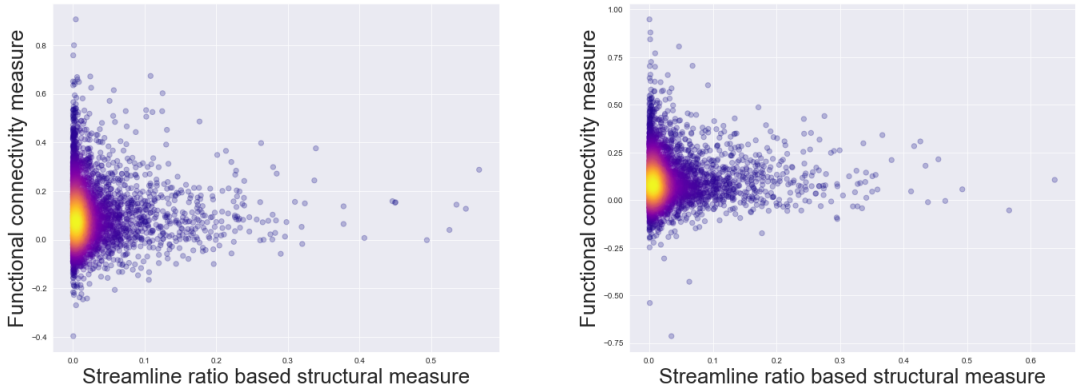

Figure C.5: Scatter plot of the relationship between the structural measure of the WMHs based on the streamlines ratio and the functional measure (full correlation, r to z transformed) for the UNC tract: for right hemisphere (left hand side), for left hemisphere (right hand side).

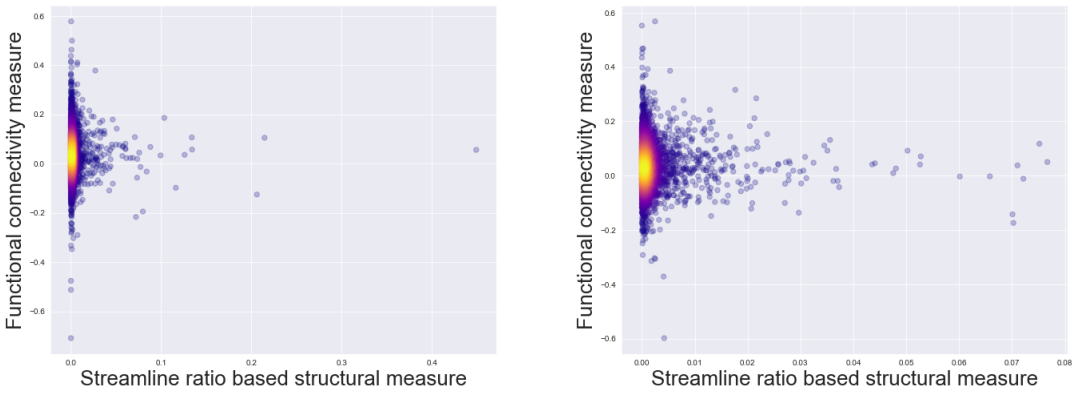

Figure C.6: Scatter plot of the relationship between the structural measure of the WMHs based on the streamlines ratio and the functional measure (full correlation, r to z transformed) for the CGH tract: for right hemisphere (left hand side), for left hemisphere (right hand side).

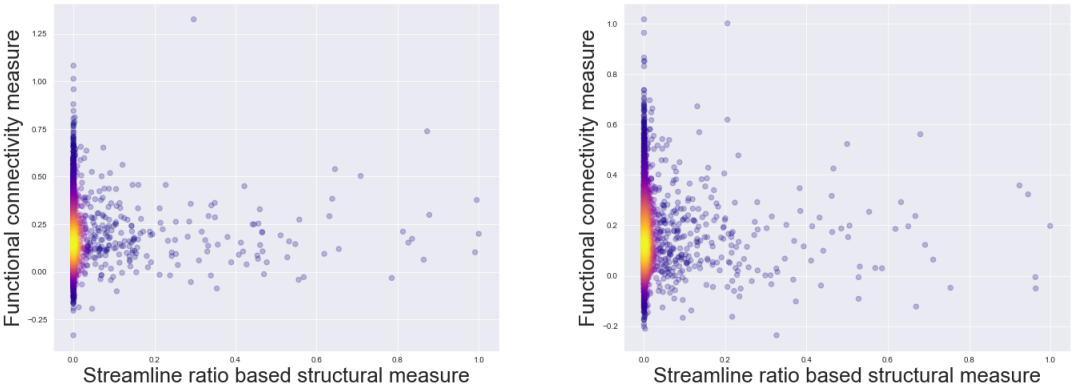

Figure C.7: Scatter plot of the relationship between the structural measure of the WMHs based on the streamlines ratio and the functional measure (full correlation, r to z transformed) for the CGC tract: for right hemisphere (left hand side), for left hemisphere (right hand side).

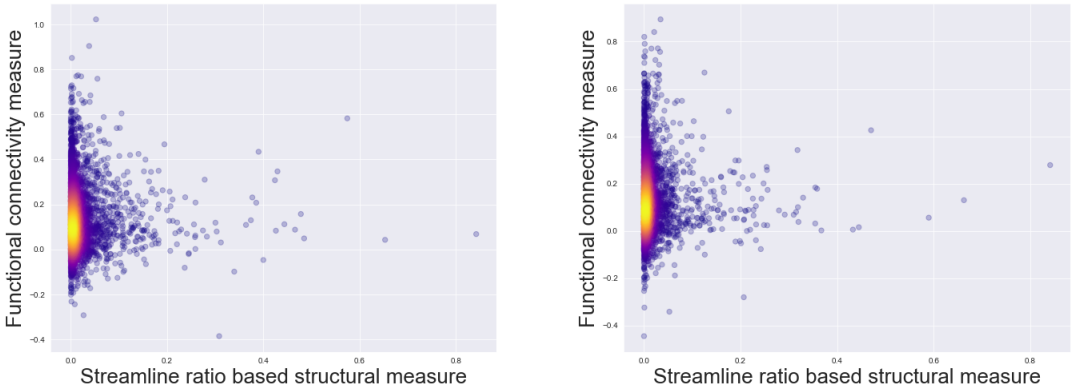

Figure C.8: Scatter plot of the relationship between the structural measure of the WMHs based on the streamlines ratio and the functional measure (full correlation, r to z transformed) for the AR tract: for right hemisphere (left hand side), for left hemisphere (right hand side).

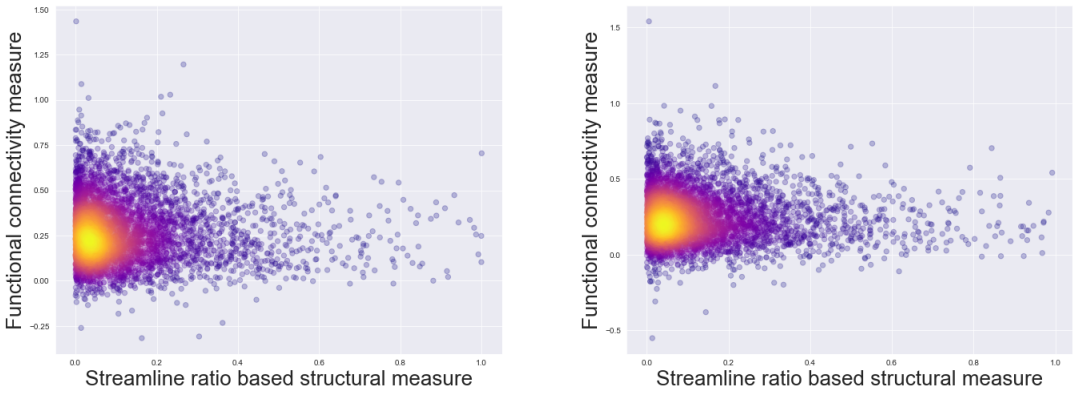

Figure C.9: Scatter plot of the relationship between the structural measure of the WMHs based on the streamlines ratio and the functional measure (full correlation, r to z transformed) for the ATR tract: for right hemisphere (left hand side), for left hemisphere (right hand side).

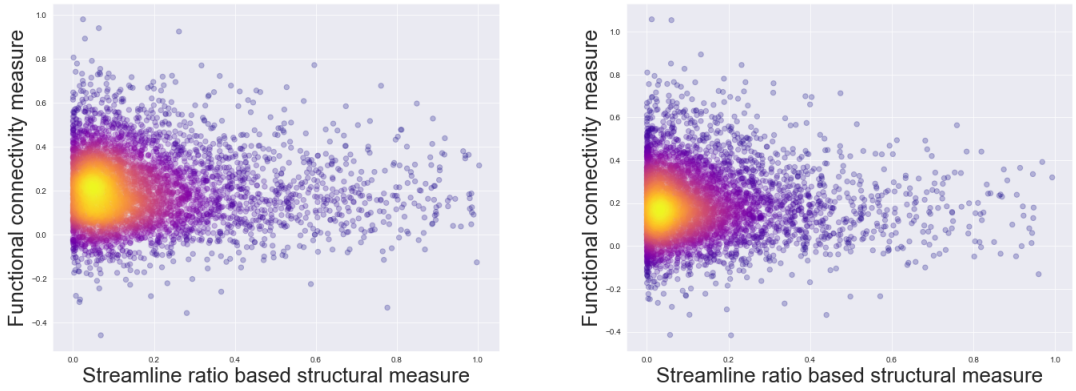

Figure C.10: Scatter plot of the relationship between the structural measure of the WMHs based on the streamlines ratio and the functional measure (full correlation, r to z transformed) for the PTR tract: for right hemisphere (left hand side), for left hemisphere (right hand side).

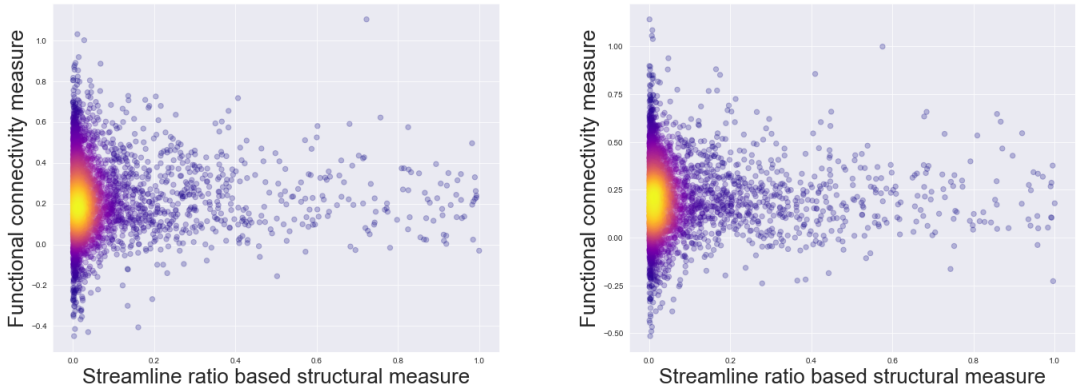

Figure C.11: Scatter plot of the relationship between the structural measure of the WMHs based on the streamlines ratio and the functional measure (full correlation, r to z transformed) for the STR tract: for right hemisphere (left hand side), for left hemisphere (right hand side).

D

Analysis of structural and functional connectivity correlation for subsets of data

For the majority of the subjects in the analysed dataset, in nearly all the white matter tracts, the disruption of structural connectivity (for both measures) is non-zero but very small. Therefore, to ensure that this non-uniformity of the independent variable does not have an impact on the conclusions of the work presented in chapter 4, we present an additional analysis. We use only subsets of the data with the highest structural measure values and repeat the analysis on these subsets.

In the original analysis, we used 5000 subjects from the UK Biobank. Here, we analyse the highest percentiles of the data, i.e. for the x_{th} percentile it would be a subset of the data that only includes subjects with a structural measure value higher than x percent, as measured across all the subjects

Figure D.1 presents results for the AR tract for the right hemisphere when using full correlation (with no WM or CSF signal removal) as the functional connectivity value and streamline ratio as the disruption of structural connectivity measure for the highest 75th, 90th, and 95th percentiles of the data, respectively. Figure D.2 presents similar plots for the same functional measure but using the structural overlap measure on the x axis. As it is difficult to formulate observations directly from these qualitative plots, we also present the rank correlation values for each of

those plots, for selected tracts, for multiple choices of the percentiles in figures D.3 and D.4, for the streamline ratio measure and overlap measure, respectively. From those figures, we can observe that the values of the correlations change slightly when limiting the subset of the data, especially when only the top $5\% - 10\%$ of the data is considered. There is, however, no clear pattern of that relationship that would apply to all the tracts. For the overlap measure, plotted in figure D.4 the values of correlations do not change a lot for lower values of percentiles, and only start to vary appreciably for the highest percentiles. That is probably related to the fact that with the higher percentiles applied, the subsets of the data used are smaller, therefore p-values (not presented in plots) become large, and correlation values are not statistically significant. For comparison, we also present analogous plots for values of Pearson correlation in figures D.5 and D.6. Here, we observe that the correlation values are nearly constant until the 95th percentile, which is the situation when only 5% of the data is left. Again, there is no clear trend as values go higher and lower for diferent tracts, and these correlations have large p-values, therefore are not statistically significant.

Based on the observations from the plots, we conclude that there is no clear indication to use one of the percentiles over the other, or to limit the subset of the data used for the analysis.

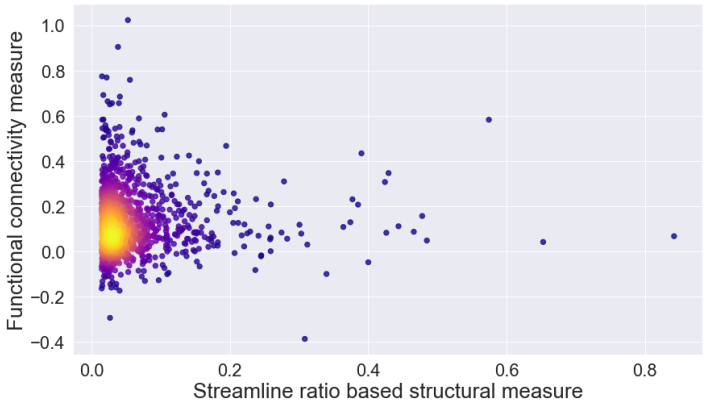

(a) Plot excluding all data below the 75th percentile of the structural measure.

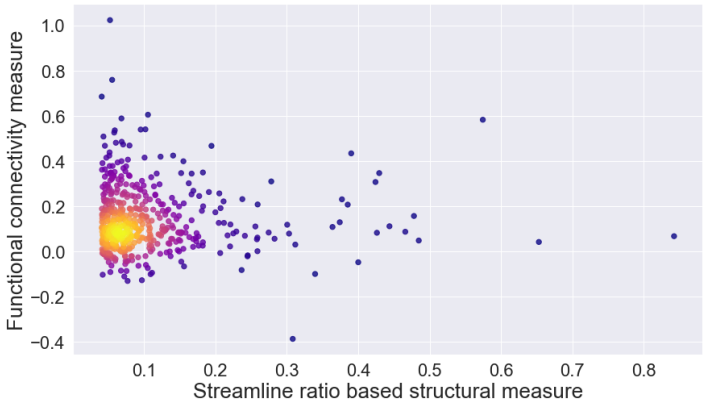

(b) Plot excluding all data below the 90th percentile of the structural measure.

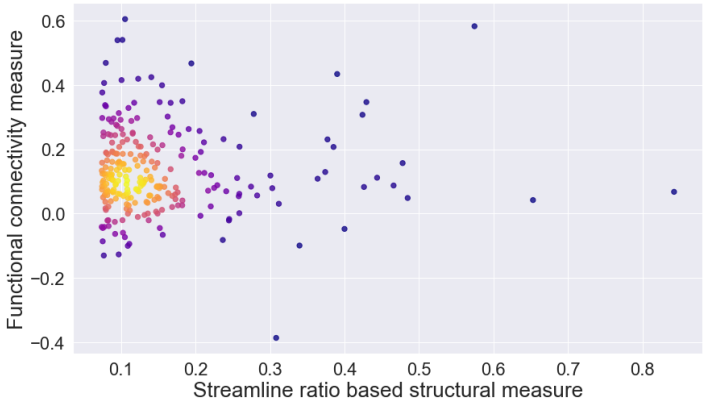

(c) Plot excluding all data below the 95th percentile of the structural measure.

Figure D.1: Scatter plot of the relationship between the structural measure of the WMHs based on the streamline ratio and the full correlations (no CSF or WM signal removed) as a functional measure for the AR tract in the right hemisphere.

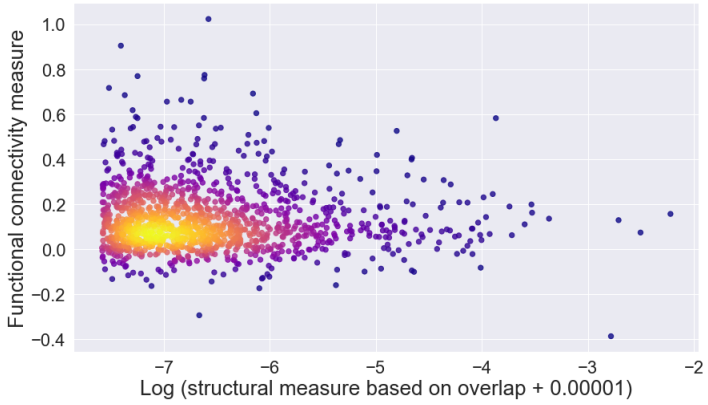

(a) Plot excluding all data below the 75th percentile of the structural measure.

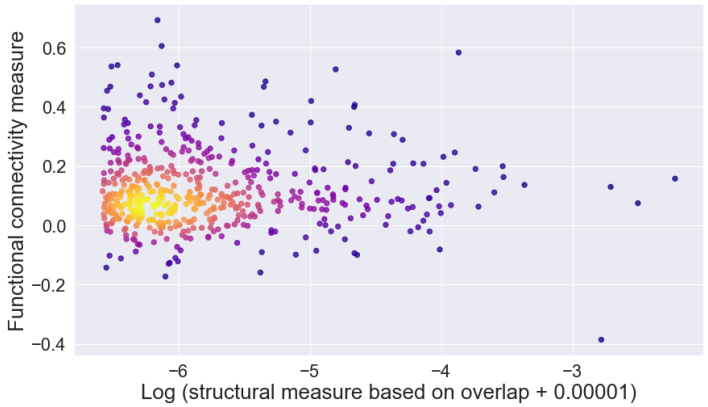

(b) Plot excluding all data below the 90th percentile of the structural measure.

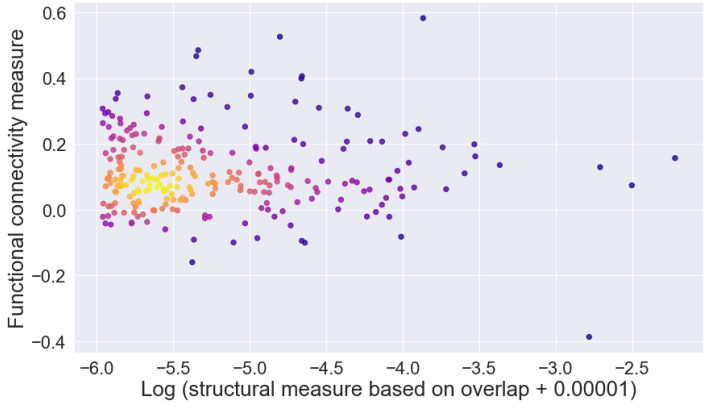

(c) Plot excluding all data below the 95th percentile of the structural measure.

Figure D.2: Scatter plot of the relationship between the structural measure of the WMHs based on the volumetric overlap ratio and the full correlations (no CSF or WM signal removed) as a functional measure for the AR tract in the right hemisphere.

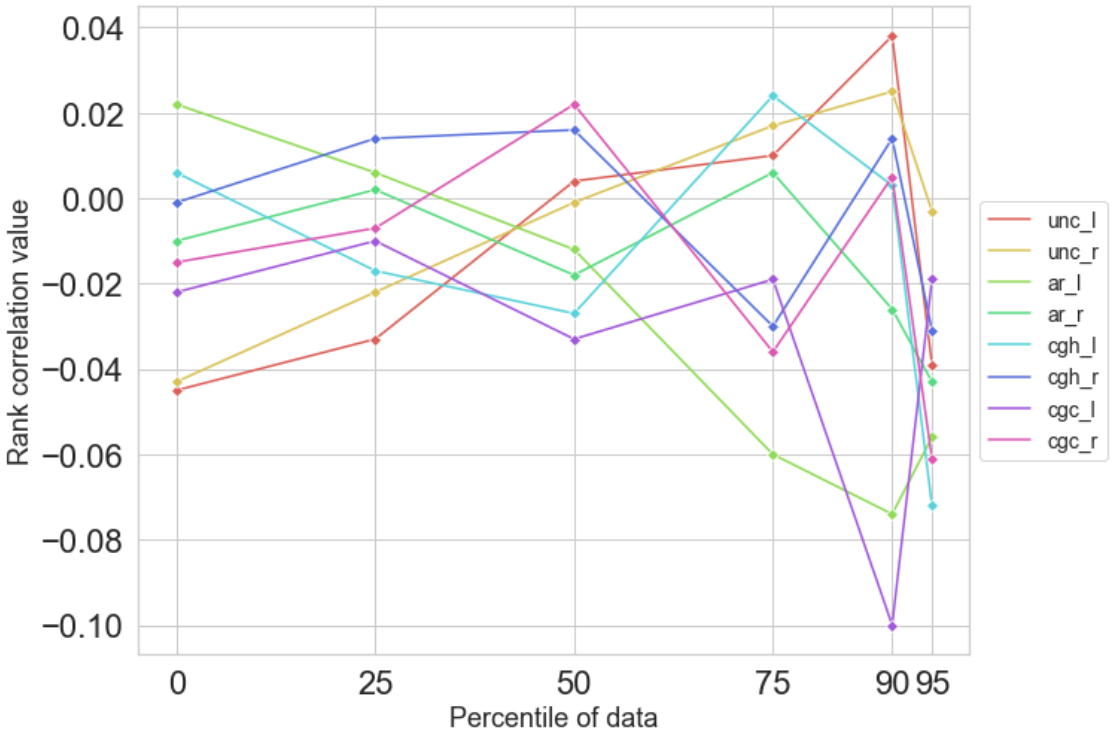

Figure D.3: The figure presents correlation values (on the y axis) obtained with different subsets of the data, described by the percentile value (marked on the x axis) for selected tracts. The values were calculated for the rank-based correlation between the structural measure based on the streamline ratio and functional connectivity based on the full correlations. The values of percentiles on the x axis are not linear, in order to present the variability for the highest thresholds. For those thresholds (90th and 95th percentiles) the correlation values vary from previous values but are also accompanied by high p-values (not pictured in the figure).

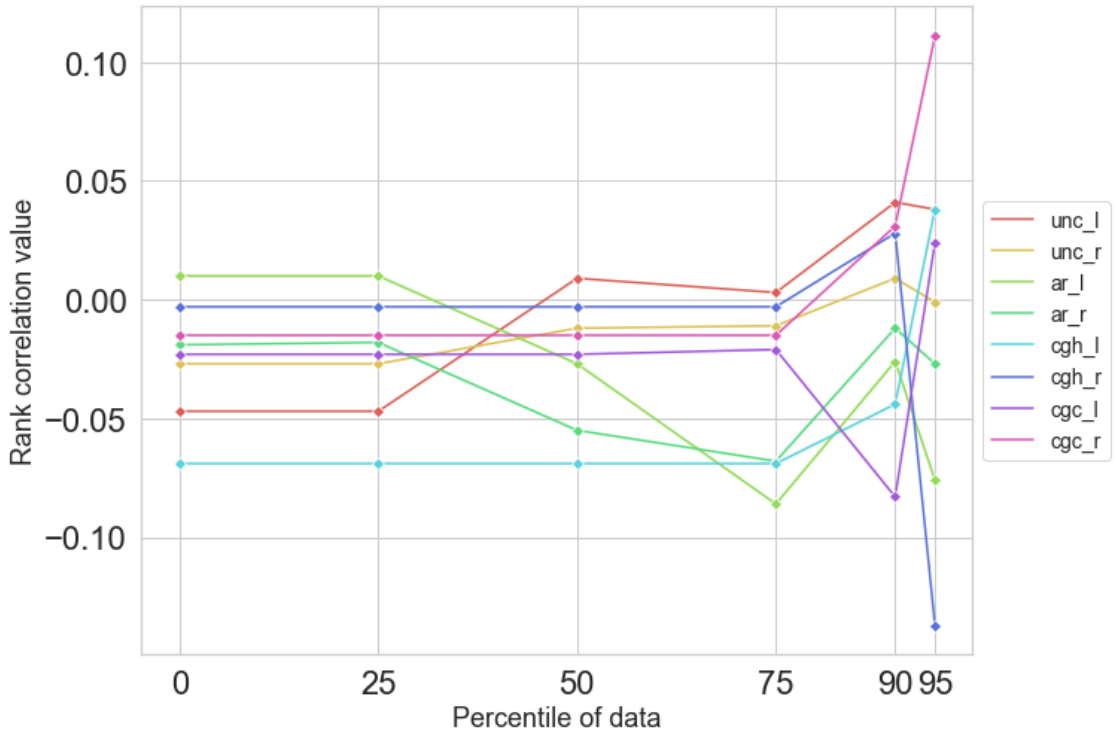

Figure D.4: The figure presents correlation values (on the y axis) obtained with different subsets of the data, described by the percentile value (marked on the x axis) for selected tracts. The values were calculated for the rank-based correlation between the structural measure based on the volumetric overlap and functional connectivity based on the full correlations. The values of percentiles on the x axis are not linear, in order to present the variability for the highest thresholds. For those thresholds (90th and 95th percentiles) the correlation values vary from previous values but are also accompanied by high p-values (not pictured in the figure).

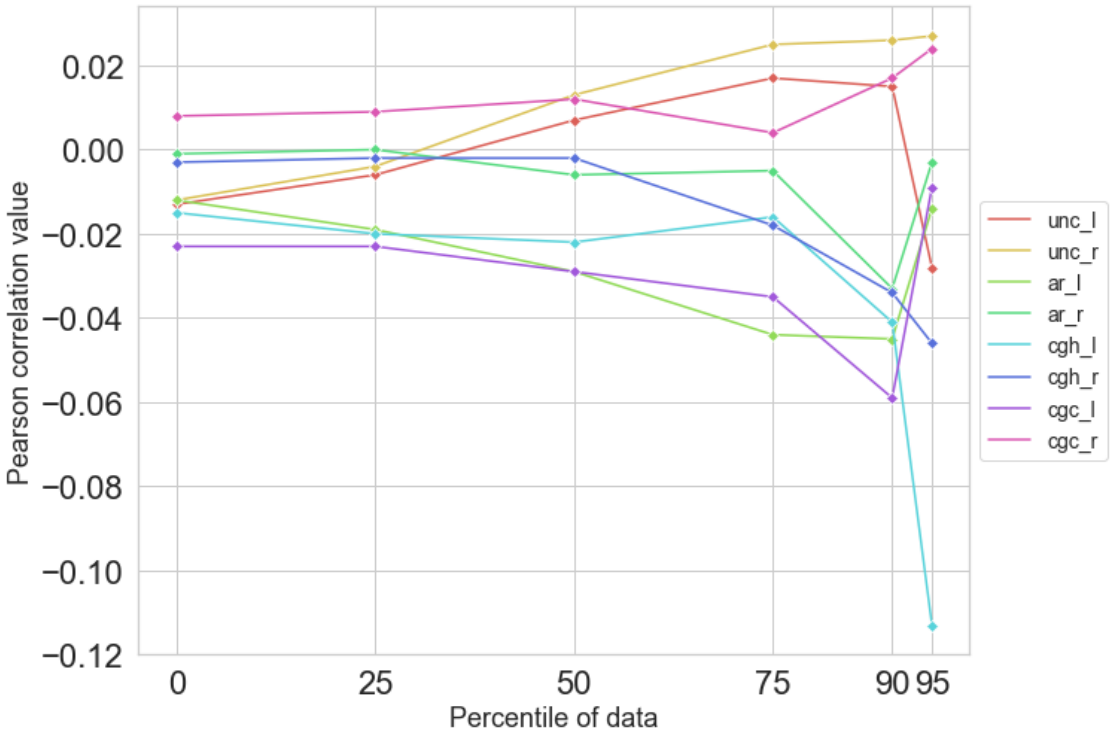

Figure D.5: The figure presents correlation values (on the y axis) obtained with different subsets of the data, described by the percentile value (marked on the x axis) for selected tracts. The values were calculated for Pearson correlation between the structural measure based on the streamline ratio and functional connectivity based on the full correlations. The values of percentiles on the x axis are not linear, in order to present the variability for the highest thresholds. For those thresholds (90th and 95th percentiles) the correlation values vary from previous values but are also accompanied by high p-values (not pictured in the figure).

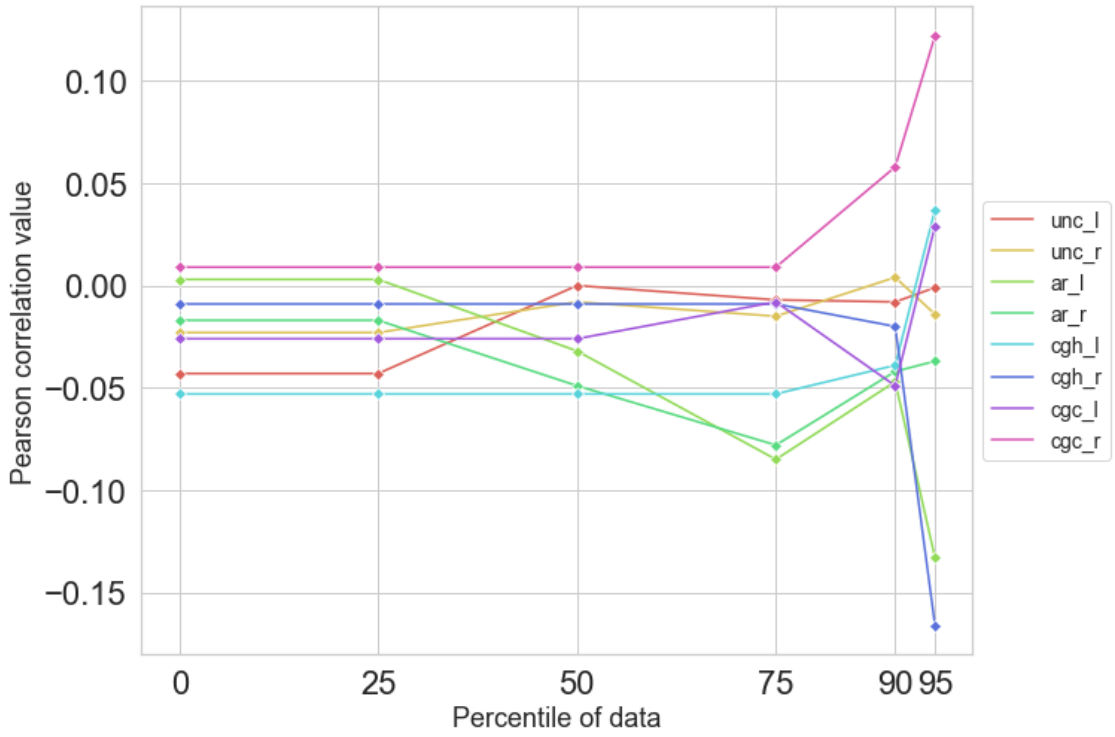

Figure D.6: The figure presents correlation values (on the y axis) obtained with different subsets of the data, described by the percentile value (marked on the x axis) for selected tracts. The values were calculated for Pearson correlation between the structural measure based on the volumetric overlap and functional connectivity based on the full correlations. The values of percentiles on the x axis are not linear, in order to present the variability for the highest thresholds. For those thresholds (90th and 95th percentiles) the correlation values vary from previous values but are also accompanied by high p-values (not pictured in the figure).

E

Voxelwise tractography analysis results for all the tracts

Contents

E.1 All the data 181
E.1.1 Two columns in design matrix 181
E.1.2 Relative difference when accounting for confounds – 4 columns in the design matrix 190
E.1.3 Results when contrasts are modified 191
E.2 Subset with narrow age range 198
E.3 Single sex subset within the narrow age range 198

In this appendix we present additional results from the analysis presented in section 5.5. In the main body of the thesis we showed only selected tracts, here we expand the presentation of the results to a larger number of tracts.

E.1 All the data

E.1.1 Two columns in design matrix

In figures E.1 and E.2 results are presented for the callosal fibres: FMI and FMA. These fibres connect corresponding areas of the cortex in both hemispheres. The results also seem to be symmetrical between the hemispheres. In both of those fibres, both positive and negative results are present. In the case of FMI there is an

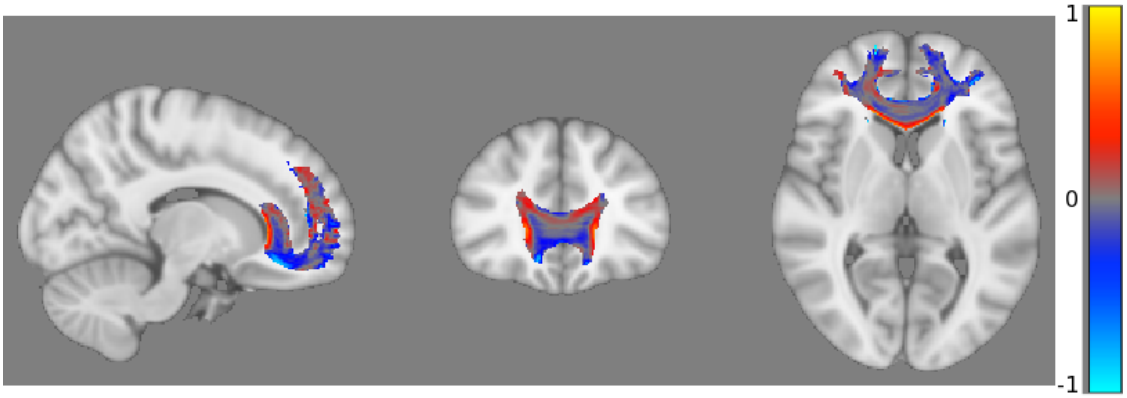

Figure E.1: Scaled β values from the voxelwise GLM comparison between cases of presence and absence of WMHs for the FMI tract.

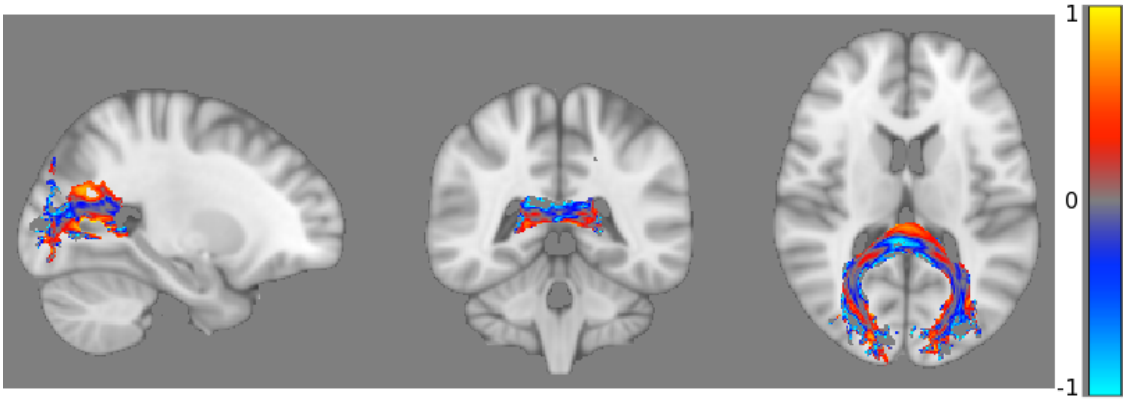

Figure E.2: Scaled β values from the voxelwise GLM comparison between cases of presence and absence of WMHs for the FMA tract.

area with values closer to zero in the middle of the tract, while FMA shows rather extreme values (and not that smoothly distributed) for the whole tract. That might again be related to the fact that the vast majority of the subjects have some WMHs on FMA. In both cases a pattern can be observed of positive (red) results mostly distributed on the medial side of the tract (on the side of the ventricles), with tract endings having rather negative values. That represents increased probabilities of voxels belonging to parts of the tract closer to the ventricles and lower tractography strength closer to the cortex in the case when WMHs are present.

Interestingly, this pattern is not necessary repeated in the association fibres. In the SLF for both sides there is very little relative effect (figures E.3, E.4). The right hemisphere tract shows slightly more effect but for both we see that most of the tract shows no relative difference, only at the edges are there some non-zero

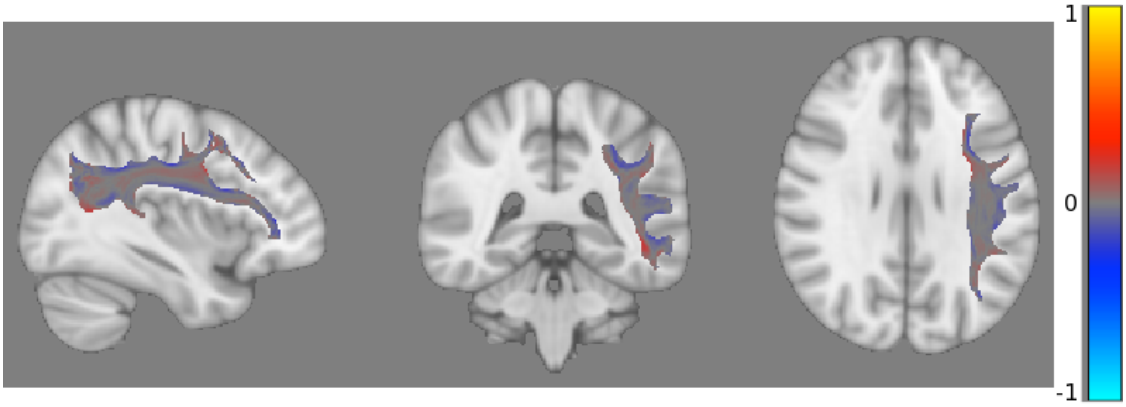

Figure E.3: Scaled β values from the voxelwise GLM comparison between cases of presence and absence of WMHs for the SLF L tract.

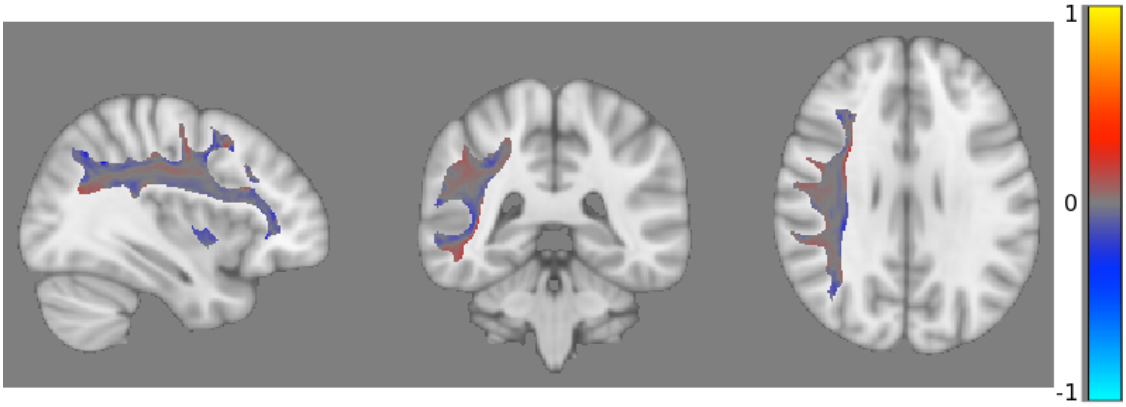

Figure E.4: Scaled β values from the voxelwise GLM comparison between cases of presence and absence of WMHs for the SLF R tract.

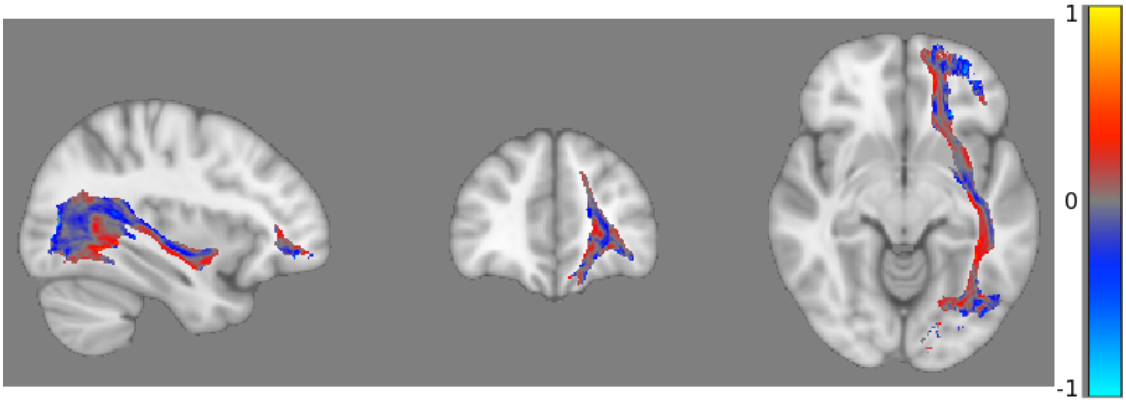

Figure E.5: Scaled β values from the voxelwise GLM comparison between cases of presence and absence of WMHs for the IFO L tract.

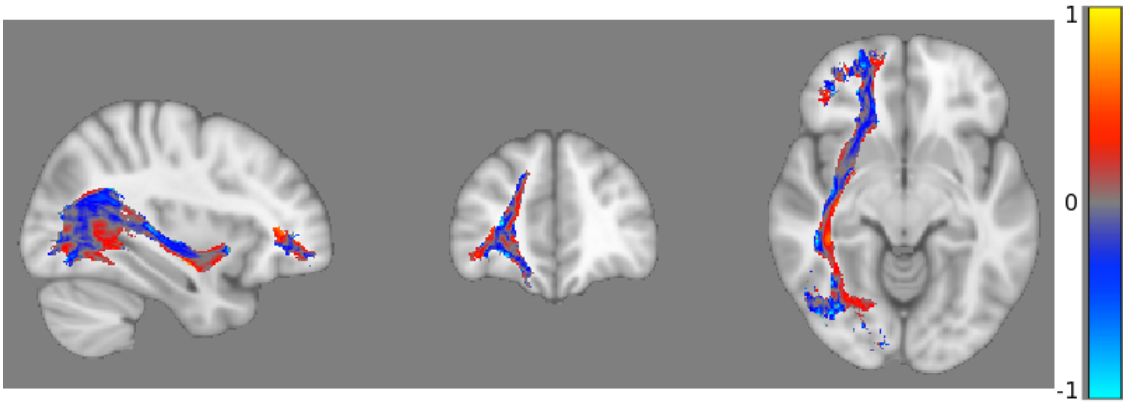

Figure E.6: Scaled β values from the voxelwise GLM comparison between cases of presence and absence of WMHs for the IFO R tract.

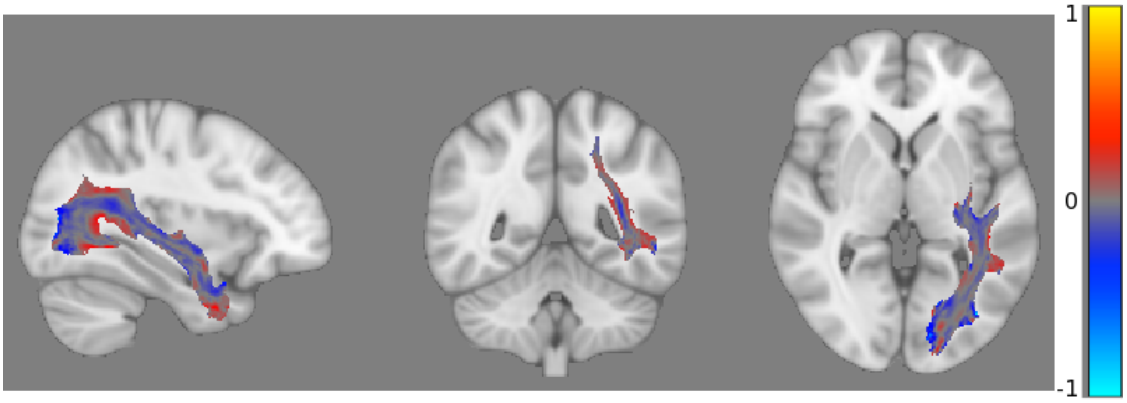

Figure E.7: Scaled β values from the voxelwise GLM comparison between cases of presence and absence of WMHs for the ILF L tract.

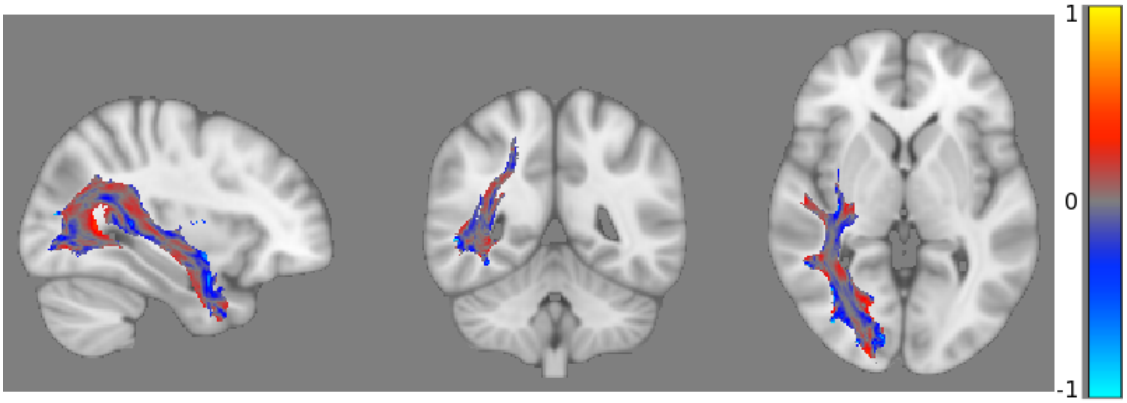

Figure E.8: Scaled β values from the voxelwise GLM comparison between cases of presence and absence of WMHs for the ILF R tract.

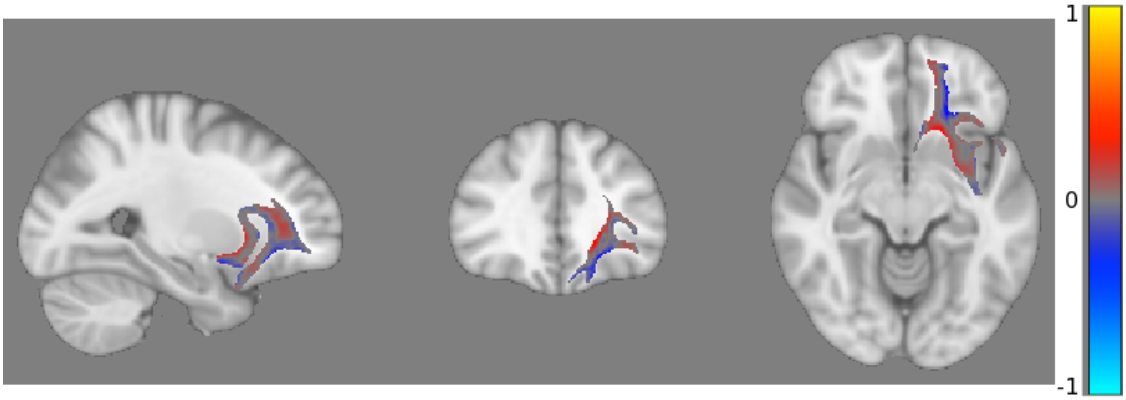

Figure E.9: Scaled β values from the voxelwise GLM comparison between cases of presence and absence of WMHs for the UNC L tract.

values. That, however, probably just reflects general variability in tractography results between the subjects (as the intensity of changes, even in the most prominent clusters, is much smaller than for the previously discussed tracts).

Stronger results are observed for the IFO bilaterally (figures E.5, E.6). In the posterior part there can be observed positive effects (increased probabilities of voxels belonging to the tract) on the deep WM side of the tract. In the frontal part there are some negative effects at the edges. Again, those relationships are not that prominent in the ILF, despite its spatial proximity to the IFO, which showed more substantial effects. However, the results for the ILF are still much more prominent than in the UNC (figures E.9, E.10). The main part of the tract, in the centre, does not show any differences. Some effects are visible around the edges of the tract – similar to the collosal fibres where we observed more positive values in the deeper part of the brain and more negative values in the frontal part, closer to the cortex. Although the pattern is visible, the values are not very high, reaching only halfway up the scale on both the positive and negative sides.

Following this are the results for the limbic tracts. In the CGH (figures E.11, E.12) there is a pattern of the superior part being more positive and the inferior more negative. This pattern is very similar for both hemispheres, with slightly higher values on the positive side in the left half. In the CGC (figures E.13, E.14) the side closer to the white matter shows more positive effects and closer to the gray

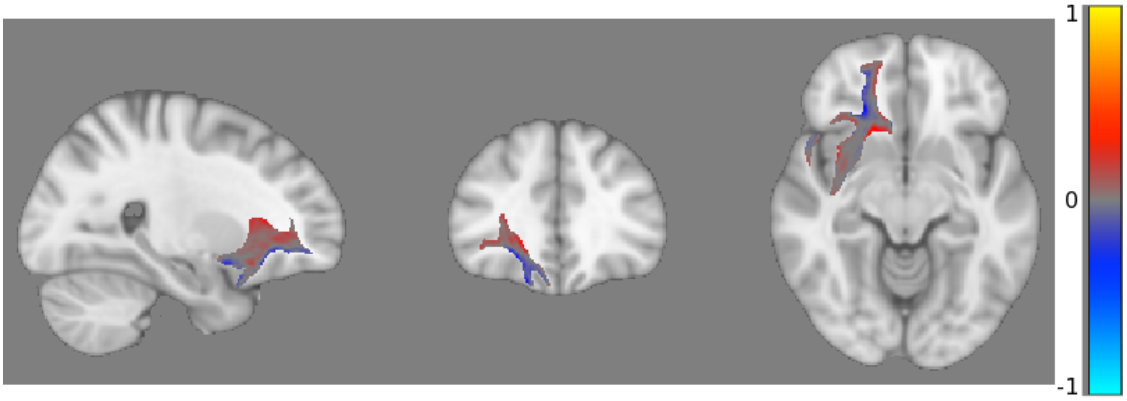

Figure E.10: Scaled β values from the voxelwise GLM comparison between cases of presence and absence of WMHs for the UNC R tract.

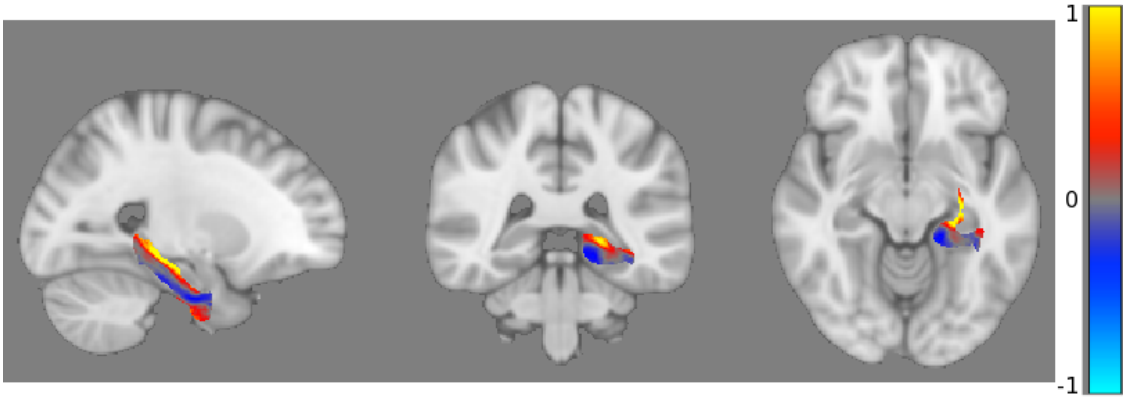

Figure E.11: Scaled β values from the voxelwise GLM comparison between cases of presence and absence of WMHs for the CGH L tract.

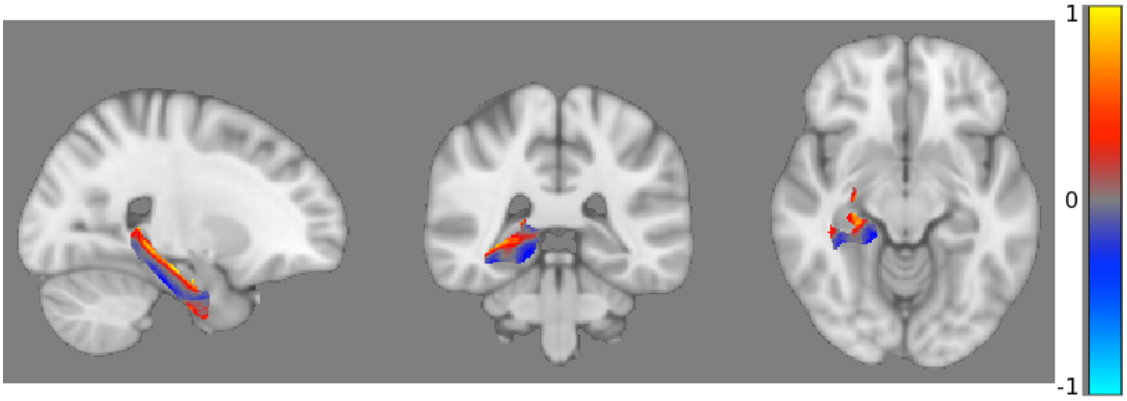

Figure E.12: Scaled β values from the voxelwise GLM comparison between cases of presence and absence of WMHs for the CGH R tract.

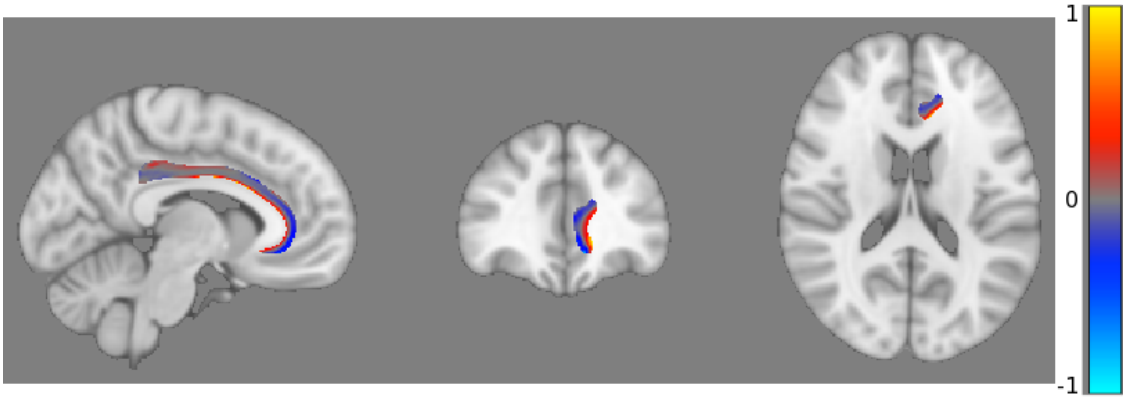

Figure E.13: Scaled β values from the voxelwise GLM comparison between cases of presence and absence of WMHs for the CGC L tract.

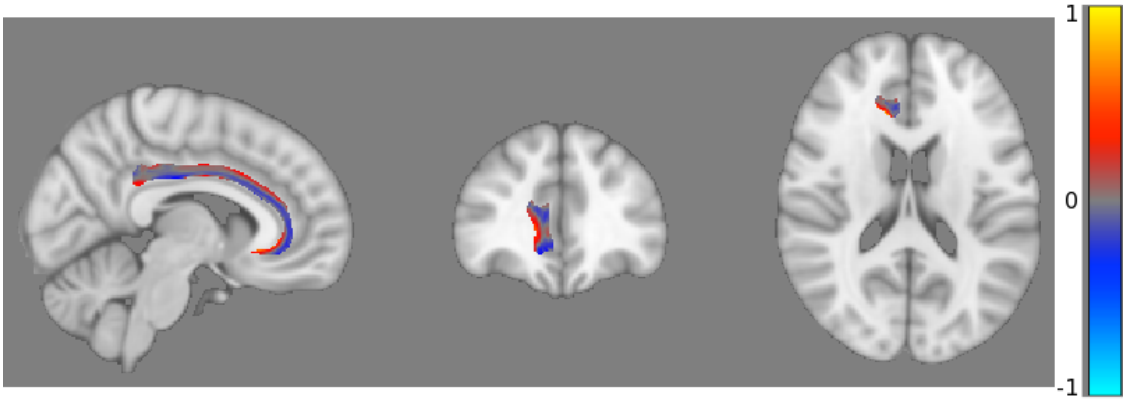

Figure E.14: Scaled β values from the voxelwise GLM comparison between cases of presence and absence of WMHs for the CGC R tract.

matter more negative ones. It is worth noting that for both hemispheres the results are very symmetrical, which is important for methodological validation purposes.

Similar patterns, although slightly less striking, are shown in the thalamic tracts as well. They are also similarly symmetrical between the hemispheres. For the AR (figures E.15, E.16) the effect is moderately strong, and slightly stronger in the left hemisphere. The pattern observed here is different than in previous tracts – the middle of the tracts show a negative effect and the outside part, the edges of the tract, show a positive difference, especially in the superior part. A similar pattern is visible for the ATR (figures E.17, E.18), with a stronger effect, especially in the left hemisphere. There is again a visible effect that was noted for the collosal fibres - with increased probabilities towards the medial part of the brain. Less of this effect is seen for the PTR (figures E.19, E.20), however the clusters of values

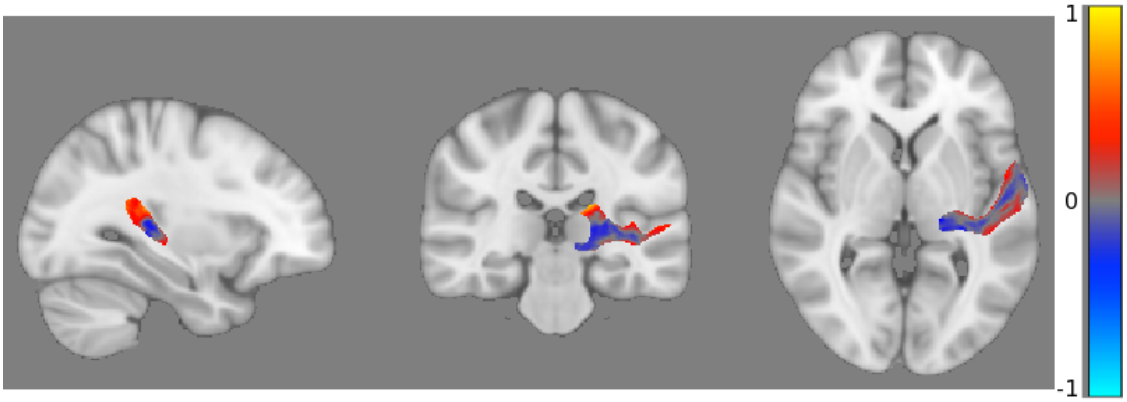

Figure E.15: Scaled β values from the voxelwise GLM comparison between cases of presence and absence of WMHs for the AR L tract.

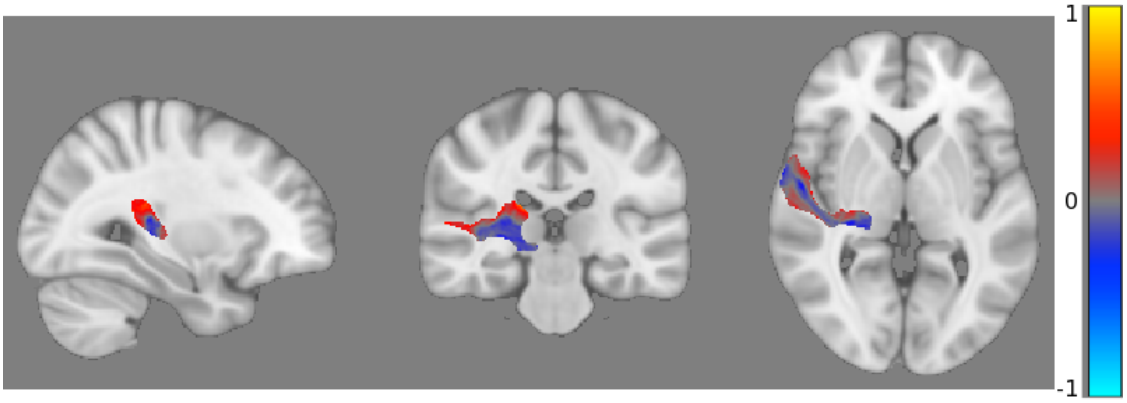

Figure E.16: Scaled β values from the voxelwise GLM comparison between cases of presence and absence of WMHs for the AR R tract.

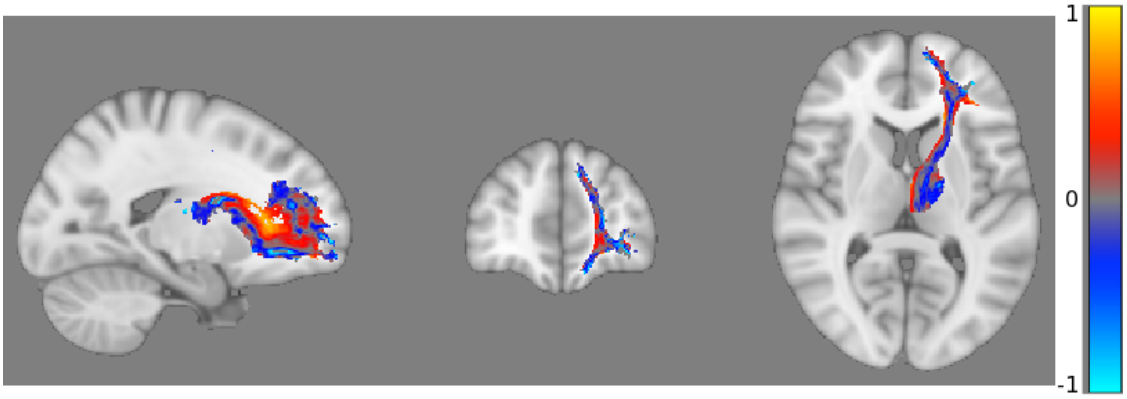

Figure E.17: Scaled β values from the voxelwise GLM comparison between cases of presence and absence of WMHs for the ATR L tract.

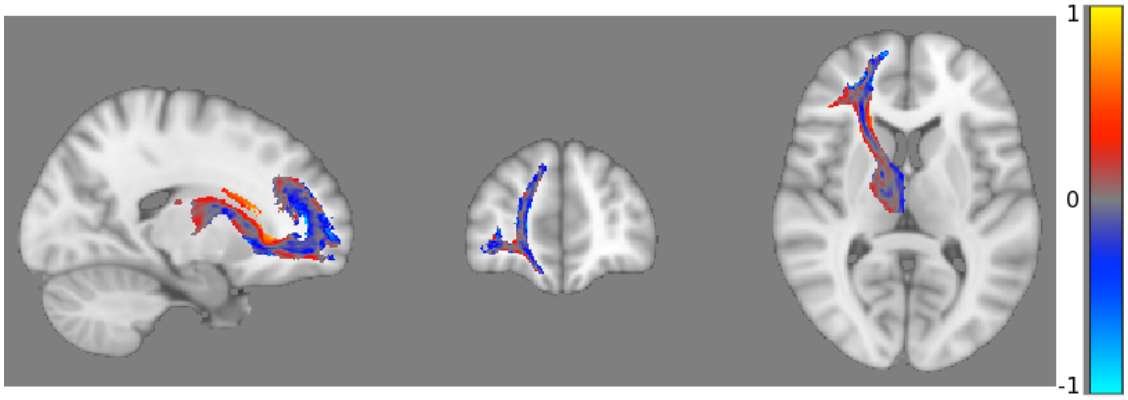

Figure E.18: Scaled β values from the voxelwise GLM comparison between cases of presence and absence of WMHs for the ATR R tract.

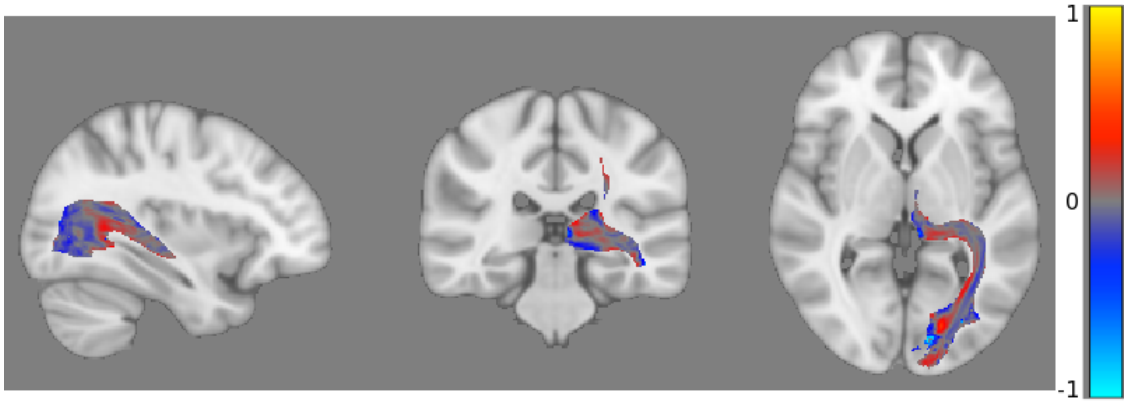

Figure E.19: Scaled β values from the voxelwise GLM comparison between cases of presence and absence of WMHs for the PTR L tract.

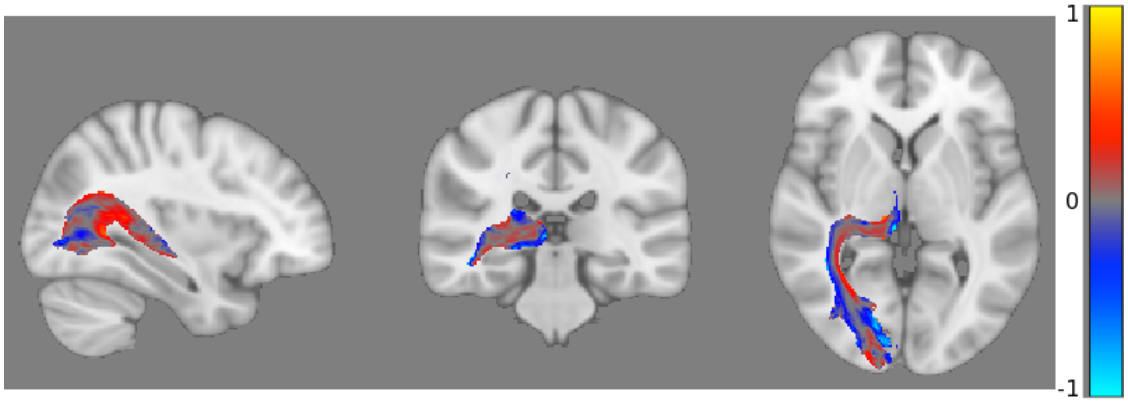

Figure E.20: Scaled β values from the voxelwise GLM comparison between cases of presence and absence of WMHs for the PTR R tract.

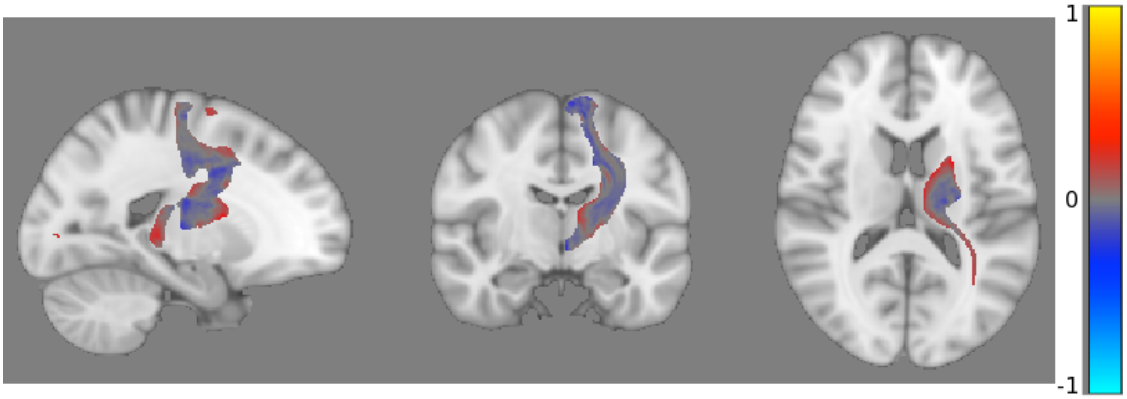

Figure E.21: Scaled β values from the voxelwise GLM comparison between cases of presence and absence of WMHs for the STR L tract.

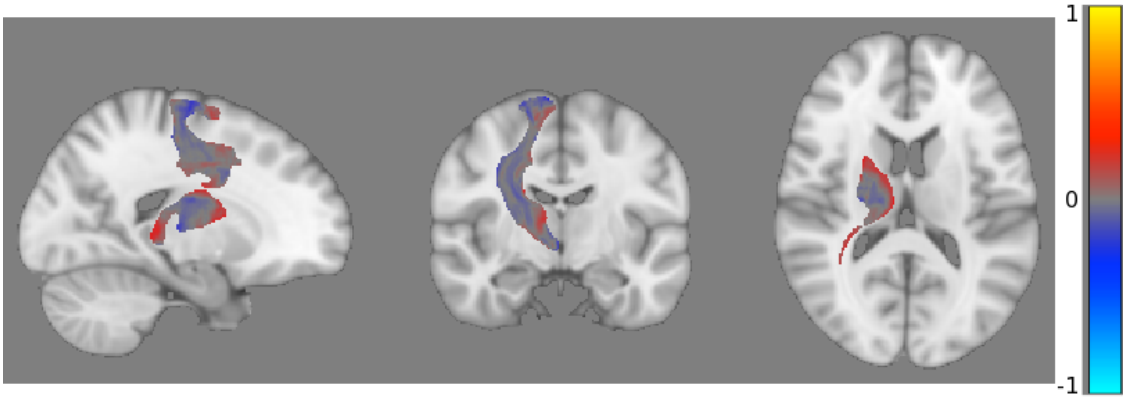

Figure E.22: Scaled β values from the voxelwise GLM comparison between cases of presence and absence of WMHs for the STR R tract.

are smoother and bigger than previously seen. The positive difference is visible, especially around the ventricles. The same can be said about the STR (figures E.21, E.22), although there is almost no effect in the middle of the tract.

E.1.2 Relative difference when accounting for confounds – 4 columns in the design matrix

There are nearly no non-zero voxels in the FMI (figure E.23), SLF (both left E.25 and right E.26), IFO left (figure E.27), ILF left (figure E.29), UNC both hemispheres (figures E.31, E.32), cingulum (both hemispheres, both fragments E.35, E.36, E.33, E.34), AR both sides (figures E.37, E.38), ATR left (figure E.39), PTR both hemispheres (figures E.41, E.42), and STR left (figure E.43). There are some very small effects in the FMA (figure E.24), IFO right hemisphere (figure E.28), ATR

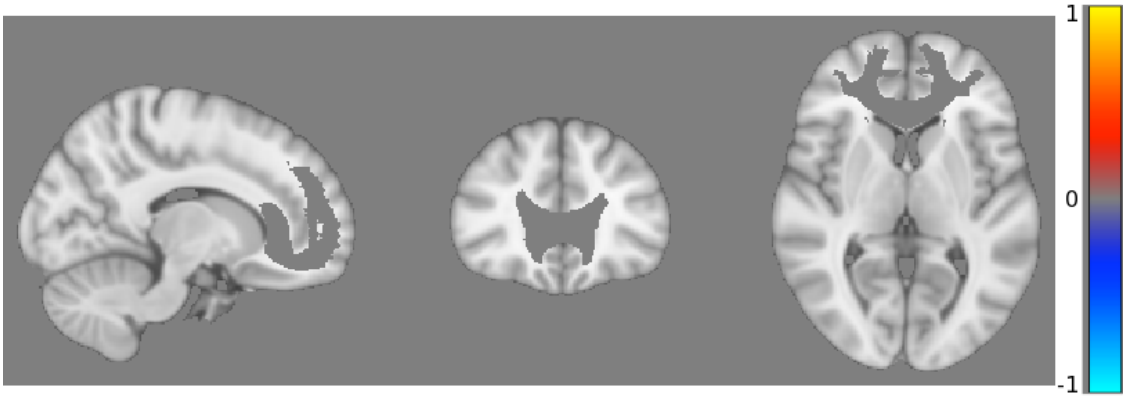

Figure E.23: Scaled β values from the voxelwise GLM comparison between cases of presence and absence of WMHs for the FMI tract with correction for age and sex.

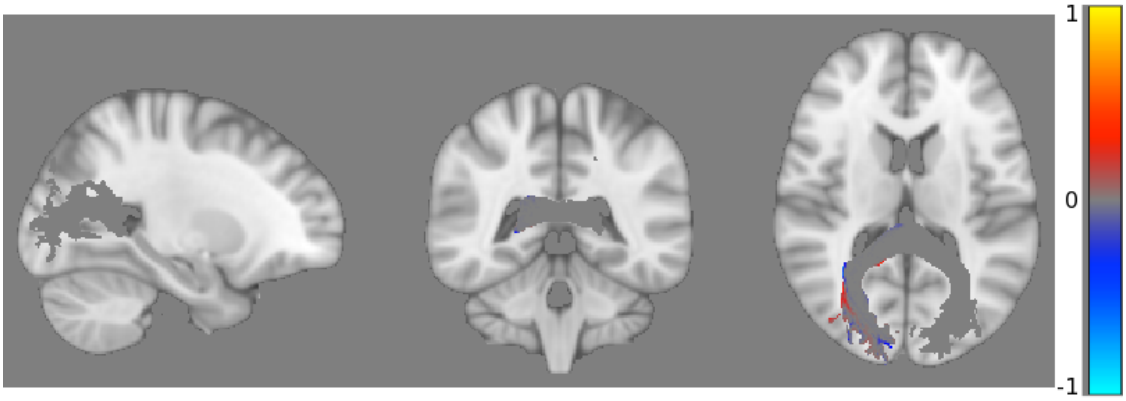

Figure E.24: Scaled β values from the voxelwise GLM comparison between cases of presence and absence of WMHs for the FMA tract with correction for age and sex.

right (figure E.40), and STR right (figure E.44). The most visible differences are in the ILF for the right hemisphere (figure E.30).

E.1.3 Results when contrasts are modified

Here, for comparison, we take the previous analysis with 4 columns in design matrix and plot the results we would obtain if the contrast was focused on either of the variables, not only WMHs presence. In addition to examples in the main body of the thesis, we show here those visualisations for FMI E.45 and PTR in left hemisphere E.46.

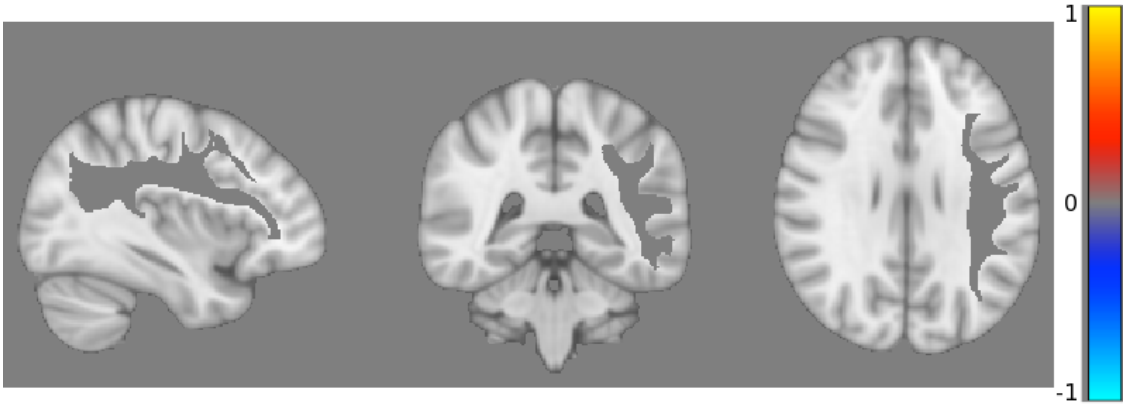

Figure E.25: Scaled β values from the voxelwise GLM comparison between cases of presence and absence of WMHs for the SLF L tract with correction for age and sex.

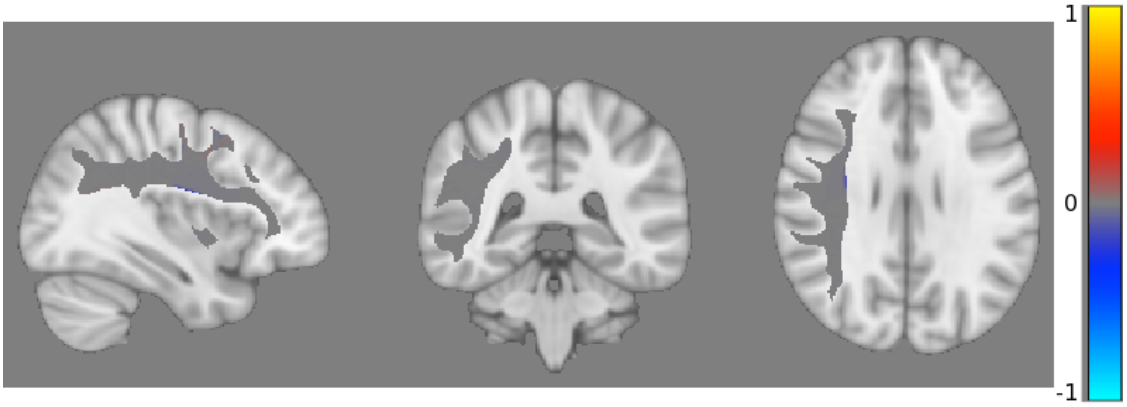

Figure E.26: Scaled β values from the voxelwise GLM comparison between cases of presence and absence of WMHs for the SLF R tract with correction for age and sex.

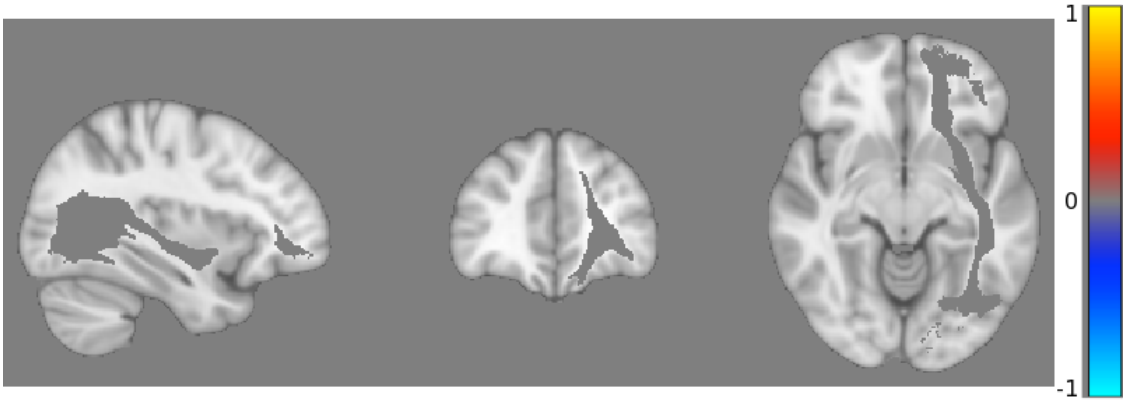

Figure E.27: Scaled β values from the voxelwise GLM comparison between cases of presence and absence of WMHs for the IFO L tract with correction for age and sex.

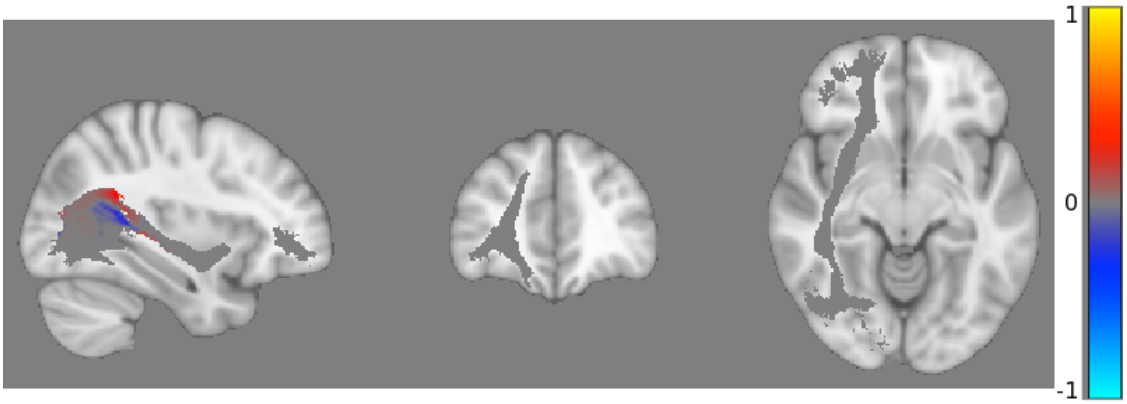

Figure E.28: Scaled β values from the voxelwise GLM comparison between cases of presence and absence of WMHs for the IFO R tract with correction for age and sex.



Figure E.29: Scaled β values from the voxelwise GLM comparison between cases of presence and absence of WMHs for the ILF L tract with correction for age and sex.

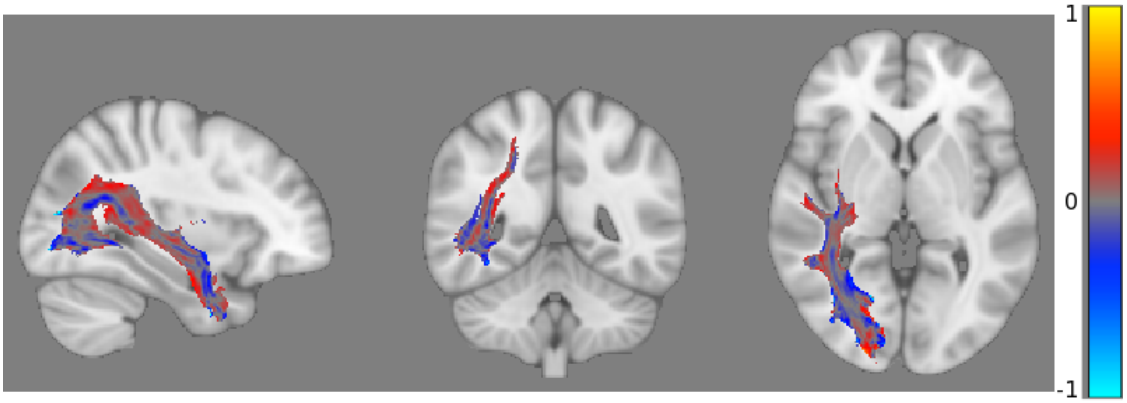

Figure E.30: Scaled β values from the voxelwise GLM comparison between cases of presence and absence of WMHs for the ILF R tract with correction for age and sex.

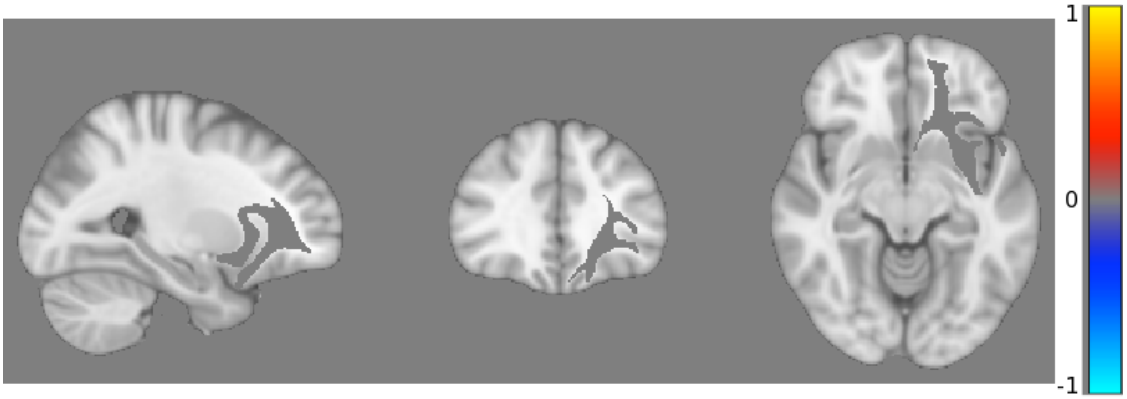

Figure E.31: Scaled β values from the voxelwise GLM comparison between cases of presence and absence of WMHs for the UNC L tract with correction for age and sex.

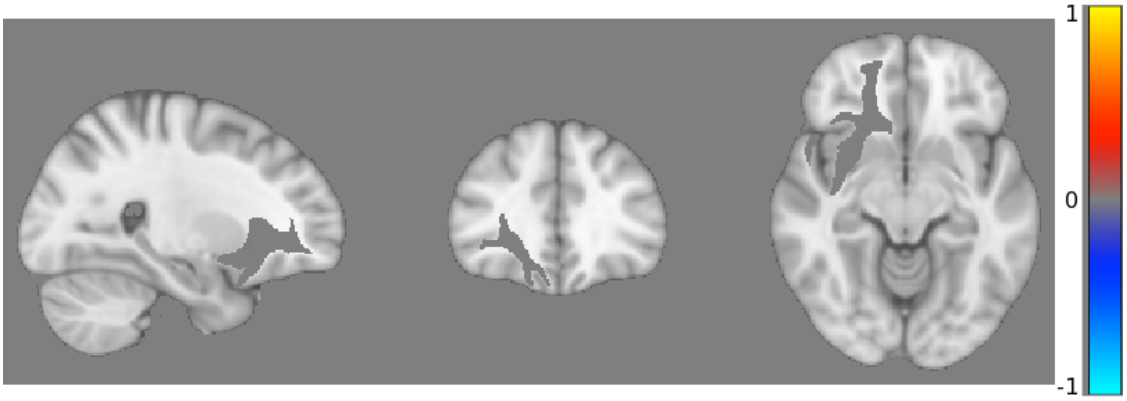

Figure E.32: Scaled β values from the voxelwise GLM comparison between cases of presence and absence of WMHs for the UNC R tract with correction for age and sex.

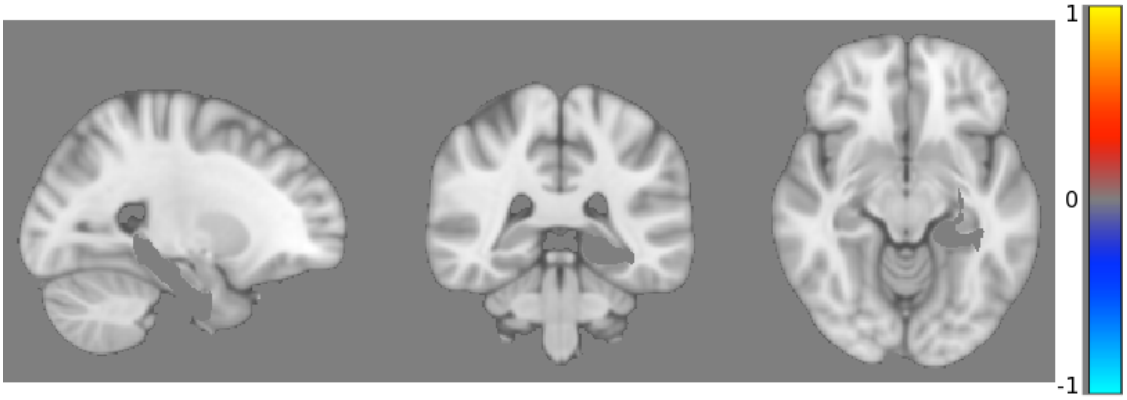

Figure E.33: Scaled β values from the voxelwise GLM comparison between cases of presence and absence of WMHs for the CGH L tract with correction for age and sex.

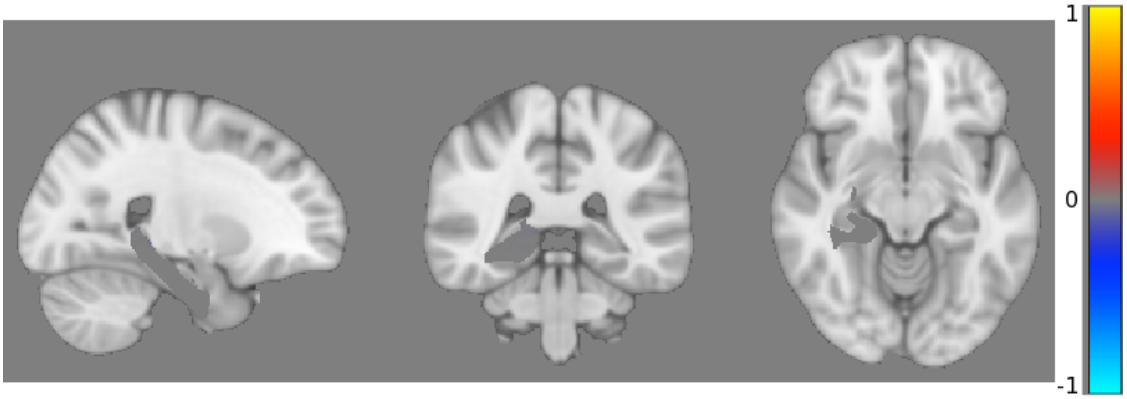

Figure E.34: Scaled β values from the voxelwise GLM comparison between cases of presence and absence of WMHs for the CGH R tract with correction for age and sex.

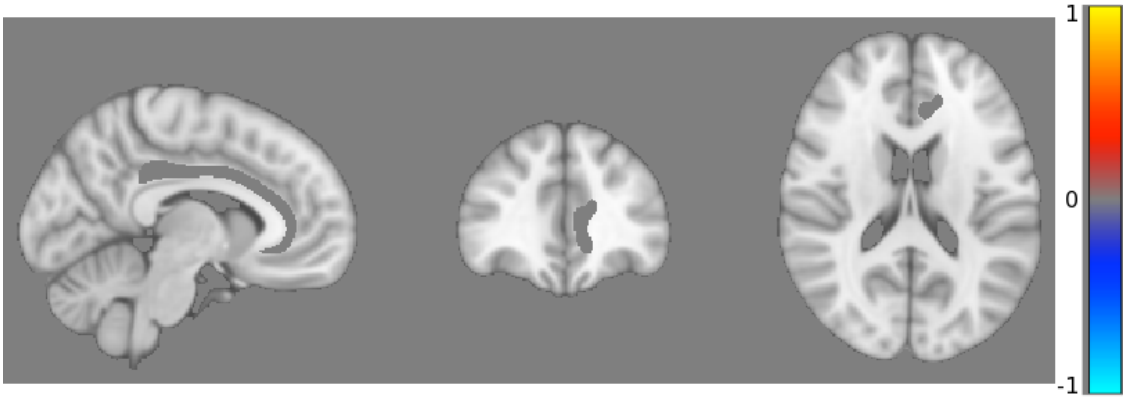

Figure E.35: Scaled β values from the voxelwise GLM comparison between cases of presence and absence of WMHs for the CGC L tract with correction for age and sex.



Figure E.36: Scaled β values from the voxelwise GLM comparison between cases of presence and absence of WMHs for the CGC R tract with correction for age and sex.

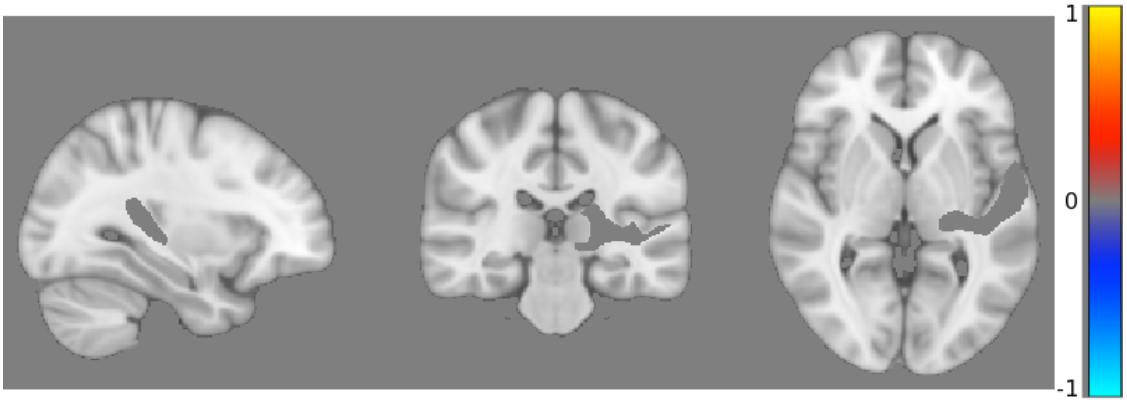

Figure E.37: Scaled β values from the voxelwise GLM comparison between cases of presence and absence of WMHs for the AR L tract with correction for age and sex.

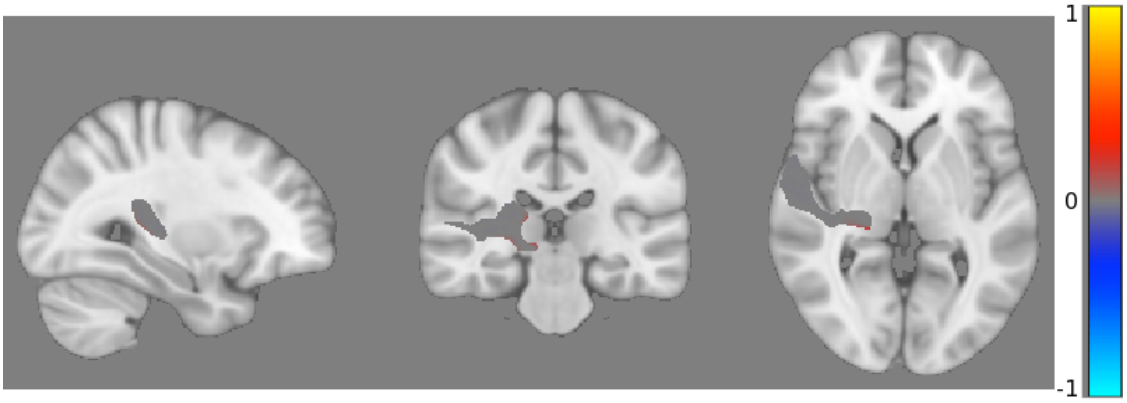

Figure E.38: Scaled β values from the voxelwise GLM comparison between cases of presence and absence of WMHs for the AR R tract with correction for age and sex.



Figure E.39: Scaled β values from the voxelwise GLM comparison between cases of presence and absence of WMHs for the ATR L tract with correction for age and sex.

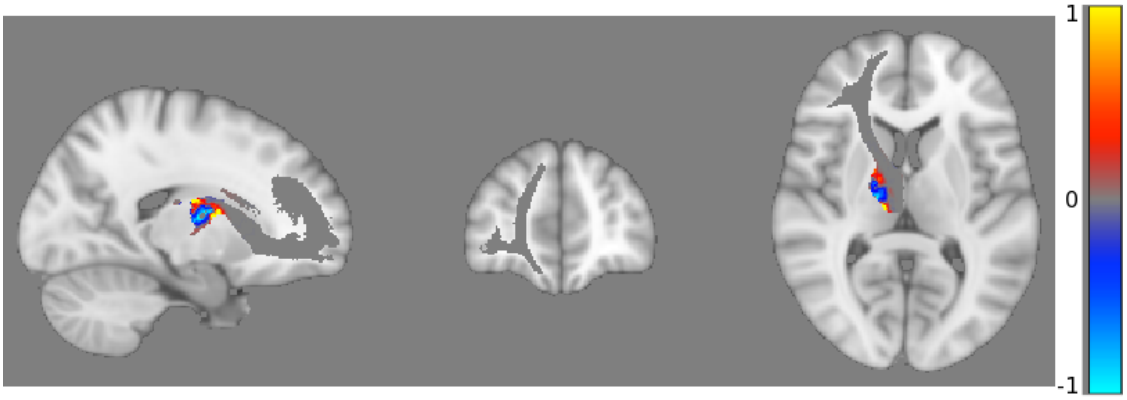

Figure E.40: Scaled β values from the voxelwise GLM comparison between cases of presence and absence of WMHs for the ATR R tract with correction for age and sex.

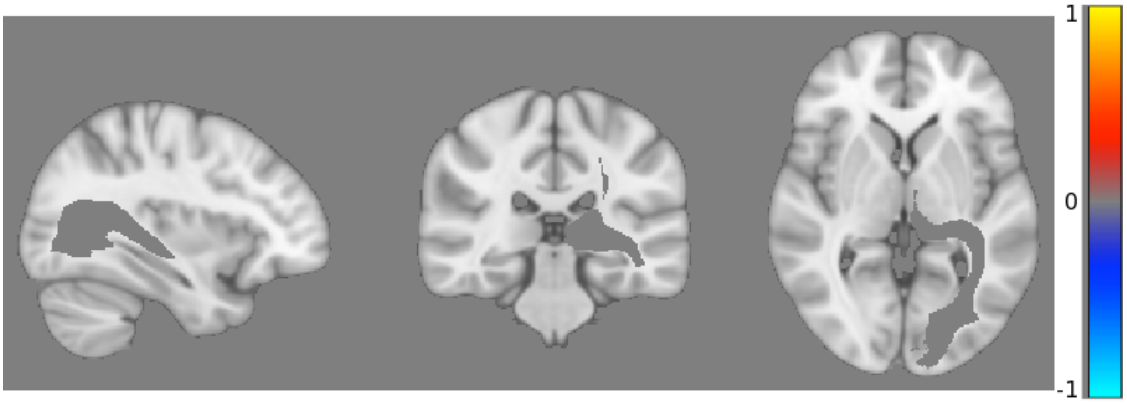

Figure E.41: Scaled β values from the voxelwise GLM comparison between cases of presence and absence of WMHs for the PTR L tract with correction for age and sex.

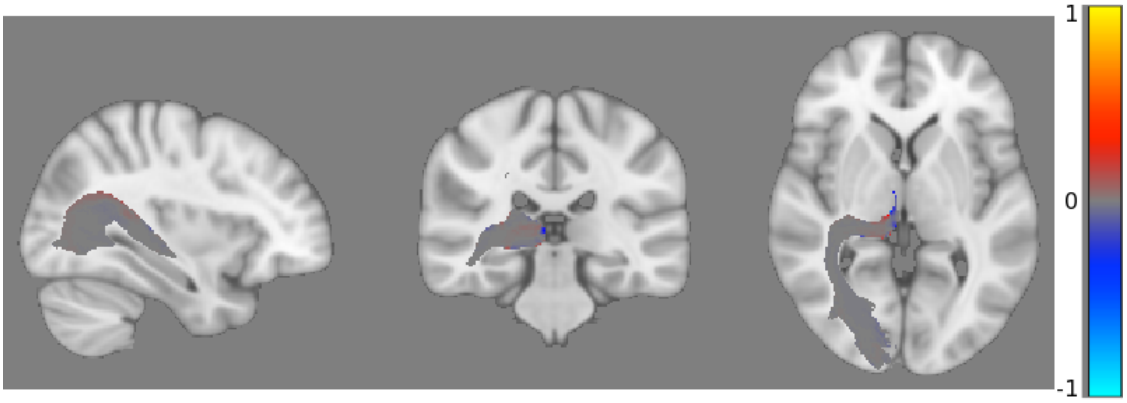

Figure E.42: Scaled β values from the voxelwise GLM comparison between cases of presence and absence of WMHs for the PTR R tract with correction for age and sex.

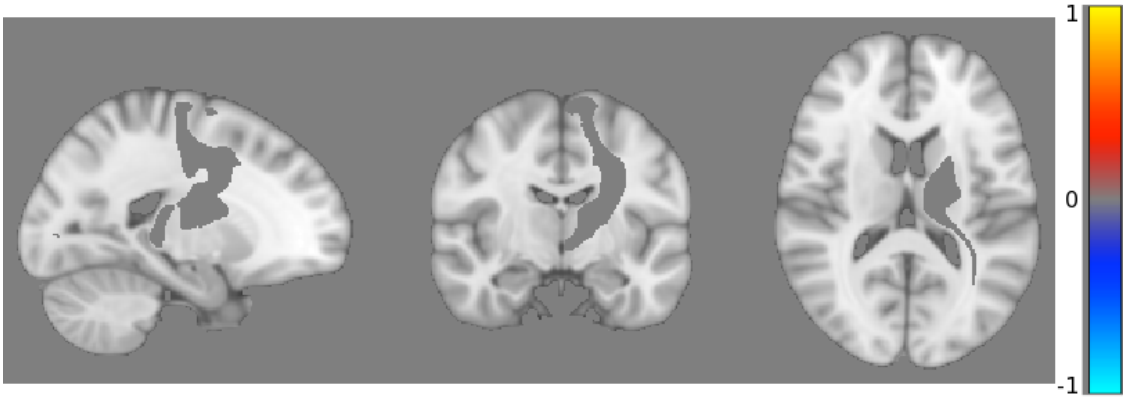

Figure E.43: Scaled β values from the voxelwise GLM comparison between cases of presence and absence of WMHs for the STR L tract with correction for age and sex.

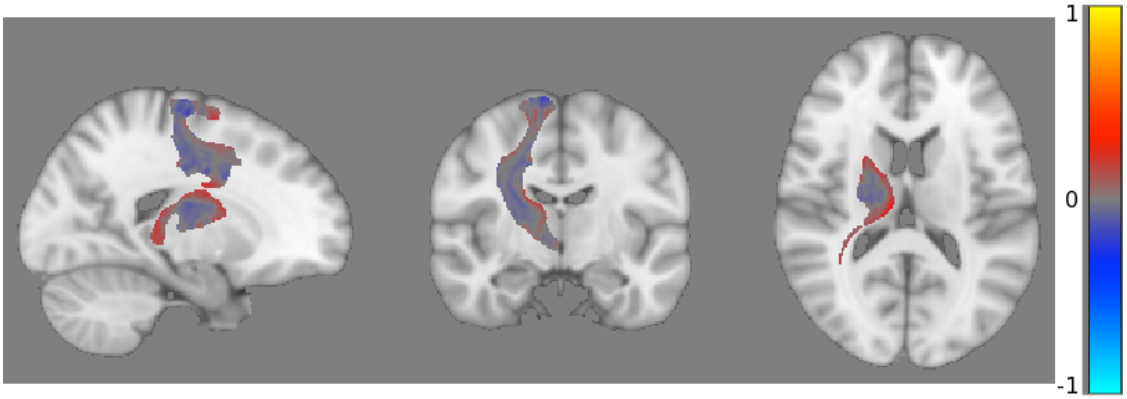

Figure E.44: Scaled β values from the voxelwise GLM comparison between cases of presence and absence of WMHs for the STR R tract with correction for age and sex.

E.2 Subset with narrow age range

We present results for additional tracts when calculated using the narrow age subset of data for the ATR in the right hemisphere (figure E.47), PTR in the left hemisphere (figure E.48), AR in the left hemisphere (figure E.49), FMI (figure E.50), IFO in the left hemisphere (figure E.51), SLR in the right hemisphere (figure E.52), and CGC in the left hemisphere (figure E.53).

E.3 Single sex subset within the narrow age range

In addition to the results presented in the main body of the thesis, we present in figure E.54 results for the CGC tract when using single sex groups within the narrow age range. In addition, we present the results for the PTR tract (figure E.55)

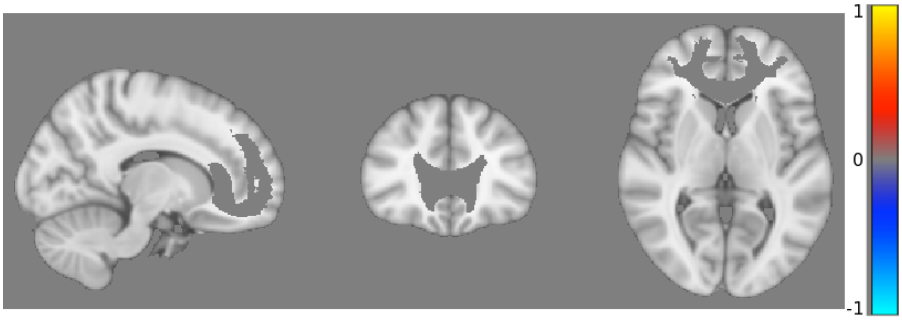

(a) Results for the case of the contrast focusing on WMH presence (default) for the FMI tract on 4998 subjects.

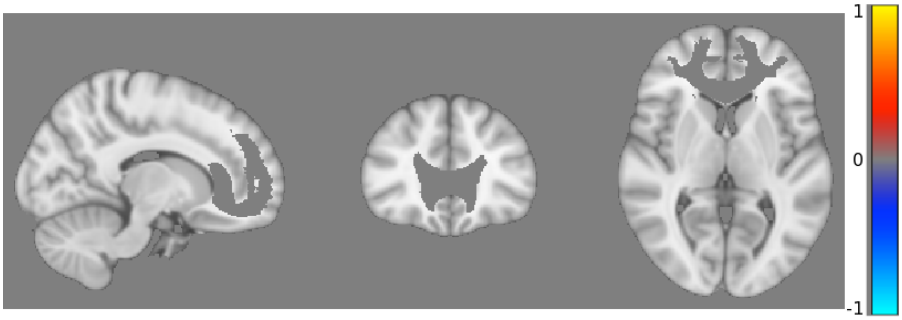

(b) Results for the case of the contrast focusing on age for the FMI tract on 4998 subjects.

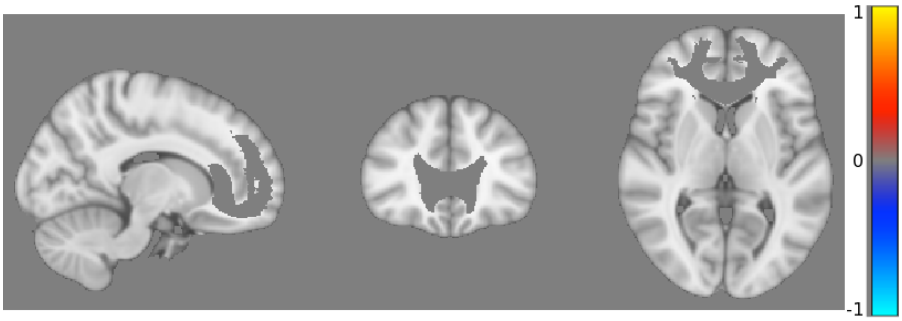

(c) Results for the case of the contrast focusing on sex for the FMI tract on 4998 subjects.

Figure E.45: Results of the analyses for all 4 contrasts for the FMI tract on the whole UK Biobank data subset used in the thesis (around 5000 subjects).

and the SLF tract (figure E.56). As in the main body of the thesis, we observe different patterns for different tracts, which vary slightly between two hemispheres but to a much smaller extent than between different tracts.

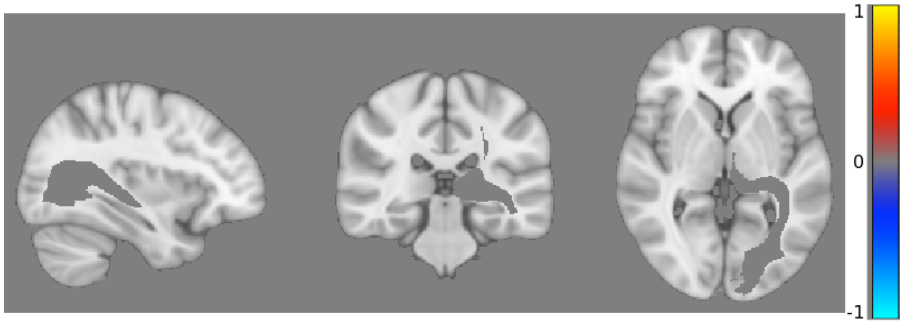

(a) Results for the case of the contrast focusing on WMH presence (default) for the PTR L tract on 4998 subjects.

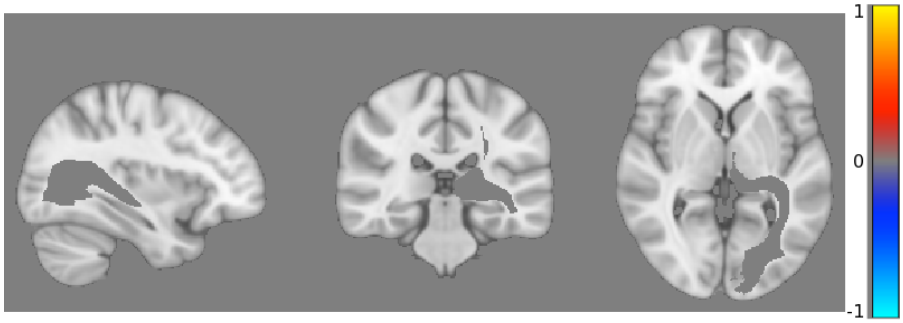

(b) Results for the case of the contrast focusing on age for the PTR L tract on 4998 subjects.

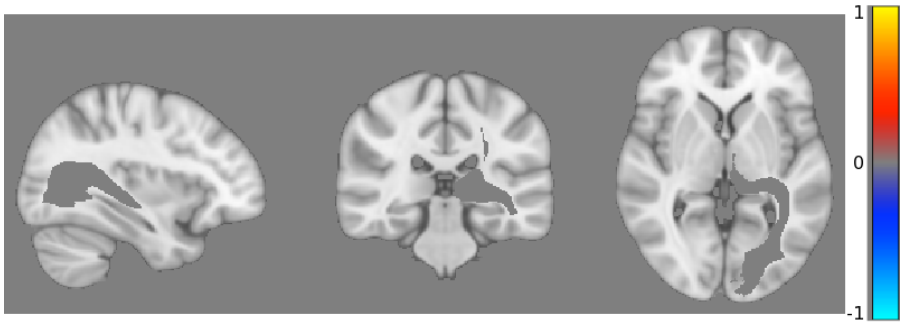

(c) Results for the case of the contrast focusing on sex for the PTR L tract on 4998 subjects.

Figure E.46: Results of the analyses for all 4 contrasts for the PTR L tract on the whole UK Biobank data subset used in the thesis (around 5000 subjects).

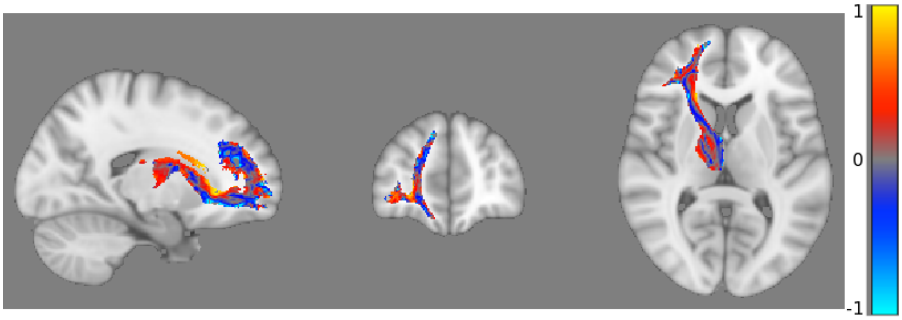

(a) Results for the case of the contrast focusing on WMH presence (the default one, contrast of interest) for the ATR R tract on the subset of 1010 subjects within a relatively narrow age range.

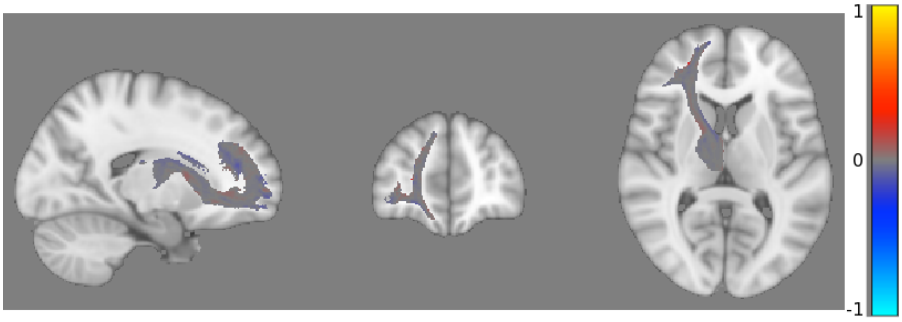

(b) Results for the case of the contrast focusing on age for the ATR R tract on the subset of 1010 subjects within a relatively narrow age range.

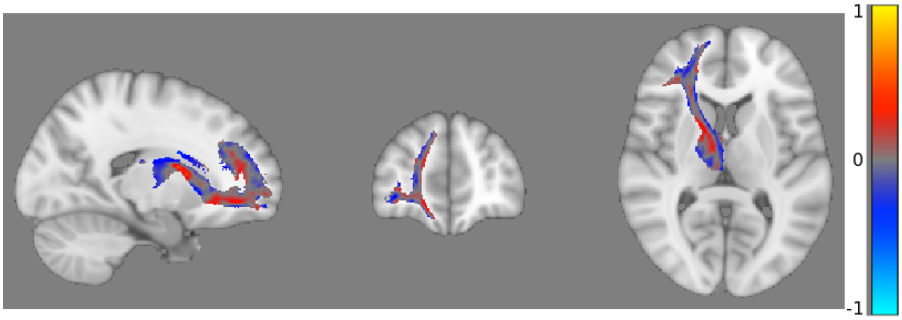

(c) Results for the case of the contrast focusing on sex for the ATR R tract on the subset of 1010 subjects within a relatively narrow age range.

Figure E.47: Results for the ATR tract in the right hemisphere for a narrow age range subset.

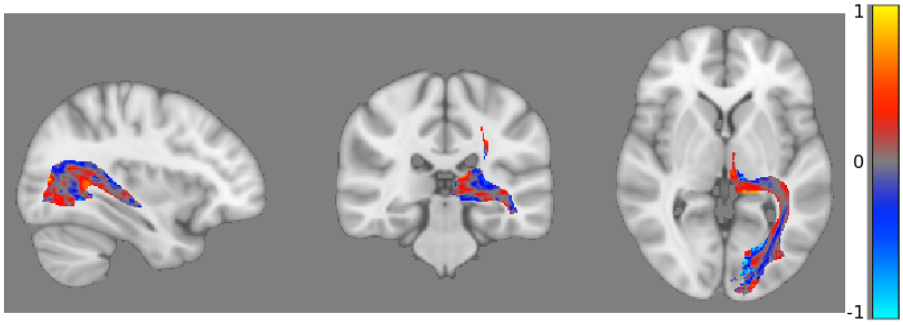

(a) Results for the case of the contrast focusing on WMH presence (the default one, contrast of interest) for the PTR L tract on the subset of 1010 subjects within a relatively narrow age range.

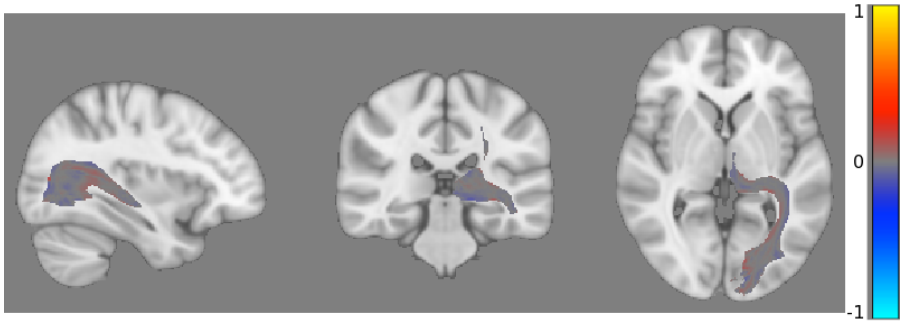

(b) Results for the case of the contrast focusing on age for the PTR L tract on the subset of 1010 subjects within a relatively narrow age range.

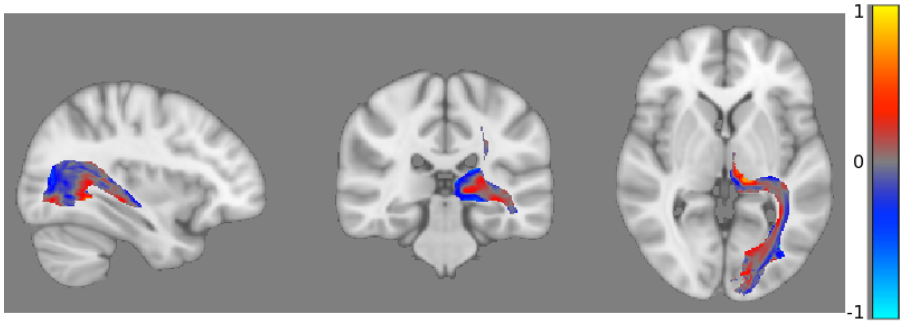

(c) Results for the case of the contrast focusing on sex for the PTR L tract on the subset of 1010 subjects within a relatively narrow age range.

Figure E.48: Results for the PTR tract in the left hemisphere for a narrow age range subset.

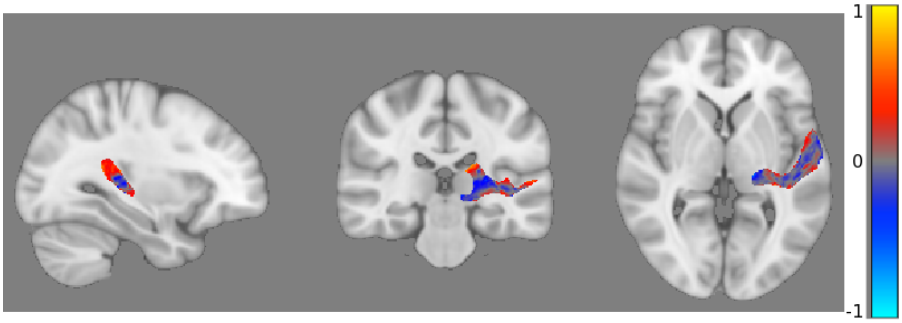

(a) Results for the case of the contrast focusing on WMH presence (the default one, contrast of interest) for the AR L tract on the subset of 1010 subjects within a relatively narrow age range.

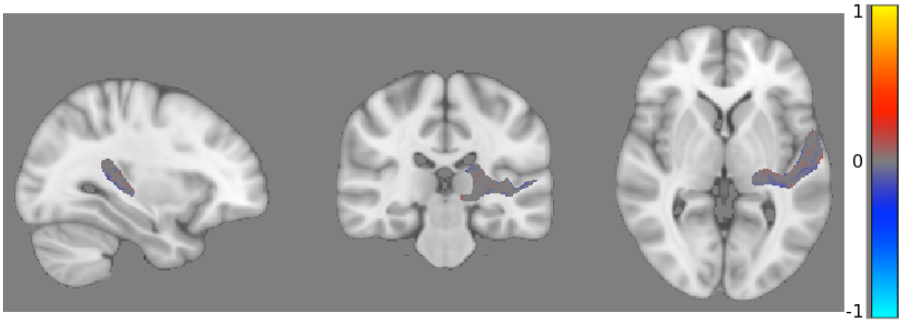

(b) Results for the case of the contrast focusing on age for the AR L tract on the subset of 1010 subjects within a relatively narrow age range.

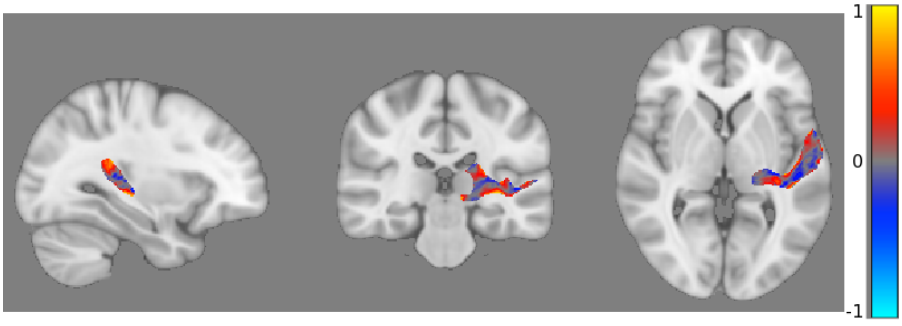

(c) Results for the case of the contrast focusing on sex for the AR L tract on the subset of 1010 subjects within a relatively narrow age range.

Figure E.49: Results for the AR tract in the left hemisphere for a narrow age range subset.

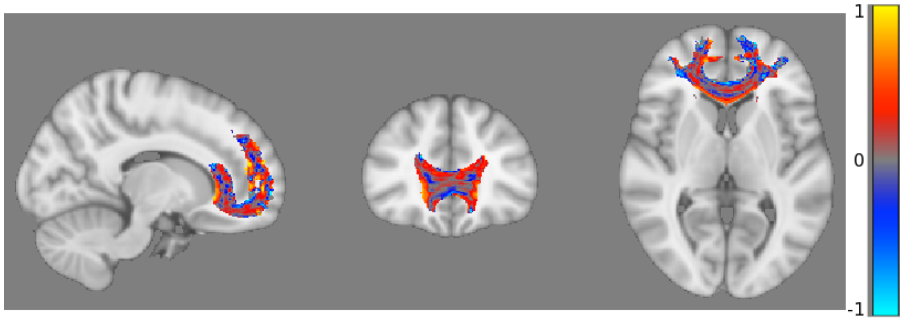

(a) Results for the case of the contrast focusing on WMH presence (the default one, contrast of interest) for the FMI tract on the subset of 1010 subjects within a relatively narrow age range.

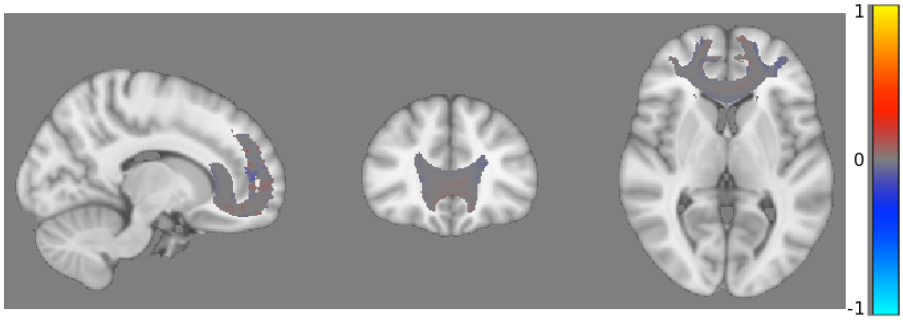

(b) Results for the case of the contrast focusing on age for the FMI tract on the subset of 1010 subjects within a relatively narrow age range.

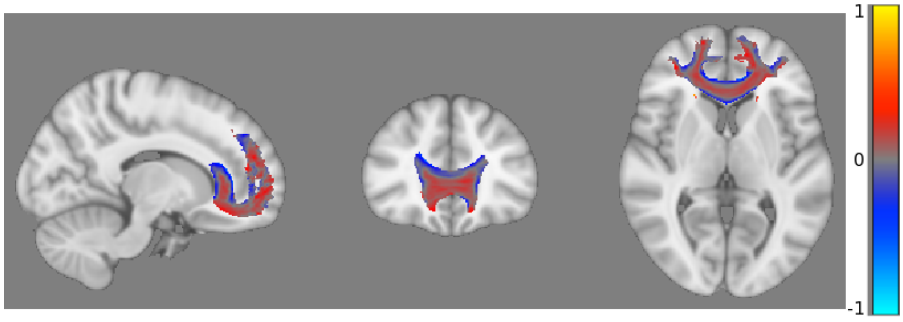

(c) Results for the case of the contrast focusing on sex for the FMI tract on the subset of 1010 subjects within a relatively narrow age range.

Figure E.50: Results for the FMI tract for a narrow age range subset.

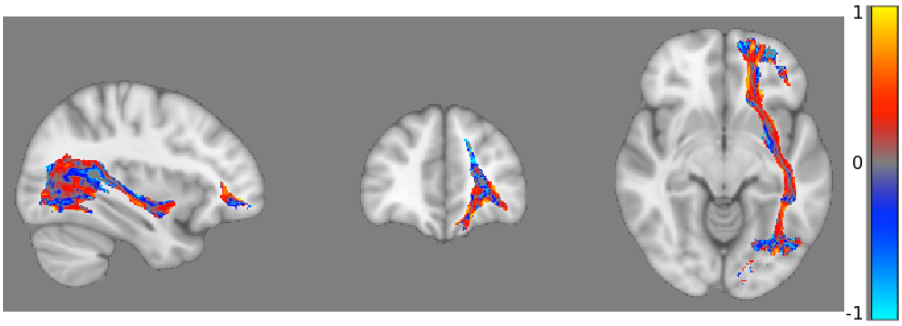

(a) Results for the case of the contrast focusing on WMH presence (the default one, contrast of interest) for the IFO L tract on the subset of 1010 subjects within a relatively narrow age range.

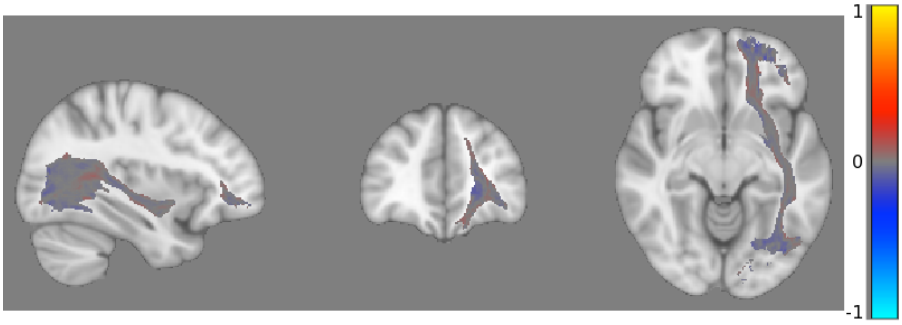

(b) Results for the case of the contrast focusing on age for the IFO L tract on the subset of 1010 subjects within a relatively narrow age range.

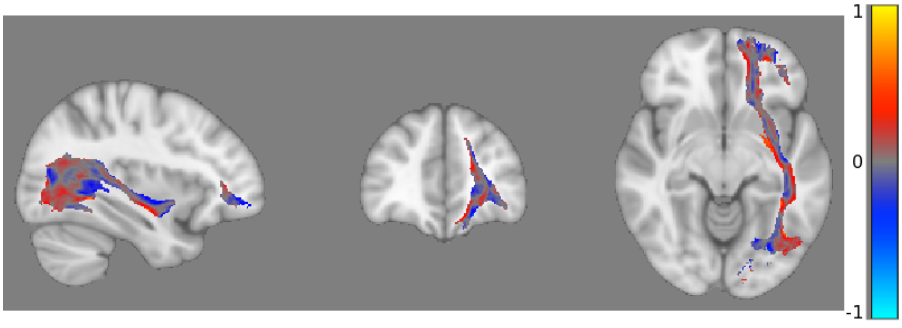

(c) Results for the case of the contrast focusing on sex for the IFO L tract on the subset of 1010 subjects within a relatively narrow age range.

Figure E.51: Results for the IFO tract in the left hemisphere for a narrow age range subset.

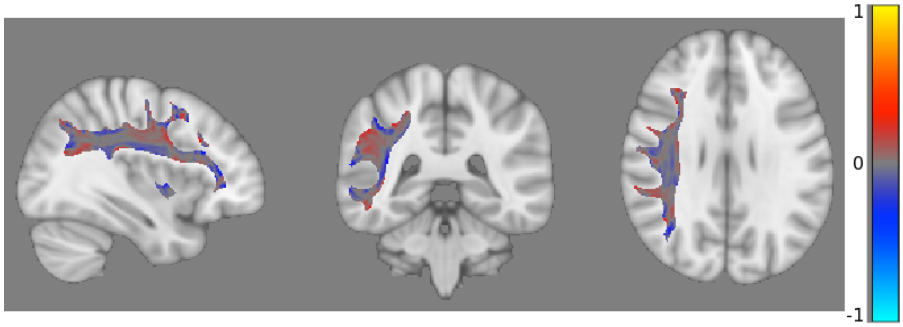

(a) Results for the case of the contrast focusing on WMH presence (the default one, contrast of interest) for the SLF R tract on subset of 1010 subjects within a relatively narrow age range.

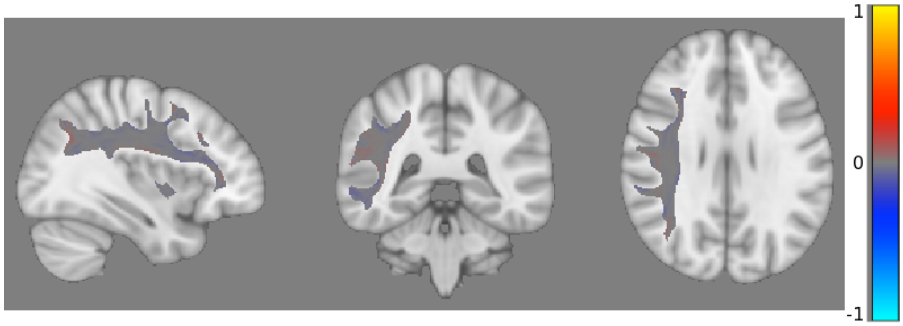

(b) Results for the case of contrast focusing on age for the SLF R tract on subset of 1010 subjects within a relatively narrow age range.

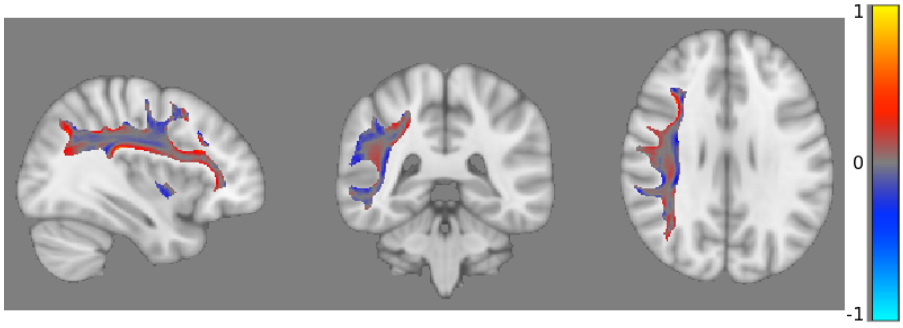

(c) Results for the case of contrast focusing on sex for the SLF R tract on subset of 1010 subjects within a relatively narrow age range.

Figure E.52: Results for the SLF tract in the right hemisphere for a narrow age range subset.

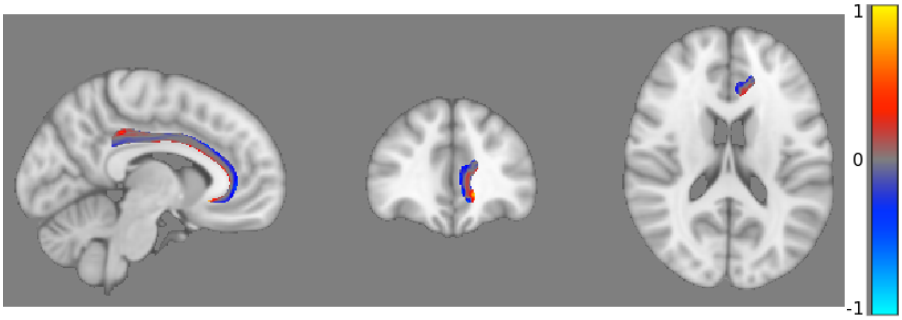

(a) Results for the case of the contrast focusing on WMH presence (the default one, contrast of interest) for the CGC L tract on the subset of 1010 subjects within a relatively narrow age range.

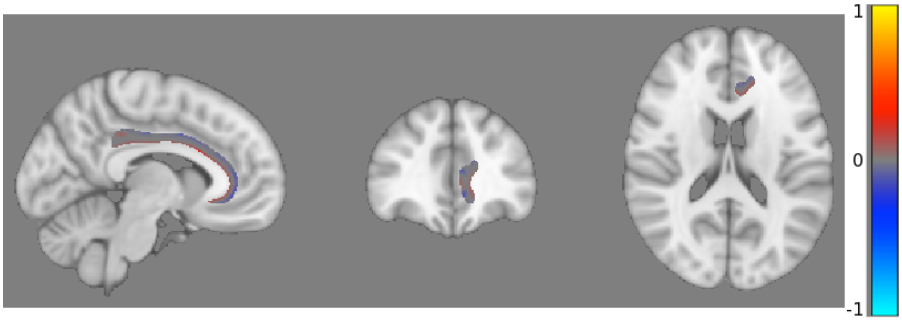

(b) Results for the case of the contrast focusing on age for the CGC L tract on the subset of 1010 subjects within a relatively narrow age range.

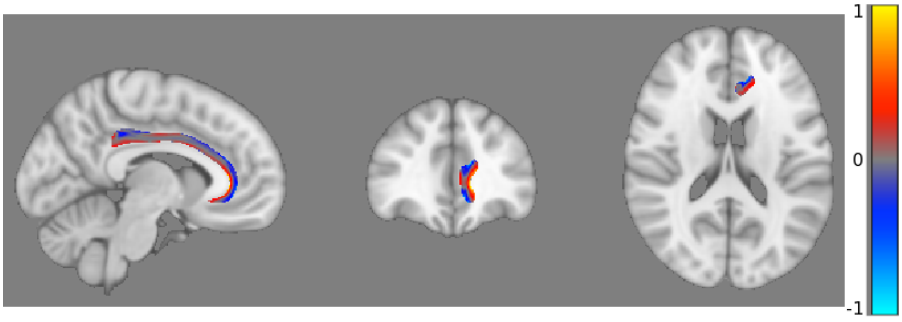

(c) Results for the case of the contrast focusing on sex for the CGC L tract on the subset of 1010 subjects within a relatively narrow age range.

Figure E.53: Results for the CGC tract in the left hemisphere for a narrow age range subset.

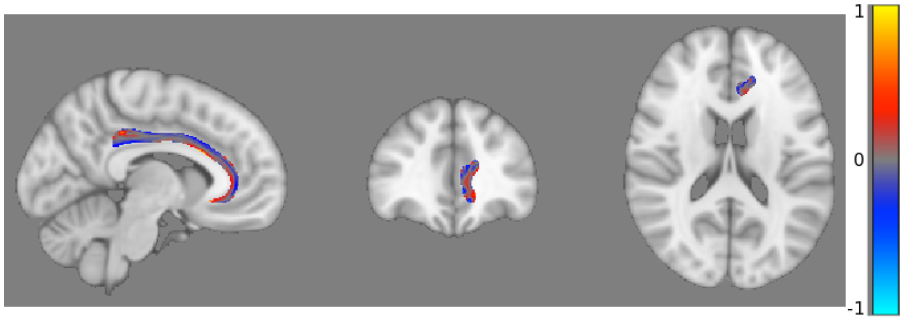

(a) Results for the case of the contrast focusing on WMH presence (default) for the CGC L tract on 523 female subjects.

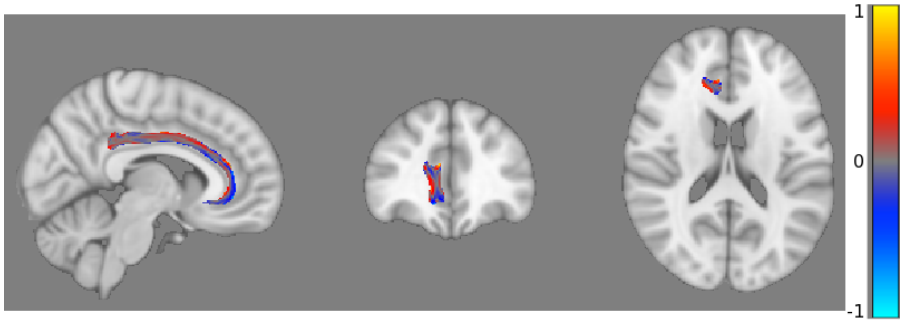

(b) Results for the case of the contrast focusing on WMH presence (default) for the CGC R tract on 523 female subjects.

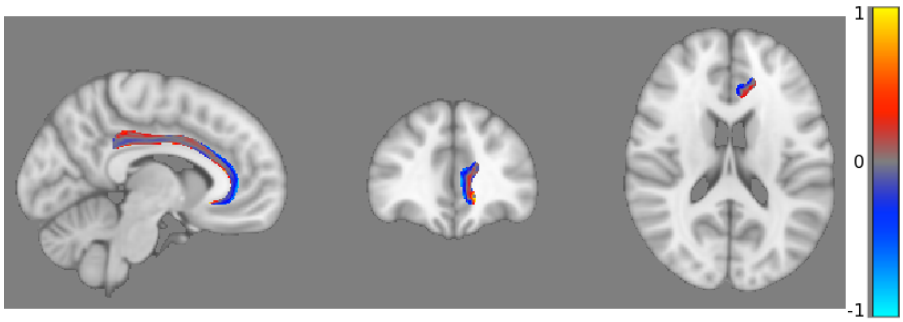

(c) Results for the case of the contrast focusing on WMH presence (default) for the CGC L tract on 487 male subjects.

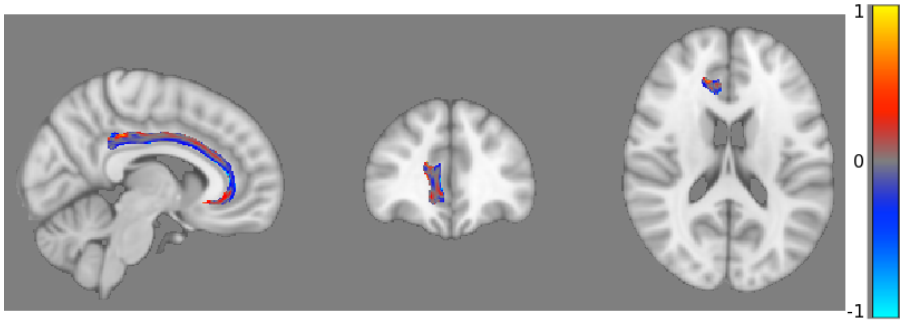

(d) Results for the case of the contrast focusing on WMH presence (default) for the CGC R tract on 487 male subjects.

Figure E.54: Results for the case of the contrast focusing on WMH presence (default) for the CGC tract on a subset of subjects within a narrow age range and within single sex groups.

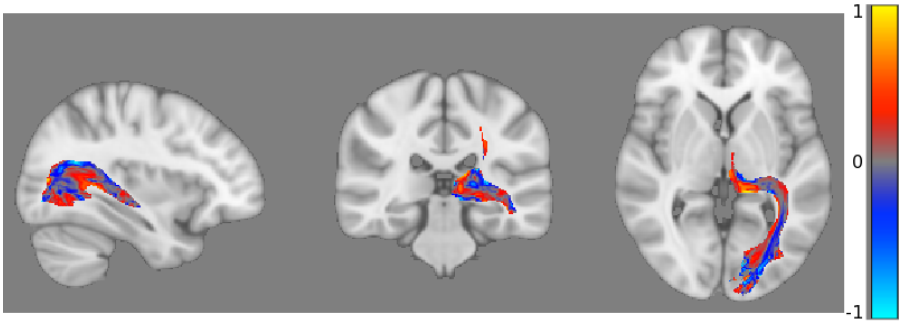

(a) Results for the case of the contrast focusing on WMH presence (default) for the PTR L tract on 523 female subjects.

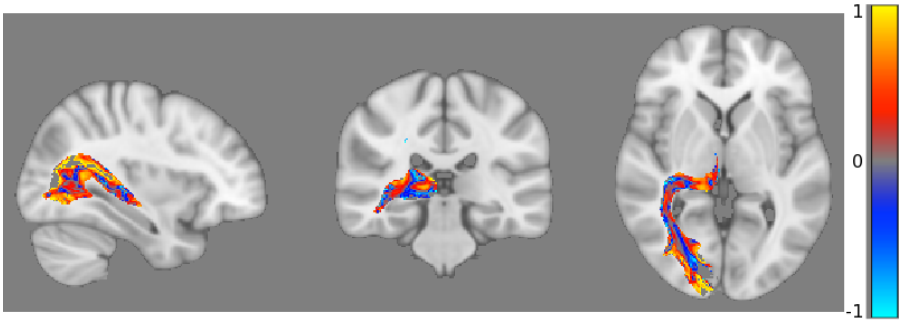

(b) Results for the case of the contrast focusing on WMH presence (default) for the PTR R tract on 523 female subjects.

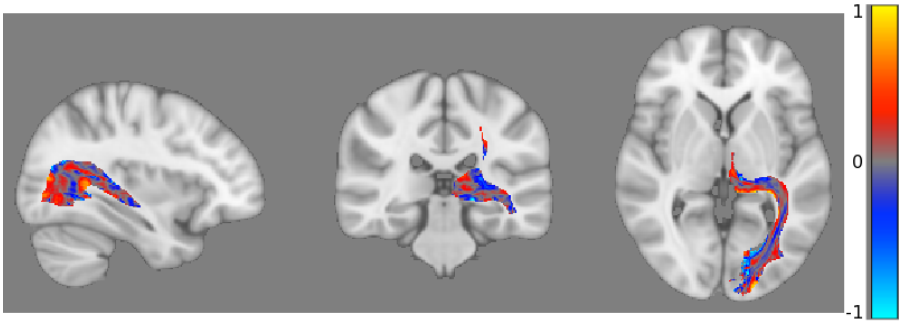

(c) Results for the case of the contrast focusing on WMH presence (default) for the PTR L tract on 487 male subjects.

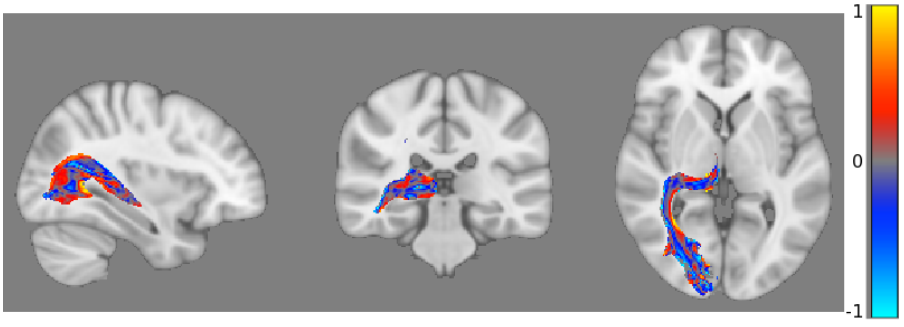

(d) Results for the case of the contrast focusing on WMH presence (default) for the PTR R tract on 487 male subjects.

Figure E.55: Results for the case of the contrast focusing on WMH presence (default) for the PTR tract on a subset of subjects within a narrow age range and within single sex groups.

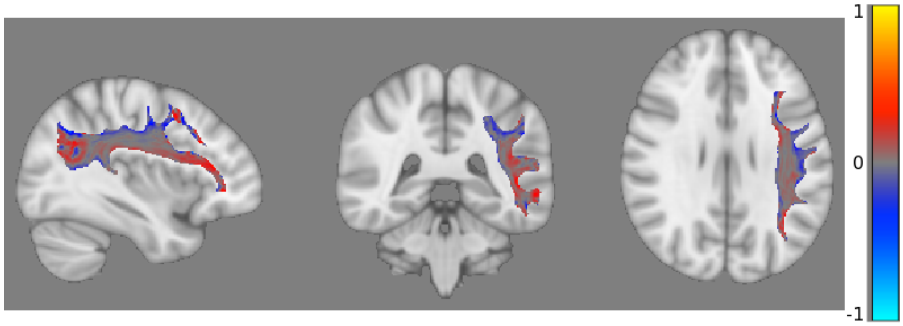

(a) Results for the case of the contrast focusing on WMH presence (default) for the SLF L tract on 523 female subjects.

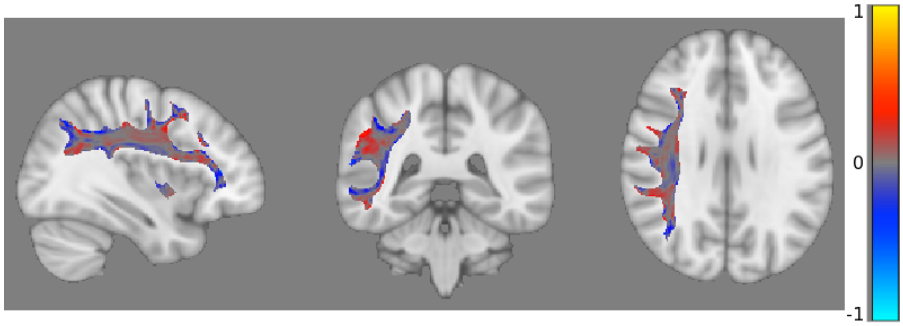

(b) Results for the case of the contrast focusing on WMH presence (default) for the SLF R tract on 523 female subjects.

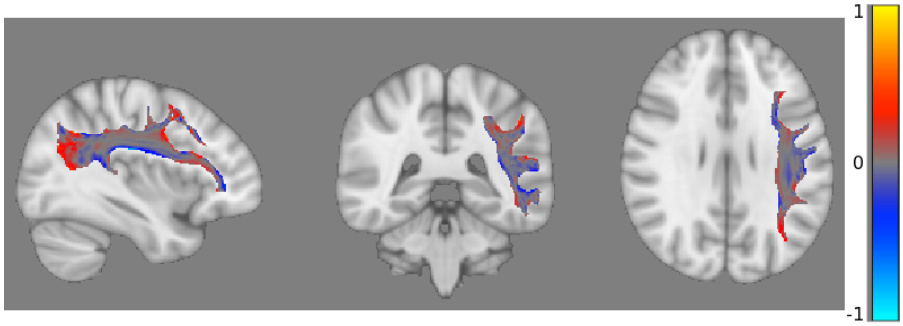

(c) Results for the case of the contrast focusing on WMH presence (default) for the SLF L tract on 487 male subjects.

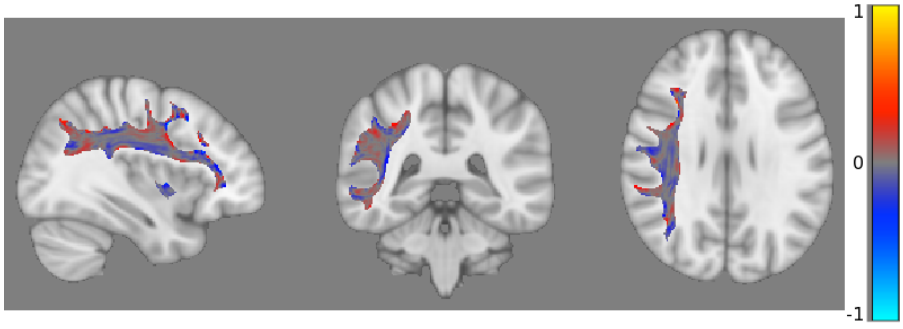

(d) Results for the case of the contrast focusing on WMH presence (default) for the SLF R tract on 487 male subjects.

Figure E.56: Results for the case of the contrast focusing on WMH presence (default) for the SLF tract on a subset of subjects within a narrow age range and within single sex groups.

F

Summary of microstructural parameters

Figures F.1, F.2, F.3, F.4, show the same data as is presented in subsection 5.6.2 of the thesis, but here they are averaged over both hemispheres. That might make it easier for the reader to compare the relationships between the parameters.

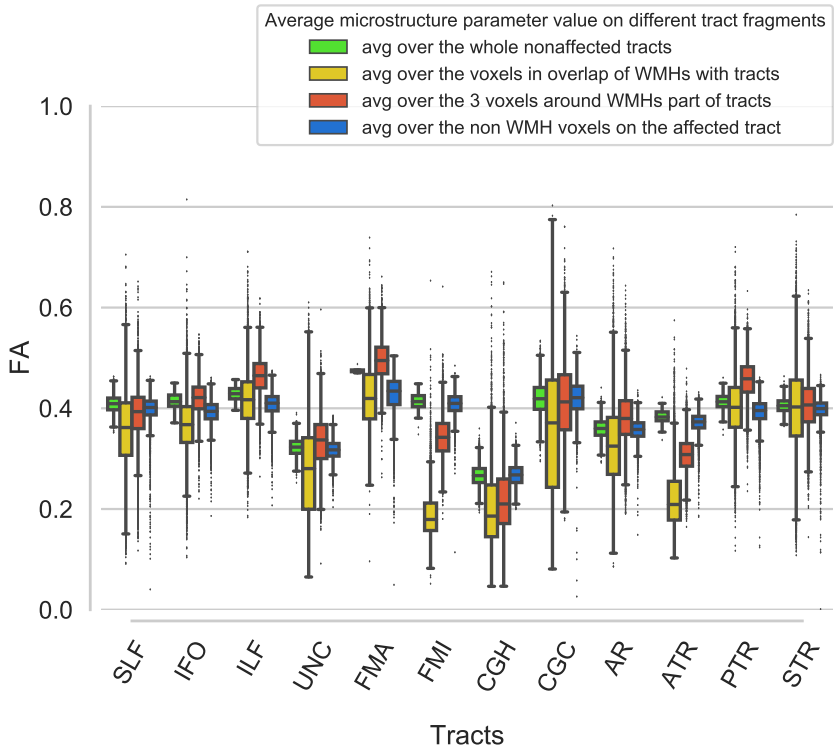

Figure F.1: FA values averaged for both hemispheres.

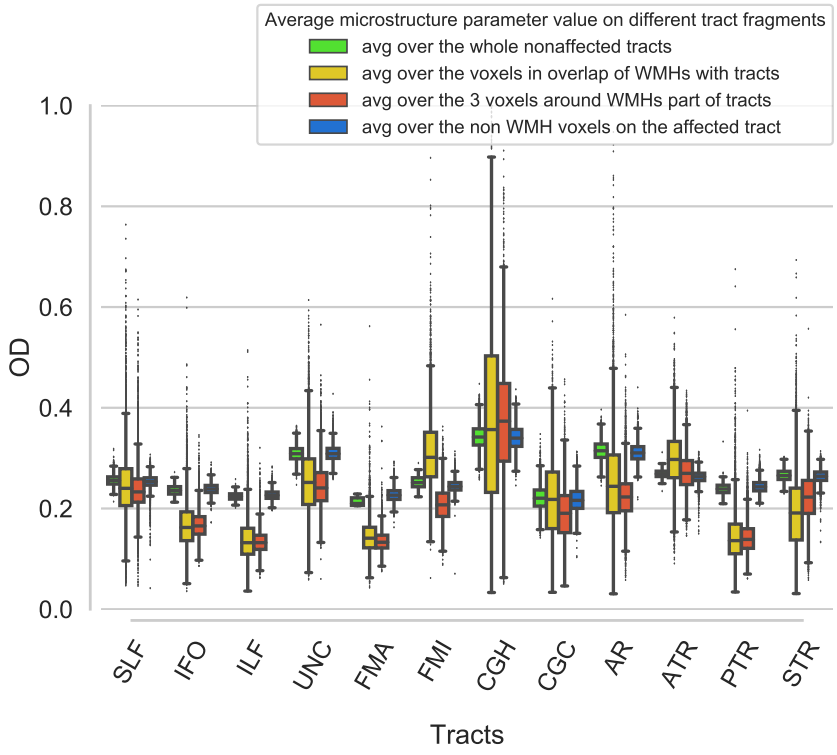

Figure F.2: OD values averaged for both hemispheres.

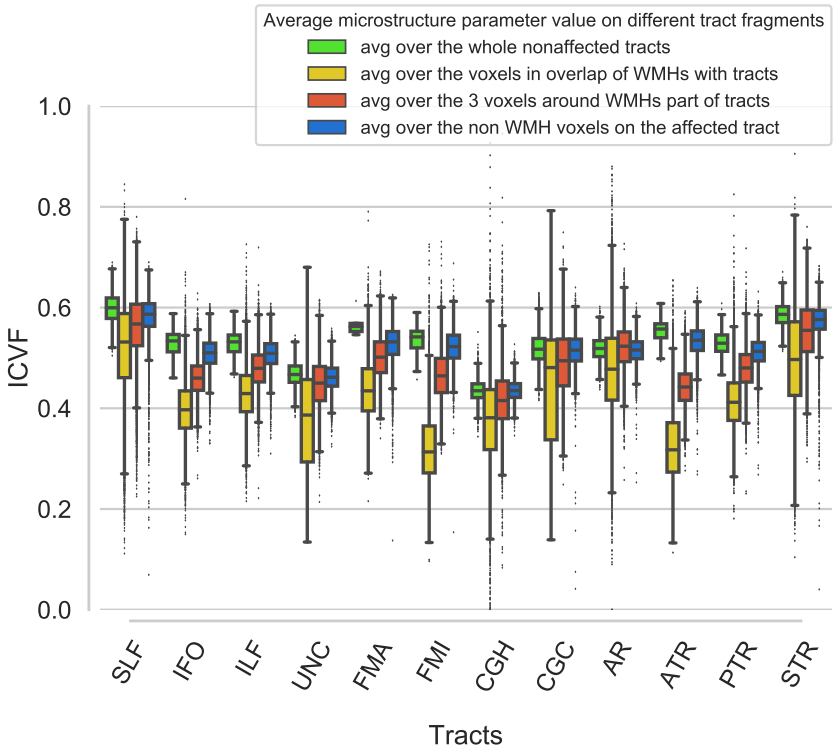

Figure F.3: ICVF values averaged for both hemispheres.

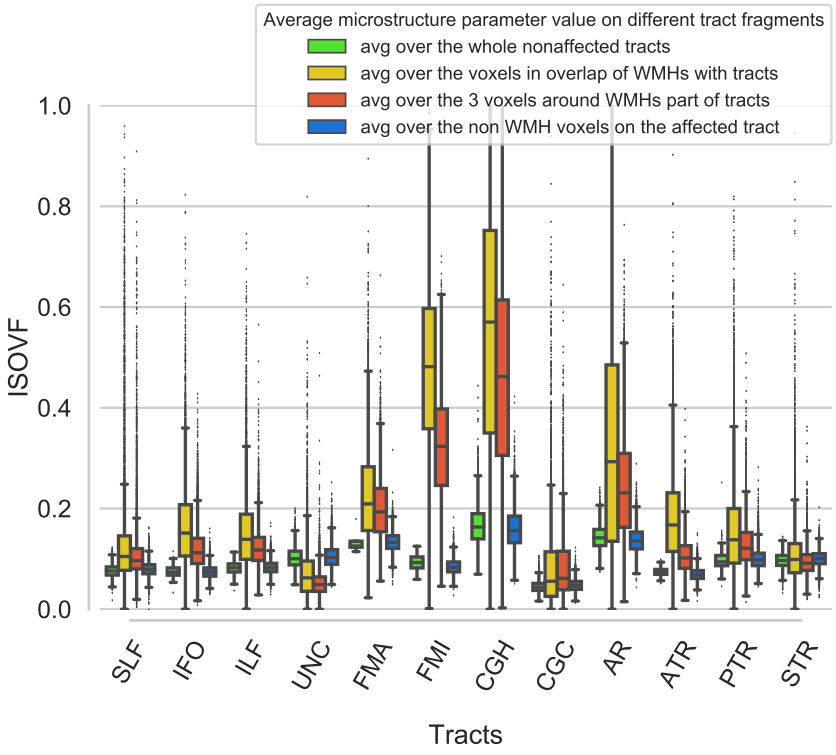

Figure F.4: ISOVF values averaged for both hemispheres.

G

Multiple Sclerosis application results for all the tracts

Contents

G.1 A modified method for MS data – creating two binary classes 215
G.2 A modified method for MS data – using the lesion load 220
G.3 Additional analysis with healthy controls 220

In this appendix we present additional results from the analysis presented in chapter 6. In the main body of the thesis we showed only selected tracts, here we expand the presentation of the results to a larger number of tracts.

G.1 A modified method for MS data – creating two binary classes

In this section we present results when subjects were assigned to binary classes for the tracts that were not presented in the main body of the thesis. In the majority of the images there are only a few voxels left after the cleaning. The only example for which the results behave differently is the CGC tract in the left hemisphere (figure G.6). Only for that tract do we observe some clusters of voxels. The β results for that tract had a much wider range (see the colour bar on the right hand

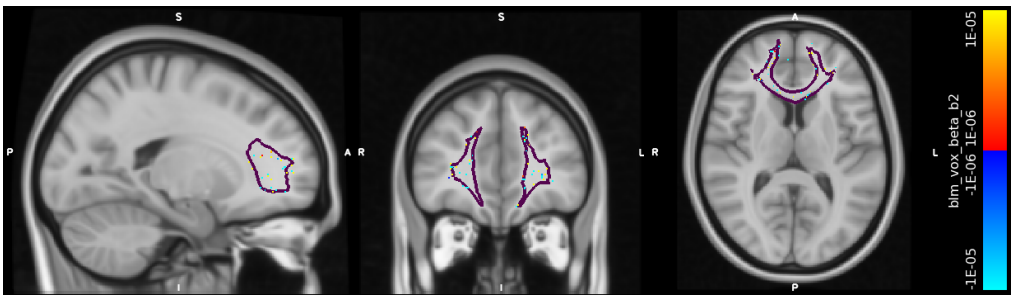

(a) FMI

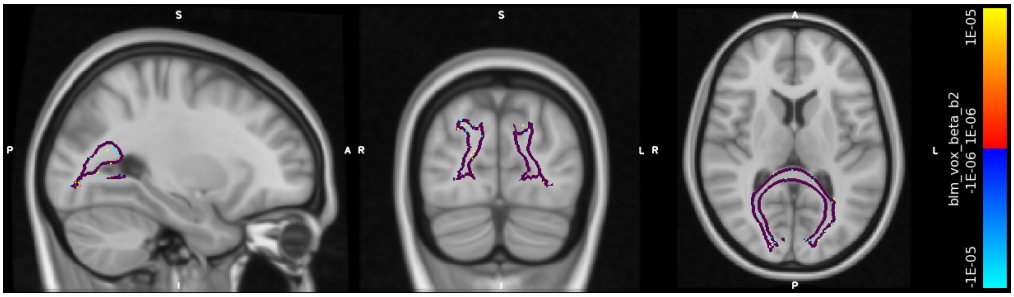

(b) FMA

Figure G.1: Results for the case of artificially dividing the dataset into two binary classes for the callosal tracts.

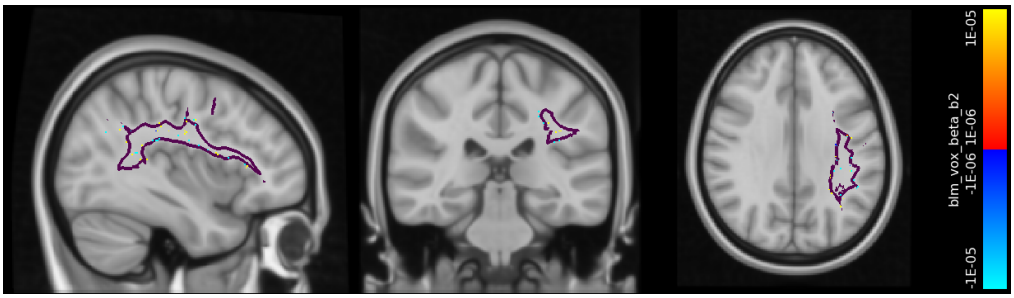

(a) SLF L

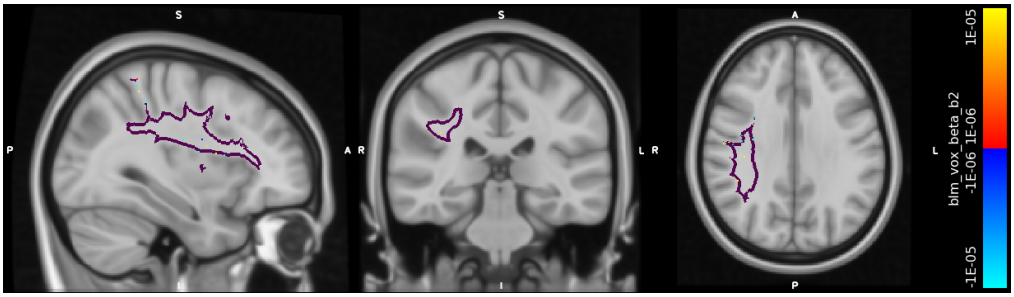

(b) SLF R

Figure G.2: Results for the case of artificially dividing the dataset into two binary classes for the SLF tract.

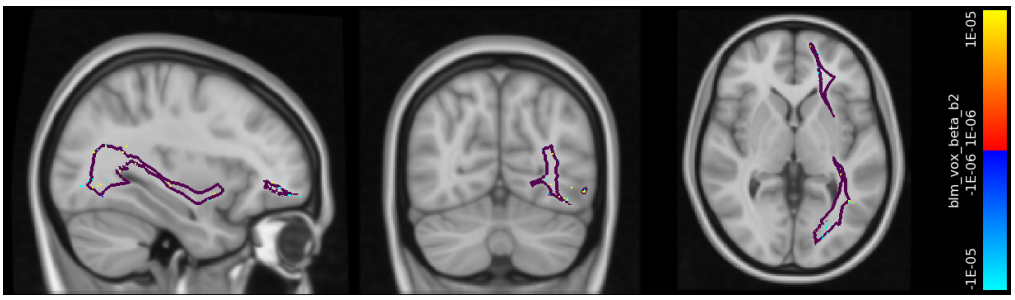

(a) IFO L

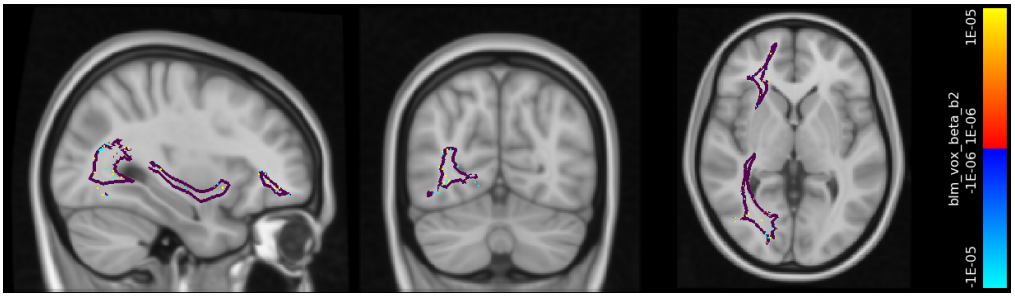

(b) IFO R

Figure G.3: Results for the case of artificially dividing the dataset into two binary classes for the IFO tract.

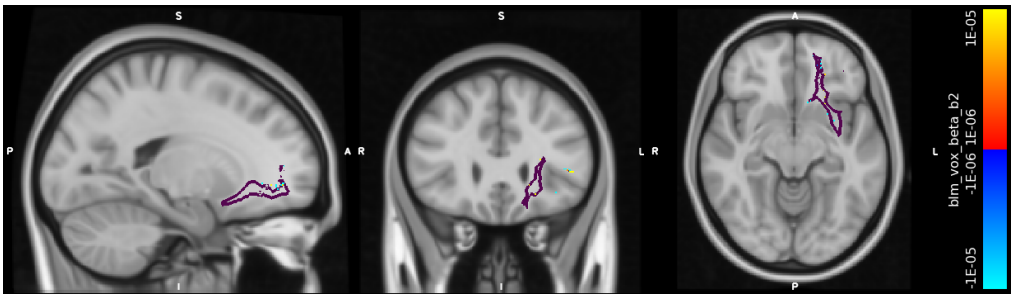

(a) UNC L

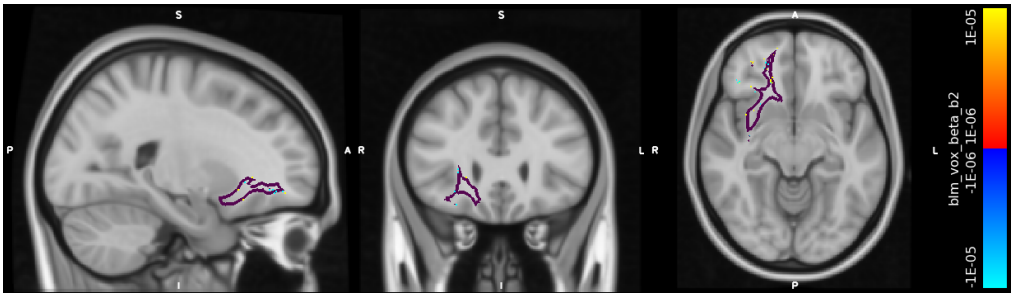

(b) UNC R

Figure G.4: Results for the case of artificially dividing the dataset into two binary classes for the UNC tract.

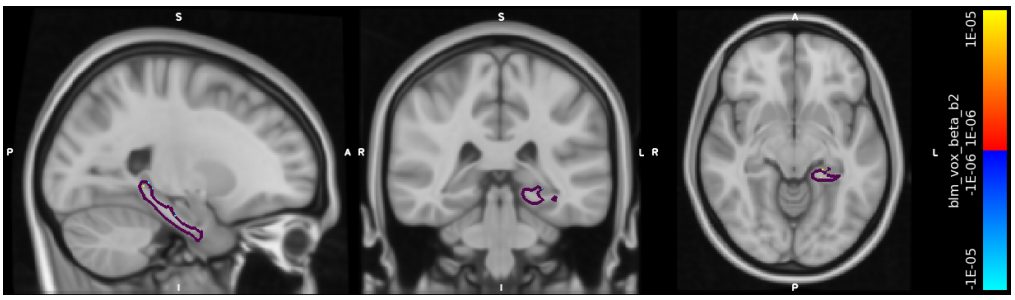

(a) CGH L

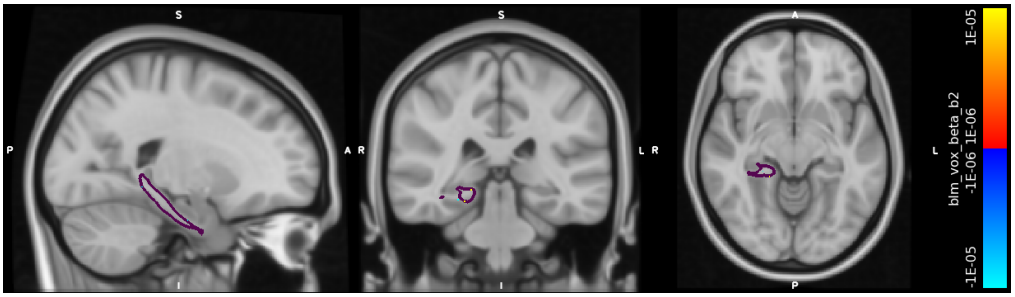

(b) CGH R

Figure G.5: Results for the case of artificially dividing the dataset into two binary classes for the CGH tract.

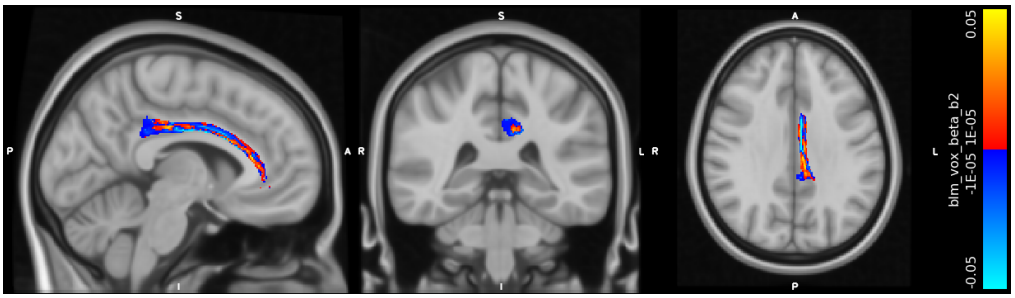

(a) CGC L

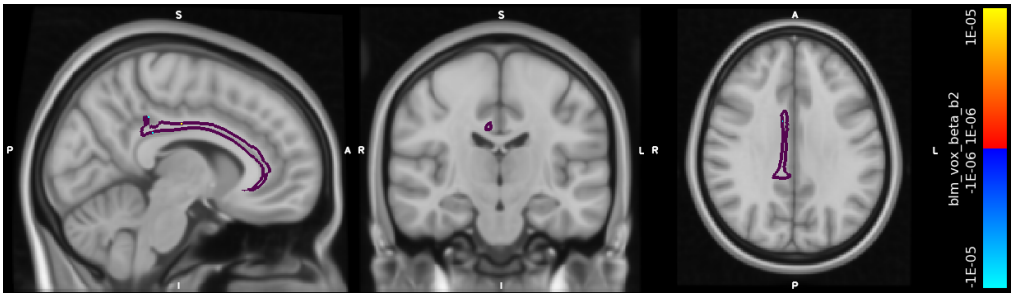

(b) CGC R

Figure G.6: Results for the case of artificially dividing the dataset into two binary classes for the CGC tract.

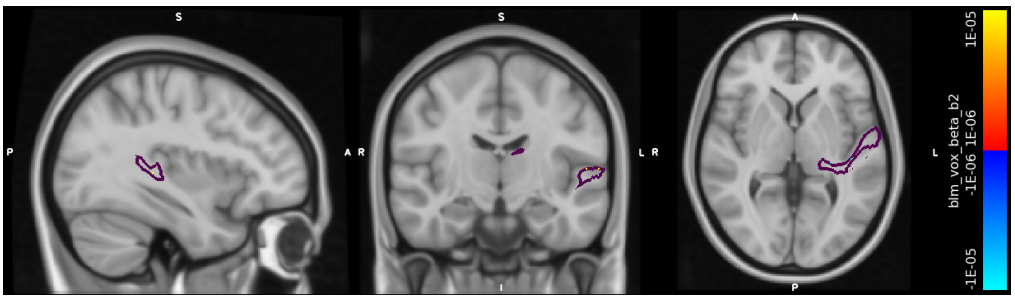

(a) AR L

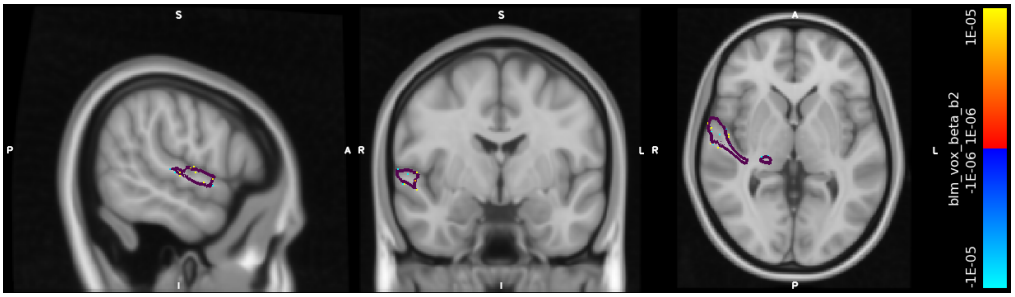

(b) AR R

Figure G.7: Results for the case of artificially dividing the dataset into two binary classes for the AR tract.

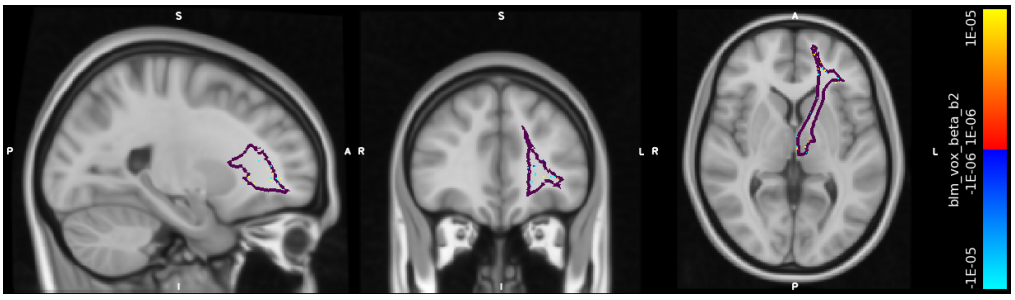

(a) ATR L

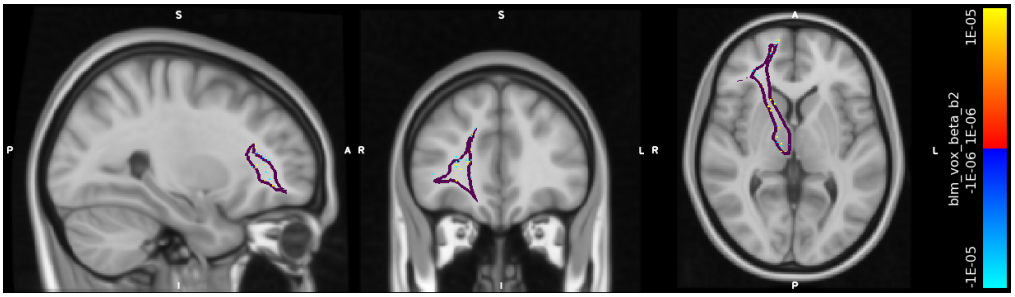

(b) ATR R

Figure G.8: Results for the case of artificially dividing the dataset into two binary classes for the ATR tract.

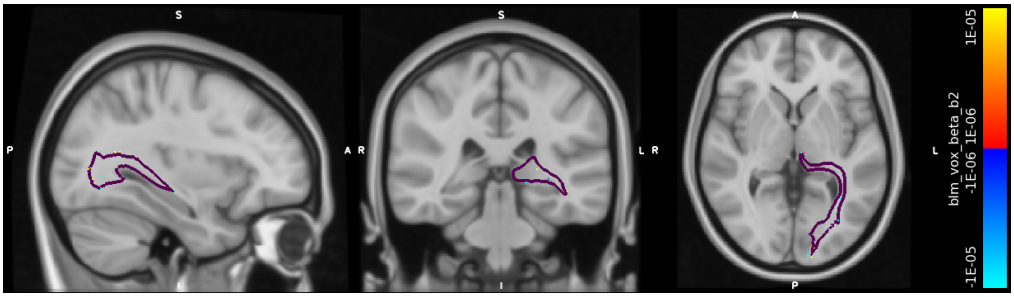

(a) PTR L

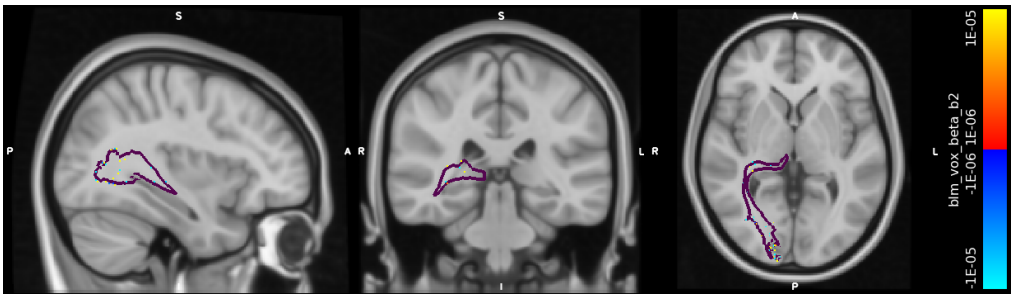

(b) PTR R

Figure G.9: Results for the case of artificially dividing the dataset into two binary classes for the PTR tract.

side) and we observed this in a large number of voxels. It is difficult to explain why the results for this tract differ from the others.

G.2 A modified method for MS data – using the lesion load

In this section we present the results for when lesion load was used as a regressor for all the tracts that were not presented in chapter 6. In this version of the analysis, the results are more consistent between the tracts. Thanks to that, it was possible to use the same colour scale for all the tracts. As mentioned in the main body of the thesis, now we see spatial clusters of similar effect sizes, which is a good indication, although those clusters are primarily along the edges of the average tract mask.

G.3 Additional analysis with healthy controls

In this section we present the results for combined MS subjects and healthy controls for the tracts that were not presented in chapter 6. In the case of the callosal tracts

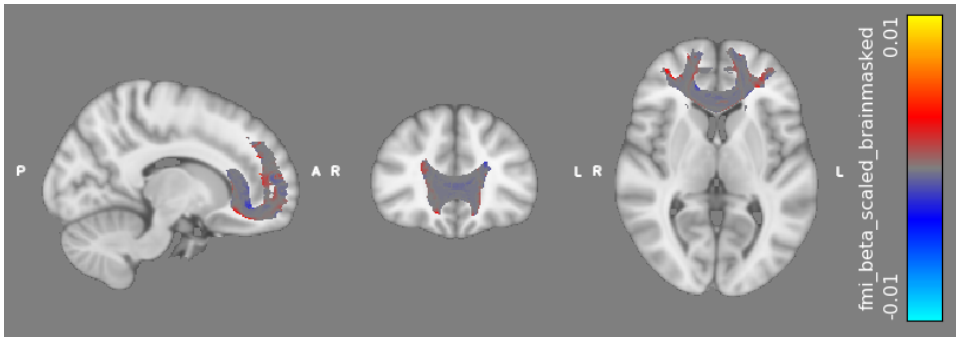

(a) FMI

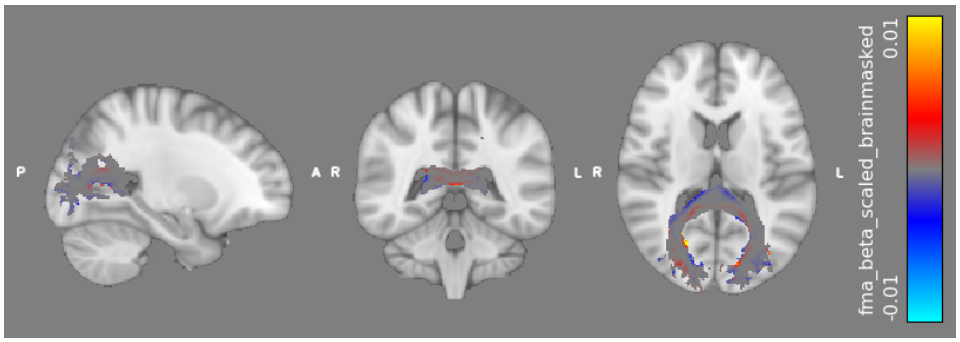

(b) FMA

Figure G.10: Results for the case of using the lesion load as a regressor for the callosal tracts.

(FMA and FMI, figure G.19), we observe the non-zero effects mostly in the posterior part of the tracts. The value of the relative β is higher than in the previous analysis when we did not use healthy participants' data. Non-zero results cover a larger part of the tract but are more noisy in the sense of forming clusters of positive or negative effects. For the SLF tract (figure G.20) the results are also stronger. We can observe some clusters of the positive effect but most of the tract shows a negative effect, i.e. in subjects with lesions on the tract there would be fewer streamlines in those regions. It could be related to the fact that SLF is a long and relatively complex tract. Results for the IFO (figure G.21) are slightly noisy but for the right hemisphere tract it is possible to observe a pattern of negative effects in the middle of the tract and positive effects around the edges. This pattern is reversed in the STR tract (figure 6.11). A negative effect cluster that is, relatively, stronger can also be observed for the CGC tract (figure G.24) in the left hemisphere, but it is not reproduced in the right hemisphere. CGH (figure G.23) had patterns that

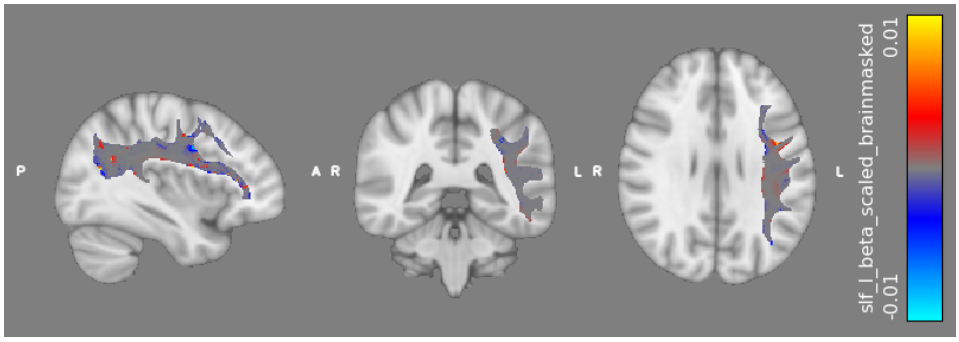

(a) SLF L

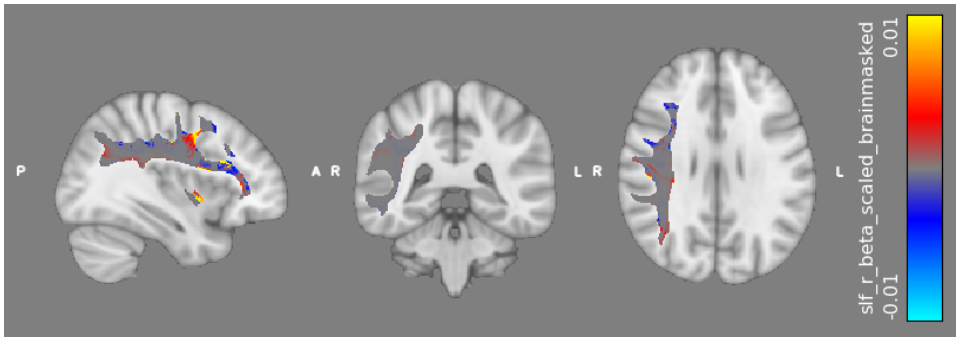

(b) SLF R

Figure G.11: Results for the case of using the lesion load as a regressor for the SLF tract.

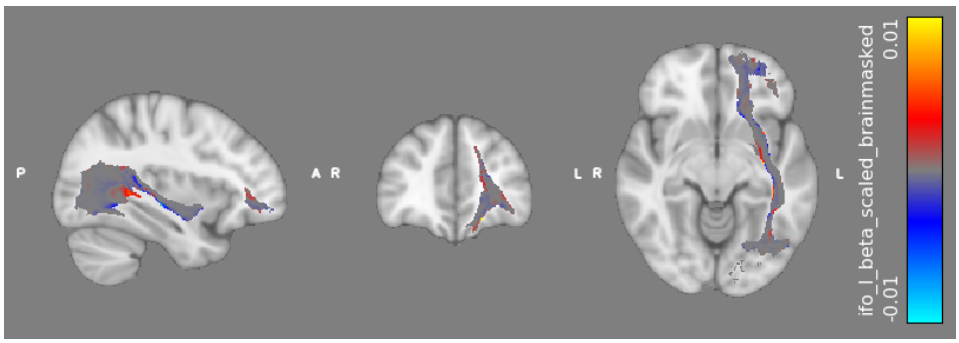

(a) IFO L

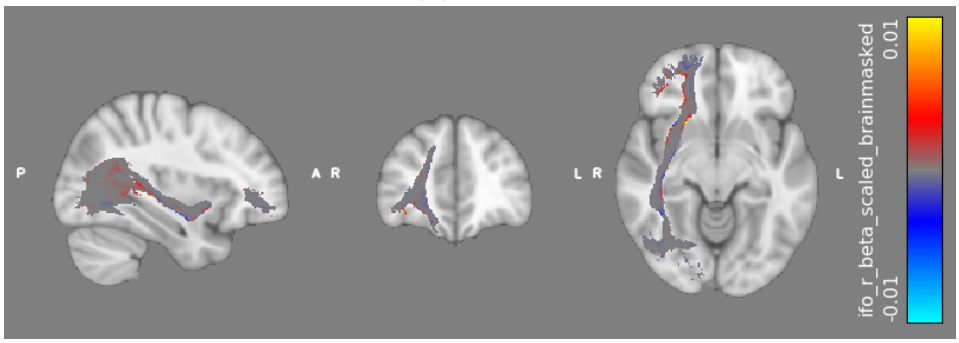

(b) IFO R

Figure G.12: Results for the case of using the lesion load as a regressor for the IFO tract.

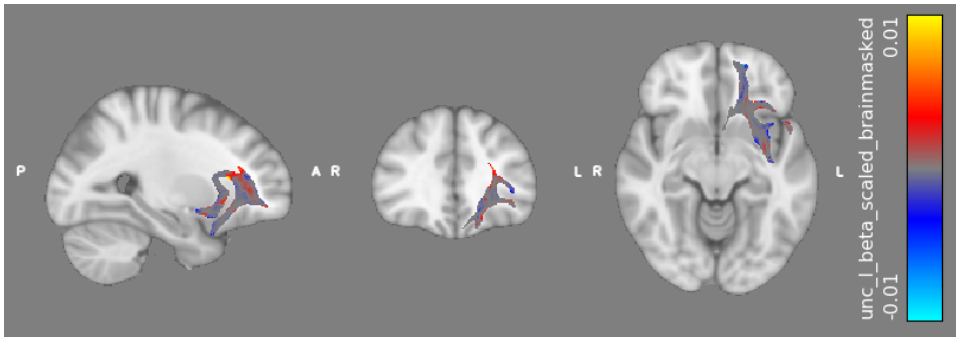

(a) UNC L

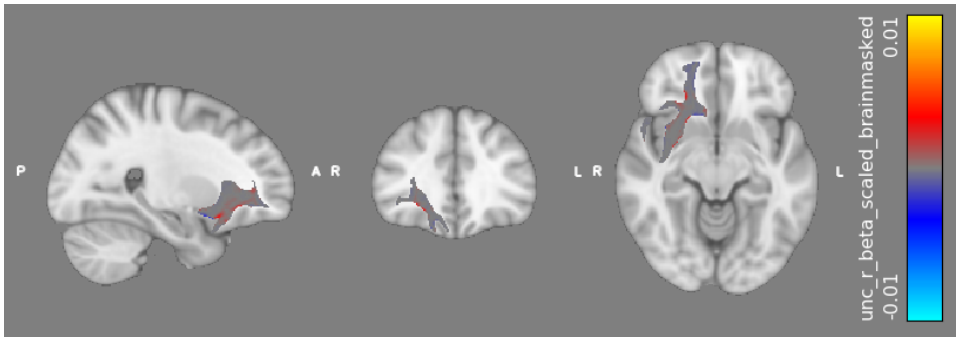

(b) UNC R

Figure G.13: Results for the case of using the lesion load as a regressor for the UNC tract.

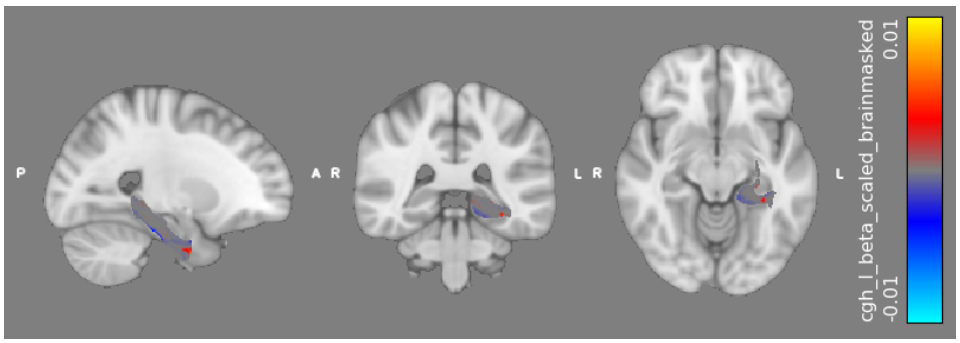

(a) CGH L

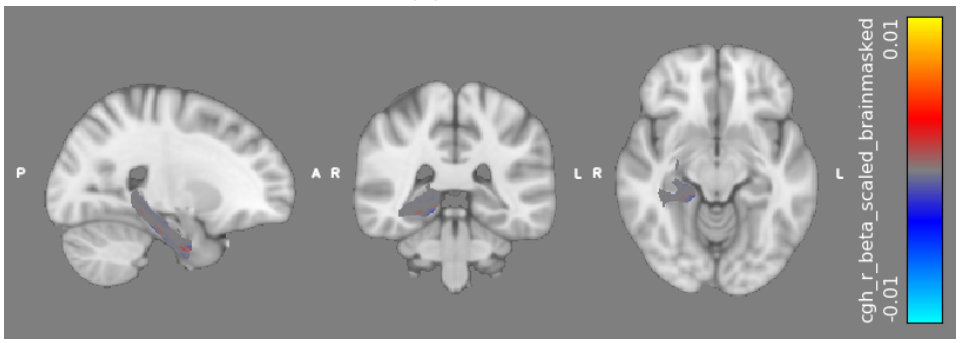

(b) CGH R

Figure G.14: Results for the case of using the lesion load as a regressor for the CGH tract.

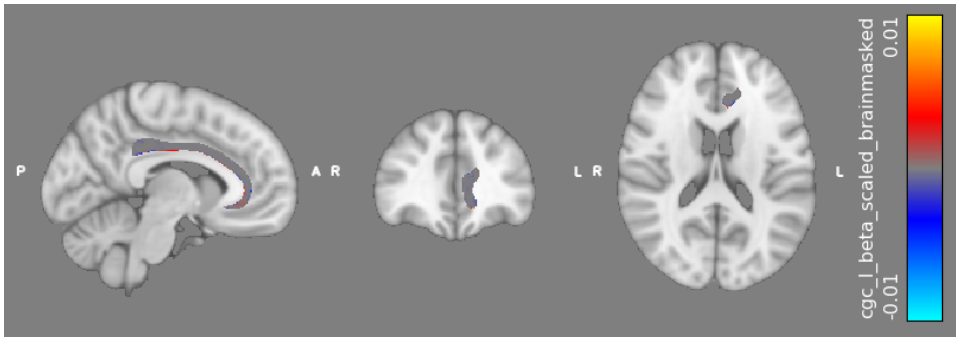

(a) CGC L

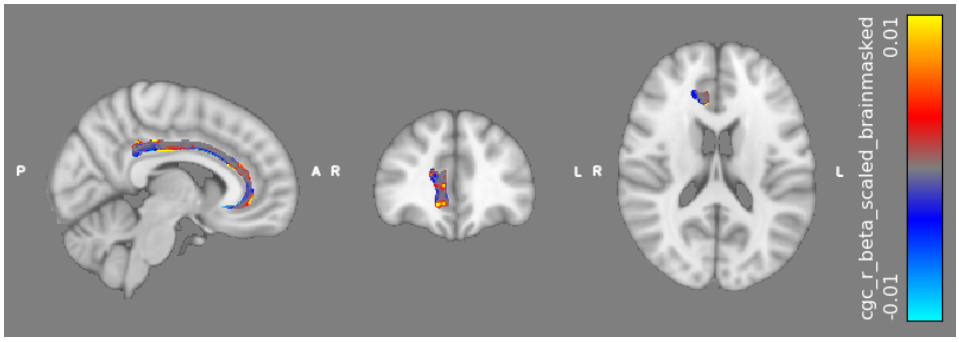

(b) CGC R

Figure G.15: Results for the case of using the lesion load as a regressor for the CGC tract.

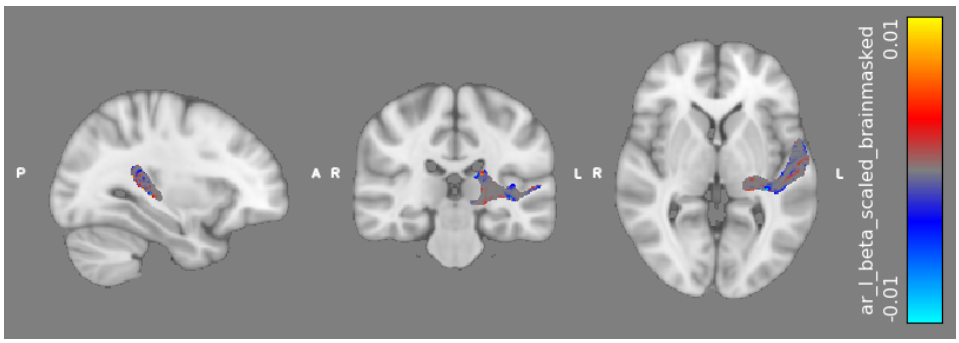

(a) AR L

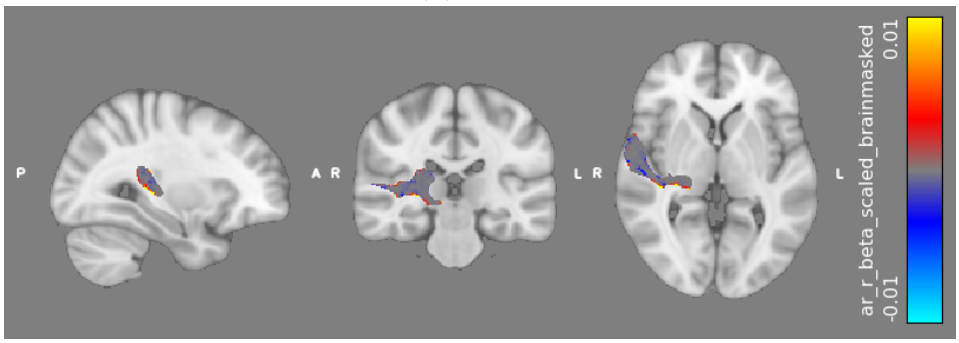

(b) AR R

Figure G.16: Results for the case of using the lesion load as a regressor for the AR tract.

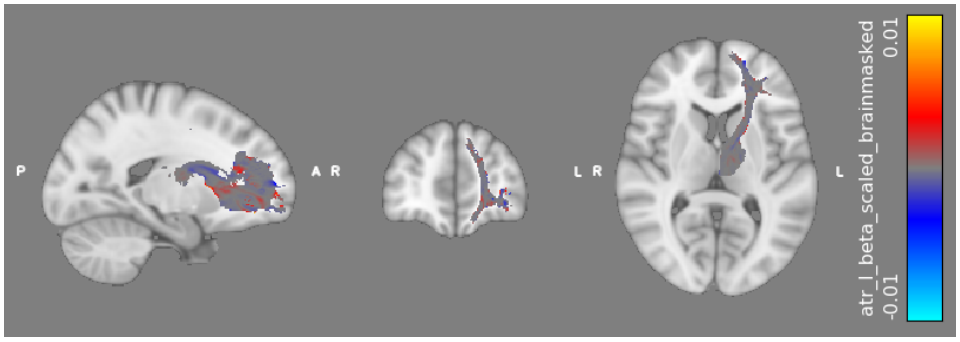

(a) ATR L

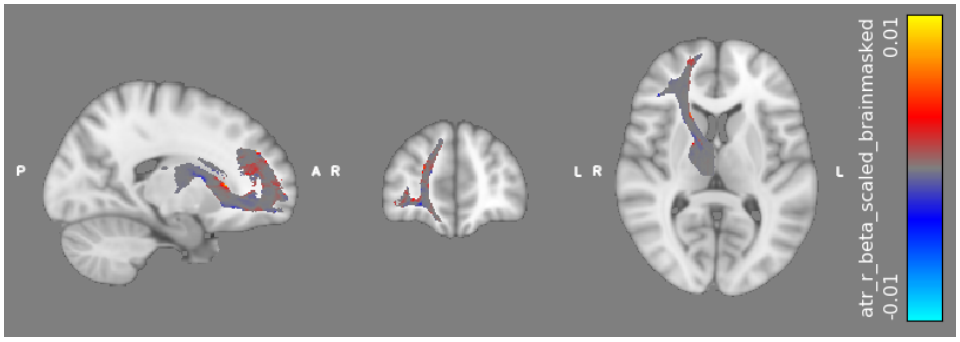

(b) ATR R

Figure G.17: Results for the case of using the lesion load as a regressor for the ATR tract.

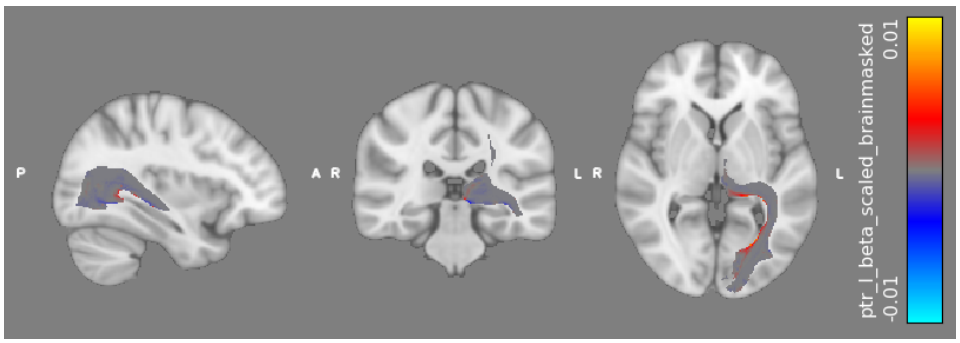

(a) PTR L

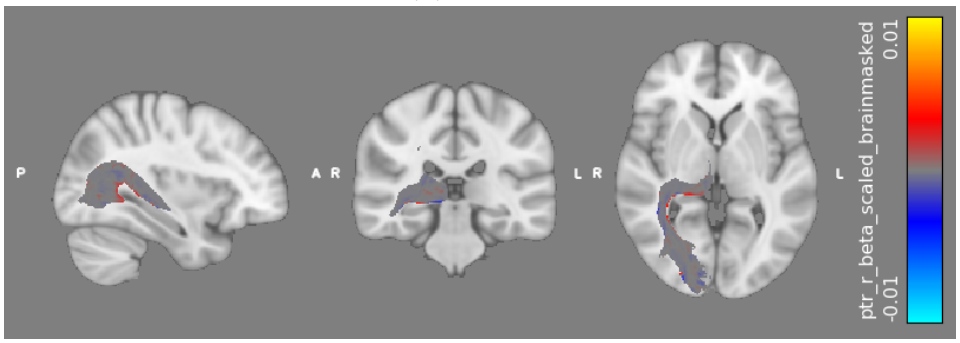

(b) PTR R

Figure G.18: Results for the case of using the lesion load as a regressor for the PTR tract.

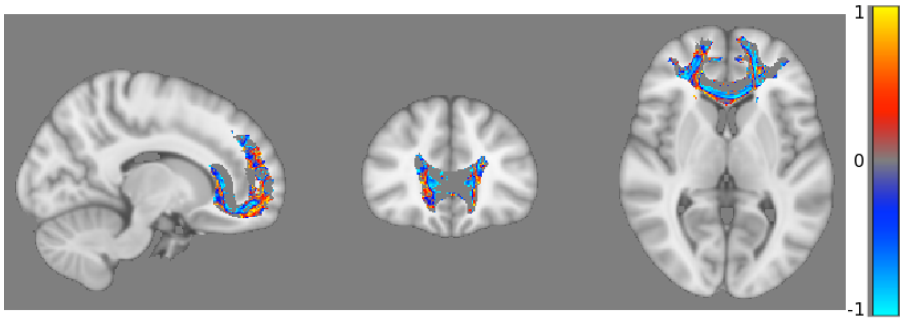

(a) FMI

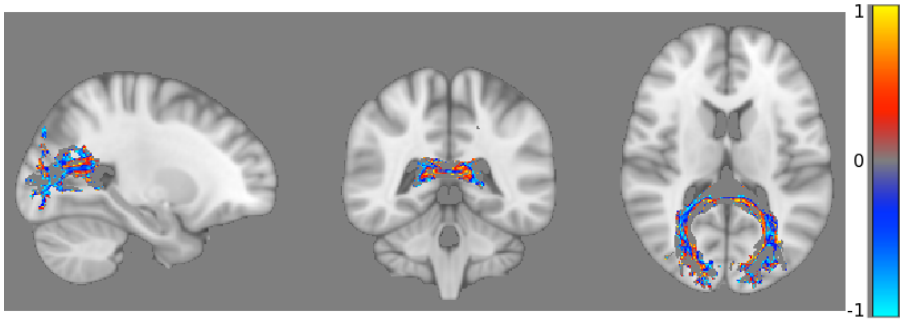

(b) FMA

Figure G.19: Results for the case of using the lesion load as a regressor in the analysis of combined MS subjects and healthy controls for the callosal tracts.

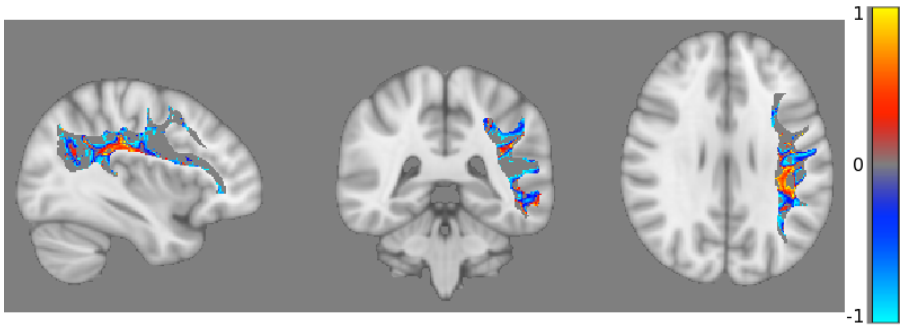

(a) SLF L

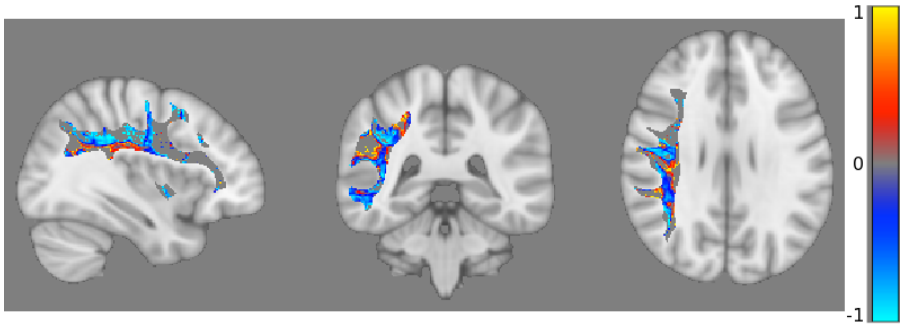

(b) SLF R

Figure G.20: Results for the case of using the lesion load as a regressor in the analysis of combined MS subjects and healthy controls for the SLF tract.

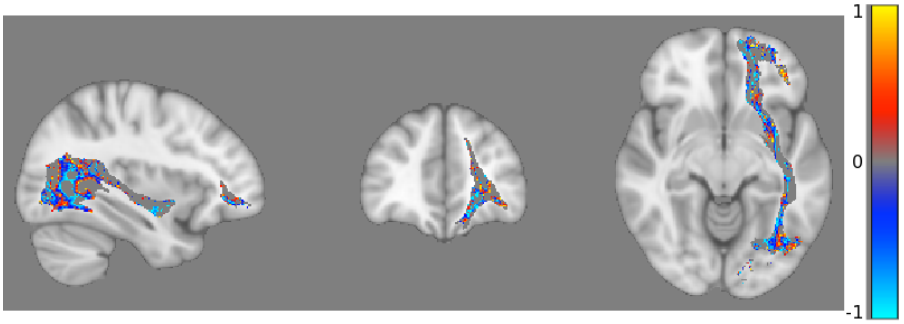

(a) IFO L

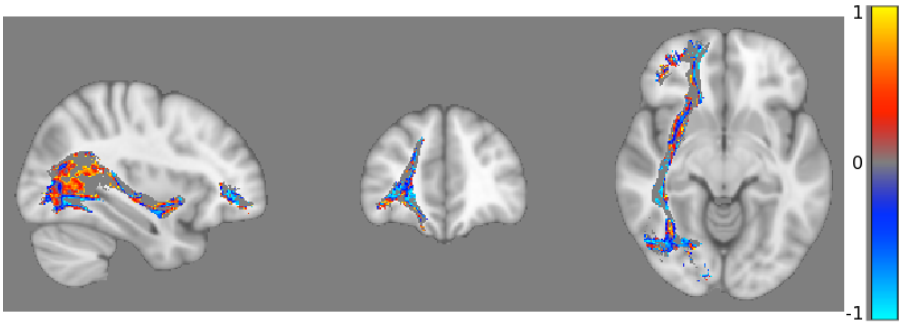

(b) IFO R

Figure G.21: Results for the case of using the lesion load as a regressor in the analysis of combined MS subjects and healthy controls for the IFO tract.

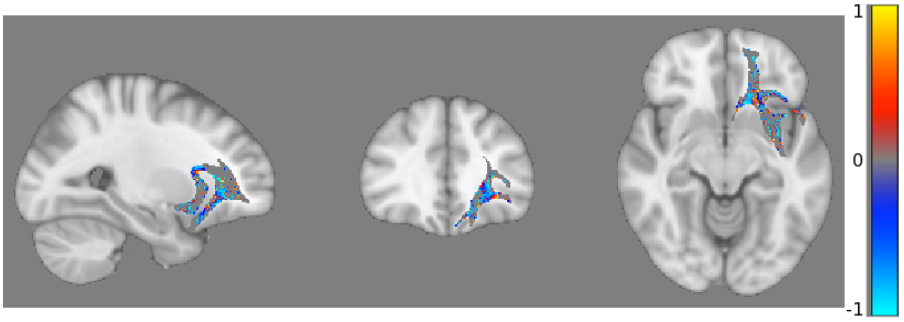

(a) UNC L

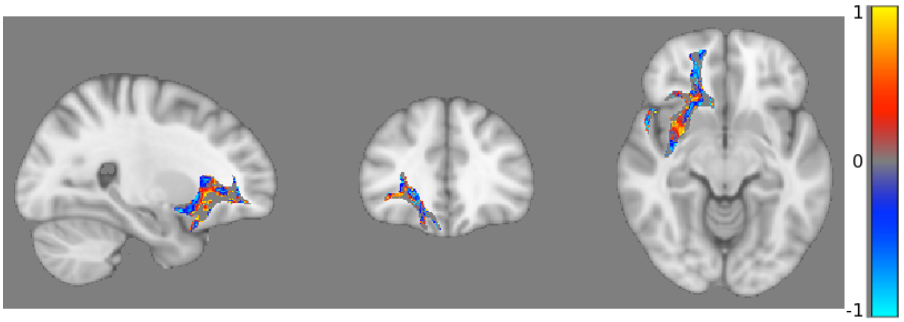

(b) UNC R

Figure G.22: Results for the case of using the lesion load as a regressor in the analysis of combined MS subjects and healthy controls for the UNC tract.

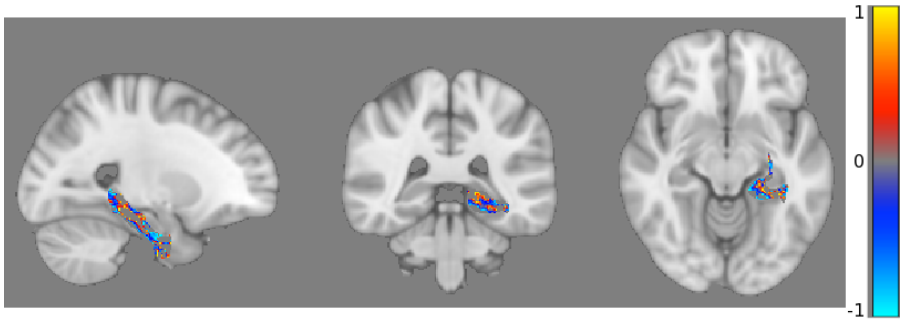

(a) CGH L

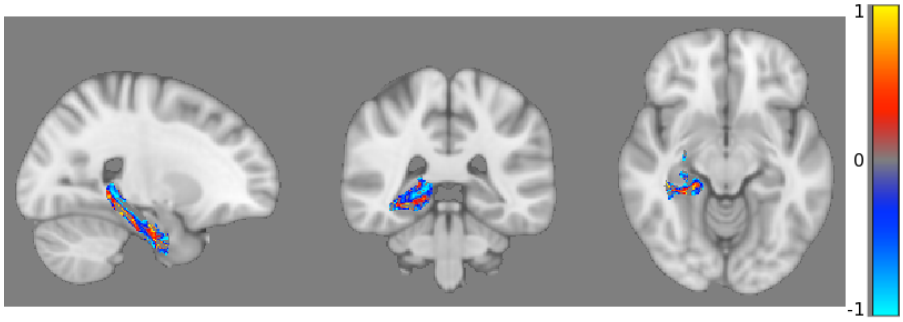

(b) CGH R

Figure G.23: Results for the case of using the lesion load as a regressor in the analysis of combined MS subjects and healthy controls for the CGH tract.

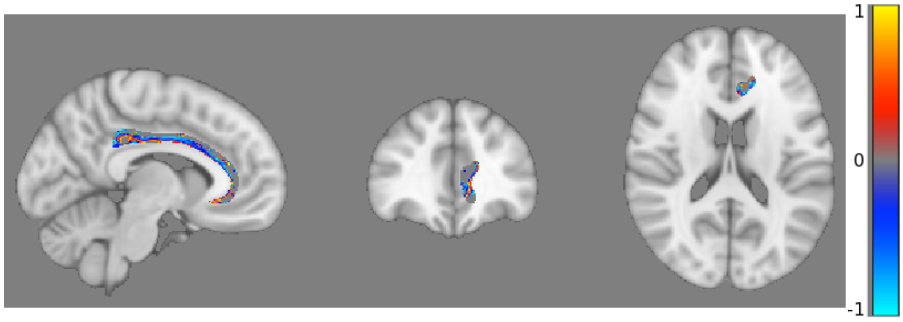

(a) CGC L

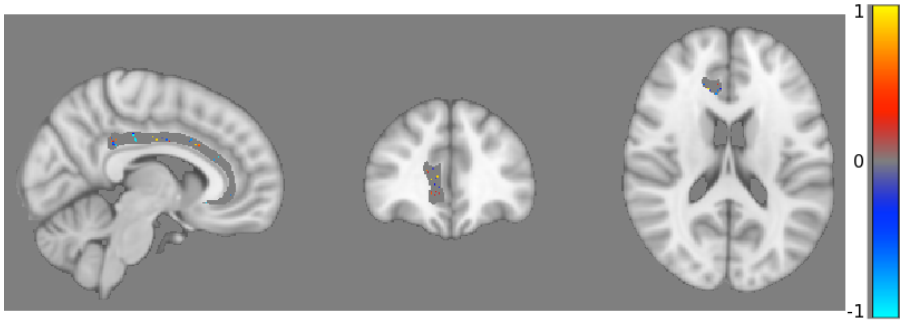

(b) CGC R

Figure G.24: Results for the case of using the lesion load as a regressor in the analysis of combined MS subjects and healthy controls for the CGC tract.

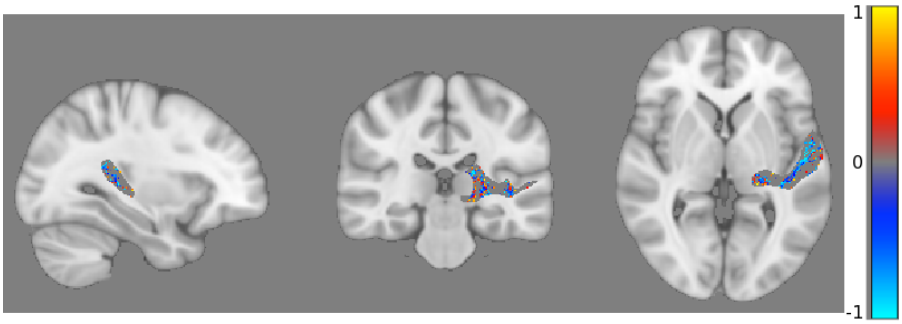

(a) AR L

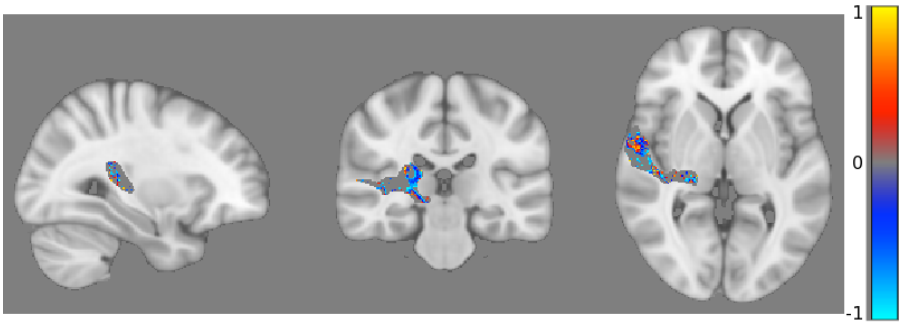

(b) AR R

Figure G.25: Results for the case of using the lesion load as a regressor in the analysis of combined MS subjects and healthy controls for the AR tract.

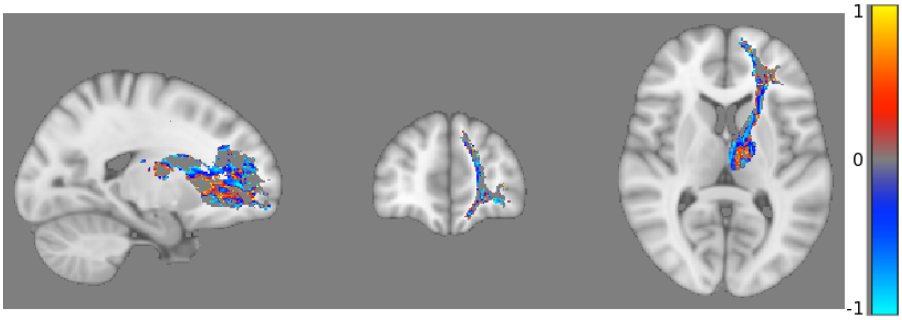

(a) ATR L

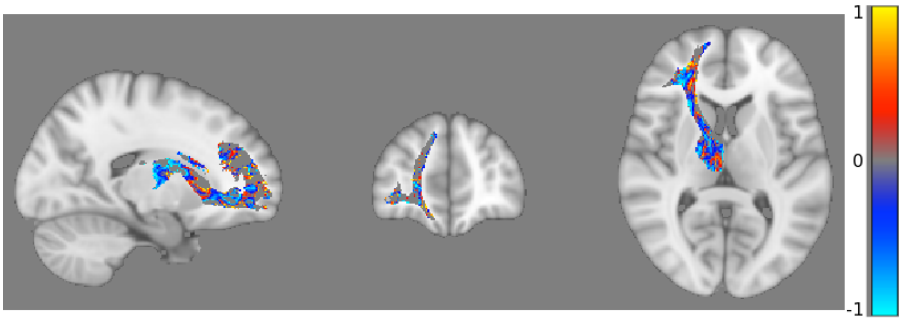

(b) ATR R

Figure G.26: Results for the case of using the lesion load as a regressor in the analysis of combined MS subjects and healthy controls data for the ATR tract.

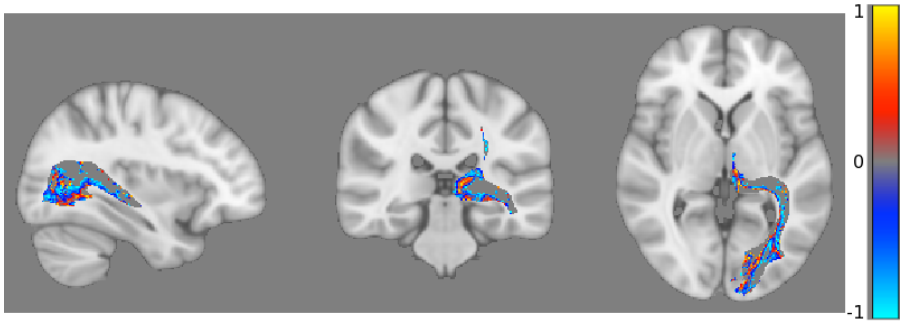

(a) PTR L

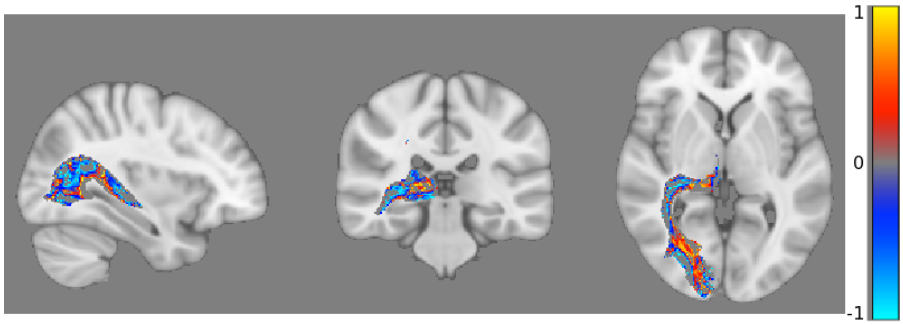

(b) PTR R

Figure G.27: Results for the case of using the lesion load as a regressor in the analysis of combined MS subjects and healthy controls data for the PTR tract.

were more similar between the hemispheres, although results in the left hemisphere were slightly noisier. Similarly, for the UNC tract (figure G.22), the results were noisier and harder to interpret in the left hemisphere, whilst in the right hemisphere both positive and negative effect clusters could be observed. The results for the AR (figure G.25), ATR (figure G.26) and PTR (figure G.27) tracts are all noisy. They show, however, some clusters of effect there, compared to the analysis with no healthy controls, especially in the longer ones, like the PTR and ATR tracts.

References

[1] Meike W Vernooij, M Arfan Ikram, Hervé L Tanghe, Arnaud J P E Vincent, Albert Hofman, Gabriel P Krestin, Wiro J Niessen, Monique M B Breteler, and Aad van der Lugt. "Incidental Findings on Brain MRI in the General Population". In: *New England Journal of Medicine* 357.18 (Nov. 2007), pp. 1821–1828.

[2] Karlijn F. de Laat, Anil M. Tuladhar, Anouk G. W. van Norden, David G. Norris, Marcel P. Zwiers, and Frank-Erik de Leeuw. "Loss of white matter integrity is associated with gait disorders in cerebral small vessel disease". In: *Brain* 134.1 (Dec. 2010), pp. 73–83.

[3] S. Debette and H. S. Markus. "The clinical importance of white matter hyperintensities on brain magnetic resonance imaging: systematic review and meta-analysis". In: *Bmj* 341.jul26 1 (2010), pp. c3666–c3666.

[4] Amandine Pelletier, Olivier Periot, Bixente Dilharreguy, Bassem Hiba, Martine Bordessoules, Sandra Chanraud, Karine Pérès, Hélène Amieva, Jean François Dartigues, Michèle Allard, and Gwénaëlle Catheline. "Age-related modifications of diffusion tensor imaging parameters and white matter hyperintensities as inter-dependent processes". In: *Frontiers in Aging Neuroscience* 7.JAN (2016), pp. 1–10.

[5] Karla L Miller, Fidel Alfaro-Almagro, Neal K Bangerter, David L Thomas, Essa Yacoub, Junqian Xu, Andreas J Bartsch, Saad Jbabdi, Stamatios N Sotiropoulos, Jesper L R Andersson, Ludovica Griffanti, Gwenaëlle Douaud, Thomas W Okell, Peter Weale, Iulius Dragonu, Steve Garratt, Sarah Hudson, Rory Collins, Mark Jenkinson, Paul M Matthews, and Stephen M Smith. "Multimodal population brain imaging in the UK Biobank prospective epidemiological study." In: *Nature neuroscience* 19.11 (2016), pp. 1523–1536.

[6] Emil C Toescu. "Normal brain ageing : models and mechanisms". In: November (2005), pp. 2347–2354.

[7] R Peters. "Ageing and the brain". eng. In: *Postgraduate medical journal* 82.964 (Feb. 2006), pp. 84–88.

[8] R. Douglas Fields. "White matter in learning, cognition and psychiatric disorders". In: *Trends in Neurosciences* 31.7 (2008), pp. 361–370.

[9] Rikke B. Dalby, Jesper Frandsen, M. Mallar Chakravarty, Jamila Ahdidan, Leif Sørensen, Raben Rosenberg, Leif Østergaard, and Poul Videbech. "Correlations between Stroop task performance and white matter lesion measures in late-onset major depression". In: *Psychiatry Research: Neuroimaging* 202.2 (2012), pp. 142–149.

[10] L. L. Herrmann, M. Le Masurier, and K. P. Ebmeier. “White matter hyperintensities in late life depression: A systematic review”. In: *Journal of Neurology, Neurosurgery and Psychiatry* 79.6 (2008), pp. 619–624.

[11] Joanna M. Wardlaw, Maria C. Valdés Hernández, and Susana Muñoz-Maniega. *What are white matter hyperintensities made of? Relevance to vascular cognitive impairment*. 2015.

[12] F. Fazekas, R. Kleinert, H. Offenbacher, R. Schmidt, G. Kleinert, F. Payer, H. Radner, and H. Lechner. “Pathologic correlates of signal hyperintensities”. In: *Neurology* 43.September (1993), pp. 1683–1689.

[13] Heidi Johansen-Berg and T E J Behrens. *Diffusion MRI: From Quantitative Measurement to In vivo Neuroanatomy: Second Edition*. Elsevier Inc., 2013.

[14] Ki Woong Kim, James R. MacFall, and Martha E. Payne. “Classification of White Matter Lesions on Magnetic Resonance Imaging in Elderly Persons”. eng. In: *Biological Psychiatry* 64.4 (Aug. 2008), pp. 273–280.

[15] Joanna M. Wardlaw, Francesca M. Chappell, Maria del Carmen Valdés Hernández, Stephen D.J. Makin, Julie Staals, Kirsten Shuler, Michael J. Thrippleton, Paul A. Armitage, Susana Muñoz-Maniega, Anna K. Heye, Eleni Sakka, and Martin S. Dennis. “White matter hyperintensity reduction and outcomes after minor stroke”. In: *Neurology* 89.10 (2017), pp. 1003–1010.

[16] Pantoni Leonardo and Garcia Julio H. “Pathogenesis of Leukoaraiosis ”. In: *Stroke* 28.3 (Mar. 1997), pp. 652–659.

[17] Benedikt M. Frey, Marvin Petersen, Carola Mayer, Maximilian Schulz, Bastian Cheng, and Götz Thomalla. “Characterization of White Matter Hyperintensities in Large-Scale MRI-Studies”. In: *Frontiers in Neurology* 10.March (2019).

[18] Fidel Alfaro-Almagro, Mark Jenkinson, Neal K. Bangerter, Jesper L.R. Andersson, Ludovica Griffanti, GwenaÃ«lle Douaud, Stamatios N. Sotiropoulos, Saad Jbabdi, Moises Hernandez-Fernandez, Emmanuel Vallee, Diego Vidaurre, Matthew Webster, Paul McCarthy, Christopher Rorden, Alessandro Daducci, Daniel C. Alexander, Hui Zhang, Iulius Dragonu, Paul M. Matthews, Karla L. Miller, and Stephen M. Smith. “Image processing and Quality Control for the first 10,000 brain imaging datasets from UK Biobank”. In: *NeuroImage* 166 (2018), pp. 400–424.

[19] Naomi Allen, Cathie Sudlow, Paul Downey, Tim Peakman, John Danesh, Paul Elliott, John Gallacher, Jane Green, Paul Matthews, Jill Pell, Tim Sprosen, and Rory Collins. “UK Biobank: Current status and what it means for epidemiology”. In: *Health Policy and Technology* 1.3 (2012), pp. 123–126.

[20] Simon R. Cox, Stuart J. Ritchie, Elliot M. Tucker-Drob, David C. Liewald, Saskia P. Hagenaars, Gail Davies, Joanna M. Wardlaw, Catharine R. Gale, Mark E. Bastin, and Ian J. Deary. “Ageing and brain white matter structure in 3,513 UK Biobank participants”. In: *Nature Communications* 7 (2016), p. 13629.

[21] Stephen M. Smith and Thomas E. Nichols. “Statistical Challenges in “Big Data” Human Neuroimaging”. In: *Neuron* 97.2 (2018), pp. 263–268.

[22] O. Sporns. “Brain connectivity”. In: *Scholarpedia* 2.10 (2007). revision #91084, p. 4695.

[23] Karl J Friston. "Functional and effective connectivity: a review". In: *Brain connectivity* 1.1 (2011), pp. 13–36.

[24] Carlo Pierpaoli and Peter J Basser. "Toward a quantitative assessment of diffusion anisotropy". In: *Magnetic resonance in Medicine* 36.6 (1996), pp. 893–906.

[25] T E J Behrens, M W Woolrich, M Jenkinson, R G Nunes, S Clare, P M Matthews, J M Brady, and S M Smith. "Characterization and Propagation of Uncertainty in Diffusion-Weighted MR Imaging". In: 1088 (2003), pp. 1077–1088.

[26] T.E.J. Behrens, H. Johansen Berg, S. Jbabdi, M.F.S. Rushworth, and M.W. Woolrich. "Probabilistic diffusion tractography with multiple fibre orientations: What can we gain?" In: *NeuroImage* 34.1 (Jan. 2007), pp. 144–155.

[27] Saad Jbabdi, Stamatios N. Sotiropoulos, Alexander M. Savio, Manuel Graña, and Timothy E. J. Behrens. "Model-based analysis of multishell diffusion MR data for tractography: How to get over fitting problems". In: *Magnetic Resonance in Medicine* 68.6 (2012), pp. 1846–1855.

[28] Hui Zhang, Torben Schneider, Claudia A. Wheeler-Kingshott, and Daniel C. Alexander. "NODDI: Practical in vivo neurite orientation dispersion and density imaging of the human brain". In: *NeuroImage* 61.4 (July 2012), pp. 1000–1016.

[29] Olaf Sporns, Giulio Tononi, and Rolf Kötter. "The human connectome: A structural description of the human brain". In: *PLoS Computational Biology* 1.4 (2005), pp. 0245–0251.

[30] Medard Kakou, Fulbert Kouakou, Dominique N'dri Oka, Alban Slim Mbende, Johann Peltier, and Stephane Velut. "Microanatomy of Thalamic Radiations". In: *International Journal of Human Anatomy* 1.1 (2017), pp. 28–37.

[31] Marco Catani, Robert J. Howard, Sinisa Pajevic, and Derek K. Jones. "Virtual in Vivo interactive dissection of white matter fasciculi in the human brain". In: *NeuroImage* 17.1 (2002), pp. 77–94.

[32] Susumu Mori, Walter E. Kaufmann, Christos Davatzikos, Bram Stieltjes, Laura Amodei, Kim Fredericksen, Godfrey D. Pearlson, Elias R. Melhem, Meiyappan Solaiyappan, Gerald V. Raymond, Hugo W. Moser, and Peter C.M. Van Zijl. "Imaging cortical association tracts in the human brain using diffusion-tensor-based axonal tracking". In: *Magnetic Resonance in Medicine* 47.2 (2002), pp. 215–223.

[33] Ruilin Wang, Qing Fan, Zongfeng Zhang, Yongjun Chen, Yajing Zhu, and Yao Li. "Anterior thalamic radiation structural and metabolic changes in obsessive-compulsive disorder: A combined DTI-MRS study". In: *Psychiatry Research: Neuroimaging* 277 (July 2018), pp. 39–44.

[34] Marc Christopher Emos and Sanjeev Agarwal. "Neuroanatomy, Internal Capsule". In: *StatPearls [Internet]*. StatPearls Publishing, 2019.

[35] Janine Bijsterbosch, Stephen M. Smith, and Christian F. Beckmann. *An introduction to resting state fMRI functional connectivity*. 2017.

[36] Alastair Compston and Alasdair Coles. "Multiple sclerosis". In: *Lancet* 359.9313 (2002), pp. 1221–1231.

[37] Fred D Lublin, Stephen C Reingold, Jeffrey A Cohen, Gary R Cutter, Alan J Thompson, Jerry S Wolinsky, Brenda Banwell, Frederik Barkhof, Bruce Bebo, Peter A Calabresi, Michel Clanet, Robert J Fox, Mark S Freedman, Andrew D Goodman, John A Lincoln, Catherine Lubetzki, Aaron E Miller, Xavier Montalban, Paul W O Connor, and Maria Pia Sormani. "Defining the clinical course of multiple sclerosis". In: (2014).

[38] Chris H. Polman, Stephen C. Reingold, Brenda Banwell, Michel Clanet, Jeffrey A. Cohen, Massimo Filippi, Kazuo Fujihara, Eva Havrdova, Michael Hutchinson, Ludwig Kappos, Fred D. Lublin, Xavier Montalban, Paul O'Connor, Magnhild Sandberg-Wollheim, Alan J. Thompson, Emmanuelle Waubant, Brian Weinshenker, and Jerry S. Wolinsky. "Diagnostic criteria for multiple sclerosis: 2010 Revisions to the McDonald criteria". en. In: *Annals of Neurology* 69.2 (Feb. 2011), pp. 292–302.

[39] Daryoush Mortazavi, Abbas Z. Kouzani, and Hamid Soltanian-Zadeh. "Segmentation of multiple sclerosis lesions in MR images: A review". In: *Neuroradiology* 54.4 (2012), pp. 299–320.

[40] Rohit Bakshi, Alan J Thompson, Maria A Rocca, Daniel Pelletier, Vincent Dousset, Frederik Barkhof, Matilde Inglese, Charles RG Guttmann, Mark A Horsfield, and Massimo Filippi. "MRI in multiple sclerosis: current status and future prospects". eng. In: *Lancet Neurology* 7.7 (2008), pp. 615–625.

[41] Valentina Tomassini and Jacqueline Palace. "Multiple sclerosis lesions: insights from imaging techniques". In: *Expert Review of Neurotherapeutics* 9.9 (2009), pp. 1341–1359.

[42] Alan J. Thompson, Brenda L. Banwell, Frederik Barkhof, William M. Carroll, Timothy Coetzee, Giancarlo Comi, Jorge Correale, Franz Fazekas, Massimo Filippi, Mark S. Freedman, Kazuo Fujihara, Steven L. Galetta, Hans Peter Hartung, Ludwig Kappos, Fred D. Lublin, Ruth Ann Marrie, Aaron E. Miller, David H. Miller, Xavier Montalban, Ellen M. Mowry, Per Soelberg Sorensen, Mar Tintoré, Anthony L. Traboulsee, Maria Trojano, Bernard M.J. Uitdehaag, Sandra Vukusic, Emmanuelle Waubant, Brian G. Weinshenker, Stephen C. Reingold, and Jeffrey A. Cohen. "Diagnosis of multiple sclerosis: 2017 revisions of the McDonald criteria". In: *The Lancet Neurology* 17.2 (2018), pp. 162–173.

[43] Mandip S. Dhamoon, Ying Kuen Cheung, Ahmet Bagci, Noam Alperin, Ralph L. Sacco, Mitchell S.V. Elkind, and Clinton B. Wright. "Periventricular White Matter Hyperintensities and Functional Decline". In: *Journal of the American Geriatrics Society* 66.1 (2018), pp. 113–119.

[44] Leonie Lampe, Shahrzad Kharabian-Masouleh, Jana Kynast, Katrin Arelin, Christopher J. Steele, Markus Löffler, A. Veronica Witte, Matthias L. Schroeter, Arno Villringer, and Pierre Louis Bazin. "Lesion location matters: The relationships between white matter hyperintensities on cognition in the healthy elderly". In: *Journal of Cerebral Blood Flow and Metabolism* (2017).

[45] Carolyn D. Langen, Hazel I. Zonneveld, Tonya White, Wyke Huizinga, Lotte G.M. Cremers, Marius de Groot, Mohammad Arfan Ikram, Wiro J. Niessen, and Meike W. Vernooij. "White matter lesions relate to tract-specific reductions in functional connectivity". In: *Neurobiology of Aging* 51 (2017), pp. 97–103.

[46] William Reginold, Kevin Sam, Julien Poublanc, Joe Fisher, Adrian Crawley, and David J. Mikulis. "Impact of white matter hyperintensities on surrounding white matter tracts". In: *Neuroradiology* 60.9 (2018), pp. 933–944.

[47] Amy Kuceyeski, Jun Maruta, Norman Relkin, and Ashish Raj. "The Network Modification (NeMo) Tool: Elucidating the Effect of White Matter Integrity Changes on Cortical and Subcortical Structural Connectivity". In: *Brain Connectivity* 3.5 (2013), pp. 451–463.

[48] Marius De Groot, Meike W. Vernooij, Stefan Klein, M. Arfan Ikram, Frans M. Vos, Stephen M. Smith, Wiro J. Niessen, and Jesper L R Andersson. "Improving alignment in Tract-based spatial statistics: Evaluation and optimization of image registration". In: *NeuroImage* 76 (2013), pp. 400–411.

[49] Ludovica Griffanti, Giovanna Zamboni, Aamira Khan, Linxin Li, Guendalina Bonifacio, Vaanathi Sundaresan, Ursula G Schulz, Wilhelm Kuker, Marco Battaglini, Peter M Rothwell, and Mark Jenkinson. "BIANCA (Brain Intensity AbNormality Classification Algorithm): A new tool for automated segmentation of white matter hyperintensities". In: *NeuroImage* 141 (2016), pp. 191–205.

[50] Moises Hernandez-Fernandez, Istvan Reguly, Saad Jbabdi, Mike Giles, Stephen Smith, and Stamatios N. Sotiropoulos. "Using GPUs to accelerate computational diffusion MRI: From microstructure estimation to tractography and connectomes". In: *NeuroImage* 188.June 2018 (2019), pp. 598–615.

[51] Mark Jenkinson, Christian F. Beckmann, Timothy E J Behrens, Mark W. Woolrich, and Stephen M. Smith. "FSL". In: *NeuroImage* 62.2 (2012), pp. 782–790.

[52] Vaanathi Sundaresan, Giovanna Zamboni, Campbell Le Heron, Peter M. Rothwell, Masud Husain, Marco Battaglini, Nicola De Stefano, Mark Jenkinson, and Ludovica Griffanti. "Automated lesion segmentation with BIANCA: Impact of population-level features, classification algorithm and locally adaptive thresholding". In: *NeuroImage* 202 (2019), p. 116056.

[53] Mohamad Habes, Guray Erus, Jon B. Toledo, Tianhao Zhang, Nick Bryan, Lenore J. Launer, Yves Rosseel, Deborah Janowitz, Jimit Doshi, Sandra Van Der Auwera, Bettina Von Sarnowski, Katrin Hegenscheid, Norbert Hosten, Georg Homuth, Henry Völzke, Ulf Schminke, Wolfgang Hoffmann, Hans J. Grabe, and Christos Davatzikos. "White matter hyperintensities and imaging patterns of brain ageing in the general population". In: *Brain* 139.4 (2016), pp. 1164–1179.

[54] Stephan Seiler, Evan Fletcher, Kinsy Hassan-Ali, Michelle Weinstein, Alexa Beiser, Jayandra J. Himali, Claudia L. Satizabal, Sudha Seshadri, Charles DeCarli, and Pauline Maillard. "Cerebral tract integrity relates to white matter hyperintensities, cortex volume, and cognition". In: *Neurobiology of Aging* 72 (2018), pp. 14–22.

[55] Melissa E. Murray, Stephen D. Weigand, David S. Knopman, Dennis W. Dickson, Matthew L. Senjem, Ronald C. Petersen, Greg M. Preboske, John H. Hollman, Clifford R. Jack, and Tanis J. Ferman. "Functional Impact of White Matter Hyperintensities in Cognitively Normal Elderly Subjects". In: *Archives of Neurology* 67.11 (2010), pp. 1379–1385.

[56] Carolyn D. Langen, Lotte G.M. Cremers, Marius de Groot, Tonya White, M. Arfan Ikram, Wiro J. Niessen, and Meike W. Vernooij. "Disconnection due to white matter hyperintensities is associated with lower cognitive scores". In: *NeuroImage* 183.August (2018), pp. 745–756.

[57] Alexander N.W. Taylor, Lana Kambeitz-Ilankovic, Benno Gesierich, Lee Simon-Vermot, Nicolai Franzmeier, Miguel Araque Caballero, Sophia Müller, Liu Hesheng, Birgit Ertl-Wagner, Katharina Bürger, Michael W. Weiner, Martin Dichgans, Marco Duering, and Michael Ewers. "Tract-specific white matter hyperintensities disrupt neural network function in Alzheimer's disease". In: *Alzheimer's and Dementia* 13.3 (2017), pp. 225–235.

[58] Minjie Wu, Carmen Andreescu, Meryl A. Butters, Robert Tamburo, Charles F. Reynolds, and Howard Aizenstein. "Default-mode network connectivity and white matter burden in late-life depression". In: *Psychiatry Research - Neuroimaging* 194.1 (2011), pp. 39–46.

[59] Yongxia Zhou, Fang Yu, Timothy Q. Duong, and for the Alzheimer's Disease Neuroimaging Initiative. "White matter lesion load is associated with resting state functional MRI activity and amyloid pet but not FDG in mild cognitive impairment and early alzheimer's disease patients". In: *Journal of Magnetic Resonance Imaging* 41.1 (2015), pp. 102–109.

[60] Rahul S. Desikan, Florent Ségonne, Bruce Fischl, Brian T. Quinn, Bradford C. Dickerson, Deborah Blacker, Randy L. Buckner, Anders M. Dale, R. Paul Maguire, Bradley T. Hyman, Marilyn S. Albert, and Ronald J. Killiany. "An automated labeling system for subdividing the human cerebral cortex on MRI scans into gyral based regions of interest". In: *NeuroImage* 31.3 (July 2006), pp. 968–980.

[61] B. T. Thomas Yeo, Fenna M. Krienen, Jorge Sepulcre, Mert R. Sabuncu, Danial Lashkari, Marisa Hollinshead, Joshua L. Roffman, Jordan W. Smoller, Lilla Zöllei, Jonathan R. Polimeni, Bruce Fisch, Hesheng Liu, and Randy L. Buckner. "The organization of the human cerebral cortex estimated by intrinsic functional connectivity". In: *Journal of Neurophysiology* 106.3 (2011), pp. 1125–1165.

[62] Stephen M. Smith, Diego Vidaurre, Christian F. Beckmann, Matthew F. Glasser, Mark Jenkinson, Karla L. Miller, Thomas E. Nichols, Emma C. Robinson, Gholamreza Salimi-Khorshidi, Mark W. Woolrich, Deanna M. Barch, Kamil Uğurbil, and David C. Van Essen. "Functional connectomics from resting-state fMRI". In: *Trends in Cognitive Sciences* 17.12 (2013), pp. 666–682.

[63] William Hedley Thompson and Peter Fransson. "On stabilizing the variance of dynamic functional brain connectivity time series". In: *Brain connectivity* 6.10 (2016), pp. 735–746.

[64] Donald R. Williams and Philippe Rast. "Back to the basics: Rethinking partial correlation network methodology". In: *British Journal of Mathematical and Statistical Psychology* (2019), pp. 1–15.

[65] Janine Diane Bijsterbosch, Mark W Woolrich, Matthew F Glasser, Emma C Robinson, Christian F Beckmann, David C Van Essen, Samuel J Harrison, and Stephen M Smith. "The relationship between spatial configuration and functional connectivity of brain regions". In: *eLife* 7 (Feb. 2018). Ed. by Chris Honey, e32992.

[66] R Deichmann, J.A Gottfried, C Hutton, and R Turner. "Optimized EPI for fMRI studies of the orbitofrontal cortex". In: *NeuroImage* 19.2 (June 2003), pp. 430–441.

[67] Christian F. Beckmann, Marilena DeLuca, Joseph T. Devlin, and Stephen M. Smith. "Investigations into resting-state connectivity using independent component analysis". In: *Philosophical Transactions of the Royal Society B: Biological Sciences* 360.1457 (2005), pp. 1001–1013.

[68] V.D. Calhoun, T. Adali, G.D. Pearlson, and J.J. Pekar. "A method for making group inferences from functional MRI data using independent component analysis". In: *Human Brain Mapping* 14.3 (2001), pp. 140–151.

[69] Julie A. Alvarez and Eugene Emory. "Executive function and the frontal lobes: A meta-analytic review". In: *Neuropsychology Review* 16.1 (2006), pp. 17–42.

[70] Saad Jbabdi and Heidi Johansen-Berg. "Tractography: where do we go from here?" In: *Brain connectivity* 1.3 (2011), pp. 169–183.

[71] Kurt Schilling, Yurui Gao, Vaibhav Janve, Iwona Stepniewska, Bennett A. Landman, and Adam W. Anderson. "Confirmation of a gyral bias in diffusion MRI fiber tractography". In: *Human Brain Mapping* 39.3 (2018), pp. 1449–1466.

[72] Wang Zhan, Yu Zhang, Susanne G. Mueller, Peter Lorenzen, Stathis Hadjidemetriou, Norbert Schuff, and Michael W. Weiner. "Characterization of white matter degeneration in elderly subjects by magnetic resonance diffusion and FLAIR imaging correlation". In: *NeuroImage* 47.SUPPL. 2 (2009), T58–T65.

[73] Guillaume Theaud, Bixente Dilharreguy, Gwenealle Catheline, and Maxime Descoteaux. "Impact of white matter hyperintensities on tractography". In: *Proc. Intl. Soc. Mag. Reson. Med* 25.January 2017 (2017), pp. 3–6.

[74] C. M. Bird, P. Malhotra, A. Parton, E. Coulthard, M. F.S. Rushworth, and M. Husain. "Visual neglect after right posterior cerebral artery infarction". In: *Journal of Neurology, Neurosurgery and Psychiatry* 77.9 (2006), pp. 1008–1012.

[75] John S Duncan. "Imaging in the surgical treatment of epilepsy". In: *Nature Reviews Neurology* 6 (Sept. 2010), p. 537.

[76] Olga Ciccarelli, Marco Catani, Heidi Johansen-Berg, Chris Clark, and Alan Thompson. "Diffusion-based tractography in neurological disorders: concepts, applications, and future developments". In: *The Lancet Neurology* 7.8 (2008), pp. 715–727.

[77] H Johansen-Berg, D A Gutman, T E J Behrens, P M Matthews, M F S Rushworth, E Katz, A M Lozano, and H S Mayberg. "Anatomical connectivity of the subgenual cingulate region targeted with deep brain stimulation for treatment-resistant depression". In: *CEREBRAL CORTEX* 18.6 (June 2008), pp. 1374–1383.

[78] Zoe Morris, William N Whiteley, W T Longstreth, Frank Weber, Yi-Chung Lee, Yoshito Tsushima, Hannah Alphs, Susanne C Ladd, Charles Warlow, Joanna M Wardlaw, and Rustam Al-Shahi Salman. "Incidental findings on brain magnetic resonance imaging: systematic review and meta-analysis". In: *BMJ* 339 (2009).

[79] Jung-Lung Hsu, Alexander Leemans, Chyi-Huey Bai, Cheng-Hui Lee, Yuh-Feng Tsai, Hou-Chang Chiu, and Wei-Hung Chen. "Gender differences and age-related white matter changes of the human brain: A diffusion tensor imaging study". In: *NeuroImage* 39.2 (2008), pp. 566–577.

[80] Juergen Lutz, Felix Hemminger, Robert Stahl, Olaf Dietrich, Martin Hempel, Maximilian Reiser, and Lorenz Jäger. "Evidence of Subcortical and Cortical Aging of the Acoustic Pathway: A Diffusion Tensor Imaging (DTI) Study". In: *Academic Radiology* 14.6 (2007), pp. 692–700.

[81] Jesper L R Andersson, Mark Jenkinson, and Stephen Smith. "Non-linear registration aka Spatial normalisation FMRIB Technical Report TR07JA2". In: *FMRIB Analysis Group Technical Reports* (2007).

[82] Ruth Geraldes, Olga Ciccarelli, Frederik Barkhof, Nicola De Stefano, Christian Enzinger, Massimo Filippi, Monika Hofer, Friedemann Paul, Paolo Preziosa, Alex Rovira, Gabriele C. DeLuca, Ludwig Kappos, Tarek Yousry, Franz Fazekas, Jette Frederiksen, Claudio Gasperini, Jaume Sastre-Garriga, Nikos Evangelou, and Jacqueline Palace. "The current role of MRI in differentiating multiple sclerosis from its imaging mimics". In: *Nature Reviews Neurology* 14.4 (2018), pp. 199–213.

[83] M. Rovaris, A. Gass, R. Bammer, S. J. Hickman, O. Ciccarelli, D. H. Miller, and M. Filippi. "Diffusion MRI in multiple sclerosis". In: *Neurology* 65.10 (2005), pp. 1526–1532.

[84] Ilona Lipp, Greg D Parker, Emma Tallantyre, Alex Goodall, Steluta Grama, Eleonora Patitucci, Phoebe Heveron, Valentina Tomassini, and Derek Jones. "Tractography in the presence of white matter lesions in multiple sclerosis". In: *bioRxiv* (2019).

[85] Jeremy D. Schmahmann, Deepak N. Pandya, Jeremy D. Schmahmann, and Deepak N. Pandya. "Superior Longitudinal Fasciculus and Arcuate Fasciculus". eng. In: *Fiber Pathways of the Brain*. New York: Oxford University Press, 2009, pp. 393–408.

[86] Frederik Barkhof. "The clinico-radiological paradox in multiple sclerosis revisited". In: *Current Opinion in Neurology* 15.3 (2002).

[87] Mara Cercignani and Claudia Gandini Wheeler-Kingshott. "From micro- to macro-structures in multiple sclerosis: What is the added value of diffusion imaging". In: *NMR in Biomedicine* November 2017 (2018), pp. 1–10.